

**Die Untersuchung der β_0/β Phasenumwandlung in
TiAl Legierungen mit Hilfe von Synchrotron- und
Neutronenbeugungsmethoden**

**Dissertation zur Erlangung des Doktorgrades an der Fakultät für
Mathematik, Informatik und Naturwissenschaften
Fachbereich Physik
der Universität Hamburg
vorgelegt von
Victoria Kononikhina**

Hamburg

2023

Gutachter/innen der Dissertation:

Prof. Dr. Andreas Schreyer
Prof. Dr. Florian Pyczak

Zusammensetzung der Prüfungskommission:

Prof. Dr. Andreas Schreyer
Prof. Dr. Florian Pyczak
Prof. Dr. Robin Santra
Prof. Dr. Christian Schroer
Dr. Andreas Stark

Vorsitzende/r der Prüfungskommission:

Prof. Dr. Robin Santra

Datum der Disputation

13.01. 2023

Vorsitzender Fach-Promotionsausschusses
PHYSIK:

Prof. Dr. Günter H. W. Sigl

Leiter der Fachbereich PHYSIK

Prof. Dr. Wolfgang J. Parak

Dekan der Fakultät MIN:

Prof. Dr.-Ing. Norbert Ritter

**Disordering β_0/β phase transformation in γ -TiAl
alloys studied by neutron and synchrotron diffraction
techniques**

**Dissertation with the aim of achieving a doctoral degree
at the Faculty of Mathematics, Informatics and Natural Sciences**

**Department of Physics
of Hamburg University**

**submitted by
Victoria Kononikhina**

**Hamburg
2023**

Abstract

An investigation dedicated to the β_0/β phase transformation in TiAl alloys by means of neutron and synchrotron diffraction is presented in this thesis. Binary and ternary TiAl alloys with 42 at. % of Al were researched. The alloy compositions were chosen mainly to systematically investigate the fundamental aspects of the β_0/β phase transformation in TiAl alloys. Phase composition, lattice parameters, site occupancy and phase transformation temperatures were determined from the synchrotron data. In addition the presence of the ordered phases, their lattice parameters and phase transformation temperatures were derived from neutron data. Due to the neutron scattering characteristics of Ti and Al only information about the ordered phases can be yielded from neutron diffraction. The results were interpreted to gain insight into the effect of the third element on all investigated parameters. Due to the restriction to ternary compositions, the correlations found could be unambiguously related to the alloying element added. By this, a sound systematic knowledge was obtained about alloying effects usable (1) for the development of new alloy compositions, applicable to turbine blades production, as well as (2) for improvement of properties of alloys being already in use. Namely the sample with 2 at. % of Mo was found to have the highest amount of the β_0/β phase, as well as the highest temperature of the $\beta_0 \rightarrow \beta$ phase transformation. With increase of Mo content both parameters increase. The sample with 2 at. % of Cr possesses a higher β_0/β phase content but a lower $\beta_0 \rightarrow \beta$ phase transformation temperature than 2 at. % of Fe. Increase of Fe and Cr contents give no obvious tendency for in/decrease of the $\beta_0 \rightarrow \beta$ phase transformation temperature but only for an increase of the β_0/β phase content. Ternary samples with 2 at% of Nb and Ta as well as the binary samples contain no β_0/β phase up to 1300 °C, where bad grain statistic made a further investigation of ordering impossible. All samples with higher than 2 at. % of β -stabilizing elements contain the β_0 phase above 1000 °C according to both synchrotron and neutron data. In addition, the samples Ti-42Al-3Fe, Ti-42Al-4Mo, Ti-42Al-6Mo, Ti-42Al-4Cr, Ti-42Al-6Cr contain the β_0 phase even at RT according to the synchrotron data. Two ways to quantify the degree of ordering for the cubic β_0/β phase are considered being the degree of ordering coefficient and the site occupancy refinement. The ways are appropriate only for synchrotron diffraction results and values of degree of ordering depend strongly on the sample composition.

From the refined lattice parameters measured by synchrotron diffraction the linear and the volume thermal expansion coefficient of all phases in the different samples during heating between 1100 and 1200 °C were determined. The values lie in the range around $5 \times 10^{-5} \text{ K}^{-1}$. The difference between lattice parameters determined by synchrotron and neutron diffraction does not exceed 0.005 Å. There is no obvious observation of a lattice parameter change due to β_0/β or even α_2/α order/disorder phase transformation.

Advantages and disadvantages of each diffraction method and the dilatometer sample environment used as heating furnace for the study of disordering phase transformations in TiAl alloys are described and suggestions for possible improvements, e.g. an application of a goniometer for a few degrees rotation of the dilatometer around the vertical axis, are given. Additionally, Scanning Electron Microscopy provided an overview of microstructures, which were classified into the four types: fine grained, nearly α_2 , as well as homogeneous and inhomogeneous duplex microstructures. With increase of the third element content the samples grain size decreases. Differential Scanning Calorimetry was used as an attempt to give an experimental evidence for the detectability of the β_0/β phase transformation in TiAl alloys by the heat flow. In this context, the very fundamental question is discussed whether the disordering β_0/β phase transformation is a second order type transformation.

Kurzfassung

Die Dissertation behandelt die Untersuchung der β_0/β Phasenumwandlung in TiAl Legierungen mit Hilfe von Synchrotron- und Neutronenbeugungsmethoden. Dabei wurden speziell binäre und ternäre Legierungen mit 42 at. % Al-Gehalt untersucht. Die Legierungszusammensetzungen wurden vor allem unter dem Gesichtspunkt ausgewählt, systematisch grundlegende Aspekte der $\beta_0 \rightarrow \beta$ Phasenumwandlung zu untersuchen. Die Phasenanteile, die Gitterparameter, die atomare Besetzung der Gitterplätze und die Phasenumwandlungstemperaturen wurden aus der Analyse der Synchrotronbeugungsdaten bestimmt. Die Anwesenheit der geordneten Phasen sowie deren Gitterparameter und Phasenumwandlungstemperaturen wurden zudem mit Hilfe der Neutronenbeugungsmethode bestimmt. Wegen der speziellen Neutronenbeugungseigenschaften von Ti und Al die Neutronen können nur die Informationen über die geordneten Phasen gewonnen werden. Alle Ergebnisse wurden dahingehend ausgewertet, neue Einblicke bezüglich des Einflusses der ternären Legierungselemente auf alle untersuchten Parameter zu gewinnen. Wegen der Beschränkung auf ternäre Zusammensetzungen konnten die gefundenen Zusammenhänge eindeutig dem zugesetzten Legierungselement zugeordnet werden. Dadurch wurde eine eindeutige systematische Wissensbasis über den Legierungseinfluss gewonnen, die weiter genutzt werden kann (1) für die Entwicklung neuer Legierungszusammensetzungen für die Produktion von Turbinenschaufeln aber auch (2) für die Verbesserung der Eigenschaften von Legierungen die sich schon im Einsatz befinden. Namentlich die Probe mit 2 at. % Mo hat den größten Phasenanteil an β_0/β Phase und die höchste Phasenübergangstemperatur. Mit zunehmendem Mo Anteil steigen beide Parameter. Die Probe mit 2 at. % Cr hat einen größeren β_0/β Phasenanteil aber eine niedrigere Phasenübergangstemperatur, als die Probe mit 2 at. % Fe. Die Erhöhung des Cr und Fe Anteils weist keine eindeutige Tendenz für einen An-/Abstieg der $\beta_0 \rightarrow \beta$ Phasenübergangstemperatur auf, sondern nur für den Anstieg der β_0/β Phasenanteile. Ternäre Legierungen mit 2 at. % Ta oder Nb aber auch die binären Legierungen enthalten keine β_0/β Phase bis 1300 °C und oberhalb macht die schlechte Kornstatistik eine weitere Untersuchung des Ordnungsverhaltens unmöglich. Alle Proben mit mehr als 2 at. % an β -Stabilisatoren enthalten β_0 Phase oberhalb von 1000 °C gemäß der Neutronen und Synchrotron Beugungsergebnisse. Die Synchrotrondaten zeigen, dass die Proben Ti-42Al-3Fe, Ti-42Al-4Mo, Ti-42Al-6Mo, Ti-42Al-4Cr, Ti-42Al-6Cr enthalten außerdem selbst bei Raumtemperatur β_0 Phase. Für die Bestimmung des Ordnungsgrades der kubischen β_0/β Phase wurden zwei Methoden verwendet: die Bestimmung des Koeffizienten des Ordnungsgrads und die Verfeinerung der Gitterplatzbesetzung. Die beiden Methoden sind nur auf Synchrotrondaten anwendbar und die Werte des Ordnungsgrades hängen stark von der Probenzusammensetzung ab.

Aus den verfeinerten Gitterparametern der Synchrotronbeugungsexperimente wurden die Längen- und Volumen-Wärmeausdehnungskoeffizienten für alle Phasen aller Proben zwischen 1100 und 1200 °C bestimmt. Die Werten liegen bei ca. $5 \times 10^{-5} \text{ K}^{-1}$. Der Unterschied zwischen den Gitterparametern, die entweder mit Neutronen- oder mit Synchrotronbeugung bestimmt wurden, ist weniger als 0.005 Å. Es gibt keine eindeutige Beobachtung einer Änderung des Gitterparameters auf Grund der β_0/β oder α_2/α Ordnungs/Unordnungsphasenumwandlung.

Die Vor- und Nachteile jeder Beugungsmethode und des Dilatometers, das als Probeumgebung wie ein Ofen genutzt wurde, für die Untersuchung der Unordnungsphasenumwandlung in TiAl Legierungen werden erläutert und daneben werden mögliche Verbesserungen vorgeschlagen, z.B. die Verwendung eines Goniometers um das Dilatometer ein paar Grad um die vertikale Achse zu drehen. Zusätzlich lieferte Rasterelektronmikroskopie einen Überblick über die Mikrostrukturen der untersuchten Proben, die sich in 4 Typen einteilen lassen: feinkörnig, nahezu reines α_2 , homogenes und inhomogenes Duplexgefüge. Mit zunehmendem Anteil an Legierungselementen verkleinert sich die Korngröße in den Proben. Die Differentialthermoanalyse wurde angewendet um den β_0/β Phasenübergang in TiAl Legierungen durch Wärmefluss experimentell nachweisen zu können. In diesem Zusammenhang wird die fundamentale Frage diskutiert, ob die β_0/β Unordnungsphasenumwandlung eine Umwandlung zweiter Ordnung ist.

Eidesstattliche Versicherung/ Declaration on oath

Hiermit versichere ich an Eides statt, die vorliegende Dissertationsschrift selbst verfasst und keine anderen als die angegebenen Hilfsmittel und Quellen benutzt zu haben. Die eingereichte schriftliche Fassung der auf elektronischen Speichermedium.

Die Dissertation wurde in der vorgelegten oder einer ähnlichen Form nicht schon einmal in einem früheren Promotionsverfahren angenommen oder als ungenügend beurteilt

A handwritten signature in blue ink, appearing to read 'M. K. H. O. L.', is written on a light-colored rectangular background.

Hamburg, den 22.08.2022

List of Publication

[KON2017] Kononikhina Victoria, S. A., Gan Weimin, Schreyer Andreas, and Pyczak Florian (2017). "Ordering and disordering of β/β_0 -phase in γ -TiAl based alloys investigated by neutron diffraction." 2016 MRS Fall Meeting.

Content

Abstract.....	0
Kurzfassung	4
Eidesstattliche Versicherung/ Declaration on oath	5
List of Publication.....	6
Chapter 1 Introduction	12
Chapter 2 Basics	16
2.1 Phase characteristics of the TiAl alloys	16
2.1.1 Description of phase's crystallography and its affecting on diffraction patterns	17
2.1.1.1 The α_2 and the α phases.....	17
2.1.1.2 The γ phase.....	20
2.1.1.3 Dependency of the $\alpha_2 \rightarrow \alpha$ and the γ solvus phase transformation temperature from the heating ramp	21
2.1.1.4 The β/β_0 TiAl	21
2.1.1.5 How β_0 phase occurs and can be detected?.....	22
2.1.1.6 $\beta_0 \rightarrow \beta$ phase transformation in binary TiAl systems	22
2.1.1.7 ω/ω_0 and τ_2 phases.....	23
2.1.1.8 Can both β_0 and β phases coexist in the same sample according to Gibbs' phase rule?.....	23
2.1.1.9 Estimation of degree of ordering.....	23
2.2 Diffraction.....	24
2.2.1 Radiations used for diffraction.....	25
2.2.2 Difference in application of synchrotron and neutron radiation for diffraction investigations of TiAl alloys from literature review	28
2.2.3 Basics of the Rietveld refinement	29
2.2.4 Debye-Waller B-Factor influence on a diffraction pattern	31
2.2.5 Isotropic phase parameters Rietveld refinements basics.....	32
Chapter 3 Experimental Methods	34
3.1 Sample production method	34
3.1.1 Weighting of pure elements	34
3.1.2 Arc melting.....	34
3.1.2.2 Melting method	35
3.1.3 Hot Isostatic Pressing.....	36
3.1.4 Heat treatment	36
3.2 Mechanical sample preparation.....	36

3.2.1 Cylinder sample cut.....	36
3.2.2 Sample preparation for SEM.....	37
3.3 Metallography	37
3.3.1 SEM.....	37
3.3.2 EDX.....	37
3.3.3 DSC.....	38
3.3.4 The RT Synchrotron radiation measurements with rotation of sample	38
3.3.5 Oxygen content determination	39
3.4 In situ heating	39
3.4.1 Heating furnaces.....	39
3.4.1.1 Standard high temperature furnace	39
3.4.1.2 Neutron and Synchrotron dilatometers	40
Neutron dilatometer	41
Synchrotron dilatometer.....	44
3.4.2 In situ diffraction methods	45
3.4.2.1 Neutron instrument and method.....	45
Method of the neutron in situ diffraction experiment	45
3.4.2.2 Synchrotron and method of in situ diffraction experiment	47
Chapter 4 Diffraction data interpretation methods and used programs	49
4.1 Model for the diffractogram refinement	50
4.2 Ordering determination via site occupancy refinement	51
4.2.1 β phase crystallographic restrictions:	51
4.2.2 α_2 phase crystallographic restrictions:.....	51
4.3 Degree of ordering by direct usage of the reflection intensities ratio	52
4.4 Reference peak for temperature correction	52
Chapter 5 Laboratory methods results and discussion.....	53
5.1 Sample compositions	53
5.1.1 Estimation of Al evaporation	54
5.2 Microstructures	54
5.2.1 Classification of observed microstructures	54
5.2.2 Influence of the amount of β -stabilizing elements on microstructure.....	58
5.2.3 Absence of α_2/α phase in the samples of the second sample set.....	59
5.3 Synchrotron RT data of rotated samples	59
5.4 EDX	62
5.5 DSC.....	63

5.6 Oxygen content	64
Chapter 6. In situ diffraction investigation results and discussion	66
6.1 Synchrotron in situ measurements results.....	66
6.1.1. β_0/β phase content and $\beta_0 \rightarrow \beta$ phase transformation temperature	66
6.1.1.1 $\beta_0 \rightarrow \beta$ phase transformation temperature.....	67
6.1.2 γ phase content and γ -solvus temperature	68
6.1.2.1 γ -solvus temperature	69
6.1.3 The α_2/α phase content and temperature of the $\alpha_2 \rightarrow \alpha$ transformation	70
6.1.3.1 The temperature of the $\alpha_2 \rightarrow \alpha$ transformation.....	71
6.1.4 Ti-42Al-2Fe: τ_2 phase presence	72
6.1.5 Determination of the degree of ordering of the β_0/β and α_2/α phases	73
6.1.5.1 Site occupancy Rietveld refinement for β_0/β phase	74
6.1.5.2 Correlation of the peaks intensities 100/200	74
6.1.5.3 Site occupancy of the $\alpha_2 \rightarrow \alpha$ phase	75
6.1.6 Lattice parameter evolution phase	77
6.1.7 Lattice parameters of the α_2/α and γ phases and their increase during heating	78
γ phase lattice parameters increase	80
6.1.8 c/a ratio for the γ phase	82
6.2 Neutron in situ diffraction measurements results.....	83
6.2.1 Standard high temperature furnace	83
6.2.1.1 Phase transformation temperatures of the first sample set.....	83
6.2.1.2 Phase composition analysis for the first sample set	85
6.2.1.3 Lattice parameters change in the first sample set.....	85
Analysis of β_0/β phase lattice parameters change by Gauss method	86
Analysis of 101 interplanar distance α_2 phase	87
Analysis of γ phase a -lattice parameter change	87
6.2.2 Implementation of the Dilatometer at STRESS-SPEC	88
6.2.2.1 The first neutron measurements with dilatometer.....	89
Influence of heating interruption on the phase transformation temperatures	89
Overlap of α_2 phase 101 peak position with the sample holder Al_2O_3 peak.....	89
6.2.2.2 The second neutron dilatometer measurements	90
Influence of collimator problem.....	90
The second sample set phase transformation temperatures	90

Chapter 7 Discussion of the influence of the alloying elements on the TiAl alloys properties	92
7.1 The influence of the third elements on the phase composition and phase transformation temperature	92
7.1.1 The influence of the third elements on the phase composition determined from synchrotron data	92
7.1.1.1 The influence of Cr and Mo on the change of phase contents with temperature.....	92
7.1.1.2 The influence of Fe on the change of phase contents with temperature ...	95
7.1.1.3 The influence of Nb and Ta on the change of the phase contents with temperature.....	96
7.1.1.4 The influence of Al concentration on the phase composition.....	97
7.1.2 Comparison of the phase content from neutrons and synchrotron results ...	98
7.2 The influence of the elements on the properties of each phase.....	98
7.2.1 Comparison of lattice parameter determined by Rietveld refinement of neutrons and synchrotron diffraction data with literature	98
7.2.2 Site Occupancy.....	101
An influence of τ_2 phase presence on the SO refinement of β_o/β and α_2/α phases	101
Position of the third element.	102
Chapter 8 Discussion of the methods.....	103
8.1 Experimental procedure	103
8.1.1 Precision and accuracy of performed measurements	103
8.1.2 Precision and accuracy of interpretation process	104
Some additional assumption for microstructure	105
8.2 Complementarity of the different methods for study of β ordering phase transformation in γ -TiAl alloys	105
8.2.1 Comparison of experimental and evaluation methods.....	105
8.2.1.1 Comparison of phase transformation temperatures between neutron and synchrotron with the same Gauss-fit evaluation method	106
8.2.1.2 Comparison between the Rietveld and Gauss (single peak) as evaluation methods	106
8.3 Degree of ordering determination and other way quantitatively characterize the ordering	107
8.4 Future work.....	108
Conclusions.....	110
Conclusions for improvement of technique of measurements.....	112
Acknowledgements.....	113

Bibliography	114
Appendix 1 Elementary theory of order for alloys with bcc lattice.....	129
Appendix 2a Debay-Waller Factor	134
Appendix 2b Grain statistics	136
Appendix 2c Correspondence of the SO and Phase composition graphs.	141
Appendix 3a Difference between nominated and weighted element composition in grams	148
Appendix 3b Estimation of the sample chemical composition under an assumption of only Al loss during arc-melting based on the mass of the melted button.	149
Appendix 3c Difference of the middle, estimated by many points according to RT with Rotation DESY measurements, and nominal sample composition.....	150
Appendix 3d Difference of the element content in different phases for the second sample set acc. EDX	151
Appendix 4 Spectrums at HT and temperatures of β phase appearance in binary and ternary alloys without ordered β_0 phase at RT	154
Appendix 5 Phase transformation temperature determined by DSC as well as synchrotron and neutron diffraction methods, interpreted by 2 methods: Rietveld refinement and Gauss fit of one reflex.....	156
Appendix 6 Neutron and synchrotron phase content comparison at RT by Rietveld refinement	158
Appendix 7 The comparison of the lattice parameters values between Rietveld refinement of two diffraction methods at RT	159

Chapter 1 Introduction

The TiAl alloys have been gaining importance as a class of intermetallic alloys, owning promising properties, like light weight and high temperature resistance materials, for their application in aero and automobile industries. One of the most impressive application examples is a replacement of Ni-based turbine blades by TiAl ones in the last (low temperature) stage of advanced aero engines for the most developed passenger airplanes e.g. Airbus A320neo.

While Ti-based alloys have been utilized in many applications such as aerospace, biomedical, automotive, nautical, chemical, and other industries due to their high specific strength, good biocompatibility and excellent corrosion resistance [OKUL2015], [LEYE2003], the application of intermetallic TiAl alloys is currently limited to aero and automotive fields. No information about TiAl medical applications was found in literature yet, however, TiAl alloys were shortly mentioned to be used in membranes [WEBP]. “An application of TiAl alloys in the Formula 1 engines was very successful between 2000 and 2004, but then its application was restricted by changes in Formula 1 regulations. Since 2014 updated regulations again allow the use of TiAl alloys in Formula 1 race sport engines, but production volumes are rather limited” [GÜTH2018]. Thus up to today the most widespread application of TiAl is in turbine blades. As of 2013 more than 40,000 low-pressure turbine blades have been manufactured from TiAl alloys for the GENx™ 1B (Boeing 787) and the GENx™ 2B (Boeing 747-8) [BEW2013] Figure 1. There is an overview about aircraft engines equipped with TiAl LPT blades given in Table 1 [GÜTH2018].

There is great political pressure on aircraft manufactures concerning energy efficiency and environmental compatibility, e.g. significantly decreased CO₂ and NO_x emissions, and also a noticeable reduction of noise [CLE2013]. This can be achieved through the use of novel materials as TiAl alloys. However, their application increases the production cost. Therefore novel processing designs are needed to reduce cost and to improve acceptance of such materials in industries. Further modifications of production routes under investigations are expected to get real leverage as for turbocharger producers, as well as aero-companies and even aircraft passengers due to expected lower prices.

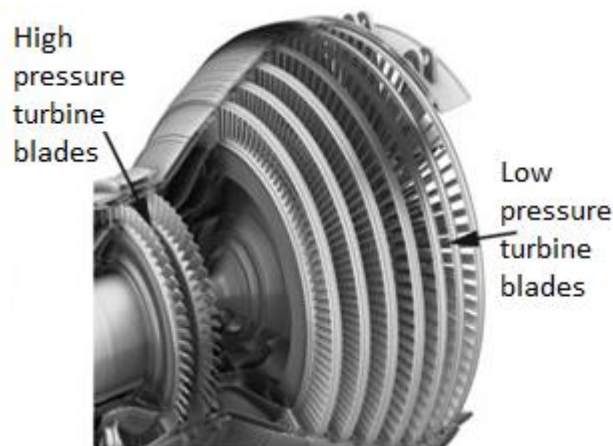


Figure 1 Rendition of the turbine section of the GENx-1B aircraft engine as used on the Boeing 787. The turbine consists of two high-pressure stages and seven low-pressure stages, including two stages of low-pressure TiAl turbine blades. [BEWL2013]

Application of TiAl blades makes the engine lighter not only by decreasing of turbine blades weight. The real weight saving (20-50% [LASA2006]) will be provided in the turbine disk. The

lower blade weight decreases the centrifugal force exerted on the disk, thereby decreasing the associated stresses and consequently the necessary mass of the superalloy disk [LORI2000].

Table 1 Overview about aircraft engines equipped with TiAl LPT blades [GÜTH2018]

Aircraft Engine	Aircrafts Powered	Entering into Service	TiAl Alloy composition (at. %)	Manufacturing technology
GE9x	B 787 B 747 - 8	2011	Ti-48Al-2Nb-2Cr	Investment casting
PW1100GTF/L EAP	A 320neo	2016	Ti-43.5Al-4Nb-1Mo-0.1B (TNM+)	Isothermal forging
LEAP	A 320neo B 737 max C 919	2016	Ti-48Al-2Nb-2Cr	Direct machining of cast semi-finished parts
GE9x	B 777max	2020 (estimated)	Ti-48Al-2Nb-2Cr	Additive Manufacturing

Besides the mentioned advantages of TiAl alloys as half the density of Ni-based alloys, good oxidation and creep properties, there is a need to improve the processing for higher cost effectivity [Lasa2006] and better material behaviour at the working temperatures. TiAl alloys are only partly suited for forging and rolling. The β (BCC) phase is an open structure compared to α_2 and γ and thus diffusion should be faster being detrimental for creep strength of turbine blades at service temperatures [RAJI2020] at 800-900 °C. A presence of the ductile, disordered, body-centered cubic (bcc) β phase, promotes the hot-deformation behaviour [SCHM2013], because dislocation motion as well as dynamic recrystallization is easily facilitated in this phase due to the high amount of slip systems [SCHM2010].

The challenge to be met is to achieve the best materials properties. The so called “ordered beta” (β_o) (simple cubic, or B2 structure) has only three independent slip modes, which are insufficient for the deformation of polycrystalline material [APPEL], therefore has an good influence on creep strength behaviour. However it can make material brittle at room temperature. Thus change of the creep properties under the $\beta_o \rightarrow \beta$ phase transformation represents a vital interest. Therefore the current project is dedicated to the fundamental investigation of $\beta_o \rightarrow \beta$ phase transformation in TiAl as well as to the dependency of the phase transformation on the presence of one β -stabilizing element. At the project’s start the $\beta_o \rightarrow \beta$ phase transformation was not very well researched in a huge amount of possible alloy compositions. Therefore, the need for fundamental investigations occurs. The influence of one (not a few simultaneously) additional element introduces the highest interest because under simultaneous application of a few elements the influence of each of them could counteract or an impossibility to separate their influence could occur. Thus **the first aim of current research is:**

- To determine the $\beta_o \rightarrow \beta$ phase transformation temperature in ternary TiAlX alloys with experimentally found Al content of 42 at. %. The influence of the third β stabilizing element X and its amount on the phase transformation temperatures will be investigated. In our work such commonly used β stabilizing elements as Mo, Nb, Ta, Cr, Fe have been applied.

The β_o phase field could be found in some ternary phase diagrams [KAI2000-B2], [DEM2013, PALM2006, WITU2009-1,2, WITU2008, WATS2009]. The presence of the β_o

phase was also mentioned in articles on the solidification pathway [XU,2017], the temperature of $\beta_0 \rightarrow \beta$ phase transformation 1210 °C for Ti-43.9Al-4Nb-1Mo-0.1B alloy was found in article [WATS2009].

For the binary TiAl alloys the existence of the β_0 phase at temperatures above 1000 °C has been found for the first time as a result of a DSC study by [OHNM2000] in the year 2000. In this article the presence of stable β_0 phase in TiAl in an Al composition range between 30 and 40 at. % was confirmed when an endothermic reaction was identified as $\beta_0 \rightarrow \beta$ phase transformation. However the author of the current thesis is in doubt whether a second order phase transformations β_0/β could be visible by DSC method. For higher Al contents, the β_0 phase presence was extrapolated from TEM investigations for Ti-Al-Cr and Ti-Al-Fe ternary systems [OHNM2000]. A reference to the information from Ohnuma et al. was also found in the article of [GRYT2003]. However, up to now there is no undoubted experimental evidence for presence of β_0 phase in binary TiAl alloys, especially, with Al contents between 40 and 50 at. % [WITU2008]. There is also literature [SCHU2006], that rebut the β_0 phase presence in binary TiAl alloys. Therefore, **the second aim of the current investigation is:**

- To determine by means of in situ neutron and synchrotron diffraction experiments whether the β_0 phase is present in binary TiAl alloys with 39, 42 and 45 at. % of Al.

In order to successfully achieve the announced aims two sample sets were produced consisting of ternary and binary TiAl alloys (see chapter 5). The alloys were investigated with DSC, SEM, EDX and in situ neutron and synchrotron measurements under heating. The results are analysed and discussed from the point of view of the third elements influence. The chemical compositions are specially developed for easier investigation of the third elements influence on the disordering phase transformation. There is no expectations on the application of the compositions for turbine blades production. However the potential for being applied could be discovered by additional mechanical tests, which are not covered by the current PhD topic.

It is possible to separate quickly and undoubtedly β_0 and β , and other phases by using diffraction data [ST-N2011, 2017]. A much more time consuming way would be a transmission electron microscopy investigation, which additionally would not include in situ investigations. The presence of the superstructure β_0 (100) peak is the main parameter to distinguish between β_0 and β phases in diffraction experiments. The superstructure peak could be detected by both neutron or synchrotron X-ray diffraction techniques, however with different contrast. The better ability of neutrons for determination of the $\beta_0 \rightarrow \beta$ phase transformation in TiAl alloys relies on the difference in the neutron scattering length densities between Ti and Al. However, no fundamental reflection from β_0/β or α_2/α phases can be detected by neutrons for a Ti:Al concentration ratio of almost 50:50. By synchrotron both fundamental and superstructure peaks are visible, however the intensity of the superstructure one could be not high enough for an unambiguous determination of the $\beta_0 \rightarrow \beta$ phase transformation. Thus, the application of both synchrotron and neutron methods will give the most effective and comprehensive research.

Synchrotron X-ray diffraction is a powerful method to determine several parameters for different phases simultaneously. The benefit of synchrotron X-ray diffraction compared to neutron diffraction is much higher flux, providing good counting statistics (even with lower penetration depth of synchrotron X-rays (1 cm) compared to neutrons (several cm)), and a higher amount of detected peaks (due to smaller scattering angle of synchrotron radiation as for neutrons) and therefore much better precision in determination of lattice parameters. All of that is very convenient for highly time-resolved in situ measurements.

The neutron diffraction is a very powerful method for in situ investigations of big samples due to high penetration depth however due to lower beam intensity the counting statistics could be worse especially at HT and in coarse grained samples. The SEM data for both sample sets were used for determination of different types of samples' microstructure. The DSC for an estimation the phase transformation temperatures in our samples compositions. The methods and reasons for their application will be discussed later in text.

A rich literature set has been elaborated concerning application of synchrotron X-ray diffraction [ERDL2017, ERDL2016, ERDL2015, ST-N2011, SCHM2011-1,2, SCHM2012, SCHW2014, BOLZ2015] and application of neutron diffraction [ERDL2016, ST-N2011, SCHM2011-1,2] to study TiAl alloys. The method of the neutron in situ experiment of this study is described in [KON2017]. Information about appropriate crystal models could be found in [APP2011] and [STAR2010]. There were some basics taken from the articles, which allowed measurements to be performed.

It is important to mention at the start of current thesis, that under the term "ordered" phase one should understand that the special kinds of atoms occupy special atom positions in the lattice, whereas in "disordered" phases all atoms have the equal probability to take any position. As it is known from the basics of solid state physics both phase modifications, as crystalline materials, have a long range order. During transformation from ordered to disordered phase either the unit cell parameters or the space group will be chosen in slight different way, but the long range order is always present. The meaning of thermodynamic kind of the phase transformation as the first or the second order, should not be mixed with an attempt to determine the degree of ordering for the β_0 phase.

The current work consist of the introduction, 8 chapters, conclusion, list of literature, and 7 appendixes:

Chapter 2 describes the basic knowledge needed for easier understanding of performed investigations: about TiAl alloy phases, thermodynamics, ordering, and diffraction.

Chapter 3 explains all applied experimental methods, reasons for their application and sample environments.

Chapter 4 exhibits the interpretation methods, applied models and programs.

Chapter 5 includes a comparison of the results of different laboratory methods.

Chapter 6 is divided into two parts. The first one exhibits results of interpretation of the in situ synchrotron diffraction experiments. The second part contains the neutron diffraction data interpretation results, compared partly with literature data.

Chapter 7 discusses influence of the third element on samples phase composition, phase transformation temperatures along with phase properties by comparison of neutron and synchrotron results.

Chapter 8 discusses the methods of experiments as well as measurement accuracy and complementarity of methods for investigation of the β_0/β phase transformations.

Conclusion summarizes the influence of the used β stabilizing elements, gives answers to the main questions of the current project according to the β phase phenomena and mentions some useful peculiarities which should be improved in the future for more precise measurements and data analysis.

Chapter 2 Basics

The main results of this PhD work are based on diffraction of neutrons and synchrotron radiation. Thus, an introduction concerning the diffraction methods and the data interpretation will be described here. As long as a full explanation of the diffraction theory is a book on its own only those parts of the diffraction theory will be shown here, that are important for data analysis of the performed experiments. For an interested reader some books will be recommended further.

At first, however, some basic crystallographic knowledge about the phases in TiAl alloys will be described in order to use them later for an explanation of the peculiarities of the diffraction investigations of TiAl alloys.

2.1 Phase characteristics of the TiAl alloys

In intermetallic γ based TiAl alloys five main phases are known to be stable at different temperatures and Al contents below 50 at. %: an α and an α_2 , a β and a β_o , and a γ (see phase diagram in Figure 2) phases. Two of these phases (the α and the β) are disordered and three ordered (the α_2 , the β_o , and the γ) with the α_2 and the β_o being the ordered counterparts of the α and the β . Since all the above phases could be present in our TiAl systems, their basic crystallographic data are presented in this chapter. Looking at phase diagram in Figure 2 at temperatures below 1000 °C the region of Al content from 25 to 60 at. % could be divided into three parts. There is a pure α_2 phase region with Al concentration up to 35 at. %, a binary $\alpha_2+\gamma$ phase region between 35 and 50 at. % Al and a pure γ TiAl phase region at Al concentrations above 50 at. %. Above 60 at. % Al also other phases exist in the phase diagram, which were not observed in our samples and therefore are not discussed in more details. In our Al content region and solidification via the β or the α phase can occur. In ternary TiAl alloys the β phase often transformed to its ordered form the β_o . However the presence of the β_o in binary alloys is currently a matter of a debate. Ohnuma et al. [OHNM2000] presented results they took for experimental evidence for β_o in binary alloys.

When comparing with binary TiAl alloys or pure Ti-alloys the β -stabilising properties of elements could be expressed in so called Mo-equivalent [WILLY2017], [WEISS1998], which, however, is introduced for the ternary and more component system compared with β -stabilising properties of Mo. The influence of pure elements could be expressed in amount of wt.% which is needed to retain 100% beta upon quenching: Mo – 10, Nb - 36, Ta - 45, Fe - 3.5, Cr - 6.5 wt.% [WEISS1998]. The lower is the number, the better are β - stabilising properties. According to this properties composition of our alloys was chosen which will be described in details in chapter 5.

In ternary and more complicated alloys the β_o/β phase transformation temperature differs depending on the kind and amount of additional β -stabilizing elements. As mentioned in the introduction, the current work is particularly dedicated to the determination of the influence of the third elements in ternary alloys on the $\beta_o \rightarrow \beta$ phase transformation in TiAl alloys, which could be similar to their β -stabilizing properties. The influence of such additions will be discussed in the chapters 6 and 7 (results section) of the current work.

In ternary alloys, especially with Nb, Ta and Fe, some additional phases, namely a ω_o/ω [TRET2005-1,2] and a τ_2 [PALM1995] could occur at temperatures below 1000 °C and therefore their crystallographic data are also described in this part. The ω_o/ω should not be mistaken with the orthorhombic O phase, therefore its crystallographic information is also included into Table 2. However no O phase was found in our samples.

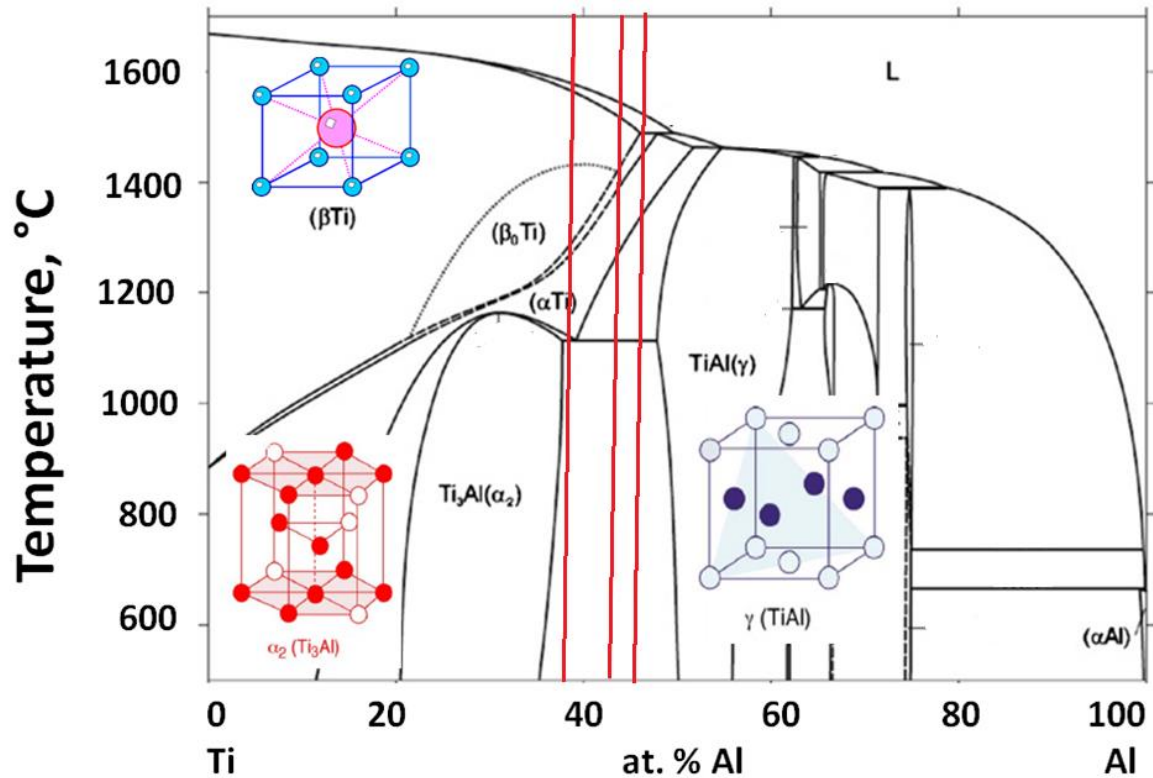


Figure 2 Binary TiAl phase diagram: modified after [WITU2008-3]. The red lines indicate the binary sample compositions of Ti-39, 42, 45 at. % Al, which are investigated in the present work.

2.1.1 Description of phase's crystallography and its affecting on diffraction patterns

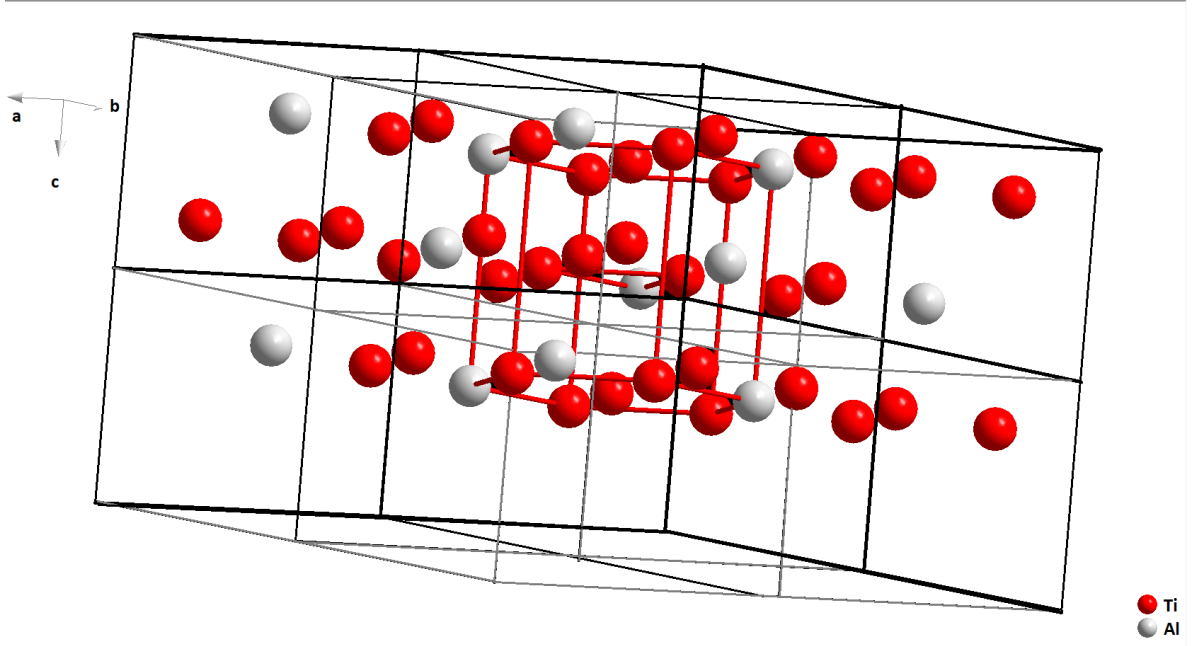
The lattice parameters of the above mentioned phases at room temperature are given in Table 2.

2.1.1.1 The α_2 and the α phases

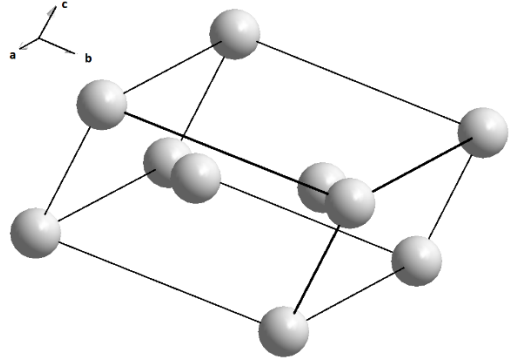
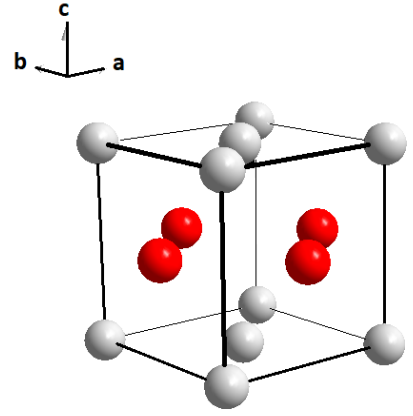
Both phases crystallize in $P6_3/mmc$ hexagonal structures. The main difference between the α_2 and α phases is the atomic order: the α_2 is the ordered phase, the α is the disordered one. Figure 3a shows a section of eight unit cells of the α_2 phase. The atom layers form the stacking sequence ABAB in c-direction and are shifted by $(1/3, 2/3, 1/2)$. In the ordered α_2 phase a layer consists of two alternating atom rows, one pure Ti row and one consisting in turn of Ti and Al. In the disordered α phase the Ti and Al atoms are randomly distributed. The ordering change yields to different unit cell dimensions and therefore different atom positions. In the α_2 phase (for ideal ordered Ti_3Al) Ti atoms sit on 6h positions and Al on 2d positions, however in the α phase only 2d positions are occupied resulting in its 4 times smaller unit cell. Thus, the base-plane lattice parameter a of α_2 phase is twice as large than that for the α phase (the lattice parameters of the above mentioned phases at room temperature are given in Table 2).

Table 2 Crystallographic parameters of the TiAl phases. Lattice constants for the β_0/β , the ω_0/ω phases, the O-phase the γ and for the α/α_2 phases from [STAR2010], for τ_2 from [GRYT2003]. More detailed space groups, Pearson symbols and Structure reports are given from [ITC2005].

Phase	Stoichiometric composition	Pearson symbol	Space group	Structure reports	Lattice parameters, Å
α	Ti	hP2 = hexagonal primitive with 2 atoms in the unit cell	$P6_3/mmc$	A3	a = 2.9505 c = 4.6826
α_2	Ti ₃ Al	hP8 = hexagonal primitive with 8 atoms in the unit cell	$P6_3/mmc$	D0 ₁₉	a = 5.750 c = 4.638
γ	TiAl	tP4 – established as fcc related lattice with 4 atoms in the unit cell	$P4/mmm$	L1 ₀	a = 4.012 c = 4.065
β	Ti	cI2 – cubic body centred (I from “innenzentriert” (German)) with 2 atoms in the unit cell	$Im\bar{3}m$	A2	a = 3.32
β_0	TiAl	cP2 – cubic primitive with 2 atoms in the unit cell	$Pm\bar{3}m$	B2	a = 3.210
ω	Ti	hP3	$P6/mmm$	C32	a = 4.625 c = 2.813
ω_0 (τ)	Ti ₄ Al ₃ Nb	hP6	$P6_3/mmc$	B8 ₂	a = 4.580 c = 5.520
τ_2	Al ₂ FeTi	cF120	$Fm\bar{3}m$		a = 12.0915
O-phase	Ti ₂ AlNb	oC16	$Cmcm$	A ₂ BC	a = 6.10 b = 9.57 c = 4.62

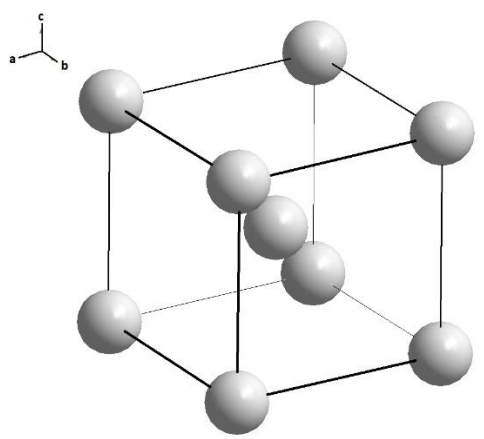
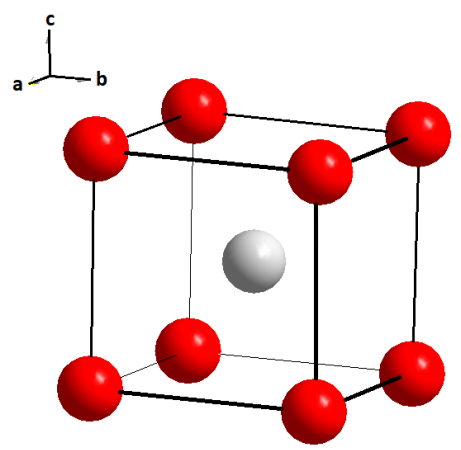


a.



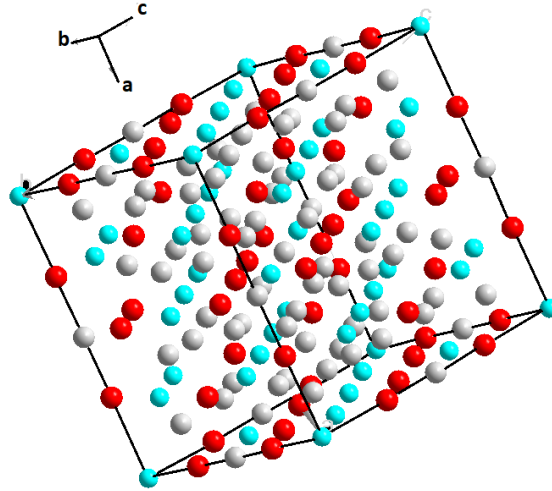
c.

b.



e.

d.



f

Figure 3 Crystal structures (a) of the α_2 phases. The atomic layers are shifted to $(1/3, 2/3, 1/2)$; (b) γ ; (c) ω ; (d) β_o ; (e) β ; (f) τ_2 phases.

The $\alpha_2 \rightarrow \alpha$ phase transition takes place at 1120 °C in binary TiAl alloys with 35 – 45 at. % Al. This temperature will be used as reference in further data analysis. As evident from Table 2 the $\alpha_2 \rightarrow \alpha$ phase transformation does not include a change in the space group, but causes a decrease in the a lattice parameter. In the model used for Rietveld refinement in the current project, similar structures with equal a and c lattice parameters are used for α_2 and α phases. Thus, no change in a lattice parameter should be observed during $\alpha_2 \rightarrow \alpha$ phase transformation in our model. The phase transition manifests itself in a disappearance of some peaks from the diffraction pattern. The disappearing peaks are known as superstructure peaks. The $\alpha_2 \rightarrow \alpha$ phase transformation manifests by the superstructure reflection disappears and thus the atom site occupancy (SO) change. The SO is considered as the main factor to distinguish between the α_2 and α phases and will be introduced in more details in chapter 4. The fundamental peaks will still be present in the α phase. For the fundamental peaks of the α_2 phase only (hkl) index labels with even h and k values are allowed by its crystallography. Their (hkl) labels will be changed if a different unit cell with two times smaller a lattice parameter will be used. In particular, then one has to renumber the peak labels, e.g. $200 \rightarrow 100$, $201 \rightarrow 101$, $202 \rightarrow 102$, $220 \rightarrow 110$ and so on. For the superstructure peak at least one of these indices (h or k) should be odd, this peak will disappear during $\alpha_2 \rightarrow \alpha$ transformation, e.g. 110 , 100 and so on.

2.1.1.2 The γ phase

The γ phase (Figure 3b) is predominantly present in the vast majority of the currently investigated alloys as well as generally in γ -TiAl alloys. It crystallizes in the tetragonal $P4/mmm$ space group [APPL2011]. Generally at slow cooling rates, the γ phase grows in form of lamellas. Nucleation of the γ lamellas starts on phase boundaries between the α/α_2 phase grains and they grow according to the Blackburn relationship:

$$(0001)\alpha_2 \parallel \{111\}_\gamma \quad (1)$$

and

$$\langle 11\bar{2}0 \rangle \alpha_2 \parallel \langle 110 \rangle_\gamma. \quad (2)$$

With medium cooling rates a massive γ_m phase can crystallize (depending on the alloy composition) and with fast cooling no γ phase would be formed [CHR2018]. However as will be shown in chapter 3 “Methods” our heat treatments only include slow cooling therefore the lamellas of the γ phase are expected to nucleate corresponding to the Blackburn relationship in the current work.

2.1.1.3 Dependency of the $\alpha_2 \rightarrow \alpha$ and the γ solvus phase transformation temperature from the heating ramp

Properties of the α/α_2 and γ phases are currently well investigated [LISS2006], [YEOH2007]. In this research project, we use the α/α_2 and the γ solvus phase transformation temperature of binary TiAl alloys as reference points in temperature determination.

The γ – solvus temperature is sometimes referred to as $\gamma \rightarrow \alpha$ temperature in the literature. Its dependency from the heating ramp plays a decisive role in the investigation as long as the γ – solvus temperature is used as a reference in Ti-42Al and Ti-45Al. Chladil et. al shows difference up to 10 °C between heating rates of 10 and 40 K/min. The heating ramps used in the present work are mentioned in chapter 3 but no systematic investigations of the influence of the heating ramp was done for our samples.

Some temperature differences between DSC and diffraction results as well as differences due to the interrupted heating during the first neutron dilatometer measurements raised the question whether $\beta_o \rightarrow \beta$, $\alpha_2 \rightarrow \alpha$, γ -solvus phase transformation temperatures depend from the heating rate. In order to acquire better evidence some literature analysis was performed and some thermodynamic basis was used. In the work of Erdely et al. [ERDL2017] the TNM alloy shows several different γ phase contents with slightly different microstructures due to different heat treatments. However, there the cooling rate has much more influence than the heating rate. In work of Xia [XIA2001] due to very high cooling rates even diffusionless phase transformations occurred. An evidence that the phase transformation temperatures are only slightly dependent or even independent from heating rate is the fact that no tendency is found, that the phase transformation temperature determined by neutrons diffraction is always lower than that determined by synchrotron diffraction. Such tendency would indeed be explained by the influence of the different heating rates.

2.1.1.4 The β/β_o TiAl

The β phase (Figure 3e) is a high temperature phase. In TiAl alloys it can be stabilized by alloying elements such as Nb, Mo, Ta, or V. The β phase crystallizes in cubic body centered (A2) structure [APPL2011]. In the A2 structure Ti and Al atoms are randomly distributed between 1a and 1b Wyckoff atomic positions and their site occupation is determined by the chemical composition. In ternary alloys with Al content above 35 at. % the β phase structure can transform to an ordered structure (known as β_o), which is characterized by intercalation of two simple cubic cells type CsCl [STRC] forming a single B2 structure [STAR2011], which is stable at a little bit lower temperature, than the β and can be stabilized up to RT. Depending on the amount of the additional β -stabilizing elements the $\beta_o \rightarrow \beta$ phase transition, also mentioned in articles as ($B2 \rightarrow A2$) transition, takes place in the temperature range of 1150-1250 °C [MAYE2017].

Ordering of the bcc solid solution to the ordered CsCl type phase (β_o) (Figure 3d) was discovered in 1958 by [BOEH1958] and confirmed in the many works mentioned in the article of [TRET2005-1] e.g. [HAMA1972, DJA1991, DJA1992-1,2, DAS1993, LI1993, LI1994, MORR1994, NAKA1995, CHEN1998, SING1997]. Currently ordering phenomena of the type

B2/A2 are known not only for TiAl but also for other alloys e.g. the B2 structure occurs in CuZn, AuCd, AuZn, CoGa, PdIn, FeCo, NiAl(Ga), FeAl(Zn,In), AgMg, NiGa, NiMn binary crystals (as mentioned at page 347 of [MEHR2007]).

Presence of β phase in TiAl alloys significantly improves their hot workability [STAR2011] thus the order-disorder transformation became cogent importance for prediction of the materials properties. Due to the high number of independent slip systems in a bcc lattice, the disordered β -phase shows an improved deformability at elevated temperature, where processes such as hot rolling and forging are carried out. Ordering reduces the number of slip systems and antiphase boundaries can be formed which reduces the ductility.

2.1.1.5 How β_0 phase occurs and can be detected?

While cooling from the liquid state an appropriate TiAl based alloy composition, first fully disordered β phase is formed. Then with decreasing temperature the ordered state becomes energetically more favourable and the ordering (change of atom position) processes could start simultaneously at several points in one crystal of the disordered phase. Often when ordering is established in the complete crystal, the symmetry of the atomic arrangement in different regions does not ideally correspond to each other. Such regions of the same symmetry of atomic arrangement are called antiphase regions. Between those regions antiphase boundaries (APB) were formed [PORT1992]. The presence of APB in the microstructure can be observed by TEM and confirms the solid-solid ordering of the B2 phase from the disordered bcc phase. Antiphase regions are also a parameter which affects the crystallite size, one of the parameters which could be refined by the Rietveld data analysis method (more details in the chapter 4).

By diffraction as in the case of the $\alpha_2 \rightarrow \alpha$ phase transition, the $\beta_0 \rightarrow \beta$ phase transition manifests itself in the disappearance of superstructure peaks from the diffraction pattern. The selection rule for the superstructure peaks in the β_0 phase is the sum of $h+k+l$ to be odd. For example, 100, 111, etc. are the β_0 superstructure peaks that should disappear as soon as the B2 to A2 phase transition takes place.

2.1.1.6 $\beta_0 \rightarrow \beta$ phase transformation in binary TiAl systems

The existence of the $\beta_0 \rightarrow \beta$ phase transition in binary Ti-Al was supported by Differential Scanning Calorimetry (DSC) measurements of the Ti-32.6 at. % Al alloy [OHNM2000]. By extrapolating the ordering temperature for Ti-Al-X (X=Fe, Cr) ternary alloys determined with DCS measurements to binary Ti-Al alloy Ohnuma et al [OHNM2000] have assumed that there is a second order transition $\beta \rightarrow \beta_0$ with temperature. The kind of the phase transformation plays a decisive role for the question whether $\beta \rightarrow \beta_0$ can be detected by different methods, especially by DSC (heat extraction). Therefore, up to now there is no direct experimental evidence for the β_0 phase existence in the binary TiAl system. In particular, Schuster and Palm [SCHU2006] argued that “ β_0 phase in binary TiAl alloys is rather unlikely but that it could not be definitely ruled out”. One of the primary goals of the current investigation is to give experimental evidence for existence or non-existence of the β_0 phase in binary TiAl alloys using the most powerful technique available – in situ neutron diffraction. The nature of the $\beta \rightarrow \beta_0$ is discussed in APPENDIX 1. According to [KAIN1994] the $\beta_0 \rightarrow \beta$ phase transformation “in the binary system is hidden by the more stable γ -phase. However, it may be observed at compositions far away from Ti0.5 / Al0.5 at higher Ti contents, where the β -phase becomes stable” – that is, not our case of composition.

2.1.1.7 ω/ω_0 and τ_2 phases

In ternary Ti-Al-X alloys (X=Fe, Nb, Ta) additional phases were found to appear. These are the ω/ω_0 – phase for the Ti-Al-Nb system [CHEN1998] and the τ_2 phase for the Ti-Al-Fe [PALM2006, RAYN1988, PALM1995, PALM1997]. Known crystallographic information about these phases is given in Table 2. Information about these additional phases will be used for interpretation of the diffraction spectra of corresponding samples. The τ_2 phase has the stoichiometric chemical composition Al_2FeTi [PALM2006] and the ω_0 a composition of Ti_4Al_3Nb [STAR2008, BYST2010, STAR2011]. The ω_0 is just an ordered modification of the also hexagonal ω phase. At temperatures below 1000 °C the β_0 -phase can decompose for example into ω , ω' and ω'' , which possess lower than bcc crystal symmetry and are extremely brittle [CLEM2008]. One should not mix up the ordered hexagonal ω_0 - Ti_4Al_3Nb with O-phase - Ti_2AlNb . Due to their low crystal symmetry ordered phases, such as β_0 and ω_0 , are often assumed to be detrimental to ductility. However the orthorhombic O phase is known to be relatively ductile and at 800 °C even ω_0 containing TiAl alloys show good plastic formability [STAR2011].

In a study of TNM alloys [SCHL2014] it has been shown that the β_0 phase coexists with the ordered hexagonal ω_0 - Ti_4Al_3Nb phase exhibiting a $B8_2$ crystal structure [CHA2011, CLEM2011]. The ω_0 and τ_2 phases appear during heating in a temperature range between 700 and 800 °C they will transform back to the β/β_0 phase at higher temperatures. Therefore their presence should not disturb us in the data analysis, but will give to the data some peculiarity.

2.1.1.8 Can both β_0 and β phases coexist in the same sample according to Gibbs' phase rule?

In the case when only temperature and concentration can be varied, according to the Gibbs' phase rule the total number of simultaneously coexisting phases in the sample cannot be more than the number of alloying elements. This means there should be only two coexisting phases in binary alloys and three phases in ternary alloys. Thus, coexistence of β_0 and β phases in binary alloys implies absence of other phases. In ternary alloys coexistence of β_0 and β phase would be possible when in maximum one additional phase is present. In our ternary systems where the α_2/α and the γ phases already exist only one of both either the β_0 or the β phase should be present.

The above mentioned thermodynamic theory and the Gibbs phase rule influenced the methodology of the data analysis in that way, that the presence of the β_0 and β or the α_2 and α phases never was refined together.

2.1.1.9 Estimation of degree of ordering

Estimation of degree of ordering is realized via the so called “degree of long-range order” or shortly “degree of order”. In the ordered state a and b sites are occupied by either element A or element B. Let X_A be the mole fraction of A kind of atoms in the alloy and r_A be the probability for a sublattice sites to be occupied by the ‘correct’ A type of atomic species. Let X_B be the mole fraction of B kind of atoms in the alloy and r_B be the probability for b sublattice sites to be occupied by the ‘correct’ B type of atomic species. [PORT1992]. To estimate quantitatively the degree of long-range order it was suggested to use the parameter [PORT1992]

$$D = \frac{r_A - X_A}{1 - X_A} = \frac{r_B - X_B}{1 - X_B}. \quad (4)$$

When a completely ordered single crystal is heated above the disordering temperature the degree of long-range order D changes from 1 for the fully ordered structure to 0 for the completely random distribution [PORT1992]. In the ideal case of the β_0 (TiAl) phase contains 50 at. % Al ($X_A = 0.5$) and the degree of the long-range order is:

$$D = \frac{1 - 0.5}{1 - 0.5} = 1. \quad (5)$$

However the above mentioned formula (4) only works well for binary alloys with ideal stoichiometric composition. A deviation from the stoichiometric composition in binary alloys decreases the maximum possible degree of long-range order. More in detail: in the case of non-ideal stoichiometric composition, the probabilities for a sites to be occupied by the ‘correct’ A atoms and that for b sites to be occupied by the ‘correct’ B atoms are different. E.g., let us consider fully ordered β_0 phase containing 42 at. % Al and 58 at. % Ti. Then all the a sites will be occupied by the ‘correct’ Ti atoms, whereas b sites be occupied by 84 % ‘correct’ Al atoms and 16% ‘wrong’ Ti ones. This results in the probabilities $r_a^{Ti} = 1$ and $r_b^{Al} = 0.84$. The degrees of the long-range order for Ti and Al sublattices will be different

$$D_b^{Ti} = \frac{1 - 0.58}{1 - 0.58} = 1 \quad (6a)$$

$$D_b^{Al} = \frac{0.84 - 0.42}{1 - 0.42} = \frac{0.42}{0.58} = 0.724 \quad (6b)$$

The degree of long-range order should account for the presence of defects, i.e. atoms residing on a wrong site: when Al atoms from the b site will go to a site, the degree of ordering will decrease. In the case when Al and/or Ti atoms will go partly in interstitial positions, the degree of ordering will be changed in a more complicated way, which, probably, could not be fully estimated. Our alloys are of non-ideal stoichiometry, therefore we’ve used the formalism being aware that we introduce a small error, which is discussed in chapter 8.

The presence of additional atoms different from Ti and Al in a low content at Al and/or Ti sites causes decrease in the degree of ordering. In the case of the elemental concentrations in equal proportion of 1/3:1/3:1/3 in ternary bcc alloys a more complicated formula for degree of ordering may be needed.

Values of D , calculated for each position will decrease with increasing temperature and decrease of probability of atom to take the position. For characterisation of the degree of ordering the coefficient D could be used. However it is equivalent to the interned Site Occupancy (or the SO, that represents probability for an atom to take a position in atom). Further it will be detailed explained in subchapter 4.2. The direct application of SO values is found easier applicable in practice. As long as for each phase there are not one value of D corresponded to maximum reachable degree of ordering, the Site Occupancy is more preferred as the ordering parameter.

2.2 Diffraction

Diffraction is defined as a bending of waves around corners of an obstacle or aperture into the region of geometrical shadow of the obstacle. In material science crystal lattices play the role of obstacles to form diffraction. [IBAC2009]. In classical physics, the diffraction phenomenon is described as the interference of waves according to the Huygens–Fresnel principle (It states that every point on a wave front is itself the source of spherical wavelets. The sum of these spherical wavelets forms the wave front (Figure 4)). This characteristic behaviour is exhibited when a wave encounters an obstacle or a slit that is comparable in size

to wave wavelength. Particularly in our experiments TiAl crystal lattices act as obstacles to form diffraction.

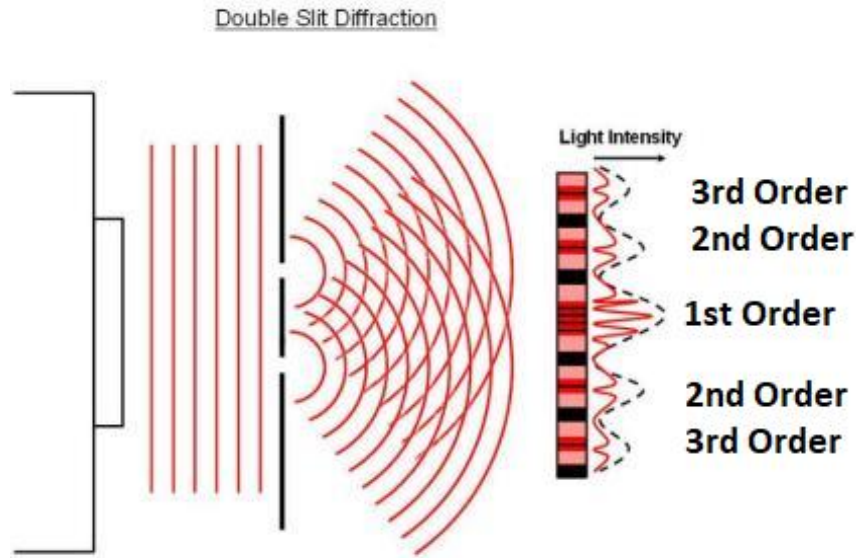


Figure 4 Wave diffraction in the manner of Huygens and Fresnel [IBAC2009], p. 67. With the 1st, 2nd, 3rd order of diffraction maximums the intensity decreases strongly.

2.2.1 Radiations used for diffraction

Different kinds of radiation (electromagnetic waves, neutrons, electrons, α -particles) are applicable for diffraction. In theory the wavelength of electromagnetic waves λ_{ph} and particles with mass (neutrons λ_n or electrons) are described by:

$$\lambda_{ph} = \frac{hc}{E} = \frac{12.398}{E[keV]}, \quad (7)$$

$$\lambda_n = \frac{h}{p} \approx \frac{h}{\sqrt{2mE}}. \quad (8)$$

In Figure 5 typical wavelengths are shown for different kinds of radiation used in materials science. For not bio objects, the wave length should cover the interatomic distance from 1 to 10 Å.

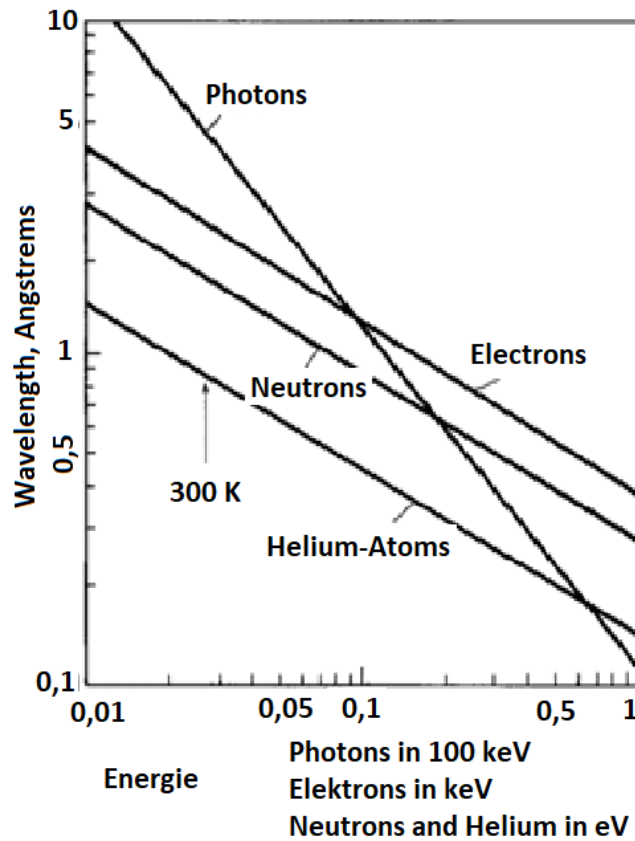


Figure 5 Comparison of wavelengths of different kinds of radiation applied for diffraction investigations in material science, translated after [IBAC2009].

The diffraction of waves with wavelength λ from crystal planes is described by Bragg's law [CHAT2010]:

$$2d \sin\theta = n\lambda, \quad (9)$$

where d is the interplanar distance, θ is the scattering angle, and $n = 1, 2, \dots$ is the order of diffraction. In Figure 6 the interference process is schematically shown leading to appearance of diffraction patterns according to equation (9).

With increasing order of diffraction n the intensity of the diffraction maximum vastly decreases (Figure 4). The lower intensity of the higher n is determined by the wave's attenuation. The diffraction maximum of first order is predominantly used in material science diffraction investigations. The second and higher order diffraction maximums have usually so small intensity, that they can be neglected.

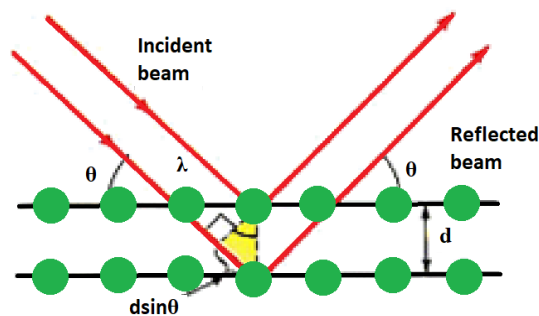


Figure 6 Scheme for fulfilled Bragg's diffraction condition [CHEM].

Main properties of neutron and synchrotron radiation are described in the book of P. Staron et al. [ST-N2017]. The book covers physical properties of photons and neutrons in chapter 4 and radiation sources in chapter 5. More detailed information concerning neutron diffraction and especially the neutron scattering lengths were covered in the Neutron Data booklet published by the Neutron Center of the Institute Laue-Langevin (ILL). A special book dedicated to synchrotron radiation: [ANIE2011] describes in a very detailed way interaction of the hard X-ray with matter and the generations of synchrotron sources.

The same mathematics describe the scattering of X-rays and neutrons, but the scattering length densities are different for neutrons and X-rays. The scattering length densities for X-rays are proportional to Z of the scattering atoms, whereas those for neutrons are unique for different isotopes. They represent the probability that neutrons are elastically/inelastically scattered. Their values must be determined experimentally and could be found in tables, e.g. [DIAN2003].

Neutrons are useful for investigations of magnetic materials as well because they have a spin of $\frac{1}{2}$. However that property was not used for our actual research. The presence of about 1, 2, and 3 at. % of Fe in some of our samples does not cause the alloys to be ferromagnetic. Since our TiAl alloys are non-magnetic, we do not account for magnetic neutron scattering.

Thermal neutrons are characterized by wavelengths of 0.06 to 4 Å. Our used wavelength is 2.1 Å as it will be shown in the next chapter. Due to the different wavelengths between neutron and synchrotron radiation used for the experiments different 2θ angles correspond to the same peaks. Thus, it is more convenient for some scientists to work in the reciprocal-space Q . The transformation of $2\theta \rightarrow Q$ is done by $Q = 4\pi \sin(\theta)/\lambda$. Results are listed in the Table 3. In our analysis the 2θ angles were used.

Neutrons for diffraction experiments are produced by reactors, separated in beams with different velocity/energy of neutrons. The penetrating power of neutrons is very high due to the lack of charge and, as a consequence, weak interaction with matter. Neutrons have much larger penetration depth into material (up to 30-50 mm) than synchrotron radiation (up to 15 mm, depending on energy). The penetrating power of neutrons depends on their energy and the atomic composition of the substance with which they interact. Some elements as e.g. hydrogen are used as moderator. The behaviour of heavier elements in metals or their alloys depends from the scattering length of the elements contained in the alloys. In the current investigation scattering properties of elements play the main role beside such properties as moderation or absorption. The neutron properties of elements are described in [DIAN2003].

Synchrotron radiation represents a wide spectrum of X-ray photons with energies in range of 150 eV to 200 keV and wave lengths of 0.06 – 80 Å (more details about the used wavelength of 0.124 Å in our beamline is described in chapter 3). The synchrotron radiation is emitted by electrons (positrons) accelerated under the influence of a constant field in a bending magnet, wiggler or undulator [ANIE2011]. Due to high energy of emitted photons the synchrotron radiation used in this study is also called hard X-ray radiation. Photons have no electric charge and, therefore, are not sensitive to magnetic properties of matter. Photons of synchrotron radiation have zero mass, therefore they are either absorbed or scattered by electron clouds. They as well have much higher than the day light photons energy, thus number of scattering events necessary to slow the synchrotron radiation is much higher than for the laboratory X-ray. The probability for synchrotron radiation to be scattered is proportional to electron density in material, that means to the Z number of atoms in the alloys. This means that they allow the penetration depth of few cm.

Table 3 Recalculation of 2θ angles from neutron and synchrotron measurements to Q-values.

Neutrons (2.1 Å)		Synchrotron (0.124 Å)	
$Q = 4\pi \sin(\theta)/\lambda, \text{Å}^{-1}$	$2\theta, ^\circ$	$Q = 4\pi \sin(\theta)/\lambda, \text{Å}^{-1}$	$2\theta, ^\circ$
1.700	33		
1.749	34		
1.799	35	0.884	1
1.849	36	1.769	2
1.899	37	2.653	3
1.948	38	3.537	4
1.997	39	4.421	5
2.047	40	5.304	6
2.096	41	6.187	7
2.144	42	7.069	8
2.193	43		
2.242	44		
2.290	45		

2.2.2 Difference in application of synchrotron and neutron radiation for diffraction investigations of TiAl alloys from literature review

Both types of radiation are suited for investigation of metals, especially TiAl alloys, which have lattice parameters in the range between 2 to 5 Å. The peculiarities in the investigation of titanium aluminide alloys using X-rays and neutrons are well described in [CLEM2013] and [CHAU1999]. Neutron measurements of β_0/β phase transitions in TiAl alloys have a strong advantage over synchrotron radiation measurements due to the high contrast between neutron scattering on β_0 and β phases. For our alloy compositions, with almost equal contents of Ti and Al and a low third element content, we have strong fundamental and superstructure peaks via synchrotron but only superstructure peaks via neutrons.

The scattering lengths of used elements are given in Table 4. The neutron scattering length density of Ti is 3,370 fm and that of Al is - 3,449 fm, [DIAN2003]. Thus the contribution of Ti and Al to the fundamental reflection of both β_0 and β phases nearly abolishes each other with a composition of Ti and Al of almost 50:50. Superstructure peaks for β_0 phase, which are determined by the difference in the Ti and Al neutron scattering length densities, are significantly better visible than with synchrotron X-ray diffraction. For different chemical compositions than that used in this study, the fundamental peaks could be detected via neutrons as found in [CHAU1999], as well as the superstructure peak intensity via synchrotron could be higher.

Table 4 Neutron Scattering lengths of used chemical elements taken from [DIAN2003].

Nb	Ta	Mo	Cr	Fe	Ti	Al
0.7054	0.691	0.6715	0.3657	0.7452	- 0.3438	0.3449

While neutron diffraction offers distinct advantages for the investigation of order/disorder transitions, synchrotron X-ray diffraction is more useful to study phase transformations and phase fraction evolutions, in which the majority of information is encoded in the fundamental peaks. Therefore neutron and X-ray diffraction are in fact complementary techniques when applied to study intermetallic TiAl alloys [CLEM2013]. Discussion of other advantages and disadvantages of synchrotron and neutron radiation according to our experience will be given in subchapter 8.2.

2.2.3 Basics of the Rietveld refinement

The analysis of all diffraction data was performed (1) using the MAUD program based on the Rietveld Refinement method and (2) by a simple Gauss fit of single peaks. For a detailed description of the interpretation method the reader is referred to chapter 4. Here the basic theoretical information is given, which is necessary to understand the factors controlling the measurement quality and the data analysis.

The code of the Rietveld refinement program minimizes the following mean least square function [CHAT2010]:

$$R_{wp} = \sum_i W_{io} (I_i^{meas} - I_i^{calc})^2, \quad (10)$$

where W_{io} is the statistical weight associated with the observed intensity $W_{io} = \frac{1}{I_i^{meas}}$.

The calculated intensity I_i^{calc} is described by the next equation [CHAT2010]:

$$I_i^{calc} = S_F \sum_{j=1}^{N \text{ phases}} \frac{f_j}{V_j^2} \sum_{k=1}^{N \text{ peaks}} L_k |F_{k,j}|^2 S_j(2\theta_i - 2\theta_{j,k}) P_{k,j} A_j + bkg_i \quad (11)$$

where S_F is beam intensity; f_j – phase volume fraction; V_j – phase unit cell volume; L_k - Lorenz polarization factor, $F_{k,j}$ - the structure factor, $S_j(2\theta_i - 2\theta_{j,k})$ – profile shape function, $P_{k,j}$ – texture factor, A_j – the absorption factor, bkg_i – background.

Lorenz polarization factor L_k depends on instrumental factors and can be written as [LUTT2015]:

$$L_k = \frac{1}{\sin 2\theta \cdot \sin \theta} \cdot \frac{1 + \cos^2 2\theta \cdot \cos^2 2\theta_\mu}{1 + \cos^2 2\theta_\mu} \quad (12)$$

where θ_μ is the angle of crystal monochromator and θ – scattering angle.

The absorption factor A_j can be approximated as [ALL2003]:

$$A \approx \exp\{-(a + b \cdot \sin^2 \theta) \cdot \mu R\} \quad (13)$$

the a, b=1.6598 or - 0.2832 , for one cylinder (capillare).

The structure factor is defined as [KRAW] :

$$F_{hkl} = \sum_n^{\text{unit cell}} f_n e^{-M} e^{\frac{2\pi i}{\lambda}(s-s_0)r_n}$$

$(s - s_0)r_n/\lambda$ represents reciprocal G-space.

The $e^{-M} = e^{-\frac{(\sin\theta)^2 B_n}{\lambda}} = e^{-\frac{(\sin\theta)^2 8\pi^2}{3} u_n^2}$ is the **Debye Waller factor**, its influence on the diffraction pattern is explained in more details in 2.2.4 and Appendix 2 covers some additional calculations. $B_n = 8\pi^2 \langle u_n^2 \rangle$ is proportional to the displacement parameter of the site n. Then $\langle u_n^2 \rangle$ is the mean-square isotropic thermal displacement of the atom on its site, usually expressed in units of squared atom distance, e.g. \AA^2 .

f_n is the **form factor**

$$f_n = \int \rho(\vec{r}) e^{iQr} d^3\vec{r}$$

Where $\rho(\vec{r})$ is the spatial density of the scatterer about its center of mass ($r=0$), and Q is the momentum transfer. As a result of the nature of the Fourier transform, the broader the distribution of the scatterer ρ in real space r, the narrower the distribution in Q; i.e., the faster the decay of the form factor.

Entering the units of λ , \AA , one can show that e^{-M} is a unitless value. Although in some papers [PENG1996] the unit \AA^2 is used, that is not fully correct and represents just an approximation as also very good explained in [KRAW].

The **profile shape function** $S_j(2\theta_i - 2\theta_{j,k})$ describes the broadening of diffraction peaks and is determined by default in MAUD program by the Cagliotti shape function [CHAT2010], [MCCUS1999]: $FWHM^2 = U \tan^2 \theta + V \tan \theta + W$. Here U, V, and W are half width parameters to be refined during the fit. The three parameters U, V, W of the Cagliotti equation for neutron investigation are dependent from such parameters as mosaicity of the monochromator and the sample and difference angle between neutrons mean beam axis and direction of every neutron:

$$U = \frac{4(\alpha_1^2 \alpha_2^2 + \alpha_1^2 \beta^2 + \alpha_1^2 \beta^2)}{\tan^2 \theta_m (\alpha_1^2 + \alpha_2^2 + 4\beta^2)} \quad (15)$$

$$V = \frac{-4\alpha_2^2 (\alpha_1^2 + 2\beta^2)}{\tan \theta_m (\alpha_1^2 + \alpha_2^2 + 4\beta^2)} \quad (16)$$

$$W = \frac{\alpha_1^2 \alpha_2^2 + \alpha_1^2 \alpha_3^2 + \alpha_2^2 \alpha_3^2 + 4\beta^2 (\alpha_2^2 + \alpha_3^2)}{(\alpha_1^2 + \alpha_2^2 + 4\beta^2)} \quad (17)$$

The formulas for the U, V, W are taken from [HEWA1975], and [MOSK2017] The $\alpha_{i(1,2,3)} = \frac{s_i}{l_i}$ are the divergences of the Soller collimators (width s by length l). The definition of $\alpha_i, \beta, \theta_m$ is shown in Figure 7 and Figure 8 in more details. In the figures a standard diffraction setup is shown. Their influence have been taken into account via reference measurements.

Using the monochromator mosaicity β and the divergence of the Soller collimator, the Cagliotti values can be calculated. More details about the parameters of the Cagliotti function can be found in [KADUK2012, HEWA1975]. However there is no information about possible differences of the Cagliotti parameters when applied to synchrotron radiation instruments. Thus also for the determination of the synchrotron Cagliotti parameters an experimental approach via measuring a reference sample was performed. It was assumed that in this case V is allowed to be negative [KADUK2012]. More detailed basic information about Rietveld refinement could be found in the book of Daniel Chateignier “Combined Analysis” [CHAT2010].

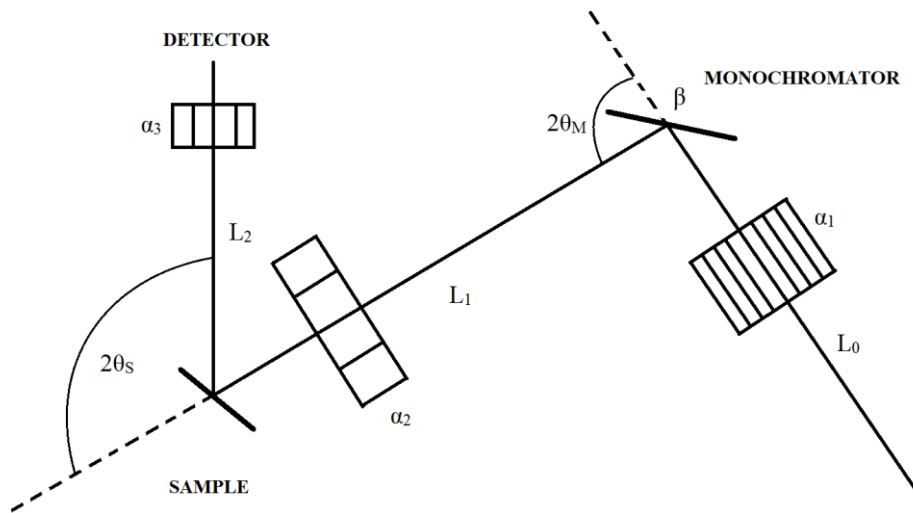


Figure 7 Scheme of powder diffractometer [MOSK2017]

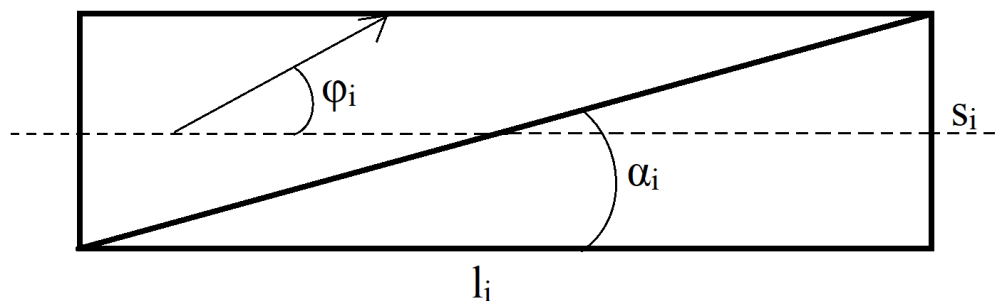


Figure 8 Collimator [MOSK2017], ϕ_i – difference between neutron trajectory and collimator axis

Actually each experimental diffraction set-up should be described by its own Cagliotti parameters determined by a reference sample measurement. In the current PhD thesis the Cagliotti parameters were refined by using a LaB_6 reference sample. Then the refined Cagliotti values were fixed and used for sample analysis.

2.2.4 Debye-Waller B-Factor influence on a diffraction pattern

The Debye-Waller or B-factor (named after Peter Debye and Ivar Waller) (see as well Appendix 2a) describes the temperature dependence of the intensity of a beam coherently scattered from the crystal. It plays a significant role in the data interpretation of the in situ experiments under heating. “Atoms are not positioned rigidly within the crystal structure, but

instead vibrate about their mean lattice site r_u with an amplitude that increases with temperature. Thus, the time-averaged atomic nuclei positions are smeared and this gives rise to a term in intensity” [HUTC2005]. Thus the intensity decrease (Figure 9, Figure 10) is determined by increased fluctuation of the atoms around their equilibrium positions with increasing temperature.

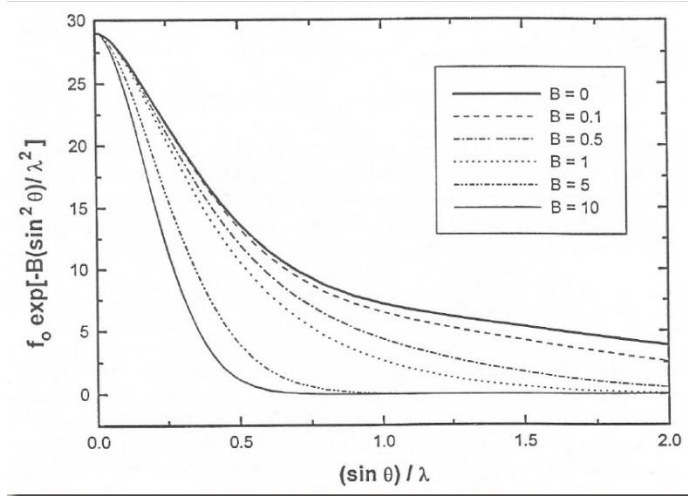


Figure 9 Acceleration of intensity decrease due to increase of the B-factor

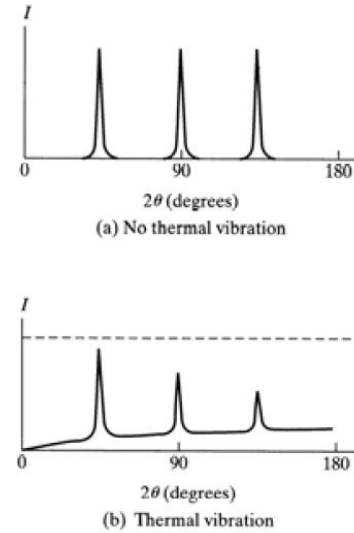


Figure 10 Change of the spectrum intensities due to appear the thermal vibration

The temperature factor is represented by the equation $e^{-M} = e^{-\left(\frac{\sin\theta}{\lambda}\right)^2 B} = e^{-\left(\frac{\sin\theta}{\lambda}\right)^2 \frac{8\pi^2}{3} u^2}$ [KRAW]. The factor e^{-M} influences the structure factor, when thermal vibrations are taken into account, as

$$F_{hkl} = \sum_n^{\text{unit cell}} f_n e^{-M} e^{(2\pi i/\lambda)(s-s_0)r_n}$$

The effects of the intensity are schematically shown in Figure 10.

In case of metals the B-factor could be assumed to be isotropic and represented by one parameter. The B-factor was refined for one atom and set equal to the refined value for all other atoms of phases of the sample.

2.2.5 Isotropic phase parameters Rietveld refinements basics

Under isotropic phase parameters one can understand such phase characteristics as crystallite size and microstrain. These parameters could be refined separately for each phase. However, a very good quality of the diffraction data (e.g. grain statistics) is necessary for their refinement.

There is a basic peculiarity in understanding the meaning of the crystallite size, refined by the Rietveld method. Not the real crystal size is refined during the Rietveld refinement. Crystallites are just smaller parts of a crystal with the same orientation of the lattices (e.g. explained in subchapter 2.1.1.5). Because the lattice of real crystals is not perfectly constructed every crystal consist of components with small differences in the orientations of their crystal planes e.g. due to small angle grain boundaries (mosaicity) or other crystal defects. Therefore,

the refined crystallite size values vary strongly from the real crystal size values. The crystalline size could be smaller or larger than the real crystal size (meaning the size of a separated, not doubled grain). The Rietveld refinement can give the size of the area with the same lattice orientation in neighbouring grains, which can be more than one grain.

No stresses and strains are assumed to be present in our samples. During sample production no stresses have been applied to the samples purposefully. The annealing performed after arc-melting for 5 or 7 days (chapter 3) is assumed to relax all initially present thermal stresses. The in situ heating experiments were performed over a big temperature range and sometimes with high heating rates. Thus, due to recrystallization microstrains should appear, that could yield to a small divergence of the lattice parameters and widen the peak. However, especially during heating the growth of microstrain is assumed to be not high due to an accelerated recovering. Microstrains which occur during cooling would be more important to take into account. Usually higher fluctuations of microstrain were visible above 1000 °C at temperatures where the $\alpha_2 \rightarrow \alpha$ and $\beta_o \rightarrow \beta$ transformations are expected. Such fluctuation can make the data interpretation difficult. Thus the microstrains were fixed during initial refinement.

Chapter 3 Experimental Methods

Experimental methods as well as sample production will be described in this chapter. First a full history of the samples is shortly summarized in this paragraph. Two sample sets with slightly different alloy compositions (composition described in detail in chapter 5) were produced. Our alloys were produced by arc melting (subchapter 3.1.2) and heat treated (3.1.3) at 1100 °C. Then cylinders were spark eroded from the center part of a melt button (3.2.1). The cylinders were used for in situ measurements with synchrotron and neutron diffraction. An edge part of each button was polished for application of SEM (3.3.1), and EDX (3.3.2). DSC (3.3.3) has been applied to small pieces from the center part of the button for the first sample set only. The mentioned additional methods SEM, EDX, DSC give comprehensive information needed for the in situ data interpretation. The complementarity of the different methods to study the β_0/β ordering phase transformation in γ -TiAl alloys will be discussed in chapter 8. Chapter 8 will also contain the discussion of the precision of each method and of possible errors. Methods of the in situ synchrotron and neutron experiments are described at last (3.4).

3.1 Sample production method

The sample production includes following stages:

- (1) weighting of the pure elements in a proportion, corresponding to sample composition;
- (2) melting of the pure elements to one alloy sample in a button;
- (3) heat treatment for microstructure homogenization;
- (4) especially for *in situ* methods: spark erosion of cylinders from a central part of the button for neutron and hard X-ray diffraction investigations;
- (5) polishing the edge button part for SEM and EDX measurements;
- (6) cut of small pieces for DSC measurements from the rest of central button.

3.1.1 Weighting of pure elements

After a nominal composition of the sample was chosen, the weight of the pure elements should be calculated from atomic % to grams. The mass of a melted alloy button was expected to be 32 g. Pure-Ti sponge needed to be melted into small buttons (for deleting the volatile components from the sponges pores) before it can be used. The pure materials were weighted with a precision of 0,001 g. The difference between nominal amount of pure elements and the amount of the weighted material is below 0.2 mass % and is listed in Appendix 3A.

3.1.2 Arc melting

The arc melting method has been used for the production of almost all alloys in this project. The arc-melting method is known to provide some advantages:

- Alloys exhibit a satisfying microstructural homogeneity, homogeneous alloying element distribution as well as low concentrations of unwanted impurities (O, N) well below 700 wt-ppm. [CLE2013]

- Possibility to produce alloys under vacuum or Ar atmosphere is a special advantage for TiAl production. Ti and TiAl alloys cannot be melted in open air furnaces because this would yield to strong oxidation.

There is a large difference in the melting temperatures of the pure elements used to produce Ti-Al alloys. As one can see from Table 5 Mo, Nb and Ta have higher melting temperatures, than the boiling temperature of Al. Therefore, Al evaporation is observed during sample melting and the real composition of our samples differs up to almost 1 at. % from the nominal one (see chapter 5 and Appendix 3B).

3.1.2.1 Description of the used arc melting furnace

The Arc melting furnace D-7400 produced by Edmund Bühler, Tübingen, was applied for sample production. Several kiloamperes of direct current are used to start an arc between the electrode and the element pieces, to derive a continuous melt. The crucible made of copper is water cooled. More technical details could be found in [ARC-MELT].

3.1.2.2 Melting method

High reactivity with oxygen and hydrogen from the ambient environment can cause the alloy to become more brittle [APPL2011]. Therefore melting was done under Ar atmosphere to prevent oxidation and a pure titanium button was used as getter for the residual oxygen in the chamber. The buttons were remelted 5 times to ensure chemical homogeneity. The buttons have a weight of about 30 g.

The melting point of the elements (see Table 5) should be taken into account when the pure elements are laid in the copper crucible. For our alloys we used the following order of the metals: at first aluminium as lowest melting element on the bottom, then Ti and at last the metals with high melting points. The water cooling of the copper crucible yields to quenching of the metastable high temperature microstructure down to room temperature. Thus, an investigation of a sample with metastable microstructure will give unrepeatable results. Therefore, a heat treatment has been applied for homogenization of the microstructure.

Table 5 Melting and boiling temperatures of the pure elements important for the investigation

Element	Melting point, °C	Boiling point, °C
Aluminum , 99.9%, buttons 3 – 20 mm	660,3	2470
1. Titanium sponge , 25±12mm, 99,76%	1668	3287
2. titanium sponge , 3-19mm, 99,95%		
Electrolytic Fe , 99.9% pieces 5 – 30 mm	1538	2862
Cr , 99.9%, flat pieces 2-30 mm ²	1907	2672
Boron pieces , crystalline, 10-10mm, 99.5% (Alfa Aesar)	2076	3927
Niobium turnings , 99.6%, (Alfa Aesar),	2477	4927
Molibdenum 99,95% (Alfa Aesar 010039)	2623	4639
Tantalmetall sinter quality > 1mm aus EB – Schmelze ProdNr 01000685, Lot Nr 970203, H.C.Starck	3017	5457

3.1.3 Hot Isostatic Pressing

The production method of the majority of the used samples is the same. However, the method of Ti-42Al-8.5Nb is different as it was prepared by Hot isostatic pressing (HIP) [STAR2015]: powder atomized in the PIGA-facility at the GKSS Research Centre, filled in Ti cans, degassed and subsequently hot-isostatically pressed for 2 h at 1250 °C and 200 MPa.

3.1.4 Heat treatment

Heat treatment has been performed for homogenization of the phase composition and microstructure. The annealing temperature 1100 °C is chosen to stabilize the α_2 , the γ and probably the β phases. After subsequent slow furnace cooling down to room temperature microstructure and phase composition will be stable. Two similar heating furnaces have been used to keep the arc melted buttons at 1100 °C for 5 days (for the 1st sample set) [KON2017] and 7 days (for the 2nd sample set). No significant difference should appear in phase composition and microstructures of the first and the second sample sets due to the different annealing times. The heat treatment is performed in air without a special atmosphere, therefore the samples were oxidized. Depending on the sample composition the colour and thickness of the oxidation crust was different.

3.2 Mechanical sample preparation

3.2.1 Cylinder sample cut

From the heat treated buttons cylinders with 5 mm diameter and length of 20 or 10 mm have been spark eroded by the workshop of Helmholtz-Zentrum hereon (earlier Helmholtz-Zentrum-Geesthacht) (Figure 11). The long samples were used for in situ neutron diffraction investigations with a standard high temperature furnace and the short samples for all dilatometer measurements performed.



Figure 11 Parts of the button used for neutron diffraction analysis (cylinders) and other methods for the first and the second sample sets

3.2.2 Sample preparation for SEM

The mean diameter of the button was about 20 mm. An edge part of the button with thickness of 3 – 7 mm has been cut. The cut has been manually ground and polished with SiO₂ suspension. The prepared samples have been used also for EDX. A parallel plane to the polished surface has been prepared at opposite side in order to achieve an exact positioning of the sample in the SEM. For cleaning of the samples methanol and acetone have been applied.

3.3 Metallography

3.3.1 SEM

Scanning Electron microscopy investigations have been performed for evaluation of the microstructure homogeneity and grain growth using a LEO GEMINI 1530 microscope at Helmholtz-Zentrum Hereon. With a back scattered electron detector it is possible to distinguish between the α/α_2 , the β/β_0 and the γ phases in Figure 12, Figure 21, Figure 22, Figure 23, and Figure 24. The phase with the highest electron density, almost pure β Ti phase, scatters the highest amount of electrons and appears as the brightest. The γ phase is pictured as dark phase because of being the richest in Al with a lower electron content and due to a middle Al content the α/α_2 phases appears in medium grey.

It is assumed that the microstructure of the alloy button at 5-7 mm from the edge and in the middle part is the same after homogenization. However, no direct measurements in the sample middle were performed.

3.3.2 EDX

Energy-dispersive X-ray spectroscopy (EDS, EDXS or XEDS), sometimes called energy dispersive X-ray analysis (EDXA) or energy dispersive X-ray microanalysis (EDXMA), was used for the elemental analysis or chemical characterization of our samples. It relies on an interaction of some source of X-ray excitation and a sample. EDX measurements have been performed at a LEO GEMINI 1530 microscope at Helmholtz-Zentrum Hereon.

EDX analysis has been carried out for composition control after heat treatment at 1100 °C. A middle composition has been estimated with respect to the phase present at the measurement position. 10 points per phase have been measured (Figure 12). The number of points is a compromise between good statistics and the time for measurement and data analysis. From the 10 measured points for each phase the mean chemical composition of the phase has been calculated. Then using the phase content determined from RT synchrotron measurements with sample rotation the mean chemical composition of a sample was calculated. A change of the element distribution might be observed at elevated temperatures that could not be measured due to the impossibility of in situ EDX observations. For the measurements binary TiAl reference has been applied.

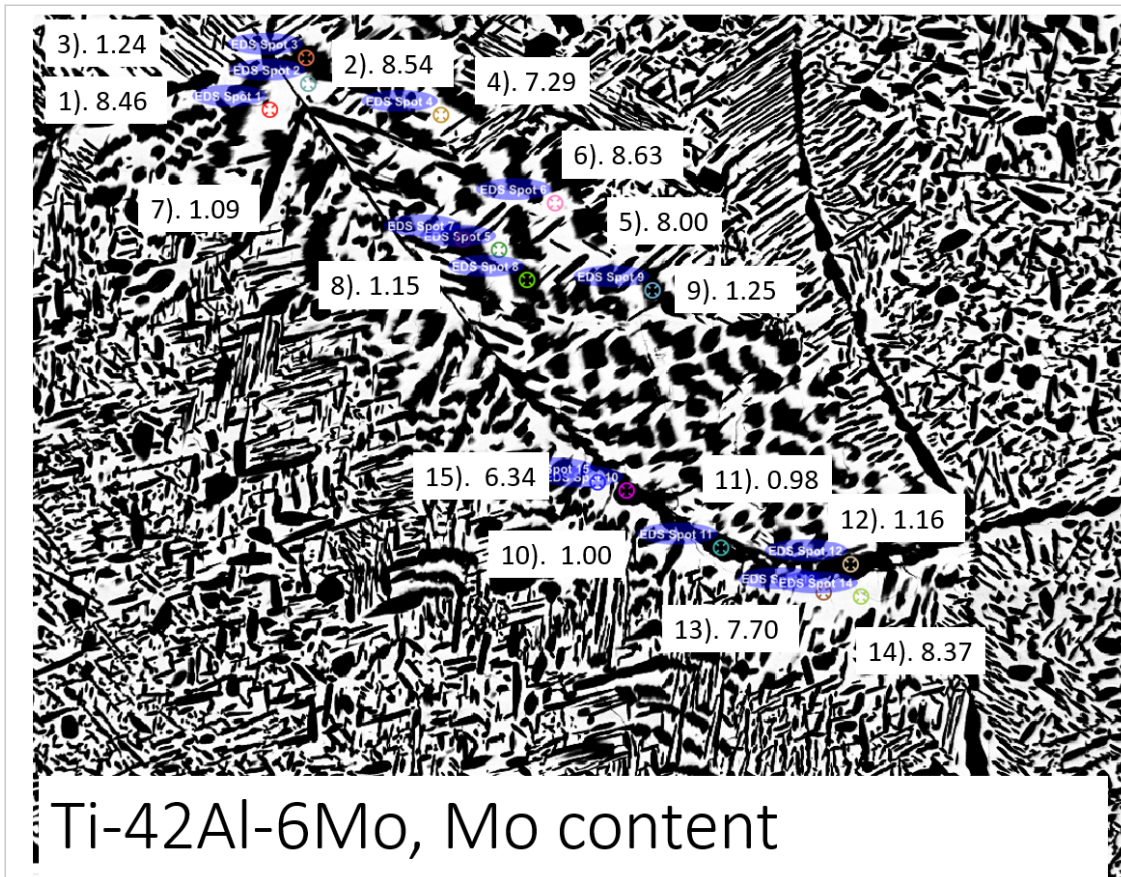


Figure 12 Example of an EDX measurement. Distribution of measurement points as well as Mo content (in atomic %) between phases of Ti-42Al-6Mo sample.

3.3.3 DSC

Differential scanning calorimetry was used to determine the disordering (ordering) temperature of the β_0/β phase during heating up to 1450 °C and cooling. At the beginning of the project it was unclear whether this phase transformation yields a detectable DSC peak. A small part of the sample (32 mg) has been heated and the changes in its heat capacity were tracked as changes in the heat flow [DSC-Guide]. Differential scanning calorimetry (DSC) measurements were performed by a DSC 404 C Pegasus (Netzsch company). Peaks of phases were identified based on the phase diagram from J. C. Schuster and M. Palm [SCHU2006].

In order to avoid oxidation Argon gas was used. The chamber was evacuated 10 times and flushed with Ar between pumping. Pressure of Argon during measurements was constant. Samples were heated from RT to 1500 °C and cooled back with rates of 20 K/min. Before and after the experiment the samples were weighted and no significant weight difference found. The samples were put into Al₂O₃ crucibles filled with Y₂O₃ powder to prevent oxidation. The second crucible on the measuring head was empty. During the DSC measurements changing of temperature and heat flow were measured.

3.3.4 The RT Synchrotron radiation measurements with rotation of sample

The investigation at RT by synchrotron generated X-rays was performed at beamline P07 (see chapter 3.4.2.2), with a simple rotating device. Rotation for 180° was performed for improvement of the grain statistics. The beam size was 1x1 mm² and a detector gain of 2 was used. The exposure time was 0.1 s and 120 pictures were summed during rotation. Three z

positions were measured, the data of the two last positions were summed and three files (two initial and one summed) were refined by Rietveld method for each sample. Values of refined parameters were compared in order to determine the most reliable data.

Such a ternary refinement was expected to determine the precision of the refined values by minimizing unphysical fluctuation of the refined parameters. Phase content, intensity, and lattice parameters have been refined. Then the averaged values of each parameter were collected in corresponding tables described in the next chapter.

If an additional phase (ω_o/τ_2) was expected to appear, two refinements were realized for presence and absence of the second phases and the amount of phases was compared. The ω_o was assumed to be present in Ti-42Al-8.5/10Ta and Nb. The amount of the ω_o or the β/β_o refined is close to each other (± 1 vol. %).

3.3.5 Oxygen content determination

Oxygen and nitrogen content has been determined at Helmholtz-Zentrum Hereon with the TC-436, a software-controlled instrument in LECO ONH836 furnace. Oxygen was detected in the form of carbon dioxide. Oxygen content was measured by infrared absorption. Because all molecules have a characteristic spectrum, infrared spectrometry is an extremely useful method for qualitative and quantitative chemical analysis.

After outgassing of an empty graphite crucible a sample is dropped into the crucible. Crucible and sample are heated by high current and the oxygen emitted from the sample reacts with the carbon from the crucible to carbon monoxide that is subsequently converted to carbon dioxide by passing through heated rare earth copper oxide. The sample gases then passed through the IR cell which detects the oxygen bound in the carbon dioxide. After this the gas flow passes through a thermal conductivity cell which detects nitrogen. Because the TC-436 uses helium as carrier gas and helium has a conductivity sufficiently different from nitrogen the change in the thermal conductive due to the presence of nitrogen could be measured.

3.4 In situ heating

In situ diffraction measurements were carried out by synchrotron and neutron radiation. Two kind of heating furnaces were applied (1) the high temperature furnace and (2) the dilatometers. There is a slight difference in modifications of dilatometer for application in the neutron and synchrotron beam, that will be described further.

3.4.1 Heating furnaces

3.4.1.1 Standard high temperature furnace

The maximum reachable temperature is 1900 °C (Table 6). Figure 13 shows an image of the high temperature furnace. The heater of the high temperature furnace (HTF) consists of a resistive Nb double cylinder element. Radiation shields, made of Nb, reduce the thermal loss. For temperatures up to 900 °C the furnace can be filled with Ar gas to improve oxidation stability [KON2017]. However, the temperatures of our investigation are much higher, namely 1450 °C, therefore, no gas atmosphere has been applied. Our cylindrical sample with a diameter of 5 mm and 20 mm length has been mounted into a Vanadium container and inserted with a long rod into the heating chamber. Figure 14 shows a cut of the high temperature furnace [MLZE].

Table 6 Experimental parameters of the standard high temperature furnace [MLZW], [MLZE]

Temperature range in vacuum (°C):	RT–1900
Temperature range in exchange gas (°C):	RT–900
Diameter of sample space (mm):	45
Total height of sample space (mm):	100
Sample rod tail:	M8 (male)
Thermometry:	type C thermocouple [MLZE]

The high temperature furnace provides information about temperature by a thermocouple positioned not directly on the sample but close to the sample holder. This results in a temperature deviation of 40 °C between read-out and sample temperature which was determined using a reference sample. The correction of the measured temperature was performed for all samples from the sample set investigated with the high temperature furnace.

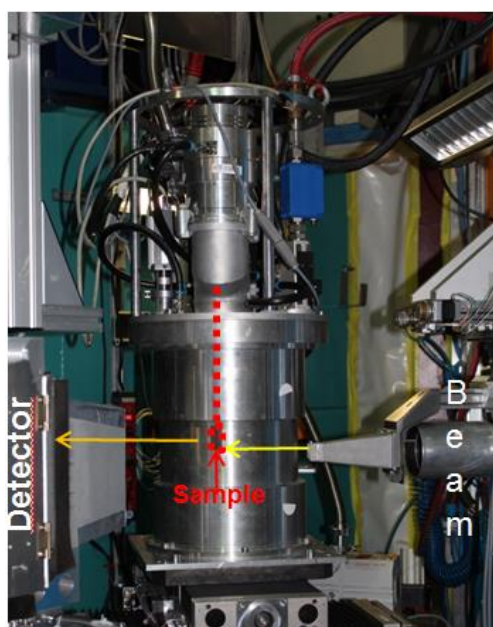


Figure 13 The High Temperature Furnace

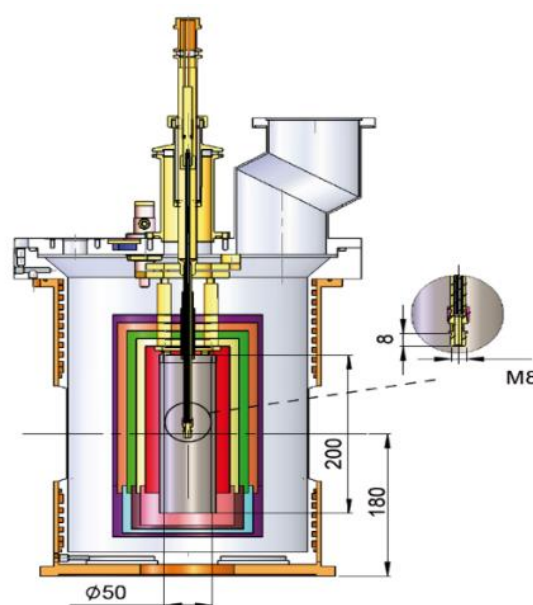


Figure 14 Cross-section over the High Temperature Furnace

3.4.1.2 Neutron and Synchrotron dilatometers

The quenching and deformation dilatometer DIL 805A/D has been produced by TA Instruments (formerly Bähr), Hüllhorst, Germany. The technical characteristics of the dilatometer are the same for both neutron and synchrotron modifications:

- sample size: \varnothing 4–5 mm; $l = 10$ mm
- inductive heating [INDHEAT] (up to 1500 °C)
- fast heating rate: up 4000 °/s (for hollow samples)
- different cooling rates up to quenching samples: quenching by blowing with gas – (Ar, N), up to 100 °C/s modelling oil (about 80 °C/s and even water 100 °C/s) quenching.
- deformation (compression, tension) with 0.01–125 mm/s and max. 20 / 10 kN.

The dilatometer measures the temperature via thermocouples. A type B thermocouple is welded directly to the sample and controls the temperature precisely. However the thermocouple type B is not sensitive for temperature measurements below 50 °C. [THCP]. The type S thermocouple has been used for RT measurements.

There can be a chemical reaction between TiAl alloys and thermocouples at high temperature. Therefore a tantalum plate of 3x2 mm² was welded between thermocouple and sample. The plate was welded at full length in order to have a good contact with the sample. The two thermocouple wires were welded in the middle of the Ta plate in 1 mm distance to each other.

A cylindrical sample of 5 mm diameter and 10 mm length was used.

The contact of the sample with the Al₂O₃ sample holder could bring a small difference of the temperature between the edge and the center. However the thermal conductivity of Al₂O₃ is smaller than that of metals thus the sample is assumed to be heated almost fully homogeneously and for data interpretation the temperature difference was neglected.

The standard dilatometer model was modified for working in the neutron and synchrotron beams by additional windows made from materials transparent for the beam: capton (for synchrotron radiation) and Al (for neutrons): Figure 15 and Figure 19 correspondingly. Windows size is larger for dilatometer at FRM II because of different scattering geometries and wider scattering angles for neutrons than for synchrotron high energy X-rays. For the transmission geometry at synchrotron 5 cm diameter round windows are sufficient.

The dilatometer log-file contains data including the most interesting parameters of time [s]; temperature [°C]; change in length [μm] and HF power [%]. The parameters allow to check the heating process. E.g. when the HF curve gradient does not correspond to the temperature curve gradient, this is usually caused by a bad connection between thermocouple and sample. The problem of bad connection usually appears at high temperatures above 1250 °C.

Neutron dilatometer

The DIL 805A/D dilatometer had been modified for working as a high-temperature equipment for FRM II reactor in 2018 for application at 2 instruments: STRESS-SPEC and SANS-1. Our experiment was performed as the first of its kind at STRESS-SPEC.

Main advantage of the neutron technique for material analysis is high penetration depth. Theoretically, a higher amount of material could be analysed. This neutron advantage is unfortunately restrained by the inductive heating of the dilatometer. Too thick samples could not be homogeneously heated by eddy current. Therefore, samples not larger than the standard dilatometer sample size of 5 mm thickness should be always used. On the one hand it is easier to have the same sample size for comparison of two diffraction methods. However, even when the sample diameter is the same as with HTF, some grain statistic problems could be avoided if a longer sample would be used during neutron measurements.

The dilatometer neutron in situ measurements of TiAl alloys have some peculiarities compared to the synchrotron measurements:

- A vertical induction coil in the heating module without deformation. In the deformation or tension module the coil is still horizontal, but both coils have a larger diameter and a larger space in the middle to let the beam pass. That theoretically can decrease the maximum achievable heating rate but it was not important for our stepwise heating.
- Larger windows to let the beam pass, because of the larger beam size.

Another material for the window: Al which is transparent for neutrons



Figure 15 Aluminum window for neutron dilatometer

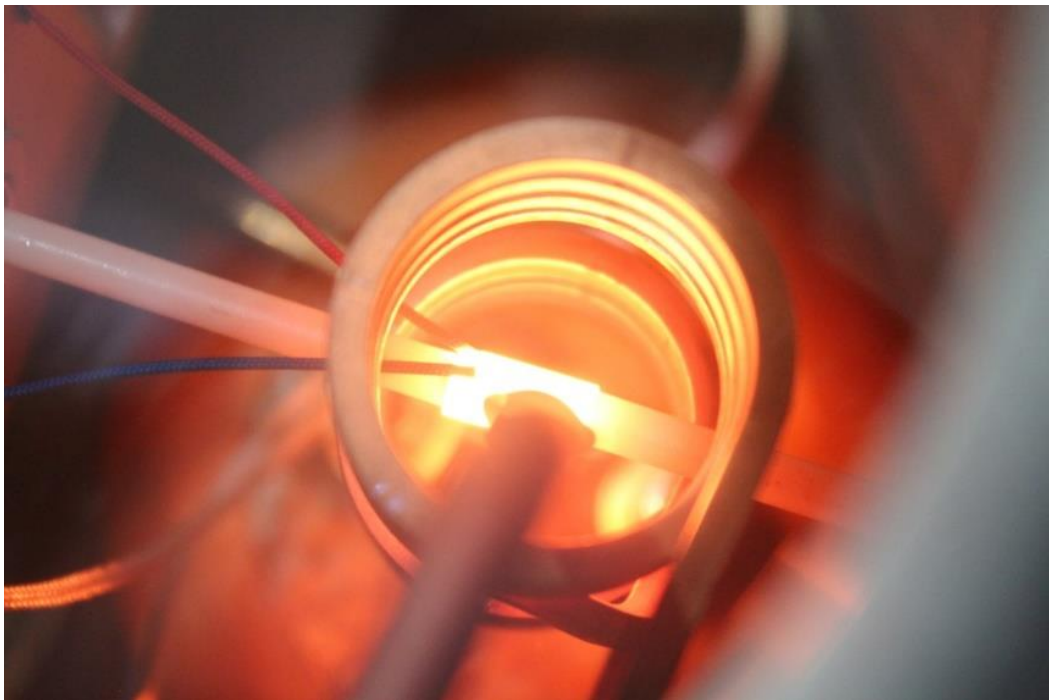


Figure 16 Vertical coil for heating module neutron dilatometer at STRESS- SPEC

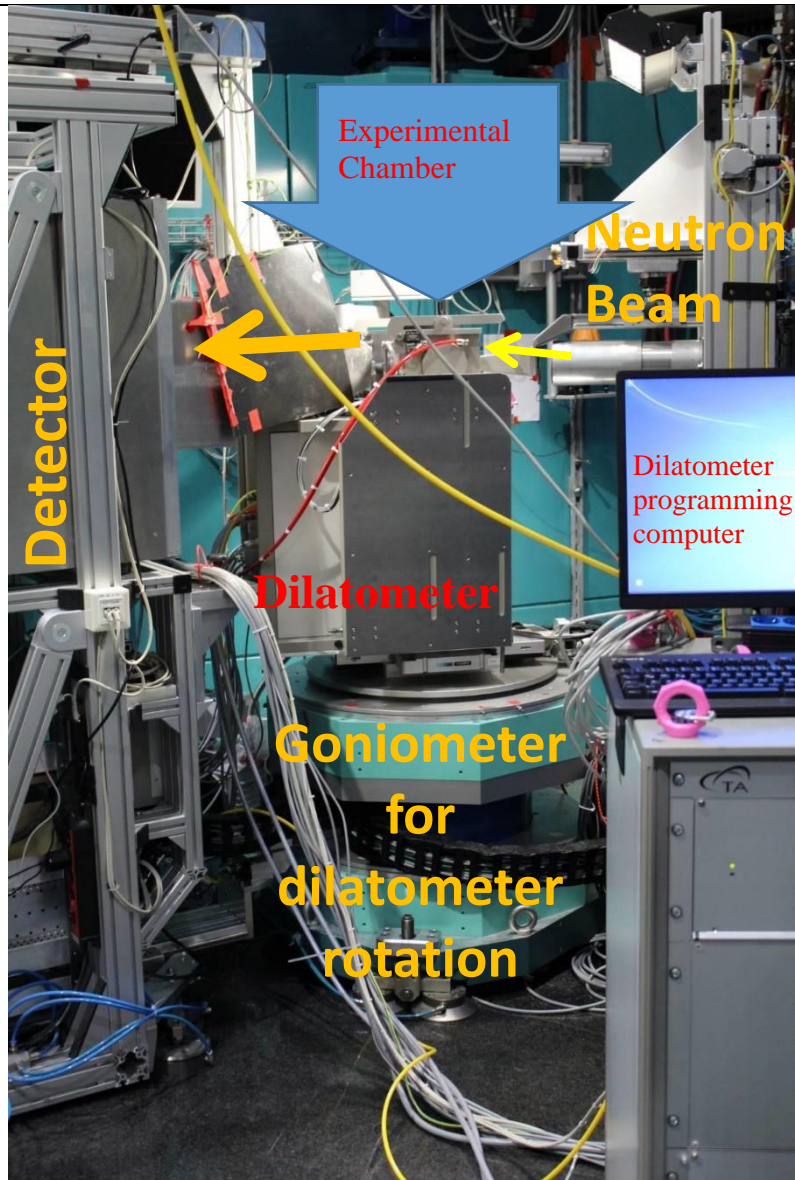


Figure 17 Quenching and Deformation Dilatometer DIL 805A/D at rotation sample table during measurements at Stress-Spec (MLZ).

Synchrotron dilatometer

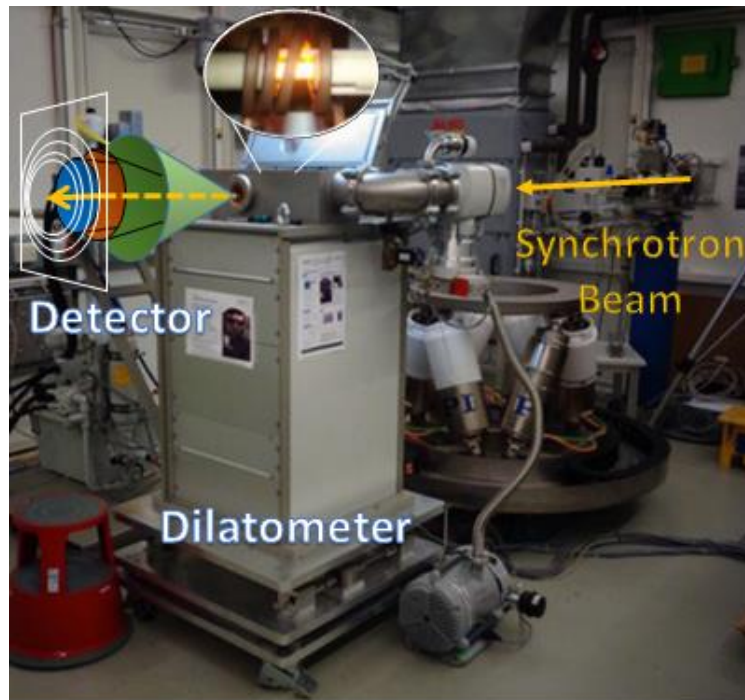


Figure 18 In situ synchrotron diffraction experiment with dilatometer DIL 805A/D in transmission geometry in the P07 beamline at PETRA III

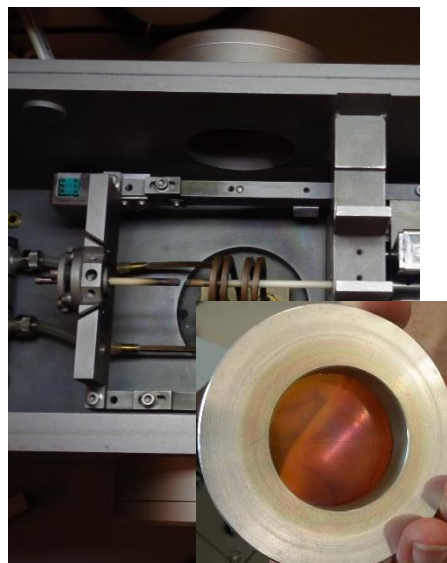


Figure 19 Experimental chamber with heating coil and capton window for synchrotron dilatometer.

The DIL 805A/D dilatometer had been modified for working in the Helmholtz-Zentrum hereon (earlier Helmholtz-Zentrum-Geesthacht) synchrotron beamline HEMS at PETRA III, DESY (Hamburg, Germany). [STAR2015] The dilatometer (Figure 18) was equipped with windows transparent for the X-ray beam [ST-N2011]. The heating coil and capton window for synchrotron dilatometer is shown in Figure 19. Capton is transparent for X-rays and does not give any additional peaks on the spectrums. Thus, due to application of the capton window it is possible to use the dilatometer for *in situ* synchrotron diffraction measurements.

3.4.2 In situ diffraction methods

3.4.2.1 Neutron instrument and method

Figure 20 shows a theoretical spectrum for neutron wave length $\lambda = 2.1 \text{ \AA}$. In the following chapter the neutron and synchrotron radiation experiment will be described separately.

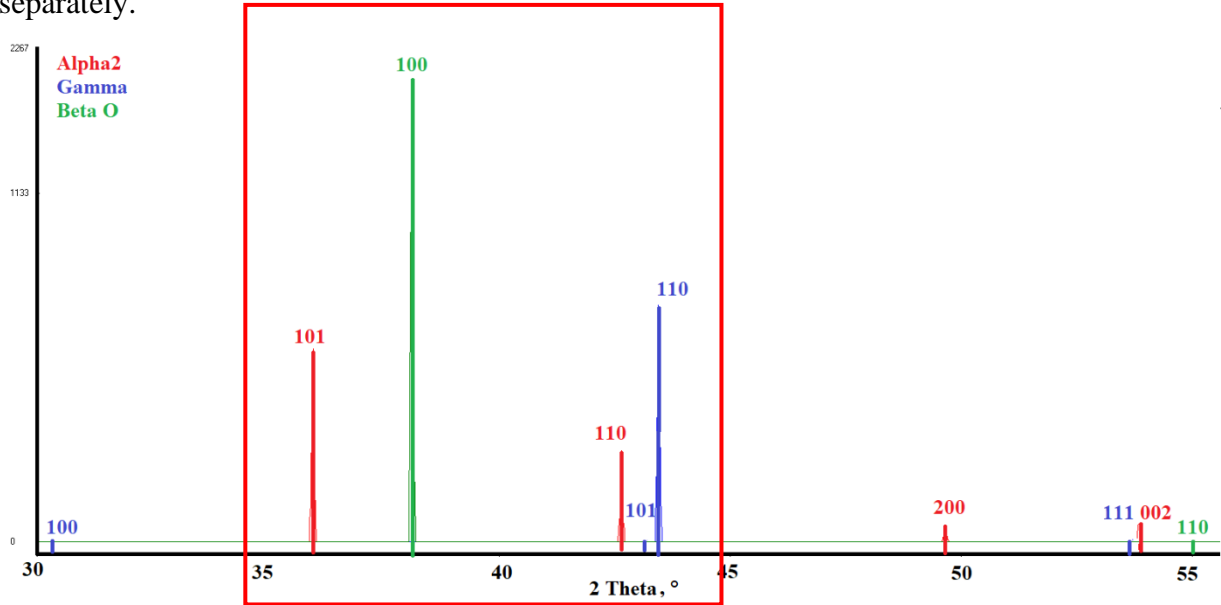


Figure 20 Spectrum of the β_0 (B2), α_2 and γ phases of TiAl alloys, calculated by program Powder cell. The 2θ are calculated for neutron radiation of $\lambda = 2.1 \text{ \AA}$. The red frame shows the region of neutron measurements.

Neutrons have been applied for diffraction analysis for the ordering disordering phase transformations because of different and much brighter contrast between β_0 and β phases in comparison to synchrotron. Due to the special contrast between scattering lengths of Ti and Al in case of our very close to 50:50 elemental content neutrons allow to detect only superstructure peaks. Neutron diffraction experiments have been performed at the materials science diffractometer STRESS-SPEC.

Method of the neutron in situ diffraction experiment

In situ ND measurements were carried out twice with different sample sets at STRESS-SPEC which is a materials science diffractometer [HOFM2015] for texture analysis or strain measurements located in the experimental hall at the thermal beam port SR-3 of the FRM II, Garching near Munich. Two different furnaces have been applied for heating: a standard high temperature furnace (HTF) and a dilatometer, which differ from each other by heating method, applicable sample size and thermocouple position. A comparison of the experimental details is given in Table 7.

Full samples have been measured. The gauge volume for the first experiment (with HTF) was $5 \times 5 \times 20 = 500 \text{ mm}^3$ and for the second was $5 \times 5 \times 10 = 250 \text{ mm}^3$. We used a wavelength of 2.1 \AA . By a 3He -PSD, $25 \times 25 \text{ cm}^2$ neutron detector an angular region of 15° has been covered. The detector covered the q -range of $1.7 - 2.3 \text{ 2}\pi \text{ \AA}^{-1}$ which enables to monitor superstructure peaks of all three ordered phases simultaneously, namely α_2 -101, β_0 -100 and γ -110.

Neutrons need an exposure time of up to 30 min per temperature point because of (1) high inelastic scattering of Ti that gives a lower peak/background ratio; (2) not too high amount of the β_0 phase in the samples and (3) low beam intensity. Therefore an experiment with a full heating and cooling cycle would take too long and even heating with a constant rate, as performed at the synchrotron, could not be realized. Consequently stepwise heating has been chosen as best compromise between time and resolution. One detector picture has been measured every 10 °C step for 20 or 30 minutes between 1100 and 1300 °C and for 10 minutes for every 25 °C step above 1300 °C. Neutron measurements with HTF have been performed up to 1450 °C. First the samples were heated with a rate of 200 °C/min from 20 to 1000 °C and held for 30 min for homogenization. Within the subsequent stepwise heating a heating rate of 10 °C/min was applied between the steps.

The neutron in situ measurements with dilatometer have been performed up to 1250 °C and were also the first test measurements for the neutron dilatometer after commissioning of the dilatometer. A few technical problems appeared during this first real dilatometer operation. The small cooling system, provided by the manufacturer does not allow to keep the dilatometer at high temperatures more than 10 minutes. Therefore above 1200 °C after every 10 minutes the experiment has been forcibly stopped by the safety program of the dilatometer and had to be restarted manually again from the temperature of the break without homogenization time for the sample. Samples have been heated inductively. The normal heating rate was chosen to be 250 °C/min and after every restart 1000 °C/min. Hence, attention should be paid to the different heating rates which are significantly higher than mentioned by Chladil et al. [CHLAD2006] Temperatures of the phase transformation determined by neutrons and synchrotron will be compared in chapter 7.

Table 7 Experimental parameters of neutron diffraction analysis at Stress-Spec

	Experiment with HTF	Experiment with dilatometer
Samples:	cylinders Ø5 mm, 20 mm length	cylinders Ø5 mm, 10 mm length
Gauge volume:	5x5x20=500 mm ³	5x5x10=250 mm ³
Monochromator:	Ge(311), $\lambda = 2.1 \text{ \AA}$,	
Detector:	3He-PSD (MWPC-multi wire proportional chamber 25 x 25 cm ² ; 256 x 256 pixels) plate-detector.	
2θ range:	32.5 – 45.5 °	
Q-range:	17.0 – 22.9 nm ⁻¹	
Exposure time:	10, 30 min or 1 hour	10, 30 min, 1 picture every 10 min
Temperature range:	1100 – 1440 °C	1100 – 1250 °C
Heating ramp:	20 K/min Step-wise heating	
Heating steps:	10, 15, 25 °C;	
Heating	25, 50 °C	10 °C
Cooling		during heating only

During the dilatometer neutron measurements with the second sample set there was no need for high temperature measurements above 1250 °C, because there are no visible peaks for most of the samples except, the sample with 6 at. % of Mo. An Al₂O₃ rod was used as a sample holder. Additionally (different to DESY dilatometer measurements) a reference Al₂O₃ rod with the same diameter as the sample holder was applied. Unfortunately, both the sample holder and the reference rod gave their own additional peaks at the position of the α_2 101 peak. Therefore, some interpretation problems appeared after the measurements because the α_2 101 peak was

used as a reference together with γ -110. Therefore no results of the second sample set are shown here.

3.4.2.2 Synchrotron and method of in situ diffraction experiment

High-energy synchrotron X-ray diffraction is a powerful tool for studies of bulk materials [LISS2006]. Especially for in situ investigations of the phase transformation behavior of titanium aluminides, high-energy X-ray diffraction (HEXRD) has evolved into a powerful and versatile characterization method [FISH2003, MARK2003, IMA2007, BRO2004, BART2002, CLE2013]. Compared with laboratory X-ray sources the high intensity of the synchrotron beam makes it easier to use an additional sample furnace to perform in situ investigations with thicker metallic walls than graphite ones [LXRHT]. At synchrotron radiation sources, a white X-ray beam is produced by the deflection of charged particles, either electrons or positrons, by means of a bending magnet or an insertion device, i.e., a wiggler or an undulator. [LAI2017, ANIE]. A monochromator is used to select a narrow energy range from the broad spectrum. The PETRA III synchrotron source at DESY, Hamburg was used for TiAl investigations.

Table 8 Experimental parameters of synchrotron measurements

Gauge volume:	5x1x1=5 mm ³
Photon energy and wave length:	EH3 the main station: 100 keV ($\lambda = 0.124 \text{ \AA}$) – main station EH1 the side station: 87 keV ($\lambda = 0.14235 \text{ \AA}$) w=99,8 w. % + ($\lambda = 0.071125 \text{ \AA}$) w=0,2 w. %
2-D detector:	PerkinElmer XRD 1621 detector; frame rate up to 10 Hz; 2048 × 2048 Pixel
Exposure time:	8 sec
Temperature range:	RT - 1450 °C
Samples:	cylinders Ø5 mm, 10 mm length
Heating:	Inductive
Temperature control:	by thermocouple at the sample close to beam exposure point.
Heating ramp:	5 K/min
Exposure time:	1,2 sek
Heating way:	continuous
Investigated Q range:	5 – 70 nm ⁻¹
Investigated 2θ range:	0.8 – 6 °
Atmosphere:	Argon

In situ synchrotron experiments for investigation of the influence of β -stabilizing elements on the disordering β_0 phase transformation in TiAl alloys were successfully performed at P07 high-energy XRD beamline (HEMS at DESY, Germany) [P07BEAM]. P07 – High-Energy Materials Science (HEMS) - has been chosen to perform the measurements because of appropriate correlation between radiation wave length and lattice constants of TiAl. For titanium aluminides, energies in the range of 87 to 120 keV (Table 8), corresponding to wavelengths of 0.143 to 0.103 Å, and wave numbers of 44.1 to 60.1 Å⁻¹ have been shown to

yield good diffraction results for specimens of 5 mm in thickness. [FISH2003]. The smaller than lattice parameter wave length gave an advantage of smaller scattering angle, that allowed to apply dilatometer as the sample furnace (due to the size of the capton window).

Main aims for experiment were

- (1) to make a phase analysis during heating and cooling samples
- (2) to determine temperatures when phase transformations occur.

Specimens were investigated in transmission geometry, as the high-energy X-rays can penetrate relatively large sample volumes: $1 \times 1 \times 5 = 5 \text{ mm}^3$. Due to their small wavelengths, they yield narrow Debye-Scherrer cones according to Bragg's law. Thus, no part of the diffraction patterns is lost, i.e. full diffraction rings have been recorded at once with the aid of a flat-panel area PerkinElmer detector. Heating has been performed with constant heating ramp in a specially modified dilatometer in a temperature range from RT up to 1450 °C followed by cooling back to RT by blowing Ar gas (Table 8). Description of the standard dilatometer configuration is given above before explanation of the neutron in situ methods.

Chapter 4 Diffraction data interpretation methods and used programs

Diffraction data interpretation was performed in 2 ways: (1) via Rietveld refinement of the full spectrum in the MAUD program [CHA2010] and (2) via Gauss fit analysis of single peaks with a python script.

Synchrotron diffraction data have been saved as tif-pictures and were azimuthally integrated into intensity over 2θ diffraction patterns (chi files) by Fit2D program. The beam center should be properly refined using a reference sample. As reference sample for synchrotron measurements LaB₆ or Ti-45Al were applied. The LaB₆ allows an automatic calibration with the Fit2D program that gives a better beam center position.

Rietveld Refinement. Prepared chi files are refined by batch-mode Rietveld refinement with the MAUD program. Basics of the Rietveld refinement are described in subchapter 2.2.3. Each experimental set-up requires the Cagliotti and Gaussian parameters. The Cagliotti and Gaussian parameters are instrumental parameters and have been fixed, once they were determined from the reference sample, for further sample parameters refinement. The sample parameters refined are: *phase fractions, background, lattice parameters, site occupancy* and equal for all atoms one *B-factor*. A simultaneous refinement of such parameters as B-factor, microstrain, crystallite size and site occupancies yielded to results bearing no physical meaning. Therefore, microstrain and crystallite size were mainly fixed.

The names of peaks fitted by Gauss curve from the synchrotron and neutron results are shown in Table 9.

Table 9 Names of peaks fitted by Gauss curve for neutron and synchrotron results

	Synchrotron	Neutrons
α_2/α	101, 200	101
β_0/β	100, 200	100
γ	100, 110, 200+002	110

The neutron diffraction detector pictures are only usable with a special program. STeCa – StressTextureCalculator is a software tool to extract texture, strain and microstructure information from area-detector measurements. It was written by colleagues of TU-Clausthal [RAND2011, BRYD2018]. The STeCa program was used for the transformation of the neutron detector pictures into diffraction spectrums, which can be interpreted. The pictures are recalculated in the intensity files and saved in the .dat format. In order to open the files in MAUD the header of the files should be changed to another one similar to that produced for synchrotron data by Fit2D program.

As it is shown in subchapter 2.4.1 there are fundamental and superstructure peaks for crystals. Only the superstructure peaks and no fundamental ones are visible of α_2/α and β_0/β phases with neutrons in intermetallic TiAl alloys with composition close to stoichiometry of the β phase. Therefore a decrease of the superstructure reflection of α_2/α and β_0/β phases is almost solely caused by a change of the ordering in the phase, but not by a change of the phase fraction.

For neutron data only the presence of a phase and some lattice parameters have been determined. In order to decrease an uncertainty of the refinement due to too high amount of

refined parameters. No microstrain and crystallite size have been refined due to too low amount of peaks. The B-factor for all neutron measurements at all temperatures was fixed at 1.5.

Gauss fit is the simplest approximation of a single peak by Gauss function and the decisive parameter then is Full Weight at Half Maximum (FWHM).

4.1 Model for the diffractogram refinement

Because Rietveld refinement is based on a comparison between the measured diffractogram and a calculation from a theoretical model, the used model should be as close as possible to reality. However, the amount of refined parameters should not elevate the amount of solving equations during refinement. Thus our models include only pure stoichiometric TiAl phases for diffractogram calculation. That means no additions of any β -stabilizing elements are included. If they would be taken into account additional assumptions would be necessary. (1) To which amount are they distributed between the phases, (2) which atom sites do they prefer and (3) how does this change at higher temperatures. Therefore the site occupancy parameters calculated by Maud do not include composition of phases, which are different from ideal stoichiometry. Additionally, no possible defects e.g. vacancies or atoms embedded in crystal are taken into account.

The site occupancy refinement was performed according to crystallographic restrictions described below, but used for synchrotron only. The amount of parameters which can be refined depends from the number of detected peaks. Usually the lattice parameters, background, thermal B-factor, and site occupancies were refined. The refined site occupancies were strongly fluctuating together with the microstrain and crystallite size. Therefore it was decided to refine no microstrain or crystallite size after test calculations were done for synchrotron and corresponding neutron data.

First trials to refine these parameters were performed for the first sample set, but no reliable results were achieved and the refinements even yielded big fluctuations of other parameters, e.g. B-factor or site occupancy. Therefore the values were fixed for all phases to 1000 nm for the crystallite size and at 0.000008 $\mu\text{m}/\text{m}$ for microstrain.

Peculiarity of the refined α_2/α phases

Because the refinement model included similar structures for α_2 and α phases, no change in a lattice parameter should be observed, and the atom site occupancy is considered as main factor to distinguish between α_2 and the α phases. In subchapter 4.2.2 the way of SO refinement is shown for the α_2 phase.

Peculiarity of the refined β_0/β phases

The chemical composition of the β_0/β phase in ternary alloys differs with the alloy composition [QIU2012-1]. In the chapter 7 an influence of β stabilizing elements on composition and lattice parameter of β_0/β alloys will be described. However in the current project in order to simplify the data analysis the β_0/β phase composition is taken as ideally stoichiometric TiAl and constant with temperature. This makes sense as long as the amount of the third element does not decisively influence the electron density of atoms in synchrotron results or the scattering lengths for neutrons. Deviation from the ideal stoichiometry, e.g., as in the current investigation with 58 at. % of Ti and 42 at % Al will lead to an imperfectly ordered crystal structure. Presence of defects in real crystals are not taken into account because to investigate them would need the highest quality of diffraction data and more additional investigations. Thus the ideal β_0 phase in B2 bcc structure implies Ti atoms to occupy 1a

position and Al ones 1b position, i.e., there are two simple cubic lattices composed of atoms of one kind (Ti or Al) (see Figure 3d, e and subchapter 4.2.1).

Peculiarity of the refined γ phase

In materials science the γ phase is often related to the fcc lattice and is treated like a cubic lattice due to its small tetragonality [BYST2010]. This similarity is also visible in its designation as tetragonal face centered unit cell. Following the crystallographic rules the tetragonal face centered unit cell is not the smallest one and therefore does not exist as primitive unit cell. However in this study the bigger unit cell (commonly used in materials science) is used in diffraction data analysis. The lattice parameters of the above mentioned phases are given in the Table 2. γ phase is shown as closely related to a face centered cubic lattice. According to the crystallographic rules the Pearson symbol of the γ phase should be tP2 (tetragonal with two atoms in the unit cell) and the lattice parameters should be $a = 2.877 \text{ \AA}$ and $c = 4.065 \text{ \AA}$ [STAR2010].

4.2 Ordering determination via site occupancy refinement

Several models exist for describing the ordering transformation in bcc phase. Currently there is no approach suggested to estimate the degree of ordering in non-stoichiometric alloys. In our approach, the degree of ordering D through the 1a site occupancy (SO) by Ti atoms is defined for binary alloys with ideal stoichiometry of β_0/β phase according to the following formula:

$$D = (1 - 2 \cdot SO) \cdot 100\%$$

Change of site occupancy from 0.5 to 1 corresponds to the degree of ordering in the range from 0 to 100%. Since 1a site is mainly occupied by Ti atoms, the SO of this position value cannot be less than 0.5. Then the SO of 1b with Al will be the same as 1a for Ti and SO of 1a with Al will be always lower than 0.5, as well as 1b of Ti. The smallest SO would give the highest coefficient D .

The MAUD program allows to refine the site occupancies for different phases. The refinement is based on the correlation between fundamental and superstructure reflection intensities. Because no fundamental peaks could be measured by neutrons, only the synchrotron data were used for ordering determination via site occupancy refinement. The full (style of old version of MAUD program) or partial (new version of MAUD program) site occupancies for several atoms in the unit cell could be refined separately or as in our case based on crystallographic relations (Table 10).

4.2.1 β phase crystallographic restrictions:

There are two atom positions in bcc crystal: 1a and 1b. Probability to take any of the two positions is equal for every atom sort to its concentration and sum of probabilities for every position is equal 1. For β phase an ideal stoichiometric 50:50 Ti:Al composition was refined, see Table 10.

4.2.2 α_2 phase crystallographic restrictions:

The hexagonal α_2 lattice has 8 atoms: two at position d and 6 at position h. The chemical formula of the α_2 phase is Ti_3Al , therefore an ideal stoichiometric 75:25 Ti:Al composition was refined.

Table 10 Dependencies in SO refinement formula for hexagonal α_2/α and cubic β_0/β phases.

β_0/β phase:	α_2/α phase:
1a Ti - Refined	2d Al - Refined
$1a\text{Al} = 1 - SO_{1aTi}$	$6hTi = 1 - SO_{6hAl}$
$1bAl = 1 - SO_{1aAl} = 1a\text{Ti}$	$2dTi = 1 - SO_{2dAl}$
$1bTi = 1 - SO_{1aTi}$	$6hAl = 0.333(3) - 0.333(3)SO_{2dAl}$

4.3 Degree of ordering by direct usage of the reflection intensities ratio

The use of diffraction methods opens the opportunity to determine the degree of ordering based on the intensity of the fundamental and superstructure peaks. The intensity correlation of a theoretical spectrum calculated by the Powder Cell program could be compared with the peaks correlation of the measured spectrums and the corresponding degree of ordering can be determined. Possible site occupancy values were entered into the Powder Cell program and intensity values of the superstructure and fundamental reflection were extracted. Then the intensity correlations of the entered site occupancies were calculated. It should be mentioned that a composition different to the stoichiometric chemical composition will be a reason for a lower degree of ordering. The B-factor increase also changes the intensity correlation. Therefore a correct value of the B-factor gives a more reliable degree of ordering.

The correlation between the intensities of the superstructure 100 and the fundamental 200 β_0/β phase peaks in experimental data has been calculated manually in Excel.

A single peak 2θ region has been chosen, the background was subtracted and the sum of intensity S under the curve was integrated. The degree of ordering D then correlates to:

$$\frac{S_{\text{superstructure refl.}}}{S_{\text{fundamental refl.}}} \quad (33)$$

4.4 Reference peak for temperature correction

A lot of articles described phase transformations of the α_2/α and the γ phases in binary alloys. Therefore the $\alpha_2 \rightarrow \alpha$ phase transformation of Ti-42Al has been used as reference for temperature control. Thus the temperature deviation has been found for neutron measurements with the high temperature furnace. The thermocouple positioned above the sample in the standard high temperature furnace at FRM II shows a temperature difference of 40 °C between experiment and theory for the very good known point of the α_2 to α phase transformation. Such a difference appeared in all samples and can be explained by the distance between the temperature detector and the specimen in the heating furnace. The uncertainty of the temperature measurement that appeared with the high temperature furnace did not appear during dilatometer measurements.

Chapter 5 Laboratory methods results and discussion

The section elucidates results of measurements performed by so called laboratory methods chiefly at room temperature (RT), excepting DSC. After a short presentation of the produced alloys a subchapter “Microstructure”, where the four main types found are described, is followed by “RT synchrotron results”. There the most trustable phase composition is presented. Then EDX results show the elemental content of the phases. The measurement points were chosen with BSE mode of SEM. At the end DSC results are presented.

5.1 Sample compositions

Two samples sets were produced. In the first sample set three binary TiAl alloys (Ti-xAl with x = 39, 42 and 45) and five ternary alloys with additional alloying elements (Ti-42Al-2y with y = Nb, Mo, Ta, Cr and Fe) were melted. The second set includes ternary alloys with different amounts of the β stabilizing elements (Ti-42Al-1, 3 Fe, 4, 6 Mo, 4, 6 Cr, 8.5, 10 Nb, 8.5, 10 Ta). Additionally two semi-binary alloys with boron additions, similar to binary alloys of the first sample set, were included (Ti-39Al-0.2B and Ti-42Al-0.2B) in the second sample set. The addition of boron has been used for a finer grain size [APPL2011]. The different amounts of the β stabilizing elements for the ternary alloys in the second sample set depend from (1) β stabilizing properties of the element (chapter 2.1 and [WILLY2017], [WEISS1998]), as well as from (2) the amount of element in an alloy already produced and investigated by colleagues: 8.5 Nb [STAR2015]. Ta is assumed to have similar β stabilizing properties as Nb. Therefore the same two amounts were used for Ta and Nb. All produced sample compositions are mentioned in Table 11.

Table 11 Nominal chemical composition of the produced samples

First sample set, at%	Second sample set, at%
Ti-42Al-2Fe	Ti-42Al-1Fe
Ti-42Al-2Cr	Ti-42Al-3Fe
Ti-42Al-2Mo	Ti-42Al-4Mo
Ti-42Al-2Nb	Ti-42Al-6Mo
Ti-42Al-2Ta	Ti-42Al-4Cr
Ti-39Al	Ti-42Al-6Cr
Ti-42Al	Ti-42Al-10Nb
Ti-45Al	Ti-42Al-8.5Ta
	Ti-42Al-10Ta
	Ti-42Al-0.2B
	Ti-39Al-0.2B

A detailed overview of the weighted amount of pure elements is listed in Appendix 3A. There an interested reader could see, that the samples have differences lower than 0.2 mass % between calculated and weighted amount. Thus, it was proved that no mistake has been allowed to occur on the step of sample weighting.

5.1.1 Estimation of Al evaporation

Some Al amount could be lost via evaporation during arc-melting due to the high difference of the melting temperatures between Ta, Mo, Nb and Al. The sum of all weighted elements and the resulted button mass after melting was compared with the calculated mass. The difference is visible in Appendix 3B. In order to estimate the error induced by Al evaporation, it was assumed that the complete mass loss resulted only from Al loss. Then the expected chemical composition under this assumption was determined. One can see in APPENDIX 3B, that the highest Al loss occurred in samples with Ta (up to 0.9 at. %) and with Mo (up to 0.4 at. %) which have the highest melting temperatures.

5.2 Microstructures

Both sample sets were analysed by SEM.

5.2.1 Classification of observed microstructures

The microstructure of the investigated samples in both sample sets could be divided into 4 groups: coarse grained, fully lamellar and duplex, and the last one could be further divided into duplex homogeneous and duplex inhomogeneous in dependence of the grain size. Figure 21, Figure 22, Figure 23, Figure 24 show the microstructures of the mentioned samples. The γ phase is characterized by the darkest colour because of its high Al content (with lower amount of electrons than Ti), the α_2 phase appears middle grey, and the β/β_0 phase as the brightest. For all exhibited pictures magnification 50X was used with acceleration voltage 20.0kV, and Back Scattered Diffraction (BSD) signal was detected from the Working Distance of 8.5 mm, No τ_2 or ω_0 phases could be distinguished in the micrographs, mainly due to their low amount, as well as due to similar brightness as β_0/β phases.

Nearly α_2 is a coarse grained microstructure of only two samples: the Ti-39Al and Ti-39Al-0.2B (Figure 21). They could be characterized by mainly α_2 phase with a grainsize from 100 to 1000 μm and different shape, from almost round to more angular shape grain form. The more complicated forms occur mainly due to smaller space between grains, but most of the grains are homogeneously grown in different directions. The γ phase is present in a much smaller amount in Ti-39Al-0.2B than in Ti-39Al and represents needle like black grains. Its amount still not enough to be determined quantitatively, thus no γ peak presented in spectrums.

Fully lamellar microstructure consists of lamellar (γ/α_2)-colonies. In most of the presented samples in this investigation the edges of lamellas are not ideally straight (pictures a – d in Figure 22). Thickness of observed lamellas is different, however, it mainly depends from cross section angle. Often, thickness of a lamella in colonies changes in the present cross section. The lamellas are mainly parallel e.g. in Ti-42Al-8.5Nb (Figure 22e). There lamellar colonies have a diameter of 50 – 100 μm . This relatively coarse grained microstructure can be attributed to HIPing at 1250 °C which is almost in a single-phase α phase field and the subsequent slow furnace cooling [STAR2015]. Additionally, a few small globular γ and β grains can be observed at triple points and colony boundaries [STAR2015]. However, the amount of the globular grains is so low, that the microstructure will still called fully lamellar. The microstructure described by A. Stark [STAR2015] is found to be similar to fully lamellar microstructure of [CLE2006] with the difference of absence of any globular grains on boundaries between lamellas. The small difference in microstructures of Ti-42Al-8.5Nb [STAR2015] and Ti-46Al-9Nb [CLE2006] could be explained by deviating elemental composition of alloys.

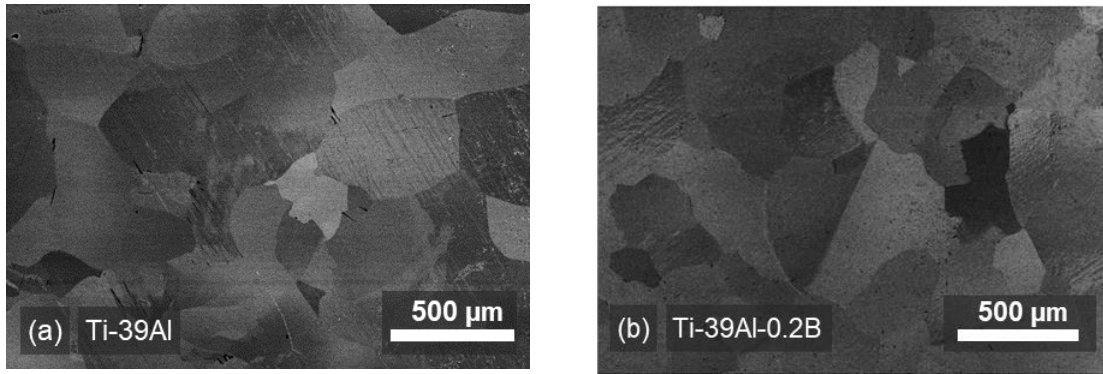


Figure 21 Nearly α_2 coarse grained microstructure

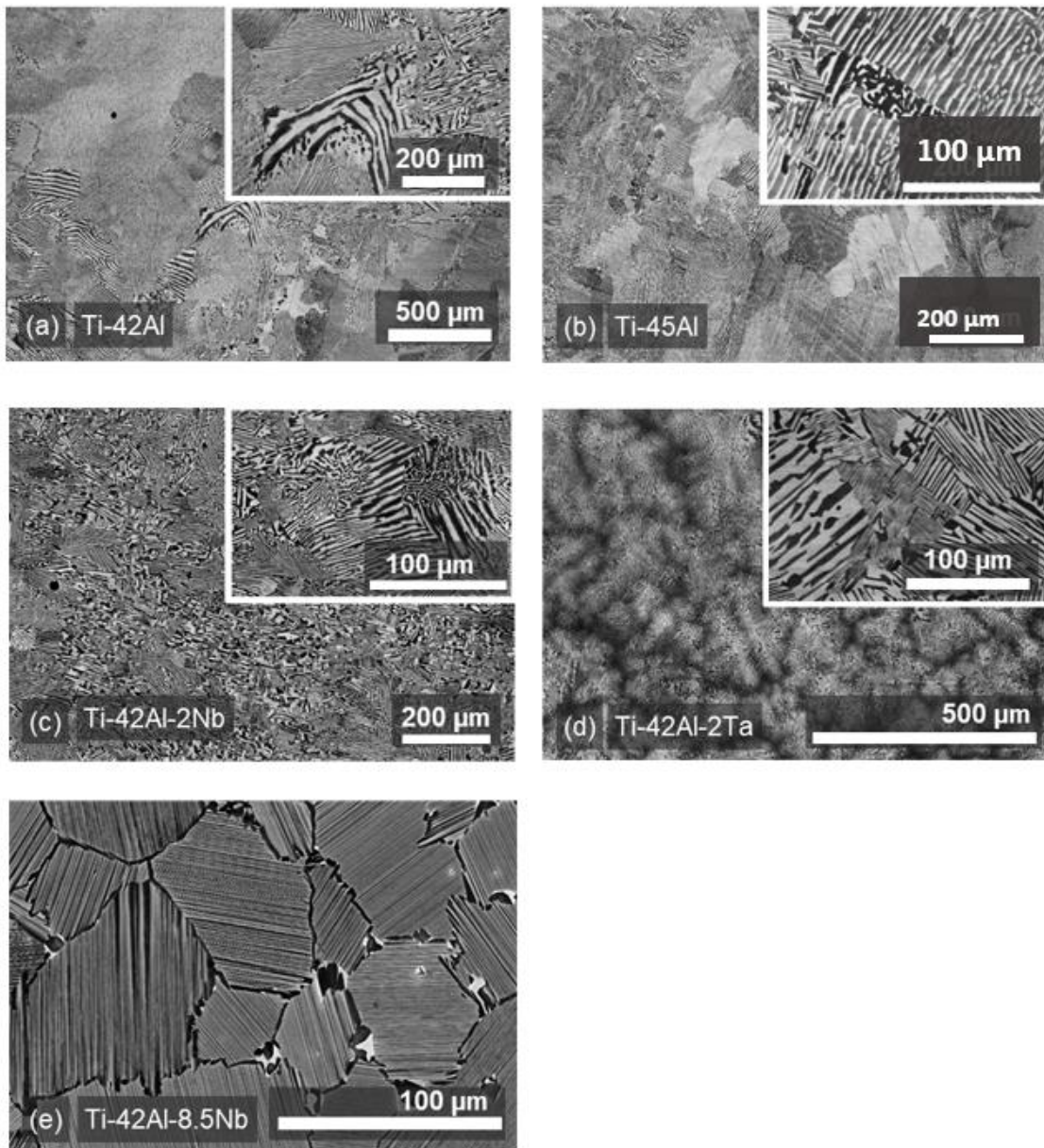


Figure 22 Fully lamellar microstructures

The duplex microstructure differs from the fully lamellar mainly by simultaneous presence of lamellas and a mix of globular γ and β_0 grains situated along the colony boundaries,

with different alignments than the gamma lamellas. A further difference between duplex microstructures could be found on grain size and therefore samples with duplex microstructure could be separated in **duplex homogeneous** (Figure 24) and **inhomogeneous** (Figure 23) structure. The formation of the homogeneous and inhomogeneous duplex microstructure could depend on the amount of grains, which nucleate and grow simultaneously, as well as on the preferred direction of the grain growth.

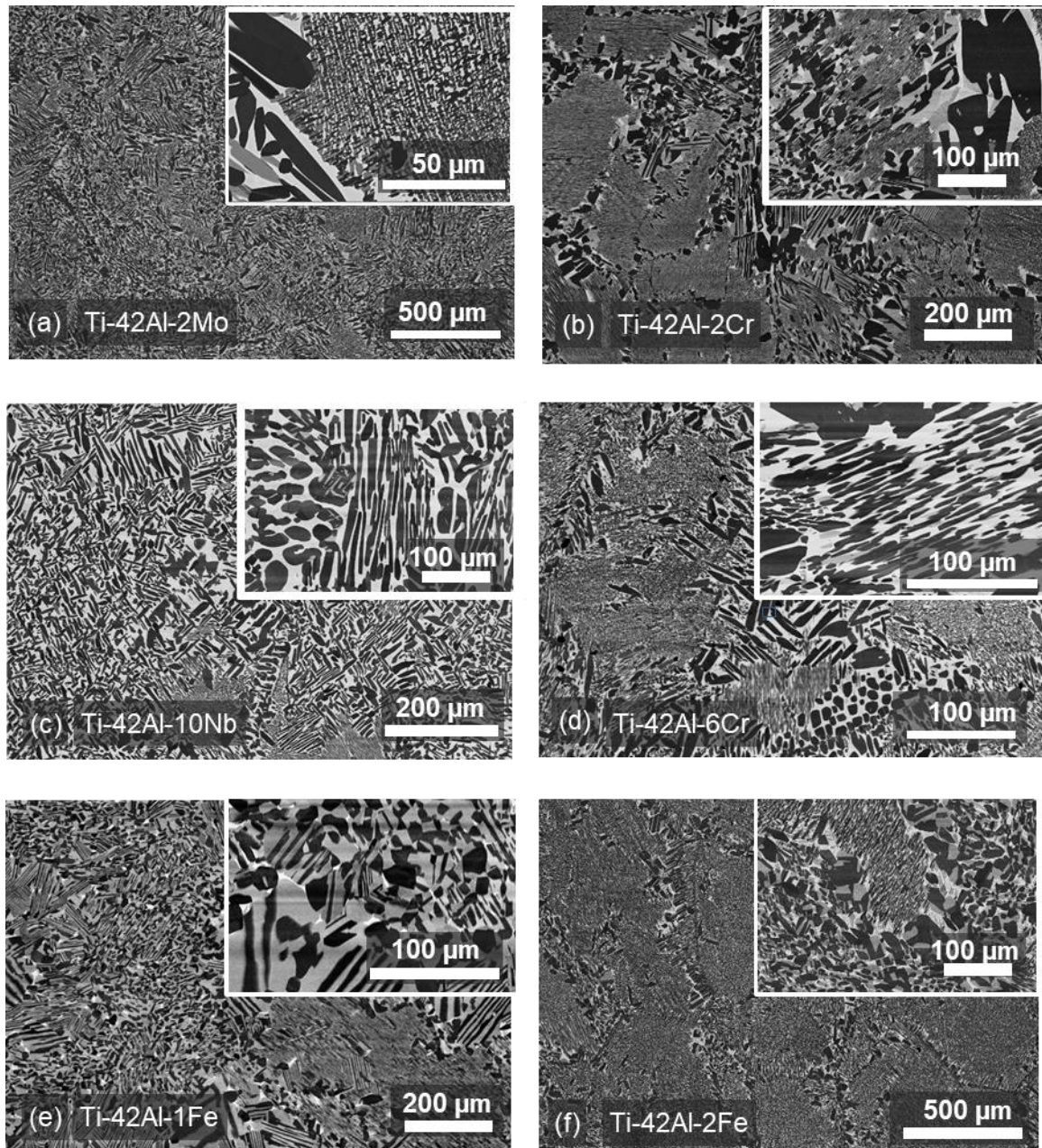


Figure 23 Duplex Inhomogeneous microstructure

In samples with **duplex inhomogeneous** microstructure one can see very good distinguishable fine lamellar areas and big coarse-grained areas. This is the type of microstructure most ternary samples of the first set with 2 at. % of β stabilizing element exhibit.

Most samples of the second sample set are characterized mainly by a **duplex homogeneous** microstructure with almost equal size of lamellas and globularized grains. Ti-42Al-0.2B, Ti-42Al-4, 6 Mo and other contain the globularized γ grains not only on lamellar

boundaries, but also inside of lamellas. It is interesting to mention that some grain boundaries are represented by only one phase - dark γ phase in Ti-42Al-4Mo.

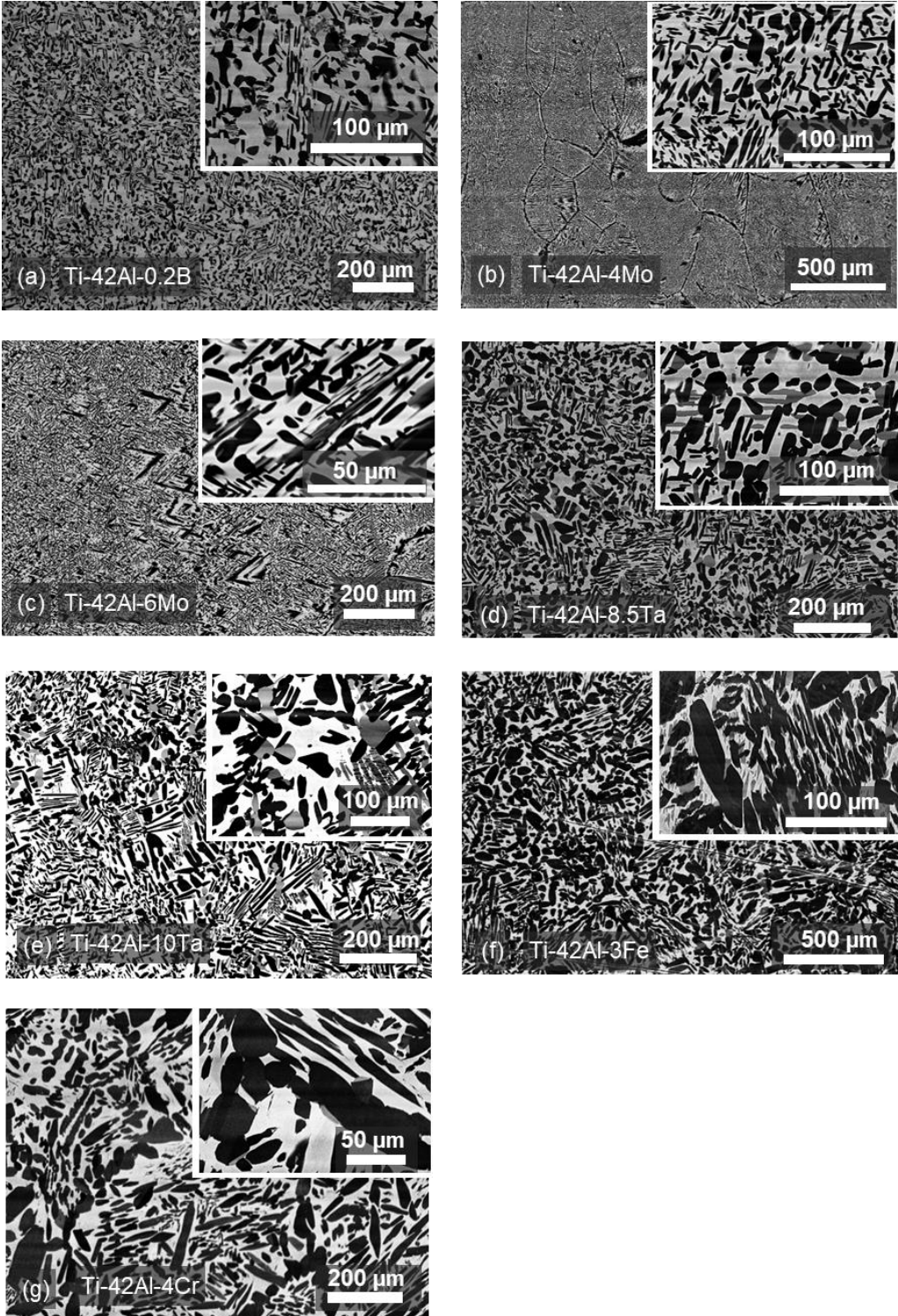


Figure 24 Duplex homogeneous microstructure

Summing up the found microstructure types one can see that ternary alloys show mainly duplex microstructures consisting of spheroidized γ grains and remaining α - γ colonies of large and small size. Spheroidized grains are localized at boundaries of the primary formed β grains. The size of the spheroidized grains is 10 to 100 μm . The big lamellar colonies are up to 50 μm

thick and 200 μm in length. The small lamellar colonies could be long or short, and show a thickness of 1-2 μm for one γ lamella. The lamellar thickness is not the ideal characteristic for γ lamellas size, because this parameter depends on the cross section of a lamella, that appears under the angle of the surface to the lamella in the sample. No preferential direction could be chosen for comparison of the γ lamellar growth orientation in full sample.

All ternary alloys from both sample sets, except Ti-42Al-2Ta and Ti-42Al-2Nb, show the β/β_0 phase in the SEM images. Whereas binary Ti-42Al and Ti-45Al as well as semi binary (Ti-42Al-0.2B) alloys consist only of γ and α_2 phase. It is interesting to mention that the amount of the α_2 phase presented in the second sample set is much smaller than in the first one. Using a program for image analysis the amount of β/β_0 phase was estimated to be about 10, 5 and 10 wt. % correspondingly for Ti-42Al-2Fe, Ti-42Al-2Cr, Ti-42Al-2Mo.

The binary Ti-39Al alloy exhibits a very coarse grained microstructure which consists predominantly of α_2 phase (Figure 21 a). No big influence of 0.2 at. % of boron addition for grain refinement could be observed in Ti-39Al-0.2B (Figure 21 b).

In Table 12 one can see lists of samples for each microstructure group. It is interesting to mention an influence of the increasing amount of β -stabilizing elements on the microstructure: the more β -stabilizing element is present the more homogeneous and fine grained microstructures are observed .

Table 12 Classification of the samples in microstructure groups

Nearly α_2 coarse grained	Fully Lamellar	Duplex inhomogeneous	Duplex homogeneous
Ti-39Al	Ti-42Al	Ti-42Al-2Mo	Ti-42Al-0.2B
Ti-39Al-0.2B	Ti-45Al	Ti-42Al-2Cr	Ti-42Al-4Mo
	Ti-42Al-2Nb	Ti-42Al-10Nb	Ti-42Al-6Mo
	Ti-42Al-2Ta	Ti-42Al-6Cr	Ti-42Al-8.5Ta
	Ti-42Al-8.5Nb (HIP)	Ti-42Al-1Fe	Ti-42Al-10Ta
		Ti-42Al-2Fe	Ti-42Al-3Fe
			Ti-42Al-4Cr

5.2.2 Influence of the amount of β -stabilizing elements on microstructure

We have produced samples with three different amounts of each β -stabilizing element. From the four microstructure types, which were found, not one microstructure type was found in all three samples with the same element. Because all our samples were produced and heat treated in a similar way, the different microstructures mainly result from the different types of β -stabilizing elements and their amounts. Thus as it is shortly mentioned in 5.2.1 subsection the more β -stabilizing element is present, the more homogeneous and fine grained a microstructures could be observed. One can observe it in more details in samples with Mo and Fe. **An addition of Mo** in the amount of 2 at. % results in a duplex inhomogeneous microstructure. A higher amount of Mo, 4 and 6 at. %, results in a duplex homogeneous microstructure. Similar to Mo the **influence of Fe** results in a duplex inhomogeneous microstructure for a small amount of Fe (1 and 2 at. %) and in a duplex homogeneous microstructure for 3 at. %. Such a tendency could be most probably explained by the influence of the β -stabilizing element on the kinetics of each

phase transformation that changes the velocity of grain growth. **Influence of Cr** is little bit different from Mo and Fe. Even if 2 at. % of Cr results in a duplex inhomogeneous microstructure and 4 at. % of Cr results in a duplex homogeneous microstructure, however, 6 at. % of Cr results in a duplex inhomogeneous microstructure again.

Samples with **Nb** and **Ta** follow the trend of microstructure refining with increasing element content. The samples with 2 and 8.5 at. % of **Nb** and 2 at. % **Ta** have a **fully lamellar** microstructure. In samples with higher Ta content up to 8.5 and 10 at. % the microstructure is **duplex homogeneous** and with 10 at. % of Nb it is **duplex inhomogeneous**.

In samples of Ti-42Al-2Ta one can observe areas of different element concentration (dark clouds). These could be explained by segregation during cooling down after melting. The homogenization time was not enough to dissolve the segregation due to the low diffusivity of the Ta atoms in comparison to other elements employed in the study.

The second sample set, due to the higher content of β -stabilizing elements, contains a very small amount of the α_2 phase. Therefore γ grains precipitated directly into the β grains.

It should be mentioned, that when comparing our sample microstructures with literature ones, the processing history should be taken into account. In literature similar segregations were found by Singh [SING1997] in Ti-48Al-4Mo (fig. 5e) or Ti-50Al-2Mo (fig. 1 of Sing).

A similar microstructure of the γ precipitation in the β grains we already observed in literature e.g. on fig. 6i of [SING1997]. Our microstructures solidified via β -phase, similar to alloys published by Erdely which were β -homogenized and isothermally annealed at 900 °C for 100 hours (figure 1d at [ERD2019], however, not very similar to cast/HIP (as in figure 1a at [ERD2019]), which exhibit stronger γ phase precipitations in β phase matrix. In the work of [SCHL2014] Fig. 3 b shows at higher magnification SEM image taken in BSE mode of the NL + γ microstructure of the heat-treated TNM alloy. There γ phase precipitates in the $\beta_0 + \omega_0$ phases.

It should be mentioned that some additional phases are indistinguishable from the β -phase by SEM in our samples. Such phases are the τ_2 phase in samples with 2 and 3 at. % of Fe, and the ω_0 phase in samples with 8.5, 10 at. % of Ta and Nb. Small amounts of those phases are found by synchrotron XRD (will be discussed in chapter 5.3). Their small amount and a similar chemical composition like β -phase could be the reason for their indistinguishability by SEM.

5.2.3 Absence of α_2/α phase in the samples of the second sample set

Parallel to microstructure types classification it was mentioned that almost no α_2/α phase in the samples was found in the second sample set. That is an important results when the diffraction data of that sample set are analyzed.

5.3 Synchrotron RT data of rotated samples

Here phase content and lattice parameter values for both sample sets are compared in Table 13 and Table 14 correspondingly. As mentioned in the chapter 3 this RT measurements have been performed additionally, with sample rotation for better grain statistics.

The data exhibited in Table 13 present the most trustable phase composition of our investigation because the grain statistic problem was reduced by sample rotation. One can see very small amounts of α_2/α phase in the samples of the second sample set with a higher than 2 at. %. content of Ta, Mo, Nb and Cr.

In samples with Ta and Nb a simultaneous presence of the ω_0 and the β/β_0 phase was found. Although that contradicts the Gibbs phase rule of equilibrium state. But ω_0 presence is supported by the superstructure 100 peak of the ω_0 while the β_0 phase presence is needed as well. Otherwise the high intensity of the common 102 ω_0 and 110 β_0 peak could not be explained. A refinement with presence of both the ω_0 and the β/β_0 phases simultaneously has been performed. The presence of both the ω_0 and the β/β_0 phases simultaneously is explained by not enough slow cooling from the homogenisation temperature of 1100 °C. This could indicate that our samples' state of phase composition slightly deviates from equilibrium state.

Table 13 Averaged phase content in vol. % between three measurements refined for each sample based on RT synchrotron data with rotation. Ti-42Al was not available for rotation measurements, therefore data from a RT measurement with rotation (except Ti-42Al) were used.

Sample	Phase content, vol. %				
	α_2/α	β_0/β	Omega O/Tau ₂	γ	\pm
2Mo	17.96	22.16			59.89
4Mo	1.4	59.8			38.8
6Mo	1.0	67.7			31.4
2Cr	27.4	21.8			50.7
4Cr	1.6	54.8			43.6
6Cr	3.2	60.0			36.8
2Ta	49.1	0			50.9
8.5Ta+Omega	19.5		38.5		41.9
8.5Ta	1.5	84.6			14.0
10Ta+OmegaO	24.5		35.8		39.7
10Ta	9.9	74.1			16.1
2Fe +Tau2	57.8	4.6	14.5		23.2
2Fe	67.6	5.2			27.2
1Fe	45.9	0			54.1
3Fe+Tau 2	31.7	13.8	33.8		21.8
3Fe	46.4	20.3			33.3
8.5Nb+OmegaO	70.3		1.6		28.1
8.5Nb	65.8	7.7			26.4
10Nb+Omega	11.8		22.4		65.9
10Nb	6.1	59.7			34.2
39Al	100	0			0
39Al	92.0	0			8.0
39Al0.2B	100	0			0
39Al0.2	96.1	0			3.9
42Al+0.2B	52.6	0			47.4
45Al	20.1	0			80.0
42Al (measured without Rotation)	53.0				47.0

Ti-42Al-3Fe sample contains some amount of τ_2 and no τ_2 phases was found at RT in Ti-42Al-1 or 2Fe. Thus one can assume that further increase of Fe content also will give presence of τ_2 phase even in higher amount. According to the refinement the τ_2 phase appears on cost of not only β_0 but α_2 and γ phases as well.

Summing up the refinement of the phase content at RT it is possible to say, that while rotation was applied the quality of data is much better. Although, there is an unexpected result. Namely in Ti-42Al-3Fe sample addition of τ_2 reduced amount of all three phases, that was not expected due to τ_2 phase is known to be connected with β phase via $\beta \rightarrow \tau_2 \rightarrow \beta$ phase transition.

The lattice parameters refined based on the RT synchrotron data with rotation, are shown in Table 14. It could be seen in Table 14 that there is a similar small difference between lattice parameters up to ± 0.05 Å between samples. As well by comparison of the data with the not rotated sample synchrotron measurements difference up to 0.009 Å in the same sample.

The difference in the lattice parameters, as it is known from solid state physics, is dependent from the atom radius of the contained elements, their amount and electronegativity. While the amount of our β -stabilizing element is not too high, but their highest amount is concentrated in the β/β_0 phase (see Table 15), therefore the highest difference is expected and observed in the β/β_0 lattice parameters between different samples.

Table 14 Refined lattice parameter from RT synchrotron data with sample rotation. No Ti-42Al sample was available for performed measurements with rotation.

Title	β/β_0 a, Å	α_2 a, Å	α_2 c, Å	c/a	γ , a, Å	γ , c, Å	c/a	ω_0 a, Å	ω_0 c, Å	τ_2 a, Å
Appel	3.210	5.775	4.638	0.803	4.012	4.065	1.013			
Ti-42Al-2Mo	3.204	5.761	4.623	0.802	4.018	4.053	1.009			
Ti-42Al-4Mo	3.198	5.787	4.579	0.791	4.015	4.052	1.009			
Ti-42Al-6Mo	3.191	5.792	4.570	0.789	4.011	4.056	1.011			
Ti-42Al-2Cr	3.181	5.752	4.613	0.802	4.014	4.050	1.009			
Ti-42Al-4Cr	3.166	5.785	4.542	0.785	4.006	4.042	1.009			
Ti-42Al-6Cr	3.183	5.767	4.589	0.796	4.012	4.045	1.008			
Ti-42Al-2Ta		5.762	4.626	0.803	4.018	4.059	1.010			
Ti-42Al-8.5Ta	3.217	5.782	4.591	0.794	4.023	4.055	1.008	4.562	5.532	
Ti-42Al-10Ta	3.216	5.779	4.606	0.797	4.023	4.052	1.007	4.562	5.530	
Ti-42Al-2Fe+Tau2	3.212	5.762	4.623	0.802	4.012	4.050	1.010			12.143
Ti-42Al-1Fe		5.755	4.619	0.803	4.013	4.052	1.010			
Ti-42Al-3Fe+Tau2	3.218	5.765	4.618	0.801	4.010	4.050	1.010			12.128
Ti-42Al-2Nb	No sample is available any more for diffraction measurements									
Ti-42Al-8.5Nb with Omega	3.221	5.762	4.640	0.805	4.023	4.066	1.011	4.576	5.525	
Ti-42Al-10Nb with Omega	3.219	5.775	4.631	0.802	4.025	4.062	1.009	4.571	5.527	
Ti-39Al ohne Beta		5.757	4.621	0.803	4.044	4.080	1.009			
Ti-39Al only alpha		5.755	4.625	0.804						
Ti-39Al-0.2B only Alpha		5.753	4.618	0.803						
Ti-42Al-0.2B ohne Beta		5.758	4.624	0.803	4.016	4.061	1.011			
Ti-45Al		5.764	4.629	0.803	4.016	4.059	1.011			

Lattice parameters are least depended from the quality of the diffraction rings. Only in much worse cases than most of our samples represent, a determination problem could occur. They will be discussed later in subchapter 7.1.1 in comparison with other methods.

5.4 EDX

EDX measurements were performed to investigate the elements' distribution between phases. Appendix 3D exhibits the average element content for β/β_0 , α_2/α , γ phases as well as the standard deviation according to weighted amounts of elements and Table 15 exhibits the same numbers without standard deviations. Some similarity of Al and Ti content could be observed between β_0/β and α_2/α phases. Therefore it is sometimes not easy to determine which phase is present, based on the brightness of SEM picture, which is dependent on the amount of heavy elements. As one could expect from the binary TiAl phase diagram the γ phase is more enriched with Al than β_0/β and α_2/α phases. A way to distinguish the β_0/β and the α_2/α phases is by the amount of the third element, which as the β stabilizing element has a higher concentration in the β_0/β phase. The third elements being in the most cases more heavy elements therefore yield to higher brightness of the β phase.

Table 15 Average elemental content of phases

Sample composition	α_2/α , at. %			β_0/β , at. %			γ , at. %		
	Al	Ti	El	Al	Ti	El	Al	Ti	El
Ti-39Al	39	61					Too low amount of γ phase		
Ti-39Al-0.2B	38	62							
Ti-42Al-0.2B	38	62					46	54	
Ti-42Al-1Fe	33	63	4				45	53	1
Ti-42Al-2Fe	37	63		32	61	7	46	54	2
Ti-42Al-3Fe				34	61	5	46	54	1
Ti-42Al-2Mo				35	60	5	46	53	1
Ti-42Al-4Mo				35	60	5	46	54	1
Ti-42Al-6Mo				36	56	8	47	52	1
Ti-42Al-2Cr	34	60	7				46	53	1
Ti-42Al-4Cr	36	60	4	33	56	11	46	52	2
Ti-42Al-6Cr	37	60	3	34	59	7	46	52	2
Ti-42Al-2Nb	37	61	1				45	54	1
Ti-42Al-10Nb				36	54	10	46	47	7
Ti-42Al-2Ta	37	61	2				45	54	1
Ti-42Al-10Ta	39	52	8	37	51	12	47	47	7

In an overall estimation the precision of the measurements could be improved if a reference sample for every ternary element composition under investigation would be available. The current precision is known to be up to ± 3 at. %. Such an high uncertainty could be explained by precision of the EDX method itself.

The third element content is higher than it was expected to see, in β_0/β phase and less in γ and α_2/α phases. This could be explained by different distribution of elements between phases.

Al is mainly concentrated in the γ phase and Ti in the α_2 phase. Thus the middle chemical composition of the sample depends (1) from phase content as well as (2) from element content of each phase. The other physical reason of difference between nominal and real sample composition, are mentioned in Appendix 3A:

- Difference in the weighted amount of elements up to 0.12 mg.
- Evaporation of the light element Al with low melting and boiling points during arc melting relative to the high melting point elements Mo, Ta, Nb. Melting point of Fe and Cr is lower therefore heating time of the element collection is less, therefore evaporation of Al was also less.
- Probably not fully homogeneous distribution of high melting point elements in the sample because the heat treatment was performed at 1100 °C, where diffusion is much slower as close to the melting point. The Table 15 and possible reasons are used further by estimation of methods errors in chapter 8.

5.5 DSC

The results of the DSC method were a first attempt to specify the temperature region of the $\beta_0 \rightarrow \beta$ and other phase transformations. A results curve is exhibited in Figure 25 below. The figure shows, how heat exchange was changed during heating and cooling in temperature range up to 1530 °C. Three changes of the heat flow have been detected and could be connected according to the known temperatures in binary alloys with (1) $\alpha_2 \rightarrow \alpha$, (2) γ -solvus, and (3) $\alpha \rightarrow \beta$ phase transformations, but not with $\beta_0 \rightarrow \beta$. The $\beta_0 \rightarrow \beta$ transformation is known to be a second order phase transformation as any order-disorder phase transformation. The second order phase transformations are not connected with heat exchange, thus invisible by DSC curve. This is in contrast to some reports in literature, where the $\beta_0 \rightarrow \beta$ phase transformation temperatures in ternary alloys of Ti-Al-Fe and Ti-Al-Cr systems were found [OHNM2000] and extrapolated to binary alloys. However, as long as the $\beta_0 \rightarrow \beta$ phase transformation is characterized as phase transition of the second order, no $\beta_0 \rightarrow \beta$ phase transformation will be visible by DSC measurements. Therefore DSC was not found to be ideal for studies of the $\beta_0 \rightarrow \beta$ phase transformation.

When the $\beta_0 \rightarrow \beta$ phase transformation would be visible, it could be covered by the $\alpha_2 \rightarrow \alpha$ transformation. The $\alpha_2 \rightarrow \alpha$ is also the ordering phase transformation, is, however, visible by DSC in several literature sources. This contradiction will be covered by the Appendix 1. exhibits the temperatures of the mentioned phase transformations in all samples of the 1st sample set. In the discussion the temperatures of $\alpha_2 \rightarrow \alpha$ and γ - solvus phase transformations could be compared with values of synchrotron and neutron data.

It is interesting to mention that during cooling one can see in Figure 25 that three peaks are appearing similar as during heating. However, there is an overcooling temperature differences between the peaks of cooling and heating. The peaks during cooling correspond to the backward phase transformations (1) $\alpha \rightarrow \alpha_2$, (2) γ -formation, and (3) $\beta \rightarrow \alpha$. One also can mention that the temperature difference of forward and backward phase transformations during heating and cooling is not equal for different phases. That could be explained by different kinetics of the phase transformations.

Summing up the DSC results, one can say that DSC allowed to detect such phase transformation as (1) the $\alpha_2 \rightarrow \alpha$ (2) the γ - solvus, (3) the $\alpha \rightarrow \beta$. One can find no temperature of the $\beta_0 \rightarrow \beta$ phase transformation. The second sample set was not yet investigated by DSC.

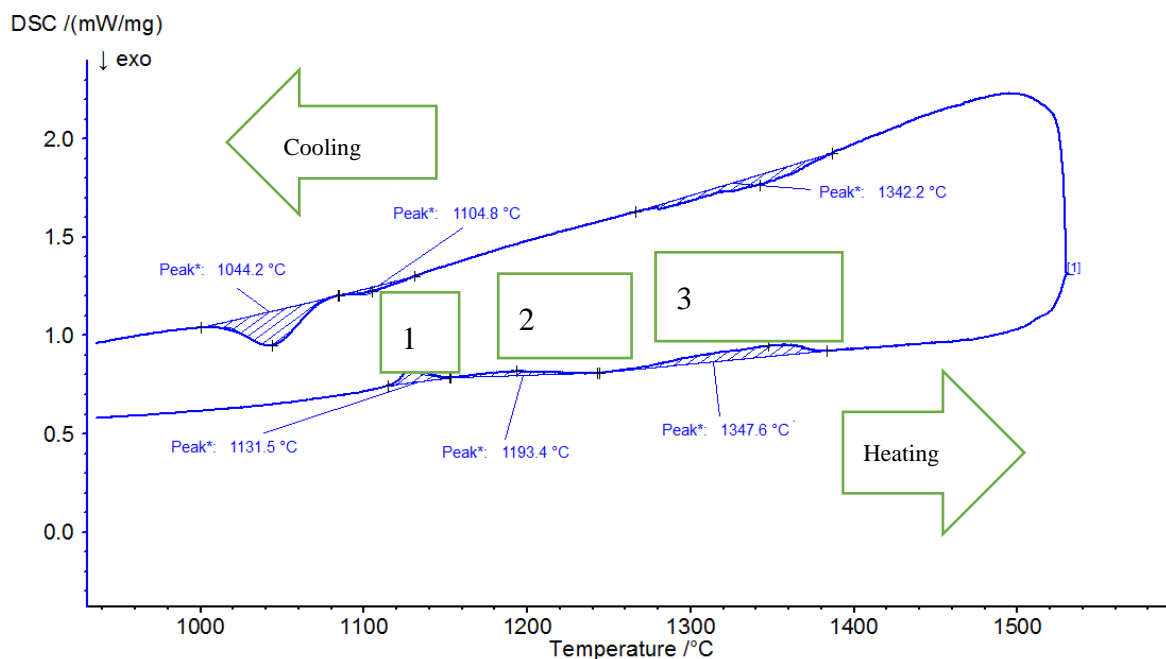


Figure 25 DSC results of Ti-42Al-2Cr 1. $\alpha_2 \rightarrow \alpha$, 2. γ -solvus, 3. $\alpha \rightarrow \beta$. Temperatures of the phase back transformations are lower than during heating, due to undercooling, which is observed in every sample.

Table 16 Temperatures of the phase transformation during heating

Sample name	$\alpha_2 \rightarrow \alpha$	$\gamma \rightarrow \alpha$	$\alpha \rightarrow \beta$
Ti-45Al	1139.0	1287.7	1460.1
Ti-42Al-2Ta	1139.5	1211.9	1393.3
Ti-42Al-2Nb	1142.0	1216.9	1380.2
Ti-42Al-2Cr	1131.3	1193.4	1347.6
Ti-42Al-2Mo	1157.5	1234.2	1348.6
Ti-39Al	1144.3		1318.2
Ti-42Al	1130.2	1206.7	1391.3
Ti-42Al-2Fe	1093.2	1241.9	

5.6 Oxygen content

The mean oxygen content of the samples increases from Ti-45Al (395) over Ti-42Al-2Mo (470), Ti-42Al-2Nb (490), Ti-39Al (536), Ti-42Al-2Ta (731), Ti-42Al-2Fe (739) up to Ti-42Al-2Cr (863) $\mu\text{g/g}$. The high oxygen content in the 2Cr sample could be explained by a high affinity of Cr to oxygen that allows to form oxides easy. In principle all refractory metals of the IV and V groups (as Nb and Ta) have a high affinity to oxygen [MEER1963] as well as Al. However there is no clear trend from the 1st sample set and the oxygen level is in the range usually found in TiAl alloys produced with the arc melting furnace. The second sample set values are as follow: Ti-42Al-8,5Ta (225); Ti-42Al-3Fe (426); Ti-42Al-10Nb (451); Ti-42Al-6Mo (466); Ti-42Al-4Cr (493); Ti-42Al-6Cr (704); Ti-42Al-1Fe (836); Ti-42Al-10Ta (865); Ti-42Al-0,2B (919); Ti-39Al-0,2B (1247); Ti-42Al-4Mo (1401) $\mu\text{g/g}$. With increase of Fe and Nb the O_2 content decreases. Cr and Ta have no straight tendency, thus no confirmation of the

version of affinity to the oxygen. Sample with 2 and 6 Mo have close O₂ content in contrast the very high value of the 4Mo. In literature [ZOLL2007] it is known that "increase of the oxygen content increases volume fraction of the α phase formed during peritectic solidification and leads to a change of the β primary solidification phase to the α phase in ternary Ti-44.2Al-1.4O, Ti-47.3Al-0.9O and Ti-47.2Al-1.5O (at. %) alloys". In our alloys the sample with 2Mo is characterised by the highest β_0 content and the smallest α/α_2 in comparison to samples with 2Cr and 2Fe, having the similar α/α_2 phase content, that does not confirm the tendency of [ZOLL2007]. The theory can be confirmed only by the binary Ti-39Al and Ti-39Al-0.2B having the higher O₂ content and consisting predominantly of the α_2 phase. However, due to altering of the microstructure during heat treatment it is hard to estimate the real solidification pathway for our alloys.

Chapter 6. In situ diffraction investigation results and discussion

In situ diffraction measurements were carried out by synchrotron and neutron radiation. At first the synchrotron data will be described then the neutron data according to decrease of the derived amount of information.

Two data interpretation methods were used to determine the α_2/α and the β_0/β phase transformations as well as the γ -solvus temperature: Rietveld refinement method and Gauss-fit of single peaks. The theory of this methods is described in chapter 2. Advantages and disadvantages of both methods for extraction of some parameters are discussed in subchapter 8.1.2.1. Problems with grain statistics occurred at HT in both synchrotron as well as neutron in situ measurements. The problems are shown in graph form in Appendix 2B. Sample Ti-39Al has especially bad grain statistics, therefore its data was found impossible to be refined properly. That is covered in Appendix 2B.

6.1 Synchrotron in situ measurements results

As mentioned in chapter 2 “Basics” our alloys consist mainly of α_2 , β_0/β and γ phases at RT, which transforms to the α and β phases at HT. Small scattering angles of synchrotron radiation allow to detect a lot of peaks of different phases simultaneously. Thus many parameters as: changes of phase amount with temperature, lattice parameter and site occupancy of α_2/α , β_0/β phases were refined and will be described here in the mentioned order for the first sample set and the semi binary (boron containing) samples from the second sample set.

In subchapter 5.3 the presence of additional phases was described as found in diffraction experiments at RT with rotation. These are ω_0 and τ_2 phases. At RT measurements carried out exactly before heating normally very small or zero content of these phases was found. With increasing temperatures up to 600-800 °C the amount of the additional phases decreases and disappears up to 1000 °C. The presence of these phases especially in the range of service temperature could change mechanical properties of the alloys. Thus, the subchapter 6.1.4 further describes phase change behaviour in Ti-42Al-2Fe due to the τ_2 phase presence in more details. Additionally it was interesting to examine whether the site occupancy of the β_0/β phase was changed due to the τ_2 phase content increase or disappearance. Above 1000 °C there is already no τ_2 phase, but the presence of standard phases the α_2 , and the γ phases, as well as the phase transformation temperature sequence will be discussed in more details and compared with literature data in subchapter 7.1.1.2.

It should be mentioned that the $\alpha_2 \rightarrow \alpha$ phase transformation and the γ -solvus temperatures are already well investigated for binary alloys. Therefore they were used as a reference to verify the quality of the refinement result. E.g. the $\alpha_2 \rightarrow \alpha$ transformation of binary Ti-42Al and Ti-45Al was expected and detected at 1120 °C. The difference in temperature of the $\alpha_2 \rightarrow \alpha$ transformation in ternary alloys could be considered as the influence of the third alloys. However an amount of α_2/α phase is too small in the second sample set, thus no phase transformation temperature is possible to determine.

6.1.1. β_0/β phase content and $\beta_0 \rightarrow \beta$ phase transformation temperature

That is one of the most important results of current investigation. The amounts of the β_0 and the β phases together were determined by synchrotron (Figure 26). In order to distinguish between the β_0 and the β phases the site occupancy parameter and the weak 100 superposition reflection intensity were used, that will be described further in subchapter 6.1.5.

In a temperature range from room temperature up to 1200 °C only three samples of the first sample set contain the β_0/β phase: Ti-42Al-2Mo, Ti-42Al-2Fe, Ti-42Al-2Cr. The amount of the β_0/β increases only slightly and homogeneously in the temperature range between RT and 900 °C in samples with Mo and Cr. Then the β_0 phase content increases up to 1100 °C decreases subsequently and increases again up to 100 %. Such behaviour of the β_0/β phase amount depends from presence of the other phases. The error bars are built as a standard deviation, have very close values to the determined symbols in lines, shown with black colour.

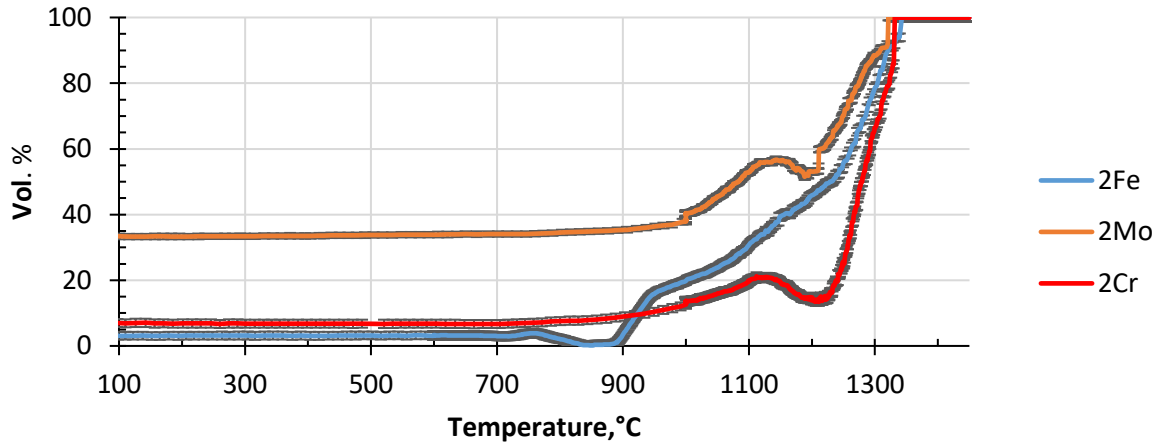


Figure 26 The β_0 and β phases content of alloys which contain β_0/β phase already at RT.

As the reader can see in Figure 26 the amount of the β_0/β phase in samples with -2Fe, -2Cr, -2Mo was fixed at 100 % after it reached a maximum value during refinement. (The temperatures are close but not equal between different samples. These temperatures are affected by worsening grain statistics and thus are not described in more details). Without manual fixation the phase amount starts to jump above 1250 °C.

6.1.1.1 $\beta_0 \rightarrow \beta$ phase transformation temperature

Table 17 contains the $\beta_0 \rightarrow \beta$ phase transformation temperature for the first sample set. The samples are arranged according to the increase of the temperature Ti-42Al-2Cr, Ti-42Al-2Fe, Ti-42Al-2Mo. The $\beta_0 \rightarrow \beta$ phase transformation temperature for the second sample set is given in appendix 5. The best case would be when both interpretation methods would give the same temperature up to ± 1 °C, however, it is restricted by the measurements precision at HT.

Table 17 Temperatures of $\beta_0 \rightarrow \beta$ phase transformation in °C.

Sample	Single peak Gauss fit 100	MAUD
Ti-42Al-2Fe	1123	1122
Ti-42Al-2Mo	1204	1197
Ti-42Al-2Cr	1111	1110

Difference between the two interpretation methods is very small and only for Mo reaches 7 °C. The phase transformations will be compared further with the neutron data.

The binary alloys, as it could be expected from the binary phase diagram, also contain some amount of the β , but not the β_0 , phase above 1350-1400 °C [APPL2011]. However, in all samples above 1250 °C grain statistic is far from that of an ideal powder sample. Therefore the determined phase fraction value is not reliable (lower as few %). Only the transformation

temperature from the α to the $\alpha+\beta$ phase field can be estimated by the first appearance of the β 110 and 200 peaks. These peaks are fundamental ones. No superstructure peak was found in the spectrum of binary and ternary alloys above 1250 °C. The β , without the presence of the β_0 , was found also in ternary alloys with 2 at. % of Ta and Nb at temperatures above 1300 °C (Table 18, Figure 27). In Appendix 4 temperature of the β phase appearance in binary and ternary alloys without the β_0 phase at RT are shown with spectrums for proof and an estimation of their quality.

All ternary samples of the second sample set exhibited the β_0 phase presence. The β_0/β phase transformation temperature, determined by Gauss-fit only is inserted to the Appendix 5 as well.

Sample Composition	°C
Ti-42Al	1338
Ti-42Al-0.2B	1330
Ti-45Al	1377
Ti-42Al-2Ta	1329
Ti-42Al-2Nb	1327

Table 18 Temperature of the β phase appearance in binary and ternary alloys without the β_0 phase at RT

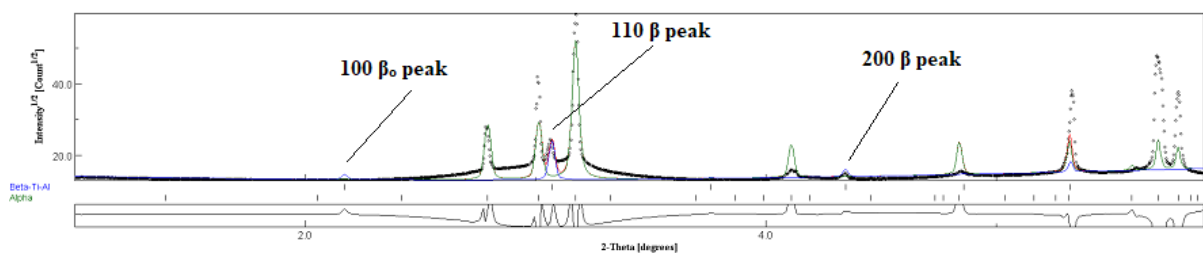


Figure 27 Spectrum of Ti-42Al-2Nb at 1330 °C. One can see the fundamental 110 and 200 peaks while the superstructure 100 peak is absent

6.1.2 γ phase content and γ -solvus temperature

A significant amount of γ phase is present in all samples except Ti-39Al binary alloy. Figure 28 shows the comparison of γ phase content between samples of the first sample set. The γ phase content stays constant from RT up to 1100 °C and slowly decreases above 1180 °C in most of the samples. Thus it is interesting to observe in Figure 28 the graphs above 800 °C only. In the binary Ti-39Al alloy very little amount of the γ phase was detected, that corresponds to the SEM images of Ti-39Al. The Ti-39Al-0.2B sample contains only α phase. The γ solvus temperatures determined by Rietveld analysis and Gauss-fit are shown in Table 19. The difference between results acquired with various methods will be explained in the 7th chapter.

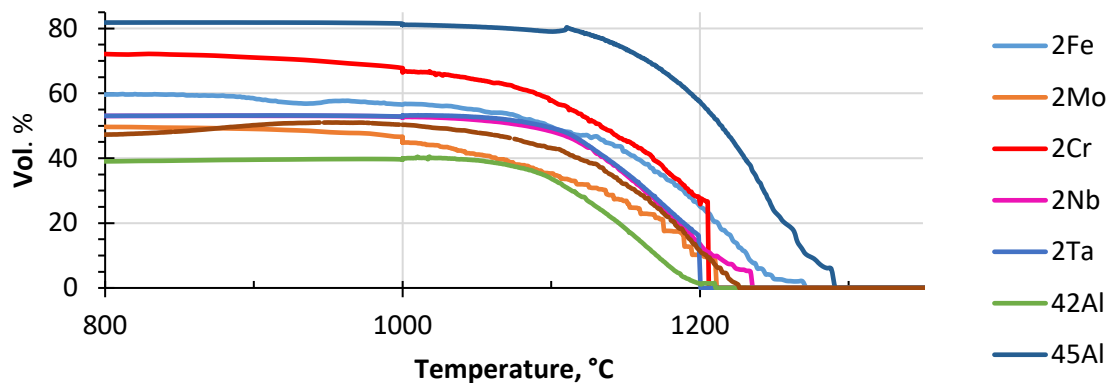


Figure 28 γ phase content in samples from the first sample set

A significant γ stabilizing effect of the different alloying elements can be observed in the temperature region between RT and 1000 °C. In accordance with decreasing γ phase fraction the samples can be put in the following order: Ti-45Al, Ti-42Al-2Cr, Ti-42Al-2Fe, Ti-42Al-2Ta, Ti-42Al-2Nb, Ti-42Al-2Mo, Ti-42Al. By comparing the same Al content the strongest γ stabilizer seems to be Cr, then Fe, Nb, Ta, and Mo which has the lowest γ stabilizing properties.

6.1.2.1 γ -solvus temperature

The γ -solvus temperature could be a reference temperature when determined for the binary alloys. According to the binary phase diagram (Figure 2) the γ -solvus temperature for Ti-42Al should be expected at 1220 °C. However the temperature according to the synchrotron data is 10 °C lower (Table 19). The difference could be explained by small deviations in the chemical composition of our sample from nominal one or by a small dependency on the heating rate, as well as precision in the temperature measurements of ± 1 % from measured temperature. In accordance with an increasing γ solvus temperature based on the Gauss fit data the samples can be put in the following order: Ti-42Al-2Mo, Ti-42Al-2Cr, Ti-42Al, Ti-42Al-2Ta, Ti-42Al-2Nb, Ti-42Al-2Fe, Ti-45Al.

One can see how the γ phase stabilizing properties change between third elements and Al content. Al is known as the strongest γ phase stabilizer. Ti-45Al sample is characterized by the highest amount of γ phase and the highest γ solvus temperature. The sequences of the increase in the γ solvus temperature and the γ phase content are partly similar to each other. E.g. in the Mo sample the amount of γ phase is low and the γ solvus temperature is low. In Ti-42Al-2Cr certainly the amount of γ phase is high but the γ solvus temperature is only slightly higher than in the Mo sample. Ti-42Al-2Nb, Ti-42Al-2Ta have a γ solvus temperature in the middle of the range of investigated alloys and also their phase content is in the middle. In Ti-42Al-2Fe a high γ phase content don't correlates with a γ -solvus temperature in the middle range.

The difference between temperatures evaluated with MAUD and Gauss fit are mainly very small (up to 6 °C), only Ti-42Al-2Fe has 11 °C and Ti-42Al-2Ta 14 °C difference. The values will be compared with neutron ones and discussed in subchapter 8.1.2.1.

Table 19 Temperatures in °C of the γ -solvus based on the Rietveld refinement method and Gauss-fit of single peak for synchrotron data

Sample	MAUD (Rietveld refinement)	Gauss
Ti-42Al	1210	1211
Ti-45Al	1288	1286
Ti-42Al-2Fe	1269	1258
Ti-42Al-2Mo	1212	1206
Ti-42Al-2Cr	1211	1209
Ti-42Al-2Nb	1235	1238
Ti-42Al-2Ta	1201	1215

6.1.3 The α_2/α phase content and temperature of the $\alpha_2 \rightarrow \alpha$ transformation

In Figure 29 one can observe the change of the α_2/α phase content with temperature. α_2 phase remains constant from RT to 1000 °C for almost all samples. Therefore the graphs in Figure 29 start from 700 °C. Only Ti-42Al starts from 800 °C due a synchrotron beam loss below 800 °C. In Ti-42Al-2Fe an appearance of the τ_2 phase interrupts the constant α_2 phase content before 1000 °C.

The α_2/α phase content in Ti-42Al-2Fe decreased between 700 °C and 800 °C from 34 vol. % by 2 vol. %, then came back to 34 vol. % from 800 °C to 900 °C, decreased again to 20 vol. % between 1000 °C and 1100 °C, increased up to 41 vol. % between 1155° and 1231 °C before finally disappearing at 1347 °C. Ti-42Al-2Mo has a constant α_2/α phase content up to 1000 °C. Then it shows a similar but less steep decrease of the α_2/α phase content by 4 vol. % than Ti-42Al-2Fe. Above 1116 °C a temporary increase of the α_2/α phase content up to a local maximum around 1200 °C is followed by a complete dissolution slightly above 1300 °C. Such a decrease at about 1100 °C (before increased from 1116 °C) could be correlated with partial replacement of the α_2/α phase by the β_o/β phase. However for Ti-42Al-2Cr this assumption is not fulfilled (see next paragraph).

Ti-42Al-2Cr and alloys without additional β_o/β phase (at temperatures above 1000 °C show no decrease of the α_2/α phase content but only a significant increase until it reaches 100 vol. % at temperatures between 1200 °C and 1300 °C. At higher temperatures the α phase starts to transform to $\alpha+\beta$ (Table 18), however, due to the bad grain statistics a quantitative phase fraction determination was not possible. As it was mentioned in 6.1.1 at HT some amount of disordered β was present and its amount was very fluctuating, thus its amount was undeterminable. Therefore the α_2/α phase content was manually fixed as 0 at temperatures listed in Table 21.

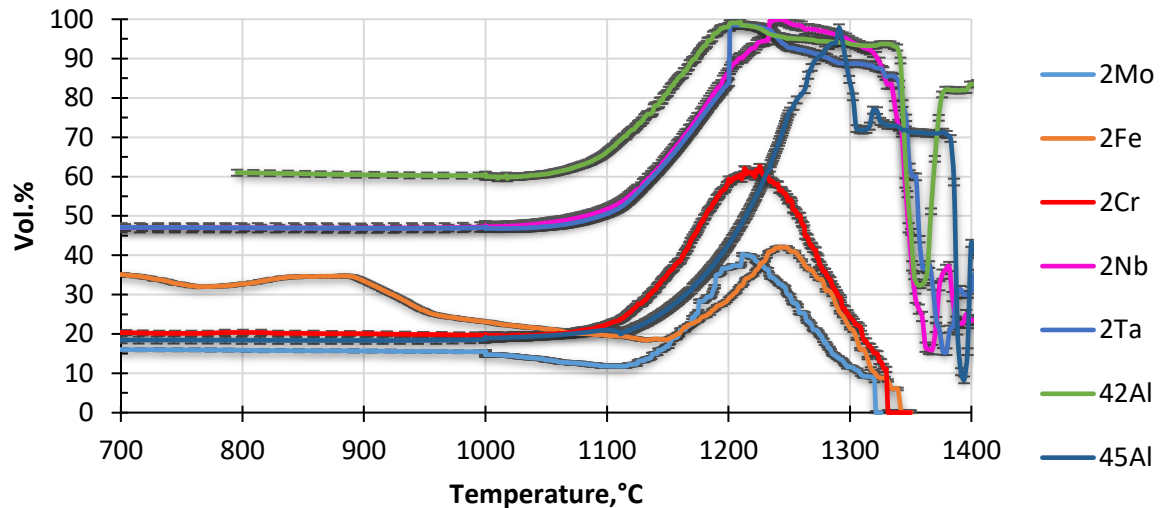


Figure 29 The α_2 / α phase content evolution with temperature. Ti-42Al graph starts from 800 °C due to empty detector pictures below 800 °C. Error bars drawn based on the standard deviation lie in the region of ± 1 vol. %.

6.1.3.1 The temperature of the $\alpha_2 \rightarrow \alpha$ transformation

The main way to detect the $\alpha_2 \rightarrow \alpha$ phase transformation is refinement of the site occupancy (SO). The theory is described in the part “Ordering determination via site occupancy refinement” of the subchapter 4.2. The results of the site occupancy refinement for the α_2 / α and the are described later in subchapter 6.1.5. The second way is a Gauss fit of the superstructure peak. Both methods are compared further. The Gauss fitting was found to be more precise based on comparison with the binary phase diagram.

The temperature of the $\alpha_2 \rightarrow \alpha$ transformation is at around 1120 °C as shown in Figure 2. However for Ti-42Al-2Nb and Ti-42Al-2Mo it is slightly increased and for Ti-42Al-2Fe the temperature differs by about 50 °C from other samples. The synchrotron values are compared with neutron ones by both evaluation methods in Appendix 5. It will be shortly mentioned in chapter 7, that Nb and Ta yield to increase of γ phase fraction. Nonetheless there could be a small influence of the used β -stabilizing elements on $\alpha_2 \rightarrow \alpha$ phase transformation temperature. With decrease of the $\alpha_2 \rightarrow \alpha$ phase transformation temperature evaluated by Gauss method samples could be put in the following order: 2Fe – 2Mo = 2Nb – 2Cr = 2Ta. The difference between phase transformation temperatures determined by Rietveld refinement and Gauss fit is due to the inability of MAUD to fit the weak superstructure peak at HT. Either the peak cannot be distinguished from background (then the temperature is lower than determined by Gauss fit), or a non-existing peak was found and refined within the background (Ti-42Al-2Mo).

After the analysis of the $\alpha_2 \rightarrow \alpha$ phase transformation it was attempt to determine the presence of the single α phase field or double $\alpha + \beta$ phase field. Due to the bad grain statistics a quantitative phase fraction determination was not possible at high temperatures and in the vicinity of single phase fields (either α or β). Therefore when a maximum of about 95 vol. % or a minimum of 5 vol. % of α phase was reached above 1200 °C the amount of the α phase was fixed to 100 vol. % or 0 vol. % respectively, in order to avoid unphysical fluctuations of phase composition. Table 21 contains the temperatures when the phase composition was fixed during Rietveld refinement.

Table 20 Temperatures of the $\alpha_2 \rightarrow \alpha$ transformation based on synchrotron data

Sample	Site occupancy Rietveld refinement, °C	Gauss, temperature of last visible 110 peak
Ti-42Al	1115	1123
Ti-45Al	1110	1116
Ti-42Al-2Fe	1160	1177
Ti-42Al-2Mo	1154	1136
Ti-42Al-2Cr	1131	1128
Ti-42Al-2Nb	1130	1135
Ti-42Al-2Ta	1136	1128

Table 21 Temperatures of manually fixed α phase composition to 100 or 0 %

Sample	Temperature of 100% fixed, °C	Temperature of 0% fixed, °C
Ti-42Al	1211	
Ti-45Al	1291	
Ti-42Al-2Fe	-	1343
Ti-42Al-2Mo	-	1322
Ti-42Al-2Cr	-	1331
Ti-42Al-2Nb	1236	
Ti-42Al-2Ta	1201	

When one would compare the tendencies of the phase transformation changes between the $\alpha_2 \rightarrow \alpha$ and $\beta_0 \rightarrow \beta$ phase transformation change due to increase of the third elements, it will be possible to see the interesting qualitative, but not quantitative, similarity. That could be the consequences of possibly same disordering nature of the phase transformation. However the low content of the third element in the α_2 / α phases contradicts to it.

6.1.4 Ti-42Al-2Fe: τ_2 phase presence

Figure 30 shows the evolution of the diffraction pattern of Ti-42Al-2Fe with temperature in more details. The formation of an additional phase, namely the τ_2 , was observed in the temperature range between 750 °C and 950 °C. During in situ synchrotron heating small peaks of the β_0 and the τ_2 phases are present up to 800 °C, where the β_0 phase disappears and appears again at 900 °C with decreasing fractions of the α_2 and the τ_2 phases. At 950 °C the τ_2 phase disappeared almost completely, and the amount of the α_2 phase is decreased from 37 to 20 wt. %. This yields a phase transformation pathway of $\alpha_2 + \gamma + \beta_0 + \tau_2 \rightarrow \alpha_2 + \gamma + \tau_2 \rightarrow \alpha_2 + \gamma + \beta_0 + \tau_2 \rightarrow \gamma + \beta_0 + \alpha_2$ (smaller amount). The states with three phases already indicate the close to equilibrium conditions (in comparison to RT). The superstructure β_0 100 peak is present below 797.11 °C and above 931.48 °C. That means that the β_0 phase retains its ordered state.

The four phases present at RT indicate a non-equilibrium condition which might be formed after the primary heat treatment at 1100 °C. After this the alloys were cooled within the furnace (about 10 °C/min) and phase transformations took place in a solid sample state. The cooling velocity might not provide enough time to perform all phase transformations necessary

to assume equilibrium state. Therefore the τ_2 and the β_0 phases were simultaneously observed in room temperature HEXRD measurements.

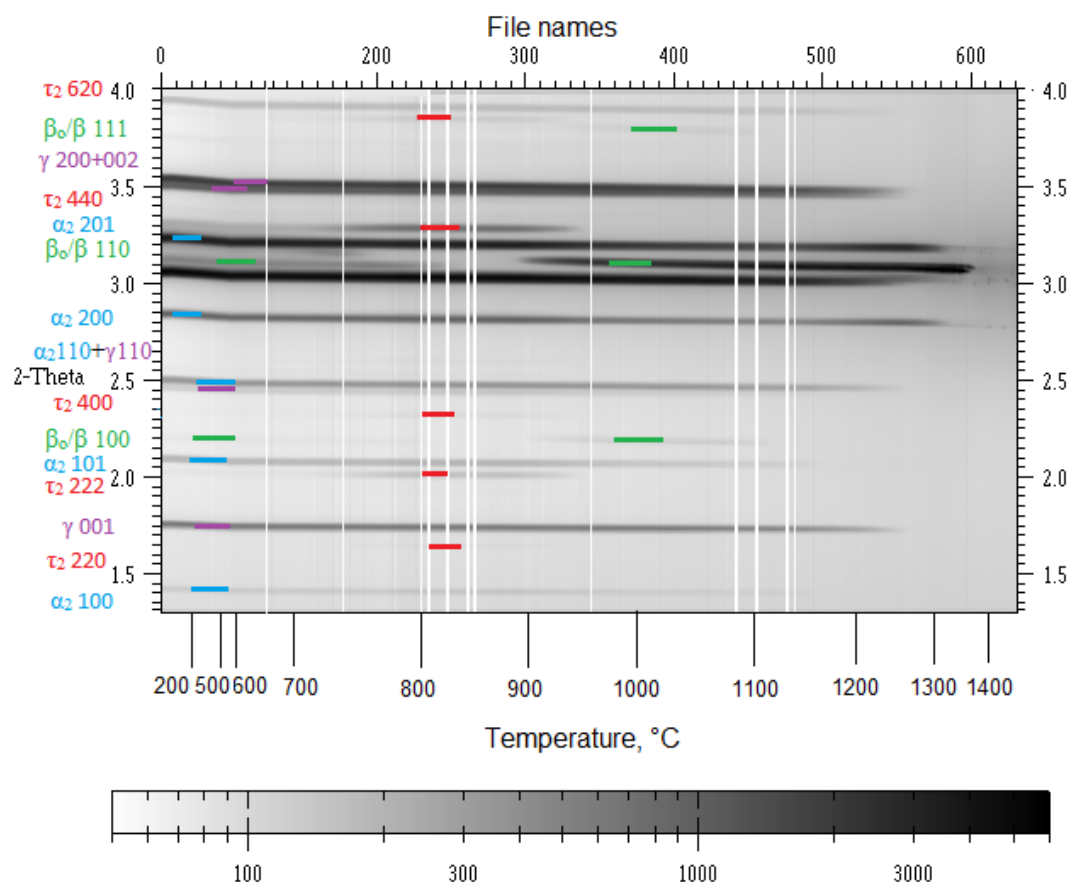


Figure 30 Evolution of the diffraction pattern of Ti-42Al-2Fe with temperature. Green are β_0/β peaks, red τ_2 phase, violet – γ and blue α_2/α peaks. At 2θ angle 2.35° there is a 400-peak corresponding to the τ_2 phase. It is present between 720°C and 896°C . After this the amount of the β phase increases up to 1000°C .

Presence of the τ_2 gave no reason for change of the α_2/α or the β_0/β phases site occupancies. Sizes of superstructure peaks intensities stayed unchanged.

6.1.5 Determination of the degree of ordering of the β_0/β and α_2/α phases

As mentioned in the theory part the degree of ordering could be determined via (1) site occupancy refinement or (2) peak correlation. In fact both methods are based on an analysis of superstructure and fundamental peaks intensities. Thus it is possible based on synchrotron data only or at least in combination with it, because no fundamental peaks are determined by neutrons. For neutrons the intensity of the superstructure peak could play the role of an ordering parameter itself, as will be described in 6.2.1.1.

6.1.5.1 Site occupancy Rietveld refinement for β_0/β phase

Site occupancy values between room temperature and 1000 °C have no visible change. Above 1000 °C the site occupancy values start to decrease up to 0.5 with increasing of the curve gradient (velocity of the parameter change) (Figure 31) of the Such gradient's behaviour corresponds to a second order phase transformation [PORT1992]. Shape of the SO curves are similar to the behaviour of the ordering parameter for the second order phase transformation in Appendix 2a.

One can observe a high fluctuation of the SO values around 0.5, especially at temperatures above 1120 °C (see Appendix 2c). The reasons for this fluctuation might be the very low intensity of the superstructure reflection at high temperatures, as well as the small amount of the β_0/β phase in the sample with Cr and the bad grain statistics. An attempt to calculate Degree of Ordering according to the formula (4) in chapter 2 from the fluctuated SO, that yield to the same high fluctuation of the Degree of Ordering.

The details of the definition of SO for cubic β_0/β are shown in Table 10.

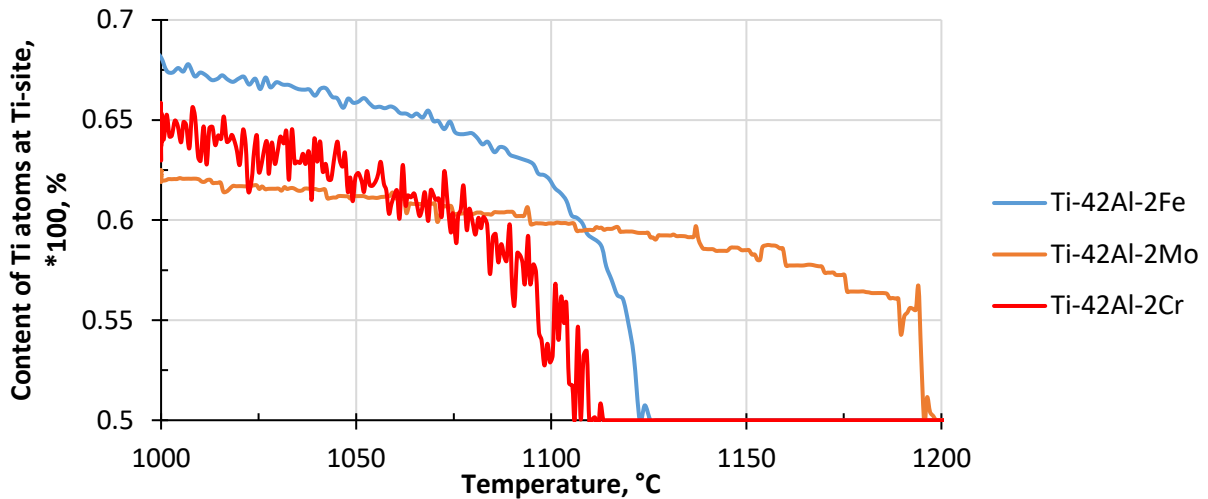


Figure 31 β_0 1a-Ti Site Occupancy. Below 1000 °C site occupancy line has a horizontal direction very close to the values at 1000 °C

6.1.5.2 Correlation of the peaks intensities 100/200

Figure 32 shows the correlation of the β_0/β peak intensities 100/200 (superstructure and fundamental) expressed in %. The intensity correlation was evaluated based on Gauss-fit of the peaks. The synchrotron data for the samples of the first data set were used, which contain the superstructure 100 peak: Ti-42Al-2Mo, Ti-42Al-2Fe, Ti-42Al-2Cr. The Intensity correlation corresponds to a manually calculated degree of ordering based on data from the Powder Cell program. The values of degree of ordering are written in the Figure 32 at the right.

Below 1000 °C the correlation was found to be nearly constant due to constant amount of β_0 phase (even the $\beta_0 \rightarrow \tau_2 \rightarrow \beta_0$ in the sample with 2Fe does not change the SO). Therefore only data above 1000 °C is shown in Figure 32. The maximum correlation values are: 12 % for 2Fe, 8 % for 2Mo and 7.5 % for 2Cr. The different temperatures where the 100/200 reflection correlation reaches its minimum are called temperatures of phase transformation and are compared in Table 22 with each other and the results of SO refinement. One can see fluctuation of the correlation peak intensities value. That is due to insufficient grains statistics.

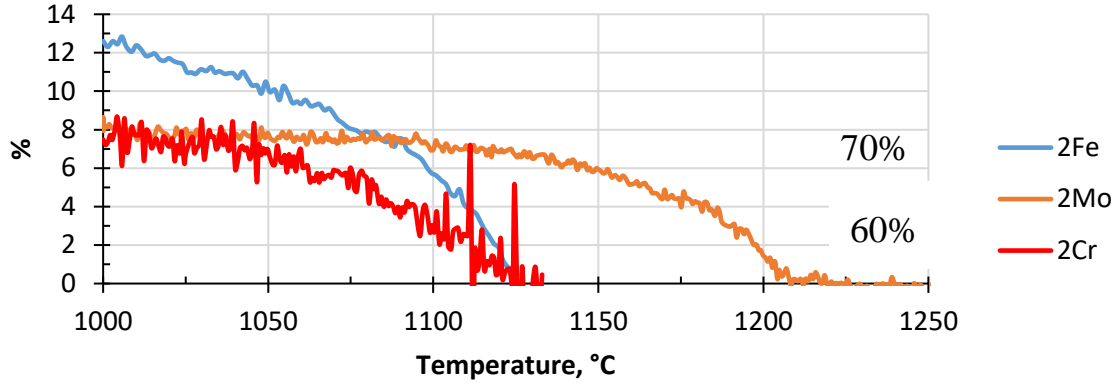


Figure 32 Intensity correlation of the β_0/β peaks 100/200. Manually calculated degrees of ordering based on values from the Powder Cell program and assumed for a B-factor of 1.4 are written at the right.

Comparison between the two methods of degree of ordering evaluation (site occupancy and peak intensity correlations) show good agreement in curve shape and temperature of the phase transformation, they differ just by a numerical factor introduced by refinement.

The fluctuation of the 100/200 peaks correlation is less than SO fluctuation due to no applied B-factor refinement, that brings more uncertainty to SO refinement.

Table 22 Comparison of two methods for degree of ordering determination based on Synchrotron radiation, 1000 °C.

Sample	Degree of ordering	Max of the reflection correlation	Temperature of the correlation min	Max of the Site Occupancy	Temperature of the SO min
Ti-42Al-2Cr	67%	7.5 %	1111	0.64	1110
Ti-42Al-2Fe	72%	12.0 %	1123	0.67	1122
Ti-42Al-2Mo	68%	8.0 %	1204	0.62	1206

6.1.5.3 Site occupancy of the $\alpha_2 \rightarrow \alpha$ phase

The site occupancy of the α_2/α phase was refined based on synchrotron data by Rietveld refinement in the MAUD program. The difference between the SO refinement formulas for cubic β_0/β and hexagonal α_2/α phase are shown in Table 10. A 6h position is occupied by Ti atoms in ideally ordered α_2 phase. The probability of Al to occupy a 6h position equal to 0 or Ti site occupancy of a 6h position equal to 1 would correspond to ideally ordered α_2 phase. In the other case the probability of Al to occupy 6h position higher than 0 means not fully ordered α_2 phase. So the minimum value of Al site occupancy up to 0.1 determined below 1000 °C corresponds to not full ordering. Change of site occupancy value from 0 to 0.25 (or from 0.75 to 1) means completion of the $\alpha_2 \rightarrow \alpha$ phase transformation. Values of 0.75 and 0.25 are determined by stoichiometric phase composition Ti_3Al . Graphs of SO change with temperature for α_2/α phase are shown in Figure 33. According to SO refinement shown in Figure 33 all samples of the first sample set reach a value of 25% almost at the same temperature. Therefore no influence from the β stabilizing element could be observed. Ti-42Al-2Fe has more fluctuation of the SO due to the τ_2 phase presence.

The close values of SO for the different alloys are explained by no addition of α_2 or α stabilizing-elements, except Al, which content stays equal at 42 at. % for all ternary samples.

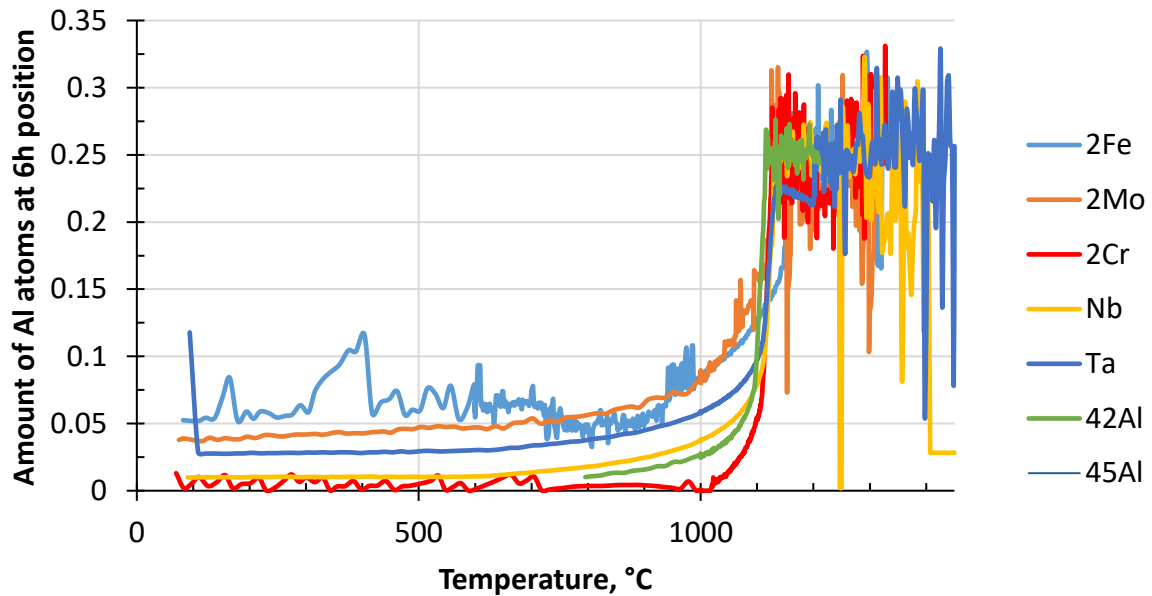


Figure 33 Site occupancy of α_2/α phase. There is a constant level of SO from RT to 800 °C. By Al site occupancy the probability of Al atoms to occupy the position 6h is meant.

In Figure 34 the change with temperature of the Gauss-fitted α_2 101 peak intensity is exhibited. It is easier to see a difference between samples by Gauss fitted intensities, than by SO graphs, mainly due to less fluctuation of the Gauss fitted intensities curves.

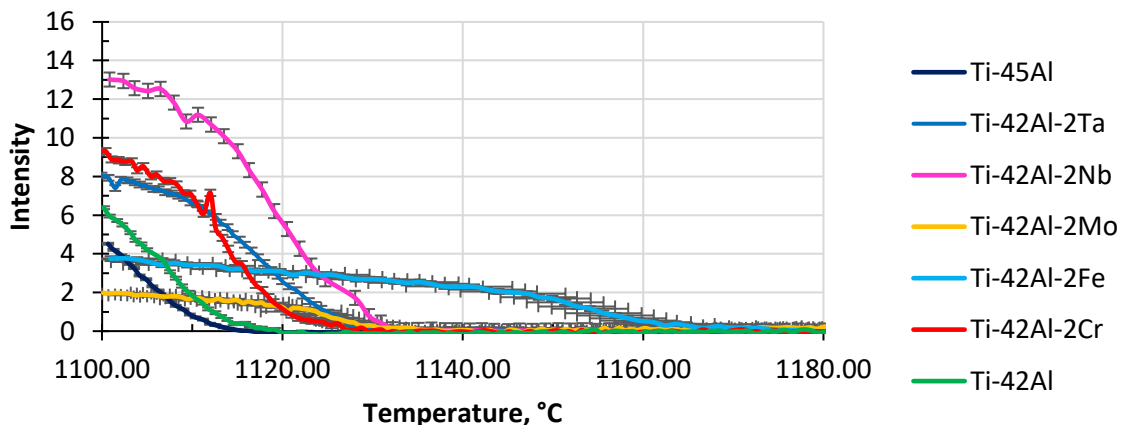


Figure 34 α_2 101 peak intensity changing with temperature

The highest α_2 101 peak intensity corresponds to Nb, then Cr, Ta, 42Al, 45Al, 2Fe, and the lowest to 2Mo. The temperature where the superstructure peak reaches its minimum is designated the $\alpha_2 \rightarrow \alpha$ phase transformation: Ti-42Al and Ti-45Al – 1120 °C, corresponding well with the binary phase diagram; Ti-42Al-2Mo, Ti-42Al-2Cr, Ti-42Al-2Nb, Ti-42Al-2Ta at about 1130 °C, and Ti-42Al-2Fe at about 1170 °C. All temperatures are listed in Table 20 as well as in APPENDIX 5 as the MAUD temperatures.

6.1.6 Lattice parameter evolution phase

As described in chapter 2 the β_0/β phase is cubic, characterized by one lattice parameter a , which is equal to the b and c parameters. Figure 33 shows the change of the lattice parameter a from RT to 1350 °C. With increasing temperature the lattice parameter a is continuously increasing for all samples due to thermal expansion but the absolute values show large differences depending on the alloy composition.

Between 700 and 1000 °C the thermal expansion increases quicker. This is very pronounced in sample Ti-42Al-2Cr and almost negligible for Ti-42Al-2Mo. Sample Ti-42Al-2Fe containing the τ_2 phase has a more complicated β phase lattice parameter evolution due to the τ_2 phase. During the τ_2 phase presence there is complete dissolution of the β_0/β phase between 800 and 900 °C. Therefore Figure 35 contains two lines corresponding to Ti-42Al-2Fe sample. The first line (2Fe(1)) is the phase a lattice parameter change before the τ_2 transformation takes place and the second one (2Fe(2)) after the τ_2 dissolution. There is a drop of the a lattice parameter from 3.252 to 3.217 Å corresponds to the peak position at the spectrums.

Figure 36 shows a section of Figure 35. Above 1100 °C the thermal expansion (gradient) decreases a bit. At temperatures above 1100 °C the thermal expansions of Ti-42Al-2Mo and Ti-42Al-2Cr alloys are close to Ti-42Al-2Fe and also the lattice parameters are almost equal. Due to the bad grain statistic above 1350 °C no realistic lattice parameters could be refined for β phase.

As one can see from both figures mentioned above the increase of the a lattice parameter due to the thermal expansion is almost linear. A change of the gradient often can be connected to a change of the chemical composition of the phase. Especially the jump in the Ti-42Al-2Fe sample can be attributed to a difference in chemical composition, when more Fe atoms are concentrated in the β_0/β phase after the τ_2 phase dissolution, however this was not experimentally proved for our sample due to impossibility of in situ EDX. Also the strong increase of the a lattice parameter in Ti-42Al-2Cr could be explained by a chemical composition change in the β phase which might have been far away from equilibrium at lower temperatures. At temperatures above 700 °C diffusion becomes a prominent process and therefore the large differences in the lattice parameter increase occurs. The almost equal lattice parameters between samples at temperatures above 1100 °C indicate that the chemical composition of the β phase is almost equal, despite of the different alloy compositions. Even if the same model of the phases have been applied, the difference in the lattice parameter could be the sign of requirement to take the third atom position into account.

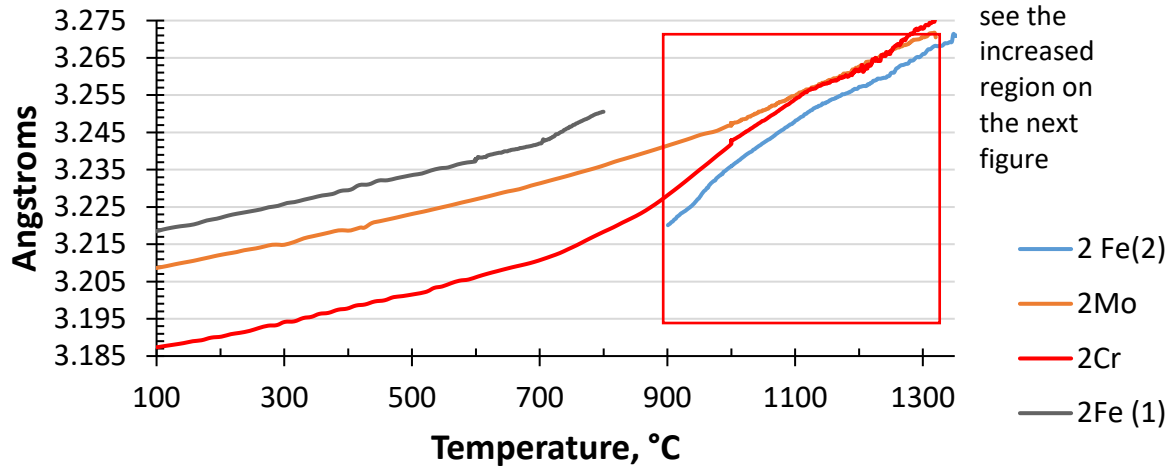


Figure 35 Change of lattice parameter a of β_0/β phase from RT to 1350 °C

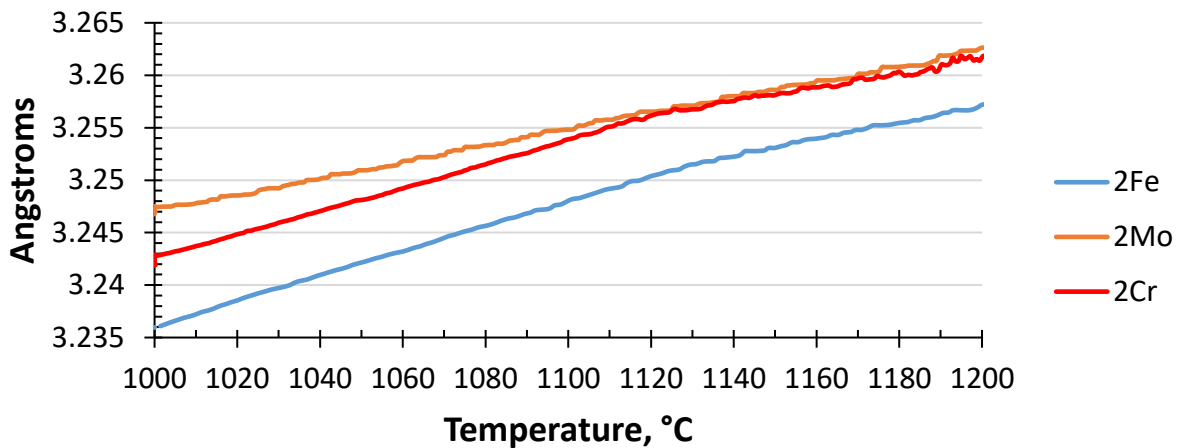


Figure 36 Change of lattice parameter a of β_0/β phase from 1000 to 1250 °C

6.1.7 Lattice parameters of the α_2/α and γ phases and their increase during heating

The evolution of the lattice parameters of the α_2/α phase during heating are shown in Figure 37 and Figure 38. Up to about 1100 °C the a and c lattice parameters increase almost linearly due to thermal expansion 4×10^{-6} to 3.7×10^{-5} depending on the sample composition and fluctuation of the lattice parameters. The a lattice parameter grows by about 0.075 Å within the range 100 - 1100 °C starting at 5.76 Å. For the c lattice parameter the increase is 0.05 Å starting at 4.63 Å. At about 1120 °C one can observe a change of the gradient in the thermal expansion of the a parameter (Figure 37 b). That could correspond to the $\alpha_2 \rightarrow \alpha$ phase transformation. It was an assumption only, that no lattice parameter change should occur. There is almost no difference in the lattice parameters between samples tells about minor role of the third element in the lattice parameters of the α_2 or α phase. That is not surprise, as long as the amount of the third element in the α_2/α phase is minimum (see subchapter 7.2.1 or the EDX results-subchapter 5.4).

We used artificially the same crystal structure for α_2 and α phase, that allows to have a continuous lattice parameter line. And difference between α_2 and α phases mainly via SO change. However some change in the a parameter of the α_2/α phases could be visible during the α_2 to α phase transformation, that corresponds to the formally other unit cell size. In Figure 37a

one can see increase of the refined value of the a lattice parameter above 1100 °C, that corresponds a temperature area of the $\alpha_2 \rightarrow \alpha$ phase transformation.

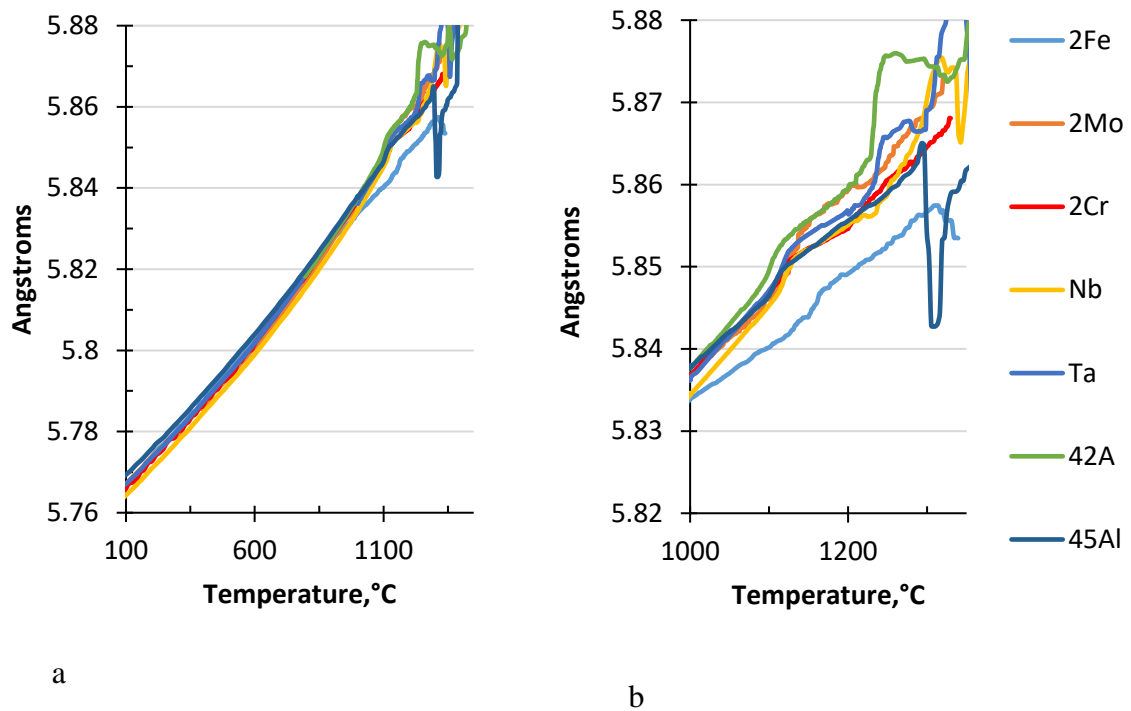


Figure 37 Lattice parameter a of the α_2/α phase with two wider and smaller temperature regions

A similar behaviour to the a parameter is not visible in the c parameter evolution. Here the oscillations above 1150 °C, visible for some alloy compositions in Figure 38b, can be attributed to shift of the 002 α peak inside the γ 111 peak due to bad grain statistic. Table 23 summarizes the maximum temperatures up to which the lattice parameter value is available, and from which the jump starts.

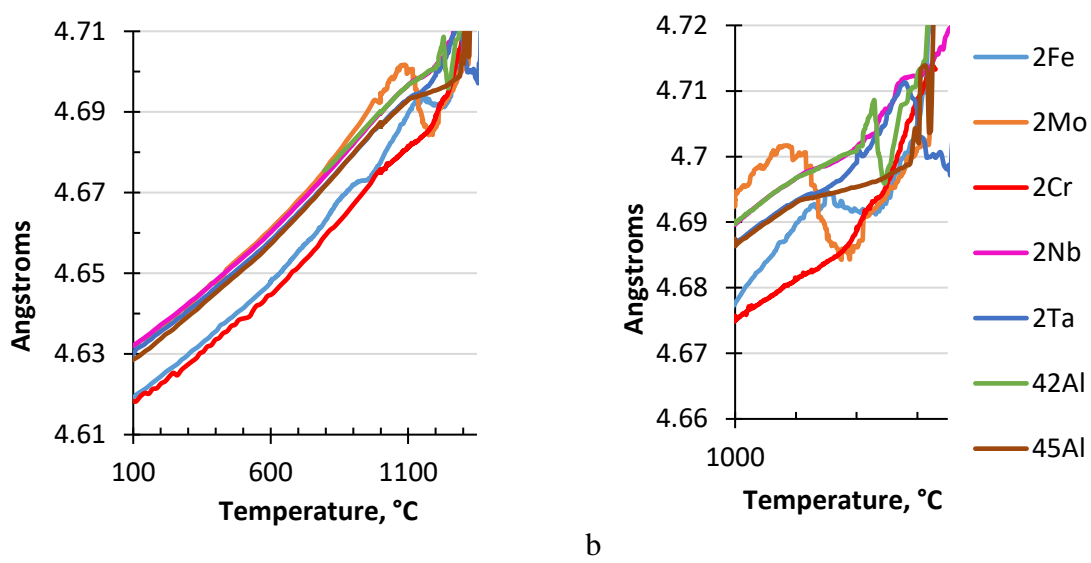


Figure 38 Lattice parameter c of the α_2/α phase within a larger and a smaller temperature region

Table 23 Temperatures of the jump of the lattice parameters lines

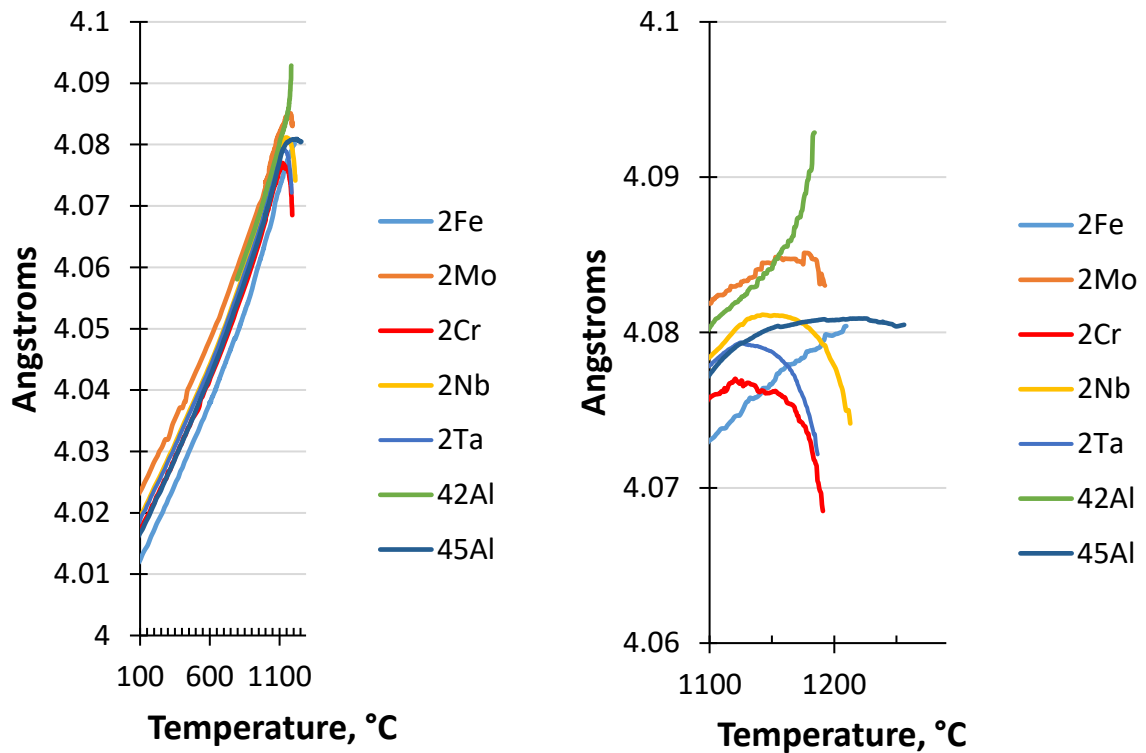
Sample	a-lattice parameter jump start	c-lattice parameter jump
Ti-42Al	1107	1230
Ti-45Al	1120	No
Ti-42Al-2Fe	1165	1140
Ti-42Al-2Mo	1140	1091
Ti-42Al-2Cr	1123	No
Ti-42Al-2Nb	1130	1274
Ti-42Al-2Ta	1124	1281

For the detection of the α_2/α phase transformation could be visible as well by analysis of the c/a ratio of the lattice parameters, that increases and then decreases for 0.002 Å.

γ phase lattice parameters increase

Figure 39 and Figure 40 show the evolution of the lattice parameters of the γ phase during heating. Both lattice parameters, a and c increase up to 1100 °C with constant rate due to thermal expansion. The increase of the lattice parameters is about 0.05 Å for a temperature range of 1000 °C. This corresponds to a linear thermal expansion coefficient of $12.4 \times 10^{-6} \text{ K}^{-1}$ which is a typical value for metallic materials [TEXP]. The lattice parameters of the different alloys do not differ significantly except for the c parameter of 2Cr and 2Fe (Figure 40). They are about 0.01 Å smaller than other alloys of the first sample set. At temperatures above 1200 °C the a lattice parameter shows an unphysical behaviour (drops and up for 42Al) attributed with Rietveld refinement of the low intensity peak. The erroneous refinement occurs due to the presence of a big α 002 reflection while the γ -111 peak almost disappears at higher temperatures and erroneously the MAUD program takes the position of α 002 for the γ -111 peak.

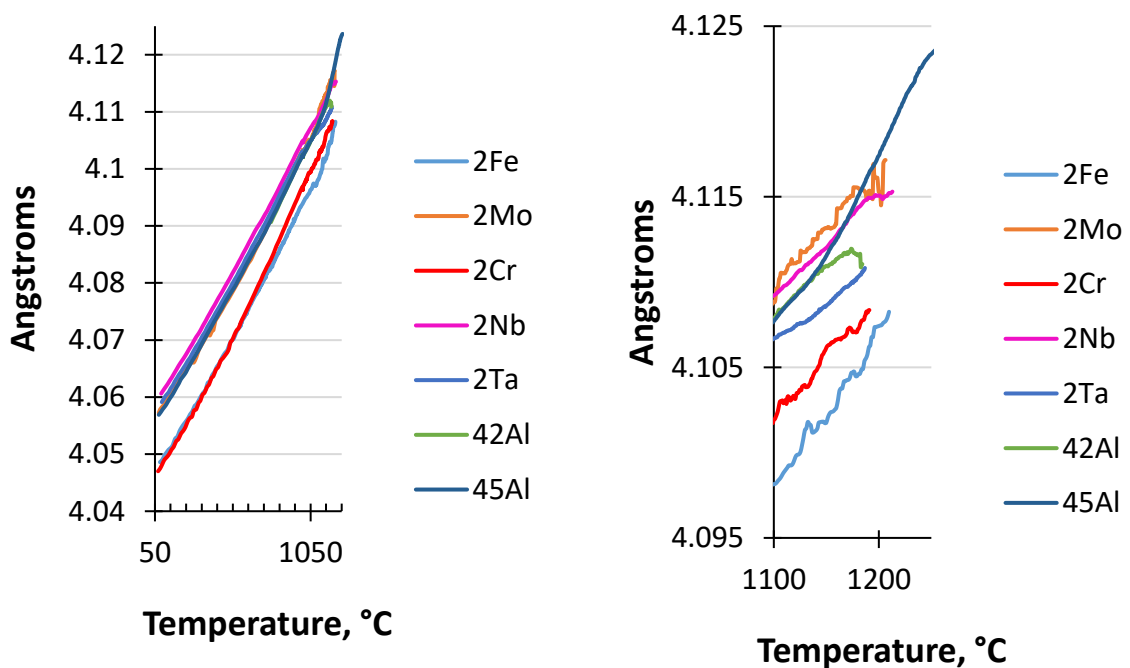
At temperatures above 1200 °C γ phase is mainly dissolved in most of the samples (see Table 19). However fluctuation of the lattice parameter was found up to 10 °C below the γ -solvus temperature. Fluctuation of the a lattice parameter started some degrees early than c parameter.



a

b

Figure 39 Lattice parameter *a* of γ phase, a – from a room temperature to 1450 °C; b – from 1000 to 1450 °C for more detailed overview. Graphs are plotted up to the γ -solvus temperature determined from the Gauss Fit.



a The *c* lattice parameter of γ phase

b The *c* lattice parameter of γ phase

Figure 40 Lattice parameter *c* of γ phase based on Rietveld refinement of synchrotron data. Graphs are plotted up to γ -solvus temperature determined from the Gauss Fit of 001 γ -peak.

6.1.8 c/a ratio for the γ phase

An important parameter for the interpretation of the lattice size change of the γ phase is the c/a ratio. Several authors have studied the influence of alloying elements on the c/a ratio at room temperature [PFUL1993, YEOH2007]. They found ratios in the range of 1.01 to 1.02. Figure 41 shows the c/a ratio evolution during heating. At low temperatures up to about 700 °C it is in the range of 1.01 for our alloys without additional β_0 phase. However, it is lower for the alloys with additional β_0 phase ranging from 1.008 for the 2Cr to 1.009 for the 2 Fe, with 2 Mo in between both values. Starting from 700 °C the ratio slightly decreases by about 0.002 for all alloys and reaches a minimum at about 1100 °C. After this it significantly increases until the γ phase is completely dissolved (except Ti-42Al and Ti-42Al-2Fe – due to unphysical behaviour of refined a lattice parameter in these samples). Such decrease could be results of small increase of the c lattice parameter above 1120 °C.

Pfullmann et al. [PFUL1993] have shown that the Al content of the γ phase strongly effects the c/a ratio with increasing values by increasing the Al content. Thus the general trend of the ratio, first slow decreasing up to a minimum at about 1100 °C and then strong increasing can be correlated to the phase diagram of TiAl (chapter 2). Here the Al content of the γ -phase is decreasing during heating from RT to 1120 °C for 1 at. % and then grows up for 1-2 at. % until the γ phase is dissolved between 1200 and 1290 °C. A similar behaviour during heating was also found by Yeoh et. al [YEOH2007]. The lower values for the β_0 phase containing alloys might indicate a generally higher Al content of the γ -phase in these alloys. This hint can be confirmed by the EDX measurements (Table 15).

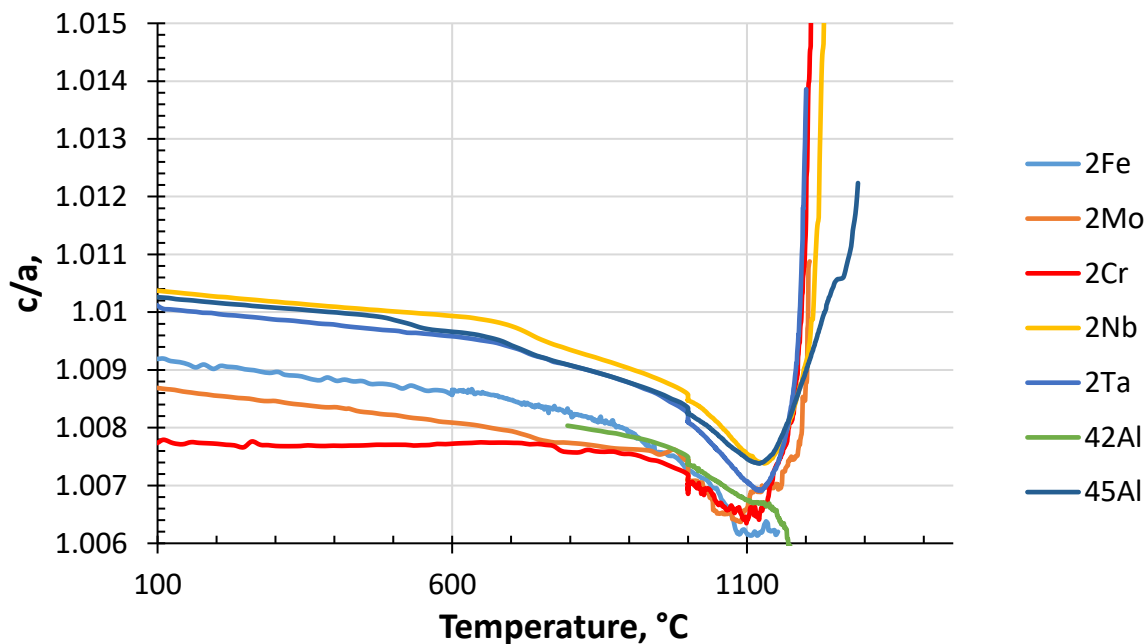


Figure 41 Change with temperature of c/a ratio of the γ phase of the first sample set. Correlation of lattice parameters (c to a ratio) of γ phase depends from Al concentration in the phase. Minimum of c/a should be at temperature of $\alpha_2 \rightarrow \alpha$ phase transformation due to change of chemical composition of the γ phase.

Further discussion about lattice parameters of the phases could be found in 7.2.1.

6.2 Neutron in situ diffraction measurements results

In this subchapter the results of the in situ neutron diffraction experiments at FRM II (Garching near Munich) will be described. One neutron beam time for the first sample set with the HTF and two neutron beam times with the dilatometer for the second sample set were performed. The first sample set was completely researched with neutrons whereas the data of the second sample set were only partly analysed. The results for the first and the second sample set will be shown in separate subchapters due to the different heating furnaces applied. For all neutron measurements grain statistic problem played a negative role for the neutron diffraction data interpretation. The examples of grain statistic influence are moved into Appendix 2b.

As it is possible to see in Figure 42 and Figure 43 the amount of detected peaks by one detector picture with neutrons is less, in comparison to synchrotron. The reasons are (1) only superstructure peaks are visible with neutrons and (2) that due to the larger wave length and the beamline setup (shorter sample to detector distance) only a small 2θ range could be measured. Thus less parameters were determined. The same interpretation methods: Rietveld refinement and Gauss fit were applied. The difference from synchrotron data analysis is the amount of parameters refined with the Rietveld method. For neutrons the difference in the values of phase transformation temperatures and lattice parameters determined by both analysis methods will be shown.

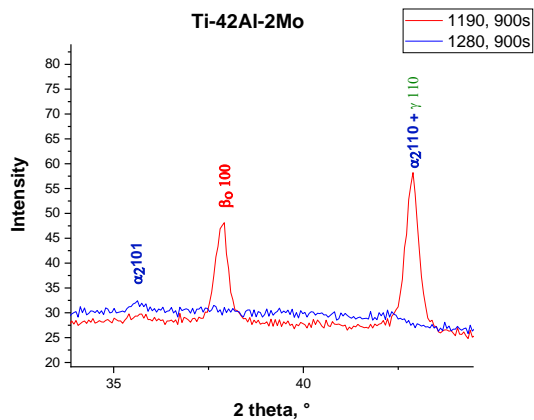


Figure 42 Neutron diffraction spectrum of Ti-42Al-2Mo sample

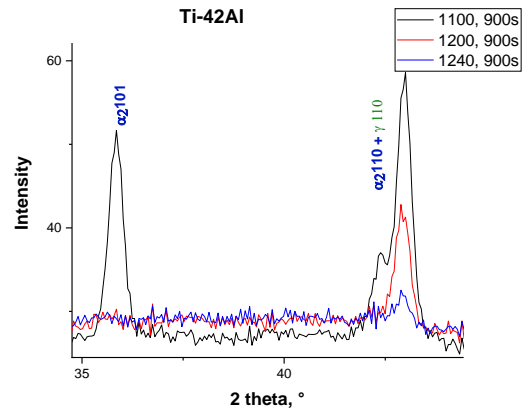


Figure 43 Neutron diffraction spectrum of Ti-42Al sample

6.2.1 Standard high temperature furnace

The properties of the standard high temperature furnace are described in chapter 3. The main disadvantage of this setup was a systematic temperature elevation of 40 °C. It was found during data analysis of reference sample Ti-42Al, which shows an elevated temperature value for the α_2/α phase transformation temperature of 40 °C. The deviation was corrected by subtraction of the 40 °C difference from every measured temperature value.

6.2.1.1 Phase transformation temperatures of the first sample set

The results of the first sample set are listed in Table 24 and in Appendix 5. There one can compare phase transformation temperatures determined by Gauss fit and by Rietveld refinement with the MAUD program. As the Rietveld refinement results it shows the temperatures where the peaks are visible for the last time. Due to a step wise heating rate the

phase transformation temperature lies inside the next step (10 °C for all alloys except the following: 15 °C for 2Cr and 25 °C for 45Al > 1260 °C) after the mentioned temperature.

Table 24 Maximum temperatures where peaks have been detected last time for the first sample set. The temperatures are corrected by (-40 °) during data analysis.

Sample	β_0 100		α_2 101		γ 110	
	Gauss	MAUD	Gauss	MAUD	Gauss	MAUD
Ti-42Al			1120	1120	1190	1210
Ti-45Al			1120	1130	1285	1310
Ti-42Al-2Fe	1120	1130	1160	1160	> 1210	>1210
Ti-42Al-2Mo	1230	1250	1140	1150	1210	1220
Ti-42Al-2Cr	1090	1110	1110	1125	1170	1170
Ti-42Al-2Nb			1120	1130	1190	1190
Ti-42Al-2Ta			1100	1130	1180	1190

Following peculiarities could be mentioned from Table 24:

The difference between temperatures determined by MAUD and the Gauss fitting method are 20 °C or less (except γ 110 of the Ti-45Al). It is noticeable that the temperatures calculated by MAUD are often higher. This is based on the liability of Rietveld refinement to treat background intensity as a peak even when the peak of interest is not present anymore. Thus MAUD overestimated the temperature values.

Ti-42Al-2Mo contains β_0 phase, which disappears at the highest temperature (of the first sample set), above 1230 °C. This indicates that Mo has the highest β stabilizing properties. The γ 110 peak disappears based on Gauss-fit and MAUD evaluation above 1210 - 1220 °C and α_2 101 above 1140 - 1150 °C correspondingly.

Ti-42Al-2Fe also contains β_0 phase, which disappears at temperatures above 1120 °C. For the γ 110 and α_2 101 peaks no difference between Gauss-fit and MAUD evaluation exists and they disappear above 1210 °C and 1160 °C correspondingly. The 1160 °C is the highest temperature at which the α_2 peak is visible in the first sample set thus one can talk about the highest α_2 stabilizing properties for Fe.

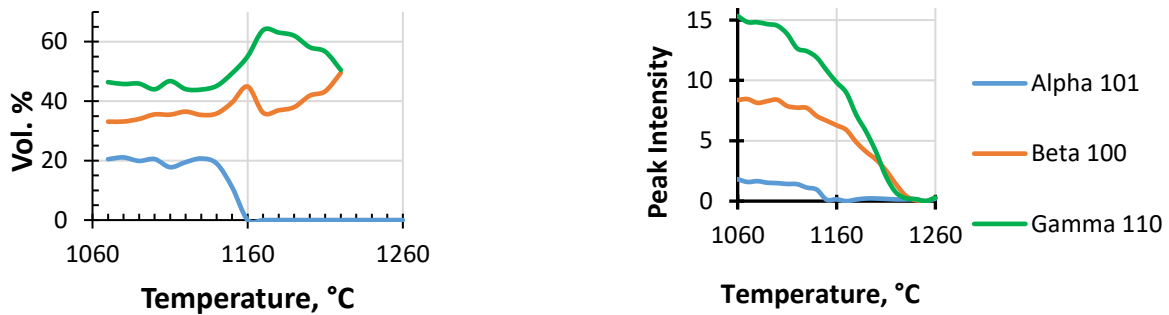
Ti-42Al-2Cr similarly contains β_0 phase, which disappears at the lowest temperature above 1090 - 1110 °C. The γ phase 110 peak from Gauss-fit and MAUD refinement disappears at the same temperature, 1170 °C, and α_2 at 1110 - 1125 °C.

Ti-42Al-2Nb and Ti-42Al-2Ta contain no β_0 phase. The γ phase 110 peak from Gauss-fit and MAUD refinement disappears in both samples above 1180 - 1190 °C The α_2 101 disappears the maximum above 1130 °C in both samples.

The binary alloys contain no β_0 or β phase. The temperatures of disappearance of α_2 101 in Ti-42Al was used as reference and in Ti-45Al is the same after correction to -40 °C and γ phase 110 peak disappearance temperatures (determined by Gauss) correspond to the values predicted by the binary phase diagram.

6.2.1.2 Phase composition analysis for the first sample set

It was possible to perform a quantitative phase composition analysis by Rietveld refinement from the neutron data up to the first order-disorder phase transformation. It must be mentioned that after this temperature, the calculated phase content is no longer true. Figure 44 exhibits a comparison of (a) the phase composition calculated by Rietveld refinement for Ti-42Al-2Mo and (b) the intensity evolution of the superstructure peaks. It can be seen in Figure 44(b) that the first order-disorder transformation which occurred is $\alpha_2 \rightarrow \alpha$, based on the disappearance of the α_2 101 superstructure peak. The disappearance of the α_2 phase in Figure 44 (b) contradicts to an increase of the amount of β_0 and γ phases in Figure 44 (a). This jump is an unavoidable misrefinement for neutron results. After the ordered phase (α_2 or β_0) transformed to the disordered one (α or β), the disordered phases are invisible with neutrons (see chapter 2 “Basics”) especially for TiAl alloys, but still present. Thus no correct phase composition could be refined by Rietveld analysis above the first disordering temperature.



a Phase composition of Ti-42Al-2Mo refined from the neutron data by MAUD b Change of neutron reflection intensities (Gauss fit)

Figure 44 A comparison of a Rietveld phase composition refinement for Ti-42Al-2Mo (a) and intensity of superstructure peaks (b).

Comparison of Gauss and Rietveld interpretation methods for our neutron data gave the following results: on the one side the Rietveld refinement of phase content is effective close before to the temperature of the first ordering peak disappearance, but not after. A recalculation of the phase content in MAUD program should take into account the interrelation between peaks. This is impossible as long as no fundamental peaks are visible with neutrons. On the other hand the Gauss fit calculated phase transformation temperatures are more precise, however the Gauss fit does not result in a phase content.

6.2.1.3 Lattice parameters change in the first sample set

Lattice parameters were refined by Rietveld refinement and calculated from peak positions from the Gauss fit. An increase of the interplanar distance with the temperature, due to thermal expansion, was expected and observed for all investigated samples. As one can see using the example of the lattice parameter a of γ phase in Figure 48, the Gauss-fit values are less fluctuating than the results of the Rietveld refinement. No possibility was found to refine the α_2 lattice parameters a and c . Theoretically in the measured neutron spectra the α_2 phase is characterized by two peaks: 101 and 110, which cover both a and c parameters. However, in reality intensity of the 110 peak is too small and its position is hardly determinable by both methods. Thus refinement of a and c parameters of the α_2 phase gave too much fluctuation in the lattice parameter values in both Rietveld and Gauss methods.

Analysis of β_0/β phase lattice parameters change by Gauss method

In Figure 45 the change of β phase lattice parameter a , calculated by Gauss fit, could be observed. As shown in Figure 45 the difference between the a lattice parameter of the three samples of the first sample set is not more than 0.01 Å. That is minimum 5 times higher than the precision of the lattice parameter determination (0.002 Å) designated by the error of the Rietveld refinement. The sample with Mo is characterized by the largest a -lattice parameter, Cr has values very close to Mo and Fe the lowest. The increase of the a -parameter with temperature reaches also maximum of 0.01 Å that lies in the range of the difference between samples. Increase of β lattice parameter with temperature is similar in 2Fe and 2Mo observing parallel lines. With Cr addition the lattice parameter increases quicker. Similar thermal expansion should correspond to the alloys of different composition.

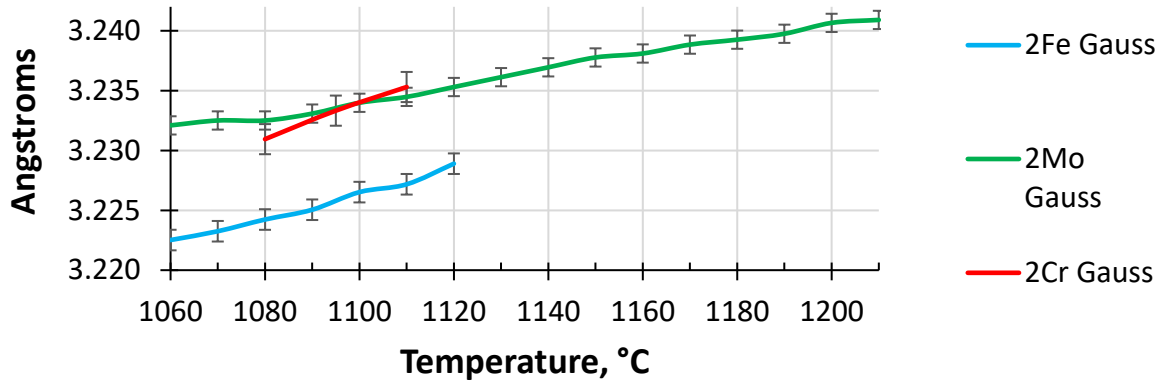


Figure 45 β phase lattice parameter a . The curves were determined by Gauss fit. Plots are drawn up to the $\beta_0 \rightarrow \beta$ phase transformation temperature.

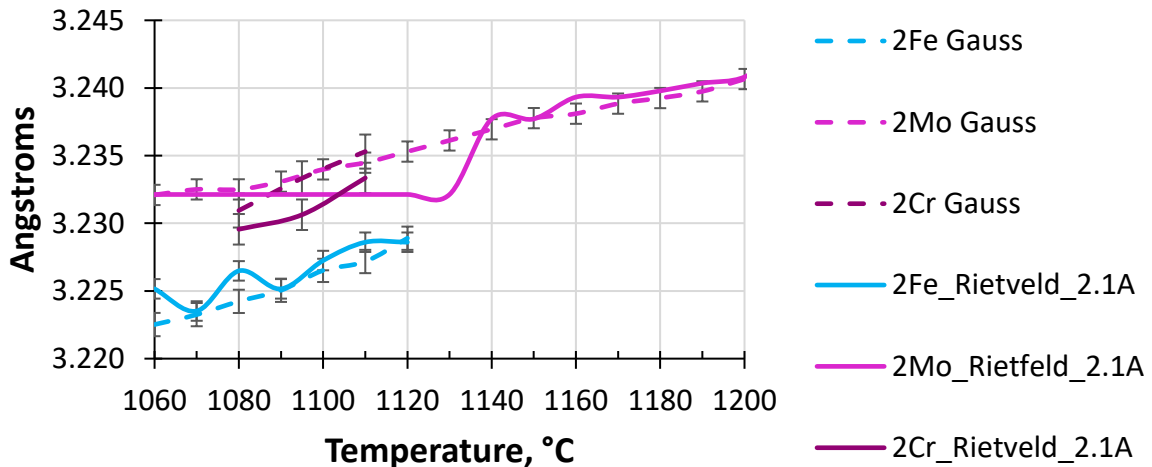


Figure 46 Comparison of the β_0/β a lattice parameter determined by Rietveld refinement and Gauss-fit. Error bars drawn based on the standard deviation lie in the range of ± 0.001 Å, that is higher than difference between the Gauss graph lines of different samples.

Figure 46 compares lattice parameters of β_0/β phase in the first sample set determined by Rietveld refinement and Gauss-fit. The best correspondence between analysing methods is found for Ti-42Al-2Mo above 1140 °C, but with the highest jump of Rietveld value between 1080 °C and 1120 °C. Ti-42Al-2Cr shows parallel lines, but with a difference of 0.002 Å, that

is a bit higher than the refinement error. In Ti-42Al-2Fe Rietveld refinement gives very fluctuating results.

Analysis of 101 interplanar distance α_2 phase

As mentioned above the lattice parameter a of the α_2 phase contributes to both measured peaks, 101 (Figure 47) and 110, whereas the lattice parameter c is only part of the α_2 101 peak. The refinement of both a and c parameters only from the 101 peak is unsolvable because the number of variables is greater than the number of equations. In order to determine the two different lattice parameters a and c one needs two equations, which could be filled by both 101 and 110 measured peaks. However, the 110 peak is positioned very close to the 110 γ peak and its intensity is small. Thus, it cannot be separated in a sufficient way from the γ peak. This problem appears during the Rietveld refinement, where the α_2 110 peak was shifted to higher 2θ angles below the γ -110 peak up to about 0.1° , as well as by Gauss-fitting. Therefore only the interplanar distance (Figure 47) is calculated from the peak position of the α_2 101 peak.

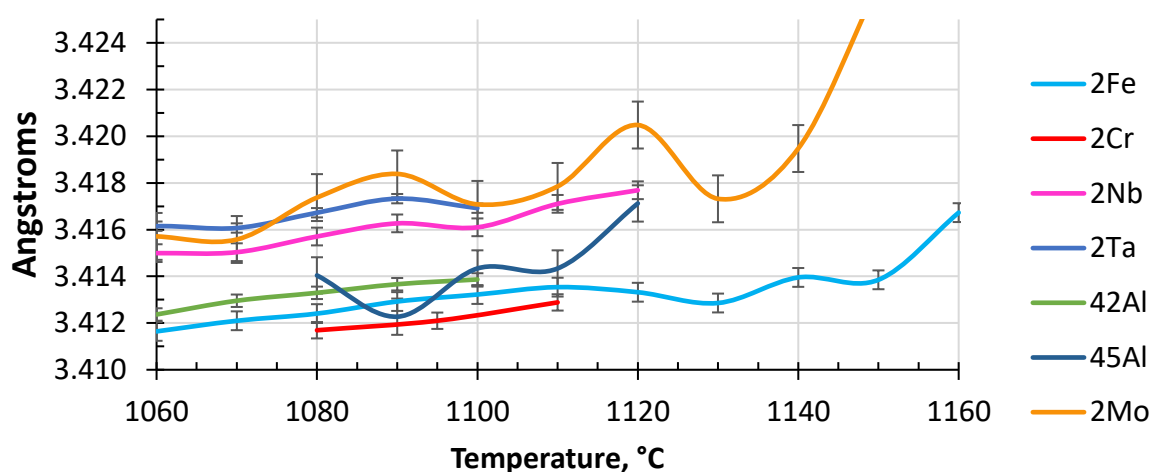


Figure 47 Interplanar distance of α_2 phase 101 peak calculated from the Gauss-fit. The lines are stopped due to disappearance of the α_2 phase 101 peak at different temperatures corresponding to the sample composition.

The Ti-45Al shows big fluctuations as well as the Ti-42Al-2Mo is fluctuating at temperatures above 1080 °C. These fluctuations could be explained by the low signal to background ratio especially for these both alloys which show the smallest α_2 content, as well as by insufficient grain statistic.

Analysis of γ phase a -lattice parameter change

Only one γ peak, 110, was measured by neutrons. The peak contains information about $a=b$ lattice parameter. Calculated from Gauss fit and refined by Rietveld method the γ phase a -lattice parameter change with temperature is shown in Figure 48 for three samples of the first sample set: Ti-42Al-2Fe, Ti-45Al and Ti-42Al. They show the most concordant and most divergent examples (from the first sample set) of a calculation by the Gauss and the Rietveld method. The temperature correlated with the number of the last spectrum, where the FWHM is still a reliable value is taken as the phase transformation temperature.

The thermal increase of the γ a parameter is linear in the temperature region of 1060-1200 °C and could be quantitatively characterized in average by 0.007 \AA . This corresponds to a thermal expansion coefficient of $12.3 \cdot 10^{-6} \text{ K}^{-1}$. That is almost identical to the thermal

expansion coefficient for the γ phase calculated from the synchrotron data (subchapter 5.1.7). With respect to thermal expansion of the γ a lattice parameter the alloys can be put in the following order: 2Mo – 2Ta – 2Nb – 2Cr – 42Al – 45Al – 2Fe. It was found that most of the lattice parameters have mainly a linear dependence from temperature, but show small fluctuations. The fluctuations could be results of insufficient grain statistic or insufficient peak position refinement.

The strong deviation of the lattice parameter estimated by Gauss and by Rietveld for Ti-42Al below 1120 °C could be explained by fitting only one Gauss peak for the 2θ region of γ 110 which is very closely spaced to the α_2 110 peak. Since Ti-42Al has the highest α_2 content this yields to a significant miscalculation (fluctuation) compared to the Rietveld method.

The maximum difference in a -lattice parameter of the γ phase between samples is 0.01 Å based on the Gauss results.

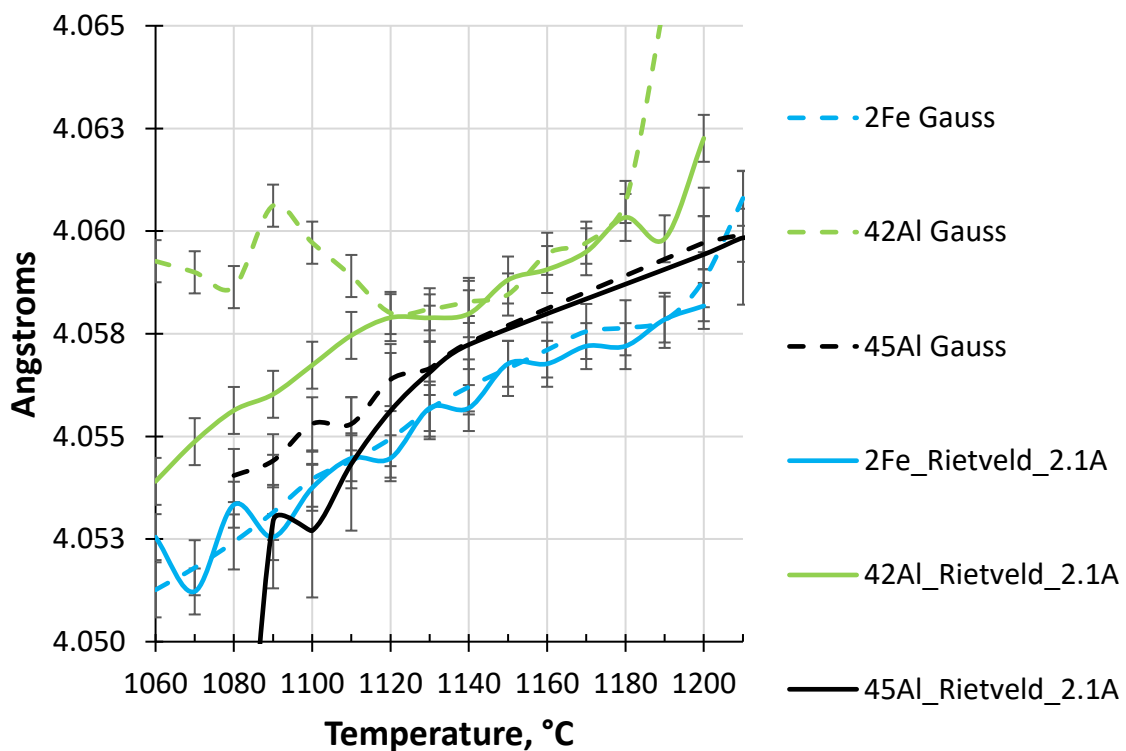


Figure 48 Evolution of the γ a lattice parameter using the examples of three alloys. Comparison of two methods precision. Error bars drawn based on the standard deviation lie in the region of ± 0.001 Å, that is higher than difference between the Gauss graph lines of different samples.

Since no detected peak characterizes the c -parameter, thus the parameter was not refined based on the neutron data. Therefore no c/a ratio is possible to calculate.

6.2.2 Implementation of the Dilatometer at STRESS-SPEC

The in situ neutron diffraction measurements with dilatometer were the first measurements in the world performed with this setup. The advantage of the dilatometer compared to the standard HTF is, that the thermocouple is directly spot welded on the sample. Thus the real sample temperature is measured and not the temperature in a certain distance from

the sample which does not correspond to the real sample temperature. However, due to the first dilatometer application (first real measurement after dilatometer commissioning) some unplanned events occurred which influenced the performed measurements in a special way. This influence will be discussed in the thesis. Most of the first problems have been professionally solved by the beam scientist up to the time of the second neutron dilatometer measurements in March 2020, however, a new problem occurred, which should be taken into account. A short list of the problems includes: during the 1st dilatometer measurements: unexpected heating interruptions due to wrong dimensions of the cooling system as well as some additional peaks of the reference rod and sample holder. During the 2nd dilatometer measurements a misalignment of a collimator gave a doubling of peaks, this doubling could be a sign of the ω_0 phase presence in samples with Nb when the temperature region below 900 °C.

6.2.2.1 The first neutron measurements with dilatometer

Influence of heating interruption on the phase transformation temperatures

During the first neutron dilatometer measurements the heating was interrupted unexpectedly because the cooling water of the dilatometer was overheated due to its low amount. The number of interruptions reached up to nine times for some samples. After interruption the same sample was reused and heated with 200°/s until the temperature of interruption.

These interruptions influence the phase transformation temperatures measured. For example on the neutron detector picture of Ti-42Al-1Fe before and after an interruption at 1200 °C one can see, that the γ 110 peak almost disappeared at 1190 °C before the heating interruption. However, it appears brighter at 1200 °C after the re-heating the sample. The resulted γ -solvus temperature is 1210 °C, which could be 10 °C lower, when the heating interruption would not happen. Comparing the RT neutron detector picture of the start and after the interruption at 1160 °C for the same Ti-42Al-1Fe one can see a more intense γ 110 peak before than after the heating interruption. Additionally the higher heating velocity gave a 20 °C higher γ -solvus temperature. Results of a short literature research is represented in the following section whether the heating rate dependency of the γ -solvus temperature was observed.

Overlap of α_2 phase 101 peak position with the sample holder Al_2O_3 peak

The fixation point of the reference rod of the dilatometer during the first neutron dilatometer measurements yielded to an additional peak superimposed with the α_2 101 peak position. In Table 25 the samples of the second sample set are separated in two groups with a single and double peak at the position of the α_2 101 peak. Both the double peaks were found to belong to Al_2O_3 . The additional peaks made the determination of the $\alpha_2 \rightarrow \alpha$ phase transformation temperature impossible. Especially for the case of the second sample set where there is a very small amount or an absence of the α_2 phase, as already mentioned in the description of the SEM results in subchapter 5.1.3. The Al_2O_3 peaks could either stem from the sample holder and the reference rod or from an Al oxide formed on the surface of the sample at HT. However, the appearance of real oxide on the sample surface was experimentally found to happen at higher temperatures than the $\alpha_2 \rightarrow \alpha$ phase transformation, especially under Ar atmosphere. Of the two peaks one corresponds to the sample holder controlling the sample position and the smaller one to the reference rod. The reference rod being on the way between sample and incoming beam, gives a slightly different 2θ position due to its different distance to the detector. Thus two separated peaks occur. The sample holder was heated from the sample

(even with other thermoconductivity) while the reference rod staid cool. Therefore the position of one peak is moving on the detector making it behave to the α_2 101 peak.

During the second neutron dilatometer measurement no Al_2O_3 peak was found because no reference rod was used and the beam size was smaller, but also no α_2 peak which corresponds with the absence of the α_2 phase in the microstructures. At higher temperature some weak oxide peaks appeared in Ti-42Al-0.2B, Ti-42Al-4Cr, Ti-42Al-4Mo, Ti-42Al-3Fe.

The presence of the Al_2O_3 peaks once or twice (doubled ring) very close to the position of α_2 101 peak made the determination of the α_2 phase content impossible. Therefore the neutron data of the second sample set were only used to qualitatively but unambiguously determine the β_0 phase presence in the samples.

Table 25 Samples with double and single peaks at the position of the α_2 101 peak of the second sample set.

Single peak at	Double peaks at
Ti-42Al-3Fe or only few points 7070 - 7073	Ti-42Al-1Fe
Ti-42Al-6Mo	Ti-42Al-Ref
Ti-42Al-8.5Ta	Ti-42Al-8.5Nb
Ti-42Al-10Nb	Ti-42Al-4Cr

6.2.2.2 The second neutron dilatometer measurements

Influence of collimator problem

During the second neutron dilatometer measurements the β_0 101 peak is "doubled". This doubling could be a sign of the ω_0 phase presence when the temperature region below 900 °C. At higher temperature that could be a result of bad collimation of scattered neutrons. However, the γ peak is mainly not "doubled". Probably it could be explained, that neutrons scattered at different 2θ angles do meet the collimator plates differently, resulting in differently separated peaks.

The second sample set phase transformation temperatures

Only one method of data analysis the Gauss fit was fully performed for neutron dilatometer data of the second sample set. Table 26 and Appendix 5 contain the temperatures according to value of FWHM abruptly changes up. The temperature correlated with the number of the last spectrum, where the FWHM is still a reliable value is taken as the phase transformation temperature.

Here results of two neutron dilatometer measurements are summarized:

Ti-42Al-1Fe has same γ solvus temperature in both the first and the second dilatometer measurement. However, no β_0 is visible in the second measurement - that could be explained by low phase content, different grain statistics and non-homogeneous distribution of phases within the sample.

Ti-42Al-3Fe: γ solvus temperature in the second measurement is higher than in the first one. The β_0 100 peak disappeared 10 °C lower in the second measurement, however, this 10 °C

difference is not more than an uncertainty between temperatures determined by FWHM and Intensity analysis at neutron dilatometer measurement.

Ti-42Al-6Mo: γ disappeared at 1250 °C in the first dilatometer measurement and at 1190 °C during the second measurement. The higher temperature in the 1st measurement could result from interrupted heating. The β_0 has a similar phase transformation temperature.

Difference in the phase transformation temperatures in all neutron data due to the possible influence of different heating rate is shortly described in chapter 2 and will be discussed further in subchapter 8.1.1.

Table 26 Temperatures where peaks have been seen the last time for the second sample set

	Beta 100	Alpha 101	Gamma 110
Ti-42Al-1Fe	1110	1110	1190/1200
Ti-42Al-3Fe	1130	X	1230
Ti-42Al-4Cr	1120 (1130)	x	1190 (1200)
Ti-42Al-6Cr	1110 (1120)	X	1180
Ti-42Al-4Mo	1250 (1260)	X	1230, (1240)
Ti-42Al-6Mo	1250	X	1260
Ti-42Al-0.2B	X	1120	1170
Ti-42Al-8.5Ta	1080		1200
Ti-42Al-10Ta			1240
Ti-42Al-8.5Nb	Double peak		1200
Ti-42Al-10Nb	1180		

Chapter 7 Discussion of the influence of the alloying elements on the TiAl alloys properties

The discussion section is divided into two parts. One part is represented by this chapter 7 and will be dedicated to comparison of the TiAl properties, found by different performed laboratory and in situ methods. The following chapter 8 covers the experience of the first neutron dilatometer measurements, to choose the best method combination for performing in situ diffraction measurements.

7.1 The influence of the third elements on the phase composition and phase transformation temperature

At temperatures where hot-deformation processes, such as forging and rolling, are conducted, the amount of ductile β phase should be considerably high in order to facilitate plastic deformation. However, at service temperature ($T < 800$ °C) the volume fraction of the β_0 phase is designed to be small in order not to deteriorate mechanical properties, e.g. creep strength. Therefore the influence of the third element on the evolution of the β_0 and other phases with temperature is discussed here.

7.1.1 The influence of the third elements on the phase composition determined from synchrotron data

7.1.1.1 The influence of Cr and Mo on the change of phase contents with temperature

There is an interesting result: one can observe an increase (local maximum) of the β_0/β phase content at about 1100 °C in Ti-42Al-2Cr and Ti-42Al-2Mo samples. This is correlated with a decrease of γ and α_2 phases content. Other samples, containing no β_0 phase, exhibit no decrease of the α_2 phase content at about 1100 °C. However, in Ti-42Al-2Cr, which contains β_0 phase, no α_2 phase decrease and only β_0 phase increase at about 1100 °C is visible or is very small.

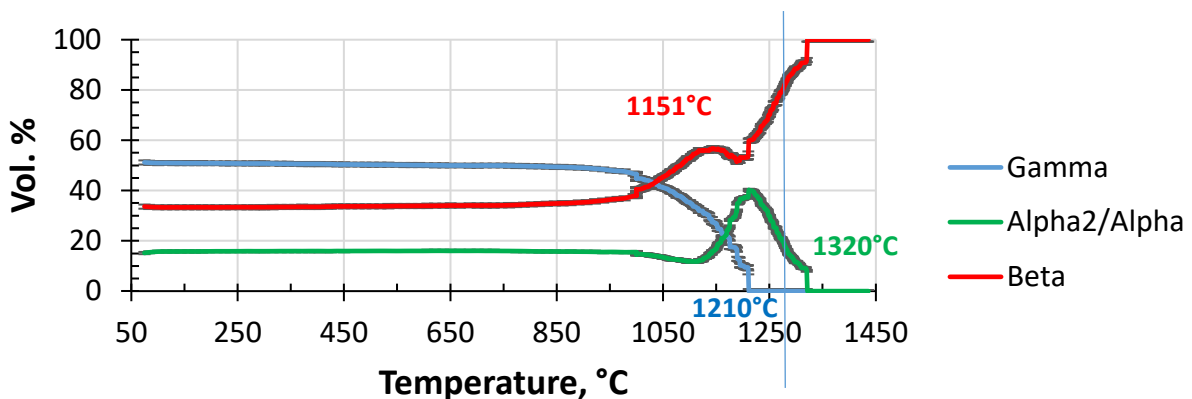


Figure 49 Phase composition, Ti-42Al-2Mo

Figure 49 shows the phase content over temperature for Ti-42Al-2Mo, where the decrease of the α_2 , and the γ phases gives rise to an increase of the β phase content before the $\alpha_2 \rightarrow \alpha$ transformation finishes at about 1110 °C. The amount of the α_2/α phase decreases by 7 vol. % in the sample with 2 at. % of Mo. At 1113 °C the decrease of the α_2 phase stopped and an increase starts again. Such behaviour of α_2 phase could be connected with the start of $\alpha_2 \rightarrow \alpha$

phase transformations (occurring for 2Mo sample at about 1124 °C). The increase of the α_2 phase makes the increase of the β_0 phase slower and at 1151 °C the β_0 phase content reaches its local maximum. Further increase of the α_2 phase yields to a decrease of the β_0 phase up to 1193 °C. After 1211 °C the α phase content starts to decrease up to its minimum value at 1320 °C. The γ phase already disappeared at 1210 °C therefore the β phase was fixed as the only phase present above 1320 °C, due to bad grain statistics at HT and impossibility to determine the presence of the α phase unambiguously.

In Table 27 one can see the correspondence of the α phase maximum to the local minimum of β_0 phase which differs by 17 °C for our Ti-42Al-2Mo sample. Here a decrease of the γ phase content played a role in increase of the β_0/β and α_2/α phase content. The decrease of the beta phase between 1110 °C and start of its increase again could not be referred to β_0 to β (1204 °C), but to α_2 to α (1136 °C) phase transformations.

Table 27 Comparison of extremum points of phase content curves between samples of 1st sample set. Ti-43.9Al-4.0Nb-0.95Mo-0.1B [SCHL2012] for HT and HEXRD

	Ti-42Al-2Mo, °C	Ti-42Al-2Cr, °C	Ti-42Al-2Fe, °C	Ti-43.9Al-4.0Nb-0.95Mo-0.1B
γ phase starts to decrease	1000	1000	900	1150
α_2 local min	1113	1000	1137	1149
β local max	1151	1110	932	1160
β local min	1194	1210	830 - 909	1250
α local maximum	1211	1231	1260	1260

A similar behaviour was found by Mayer et. al [MAYE2017] and Schloffer et al. [SCHL2012] in TNM (Ti-43.9Al-4.0Nb-0.95Mo-0.1B) shown in Table 28. The comparison of literature and Table 17 with Table 20 or Table 16 exhibits a difference in the $\alpha_2 \rightarrow \alpha$ phase transformation temperature. The smaller difference between the $\alpha_2 \rightarrow \alpha$ and the $\beta_0 \rightarrow \beta$ phase transformation temperatures in TNM alloys could occur due to the smaller amount of Mo and the addition of Nb.

An attempt to correlate the appearance of the local maximum with change of the degree of ordering is exhibited in graphs by appendix 2c. However, the difference between the disordering phase transformation temperatures and local maximums/minimums of the α_2 / α and the β_0 / β phases do not show straight correlation. Especially increase of the third element does not bring more clearness in the local maximum phenomena, mainly due to no local maximums were observed with higher element contents. In the samples from the second sample set the similar local maximum was found only in 6Cr, 8.5Ta, but not in the 4 and 6 at. % of Mo. Interpretation of the second sample set is currently in discussion, however no tendency about an influence of the third element content on the appearance or height of the local maximum is obvious.

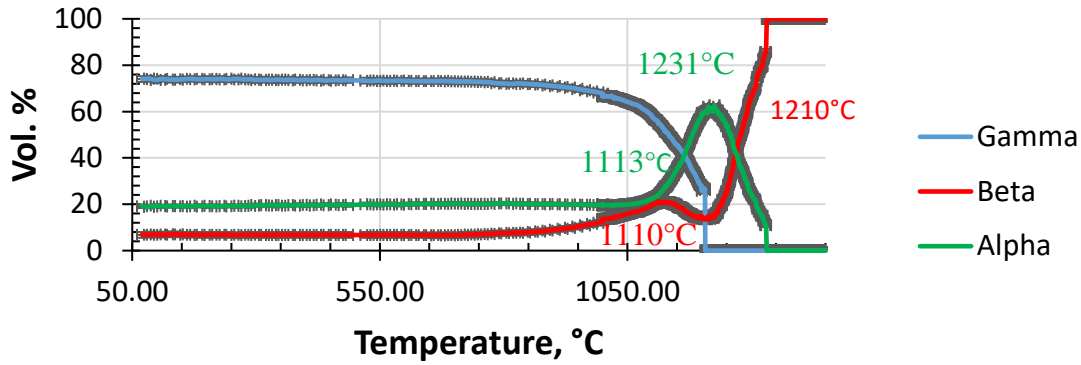


Figure 50 Phase Composition of Ti-42Al-2Cr

A different increase in the β_0 phase content is visible in the sample with Ti-42Al-2Cr (Figure 50). Here no α_2 phase decrease is visible below 1000 °C and the increase of the α_2/α phase starts above 1100 °C almost simultaneously with the β_0 phase decrease. Additionally γ phase transformed to a higher amount into the α phase than into the β_0/β phase.

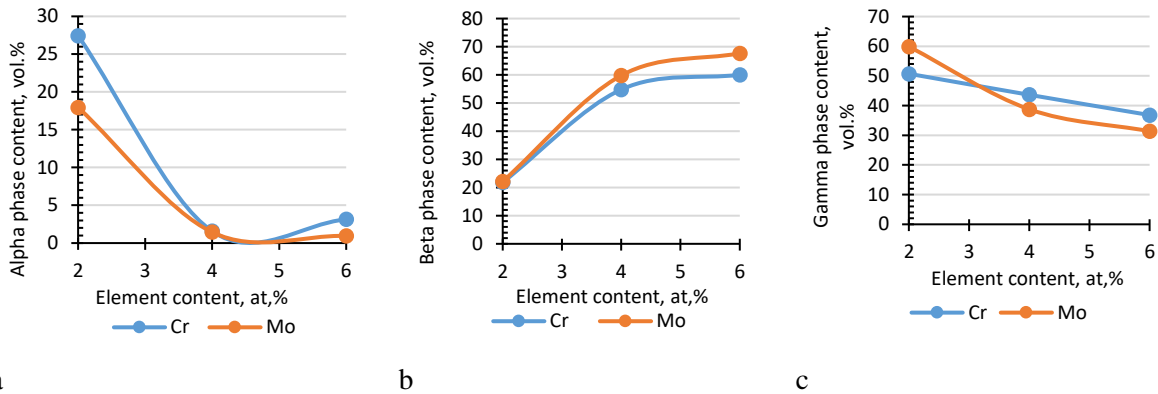


Figure 51 Phase content comparison in samples with Cr and Mo at RT.

Figure 51 shows the difference of β_0/β , γ , α_2 phase content measured at RT for samples with Cr and Mo. An increase of the Cr and Mo content resulted in an increase of the β_0/β phase content. The lines are, however, not parallel, indicating slightly different influence of the elements. Mo in a similar content as Cr gives slightly higher β_0/β phase content (Figure 51 b). The higher Cr and Mo contents as were expected are responsible for the higher β phase that should lead to the corresponding lower content of γ and/or α_2 phases.

Indeed the γ phase content decreases with increase of Cr and Mo content (Figure 51 c). and the α_2 phase content increases a bit between 4 and 6 at. % (Figure 51 a). However lines of phase content change are nor parallel. Inhomogeneous α_2 and γ phase content change between 4 and 6 Cr or Mo could be a reason of still not perfect grain statistics. Under comparison of γ phase content between all samples of the first sample set in chapter 6.1.2 Cr has the strongest γ – stabilizing properties, Mo the weakest.

In Table 28 phase transformation temperatures of Ti-42Al-2Mo alloy is compared with data of TNM alloys. All the temperatures of our sample are lower than corresponding ones of TNM alloys. The difference could be caused by lower Mo and higher Al content as well as addition of Nb. The difference in Al content according to binary phase diagram in Figure 2 has no influence on $\alpha_2 \rightarrow \alpha$ phase transformation. Thus influence of the Mo and in higher degree Nb should be decisive.

Table 28 Phase interconnections in literature.

Sample composition and source	$\beta \rightarrow \beta_0$, °C	Minimum of β , °C	Vanish of β_0 , °C	$\alpha \rightarrow \alpha_2$, °C	γ solvus, °C	Method used
Ti-43Al-4Nb-1Mo-0.1 (Clemens and Mayer 2016)	1415	1275	600	Slightly above 1110	About 1250	Calculated
Ti-43Al-4Nb-1Mo-0.1 (Cha, Clemens et al. 2011)	1210					Neutron Diffraction
Ti-43Al-4Nb-1Mo-0.1B H. Clemens Intermetallics 16 (2008) 827-833	-	1259	600	1165±5 °C	1285±5 °C	HEXRD
Ti-42Al-2Mo	1204			1136	1206	HEXRD

7.1.1.2 The influence of Fe on the change of phase contents with temperature

A similar β_0 phase content increase as in samples with Mo and Cr, but at lower temperature (950 °C), could be observed in Ti-42Al-2Fe (Figure 52). In this sample the α_2/α phase content decreases by 16 vol. %, but here the decrease was calculated from the RT level, and the τ_2 phase appearance additionally influences the α_2/α phase content decrease. The τ_2 phase is assumed to occur during cooling with furnace after heat treatment at 1100 °C.

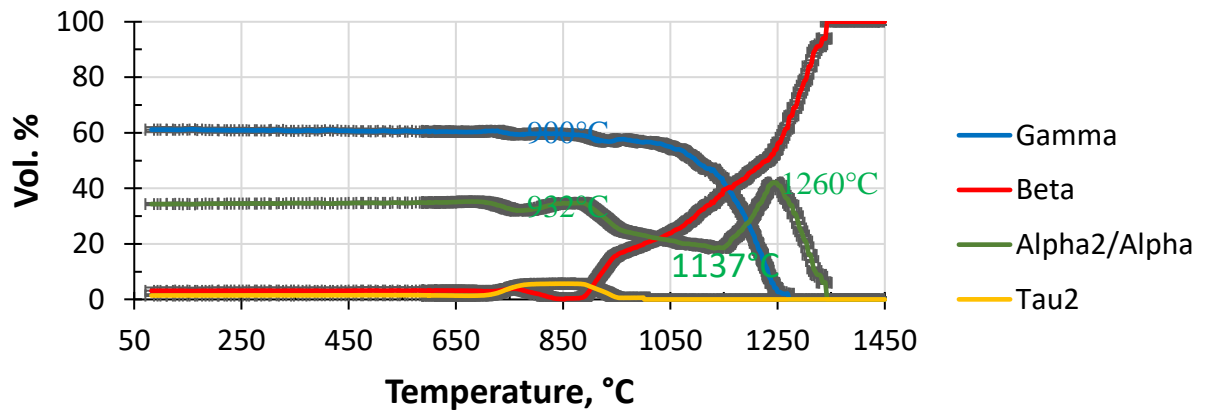


Figure 52 Phase composition, Ti-42Al-2Fe.

Synchrotron measurements with and without rotation were performed at RT, resulting in different phase contents (Appendix 6). **The β_0/β phase content** increases with increase of Fe between ternary samples (Figure 53). It could be mentioned, that before the $\beta_0/\beta \rightarrow \tau_2$ transformation occurs above 600 °C the amount of the β_0/β and the τ_2 phases is constant during heating. One can also mention an influence of the grain statistic: in the RT spectrum of the Ti-42Al-2Fe sample measured with rotation the τ_2 440 peak is higher than at RT without rotation

performed before the in situ HT measurement. At RT with rotation no τ_2 phase was found in Ti-42Al-1Fe, however without rotation at about 100 °C very small amount of τ_2 phase detected. That should not mean that τ_2 phase occurred in the range between RT and 100 °C, just the main factor is not good grain statistics. **The γ phase content** increases with increase of the Fe content at Figure 53 and to a lesser degree with an addition of the τ_2 phase. **The α_2 phase content** decreases with increase of Fe content from 2 to 3 at. %. The τ_2 phase formed mainly at expense of both γ and α_2 phases.

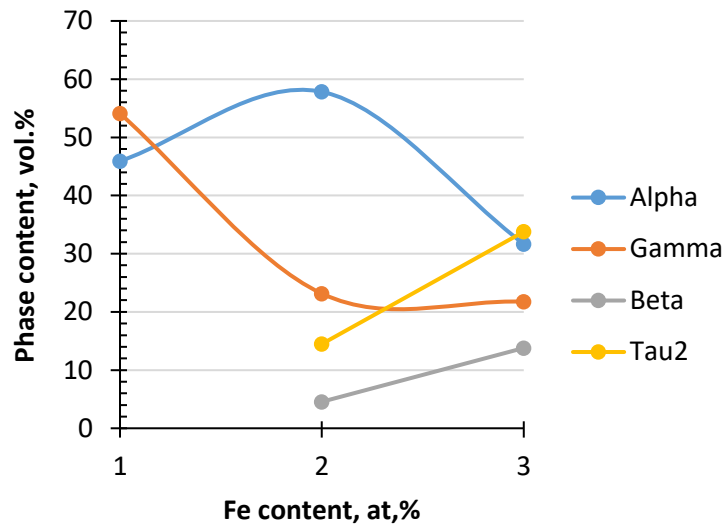


Figure 53 Change of phases content with increase of Fe content at RT according to synchrotron data with rotation.

7.1.1.3 The influence of Nb and Ta on the change of the phase contents with temperature.

Nb and Ta gave in our investigation very similar results. Both do not have any β_0/β phase presence at 2 at. %. The β_0 phase is present only in samples with the higher element contents: 8.5 and 10 at. %. The β_0 phase content increases in the full temperature range in the sequence 8.5 at. % Ta, 10 at. % Ta, 10 at. % Nb. Additionally in the samples with 8.5 and 10 at. % the two ω_0 peaks 110 and 102 can be observed at the position of the β 110 peak. It is known to be possible to distinguish between the β or the ω_0 or determine the presence of both via transmission electron microscopy (TEM). Cha et. al [CHA2011] have shown that the β_0 -phase co-exists with ω -phase (B8₂-structure). Therefore in RT synchrotron measurements the presence of the β_0 and the ω_0 phase were refined simultaneously which resulted in a higher ω_0 phase content than the β_0 content. Stark et al. [STAR2008] have also found a presence of both the β_0 and the ω_0 phases simultaneously: “After deformation at 900 °C in the middle of the ω /B8₂ double peak a third peak occurs. This is the 110-peak of the β /B2-phase which occurs besides the ω /B8₂-phase...”. The β -phase was assumed in the article as an ordered one with B2 structure although no β_0 - 100 reflection was found being an indication of order.

The presence of the ω_0 phase in samples with 8.5 and 10 at. % of Ta and Nb between 600 and 900 °C is undoubtedly shown at Figure 54 via 100 of the ω_0 beside the γ 001 peak. According to the Gibbs phase rule in a three component system only three phases could be present simultaneously. Thus an equilibrium state cannot be assumed in samples with 8.5 and 10 at. % of Ta and Nb.

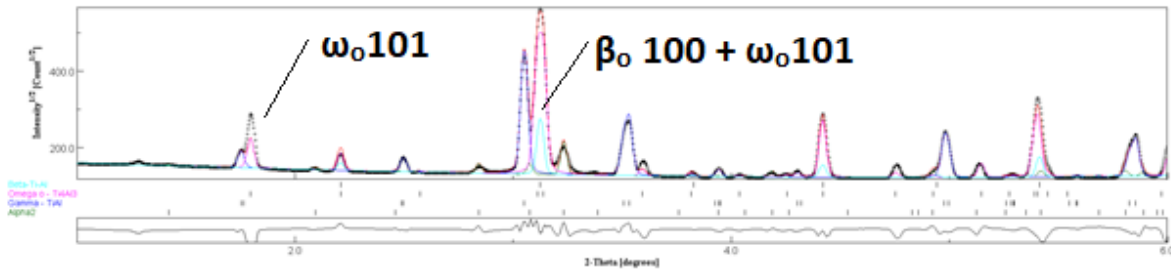


Figure 54 A Rietveld refinement of Ti-42Al-8.5Ta with 4 phases presented (α_2 , β_0 , γ , ω_0)

7.1.1.4 The influence of Al concentration on the phase composition

The influence of Al content on the phase composition can be determined for the first and second sample sets at RT based on synchrotron data in Table 13 and is represented in Figure 55.

The β_0/β phase content: There was no β_0/β phase found in binary alloys, therefore Al content between 39 – 45 vol. % has no influence on the β_0/β phase content. The change of the α_2/α and γ phases content in binary and semi-binary alloys corresponds to the binary phase diagram.

The α_2/α phase content: Ti-39Al (92.05); 39Al0.2B (92.05); 42Al0.2B (52.60); 42Al (67.01); 45Al (20.09)

The γ phase content: Ti-39Al (7.95); 39Al0.2B (7.95); 42Al0.2B (47.38); 42Al (32.99); 45Al (79.11)

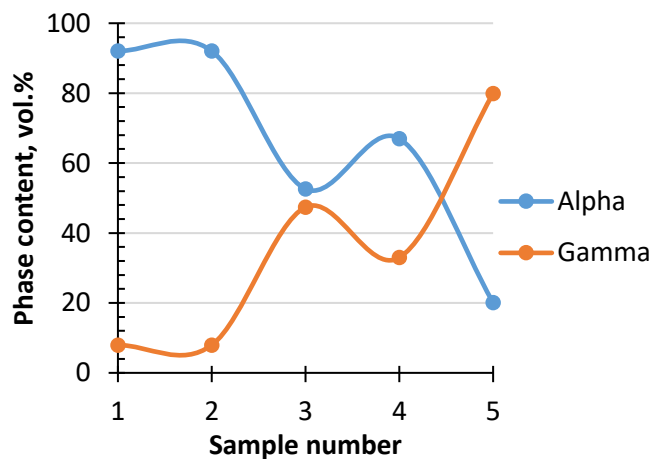


Figure 55 Phase content change with decrease of Al content: 1 - 39Al; 2 - 39Al0.2B; 3 - 42Al+0.2B; 4 - Ti-42Al; 5 - 45Al

Summing up the subchapter 7.1.1 one can see γ stabilizing properties of Al, as well as of all the 3rd elements. Increase of the γ phase amount was visible in all ternary alloys. However only in samples with Mo and Fe the γ -solvus temperature was higher than in binary Ti-42Al.

7.1.2 Comparison of the phase content from neutrons and synchrotron results

The amount of the β_0/β , the γ and the α_2/α phases according to the Rietveld refinement of neutron and synchrotron data at RT is compared in Appendix 6. The assumed error for our refinement of phase content occurring due to the grain statistics of our samples is up to 3%.

The β_0/β phase content is higher in synchrotron data, but for the γ and the α_2/α phases there is no tendency for constant elevation of the one diffraction method above the other one. There is the following reason for the β_0/β phase content difference. As no fundamental peaks are visible by neutrons, it could be that the volume of the β_0 calculated from neutron results is lower than the present amount of β_0 phase because the calculation method is based on a perfectly ordered phase. In other words the amount of the β/β_0 is higher from synchrotron data because the β/β_0 is not fully ordered and the site occupancy calculated from synchrotron data is not 100%. The degree of ordering of the β_0/β phases is an average characteristic of a sample, having regions with better and worse ordering, that will be discussed later in 7.2.2. Additionally due to a composition different to the ideal stoichiometry of the β_0 phase the ordering cannot be perfect in the alloys investigated in this work.

Differences in the α_2/α and γ phase content could be due to the difference in β_0/β phase content but as well could compensate each other. As long as in both methods the sum of phases should be 100%, the amount of the α_2/α and γ should be slightly different too. Let us further compare the neutron and synchrotron diffraction results as shown in Appendix 6. The amount of the α_2/α and γ is no one time lower or higher according to one diffraction method, then the other. As long as the difference in the content of the same phase in the same sample does not elevate 8% it is supposed the difference lies slightly above the accuracy of the HT measurements. During comparison of the amount of phases determined by both diffraction methods the influence of Mo and Fe could be confirmed: Mo is the strongest β -stabilizing element before Fe. However the increase of the β_0/β phase content in sample with Cr from synchrotron does not correspond with the decrease determined from the neutron data. Theoretically all the elements Mo, Cr, Fe, Nb, Ta have bcc structure as the β phase, but different lattice parameters, that could result in better stabilisation of the β or β_0 phases. E.g. lattice parameter of Fe is 2,87, Cr 2,91, Mo 3,15, Nb and Ta 3,30. The lattice parameter of β_0 phase at RT lies between 3,19 and 3,20 (see Appendix 7) and for β phase is about 3,3 (see Table2). One can see that if the lattice parameter of an Element is \leq than the β_0 phase has, it will preferably stabilise the β_0 phase, if higher (thus closer to the β phase) then no obvious β_0 stabilising properties.

With respect to γ -stabilization Cr is the strongest, then Fe and only slightly Mo. These three elements cause a lower α_2/α phase content, than binary Ti-42Al. For alloys without presence of the β_0/β phase, namely Ti-42Al-2Nb and Ti-42Al-2Ta presence of the β -stabilizing elements results in an increase of the γ phase content. Here the same tendency of elements as from neutron as well as from synchrotron data is confirmed for both RT and 1000 °C.

7.2 The influence of the elements on the properties of each phase

7.2.1 Comparison of lattice parameter determined by Rietveld refinement of neutrons and synchrotron diffraction data with literature

RT values. Lattice parameter difference was analysed for synchrotron and neutron diffraction methods by Rietveld refinement as well as by Gauss-fit. Appendix 7 contains a tables for comparison of the lattice parameter values at RT. The maximum difference between two diffraction methods is 0.085 Å for c of the α_2/α . The difference between samples is up to

0.057 Å for the α_2/α , 0.028 Å for β_0/β and 0.047 Å for γ phases from synchrotron data. The difference from neutron data is however smaller: 0.03 Å for the α_2/α and 0.08 Å for β_0/β (β_0/β according to neutrons present in one sample only) and 0.014 Å for γ phases. It was expected that the difference between lattice parameters for the α_2/α and γ phases would be lower than for the β_0/β phase, because the β stabilizing elements are integrated mainly in the β_0/β phase. However this was not found. One may speculate that if the β/β_0 phase is not present, the β_0/β stabilizing element enriches mainly into α/α_2 , that is confirmed by our EDX results.

In reference [HADD1994] the author explained a lattice parameter difference “by partial substitution of titanium by aluminium which has a smaller atomic radius (0.143 nm for aluminium and 0.147nm for titanium).” This effect could be also present in our alloys, when a difference between the β phase lattice parameter is discussed. From the one side the atom radius plays a decisive role in building of metallic chemical bondings in pure metals. Thus it was expected that the lattice parameter values are proportional to the atom radius: Al-1.18, Fe-1.56, Cr-1.66, Ti-1.76, Mo-1.90, Nb-1.98, Ta-2.00 Å [ARAD]. From the other side it is mentioned in the introduction that TiAl alloys are not pure metals but intermetallics, where not only a metallic but also a covalent chemical bonding type exists. Therefore the atom radius sequence is not similar to the lattice parameter change measured in the samples at RT. The covalent chemical bonding type depends from atoms electronegativity. However, its dependency is much less than in ionic bonding type. From the one side the atoms with higher electronegativity could have a higher attraction of electrons even in crystals with pure covalent bonding. The electronegativity of our atoms increases in the following order Ta-1.5, Ti-1.54, Nb-1.6, Al-1.61, Cr-1.66, Fe-1.83, Mo-2.16 [ENEG]. From the other side as long as in TiAl alloys the chemical bonding is neither fully metallic nor covalent, the order of electronegativity increase also does not correspond to the lattice parameter change of our samples. Additionally no information was found about the percentage of the metallic and covalent bonding type that results in a special volume of the unit cell. Therefore the lattice parameters of phases in different samples are determined by different correlations between change of pure atom radius and electronegativity.

Without a consideration of such a detailed atom properties one can think about the influence of the lattice parameter of the third element, which already are determined by the detailed considered properties. So lattice parameter of the BCC lattice of Fe is 2.87, Cr 2.91 Mo 3.15, Nb and Ta 3.30 Å. Due to the small amount of the 3rd element and its tendency to be incorporated in the bcc/B2 β/β_0 phase the difference in the β/β_0 only and not the α_2/α or γ phases are to be explained.

Table 2 of [SING2007] gives a similar difference of ± 0.001 Å between phase lattice parameters of their samples. The same difference was found in comparison to our sample, which is due to the different sample composition. Because of the different Al content compared to our samples as well as higher amounts of the third elements it is more complicated to determine the influence of each element.

Change with temperature. For higher temperatures the comparison is better to perform by graphs. Analysis of graphs of lattice parameters change with temperature with two evaluation methods (Rietveld and Gauss) for neutron and synchrotron results shows the following peculiarities. (1) There is a similar trend of lattice parameters increase in all methods during heating. However, a difference between lattice parameter trend lines for samples is up to 0.02 Å. Similarly to RT lattice parameters values, the determined lines not fully correlated with the change of the atom radius or electronegativity of atoms of all phases, which could be explained by a more complicated dependency of the lattice constants on both atom parameters, and also from the crystal structure. (2) The synchrotron data gives information about the lattice

parameters increase in a wider temperature range. Rietveld refinement gives higher fluctuations than Gauss fit.

The c/a ratio. A correlation of the lattice parameters namely the c/a ratio is of high interest for crystallographers and material scientists alike. The change in the c/a ratio in phases with less symmetric unit cells than cubic can help to detect phase transformations, as in the case of $\alpha_2 \rightarrow \alpha$ and γ – solvus phase transformation. Pfullmann et. al. determined the variations of the lattice parameters c/a as a function of Al content for γ phase, which “show linear relationships. With increasing Al content the a value is found to decrease and the c value to increase slightly. The result is a c/a ratio which decreases from 1.023 at 54 at. % Al to ~ 1.010 at 48 at. % Al” [PFUL1993]. In our alloys the c/a ratio lies in the range 1.007 – 1.011.

The influence of c/a ratio on ductility of TiAl alloys is discussed in [YONG1989]. “With decreasing aluminium concentration, the γ -TiAl phase exhibits a reduction in c/a ratio”. In our alloys increase of the Al content in binary alloys results in a decrease of the α_2/a lattice parameters a and c: Ti-42Al (a 5.818, c 4.675 Å, c/a 0.804) and Ti-45Al (a 5.766, c 4.628, c/a 0.803), as well as decrease of the γ lattice parameters a and c, but decrease of the c/a ratio: Ti-42Al (a 4.058, c 4.09 Å, c/a 1.008) and Ti-45Al (a 4.015, c 4.057 Å, c/a 1.01). Such behaviour of lattice parameters decrease is determined, most probably by smaller atomic radius of Al, than of Ti. However it is explicitly shown few paragraphs above the interplanar distance in TiAl alloys does not depend from atom radius or atom electronegativity purely. The increase above 1120 °C of the c/a ratio of the γ phase could be yielded by higher decrease of lattice parameter a than the lattice parameter c.

The thermal expansion coefficient. The coefficient of thermal expansion is defined as the fractional increase in length per unit rise in temperature. Lattice parameters change could be used for calculation of the thermal expansion, (in one direction (linear coefficient) or of the unit cell volume). E.g. P. Staron et al. [ST-N2021] investigated the dependency of the volume of the unit cell on temperature. However, there is difference in formula for calculation of the CTE coefficient by P. Staron, which was calculated as three times higher, than by our work linear one. The average between different samples values of a and c lattice parameters for the α_2 phase increase almost linearly due to thermal expansion up to about 1100 °C. The a lattice parameter grows by about 0.075 Å within the range 100 - 1100 °C starting at 5.76 Å which results after normalization to RT value (5.76 Å) in a linear thermal expansion coefficient of $13.0 \times 10^{-6} \text{ K}^{-1}$. However for the c lattice parameter it is 0.05 Å starting at 4.63 Å. Thus the linear thermal expansion coefficient in c-direction is $10.8 \times 10^{-6} \text{ K}^{-1}$.

The CTEs could be used to estimate residual inter-phase stresses and macro-stresses during cooling, which are of importance to estimate damage that might occur during manufacturing, processing, and heat treatments “Rapid cooling of materials can lead to internal stresses and cracking”. That was purposely avoided by the heat treatment of our samples. Thus our values are not too high. “In the TNM material, which softens around 900°C [ST-N2021], only the temperature range between RT and 900 °C is relevant for the formation of residual stresses. The strongest difference in lattice contraction (CTE) during cooling is between c(α) and c(γ), being 1.3×10^{-3} (relative value) from 900 °C to RT. Multiplying this with the modulus of elasticity of about 160 GPa for a rough estimate gives a stress value of 208 MPa. Consequently, cooling from temperatures above 900 °C can lead to significant internal stresses between the phases, which are termed micro-stresses or stresses of type II, but it will generally not lead to immediate cracking since this stress level is still far from the yield stress of TiAl alloys.” [ST-N2021]

7.2.2 Site Occupancy

Let us at first compare the SO from RT synchrotron data only, without neutron measurements values for β_0/β phase with an amount of phase in Table 29 for the two sample sets. One can see that an increase of the β stabilizing element does not necessarily yield a higher β_0/β phase site occupancy.

Then values of SO are compared with the difference between neutron and synchrotron phase amount for Ti-42Al-2Mo, 2Cr, 2Fe. A minimum SO value at RT of 0.67 corresponds to Ti-42Al-2Cr, which has not the highest difference between neutron and synchrotron phase content (3 and 4.5 vol. %). One should remember that due to rotation of the sample at RT the phase content differs from the RT phase content in dilatometer without rotation. The highest difference of 14 vol. % corresponds to Ti-42Al-2Mo (but lower in synchrotron with rotation – 3,58 vol. %), which has the highest refined value of SO (0.817). The Ti-42Al-2Fe with a bit lower SO (0.816) has not high difference between neutron and synchrotron phase content at RT (+7 and -3,2 vol. %). Thus, one can see that SO value does not directly correlate with difference in amount of β_0/β phase between neutron and synchrotron radiation in these samples. The grain statistic plays an important role. The expected dependency could be explained in following way: The higher degree of ordering would be possessed by the phase, the higher would be superstructure peaks, the higher would be refined SO values, as well as all amount of β phase visible with synchrotron would be closer to the amount of the β_0 from neutrons.

Further when temperature increases above 1000 °C intensities of all the superstructure peaks become lower (Table 26, figure 10, 6.1 Synchrotron in situ measurements results), the site occupancies of α_2 and β_0 and γ phases by synchrotron decrease, the calculated amount of the ordered phases should be decreased in both neutron and synchrotron methods. However, the decrease was not observed by neutrons. The Rietveld program tends to calculate all amount of phases as 100 %. When no fundamental peaks of α_2 and β_0 phases are visible that would give the level of real 100 % phase content, it is difficult to track the real phase content with neutrons near disordering temperature because the phase correlation is based only on the rest of the ordered phases.

Indeed differences between neutron and synchrotron α_2/α and β_0/β phase contents are expected to increase. However how one can see at Figure 44a due to explained above the amount of all α_2/α , β_0/β as well as of γ phase are overestimated and there is no increase between amount of ordered α_2 , β_0 from neutron data and disordered α , β from synchrotron data, that is an example of the unavoidable misrefinement, and not a problem of the refined model.

An influence of τ_2 phase presence on the SO refinement of β_0/β and α_2/α phases.

There was found no change of the SO value of β_0/β phase due to the addition of the τ_2 phase. There were refined site occupancies for two cases of sample with 2Fe as compared in Table 13, (1) when the presence of a τ_2 phase was taken into account and (2) was not taken into account. The amount of the β_0/β phase is not very high at RT in samples with Fe and it decreased, due to the inclusion of another phase in the refinement, thus correctness of the SO refinement of the β_0/β phase could be doubtful. It was found no change of the correlation between intensities of superstructure and fundamental peaks of the β_0/β phase by Gauss fit. Due to inclusion of the τ_2 phase in the refinement it could be observed additional difference for the α_2/α phase and its SO values, especially when the amount of α_2/α phase is small.

Table 29 An influence of the elemental content on the SO at RT. Precision of SO determination is 0.04.

Sample	β_0 SO from synchrotron RT, %	Difference between neutron and synchrotron, vol. %	Amount of β_0/β , vol. %,by Rietveld.
Ti-42Al-2Mo	81.7	14.9	33.64
Ti-42Al-4Mo	99.9		
Ti-42Al-6Mo	64.1		
Ti-42Al-2Cr	66.7	7.03	11.62
Ti-42Al-4Cr	91.7		
Ti-42Al-6Cr	85.8		
Ti-42Al-2Fe+ τ_2	81.6	3.00	3.10
Ti-42Al-3Fe+ τ_2	86.5		

Position of the third element. In the case of current investigation the position of the third element was not taken into account, because (1) in the first sample set the amount of the third element is only 2 at. %, which, probably, will give a small influence on the site occupancy; (2) even using models similar to real chemical compositions of the samples and their phases instead of stoichiometric ones (see laboratory methods results), an electron density change (of every of A or B sites) could not unambiguously be determined. Some site occupancies would be simply not distinguishable because 2 at. % of Ti₂₂ or 1 at. % of Mo₄₂ would give the same electron density change.

A good example of detailed calculations with a possible atom site occupancy of the B2 structure in Ti-Al-Mo system is given in [SIGH2008]. Additionally, preferential sites for different elements are described in [HOL2015-1,2]. Sigh [SIGH2007] and co-authors assume the site occupation of the B2 phase in Ti-26Al-20Mo and Ti-37.5Al-12.5Mo alloys and refine sample spectra using the Rietveld refinement of XRD. Assumption of Sigh shows, that the Ti atoms tend to occupy one site, let us call it A, while Al and Mo atoms occupy B site. The excess of Ti atoms occupy the B sites. As one can see from the sample composition, amount of the Mo is above 10 at. %.

Chapter 8 Discussion of the methods

This chapter describes the experience of the first neutron dilatometer measurements and issues of data analysis in theory and practice. The description of the experimental procedure here yields additional peculiarities to the procedure described in “methods”. Some peculiarities are explained in detail in Appendix 2 and are expected to support future applications of *in situ* dilatometer diffraction measurements. This is important because not only the TiAl - material science community, but as well metallographers, aircraft engineers or even alloy production industry workers could be interested to use the dilatometer for future *in situ* diffraction high temperature or tension-compression tests. The description of the data analysis probably will save some time for future investigators. In the end a comparison of the methods describes the advantages and disadvantages of every method applied to investigate the β_0/β phase transformation.

8.1 Experimental procedure

8.1.1 Precision and accuracy of performed measurements

An estimation of the errors, which can occur, was done in order to estimate the quality of the study. The errors could be separated in groups by their origin:

Instrumental error: This error is determined by the imperfection of the device, arising, for example, due to the divergence of its real conversion function from the one determined by calibration.

Methodical error: This is the error caused by the imperfection of the measurement method. It includes errors from the inadequacy of the accepted model of the object, e.g. not ideal reference with slightly different real from nominal compositions or need of application of different heating ramps for investigation of heating ramp dependent phase transformations.

Subjective error: This is due to the limitations of a person as an operator when making measurements. It manifests itself, for example, in inaccuracies when reading off the scale of the device by e.g. night shifts of experiments. This type of errors could occur during diffraction data analysis, when a lot of parameters are to be analysed simultaneously and decision depends on interpreter.

Some errors from each of this groups were found in the research during data analysis process and are described further, but are separated in groups of influence to important properties of alloys itself and measurements quality.

Inhomogeneity of elemental distribution in alloys.

Non homogeneous distribution of elements in the alloy button could result in the difference between nominal and real sample composition. Arbitrary choose of measurement points could bring some mistake due to different concentration of elements in phases. Thus the same amount of points of analysis is required to be measured in each phase.

Difference in Al content could occur due to its evaporation. The evaporation of the low melting element Al happens under melting conditions of the high melting elements Mo, Ta, Nb.

There are further uncertainties because of peculiarities of a sample or the equipment and partly due to methodical/subjective uncertainties of EDX measurements:

- Difference in the weighted amount of elements up to 0.12 mg.

- absence of the ternary reference sample for every composition and use only binary one for EDX chemical analysis.

Instrumental errors occurred mainly during temperature measurements during the in situ experiment:

- Thermocouples detect temperature via producing of a temperature-dependent voltage. Characteristic values for correlation of resistivity and temperatures are given in tables [THCP]. The temperature values are given with precision up to 0.5 °C.
- During neutron experiment with HTF a systematic deviation of -40 °C was found because the position of the thermocouple differs from the position of the sample – the problem was corrected by subtraction of 40 °C from all determined temperatures.
- The methodological error of temperature determination in diffraction data analysis is a half of the heating step that means for neutrons ± 5 °C and for synchrotron ± 0.5 °C.

8.1.2 Precision and accuracy of interpretation process

The methodological error of the data interpretation depends on the quality of the measurements (grain statistics) and the choice of an adequate refinement model. Under adequate refinement model one should understand the model, which covers the decisive properties of the investigated material and is not overloaded by specific properties which produce the double interpreted results due to not enough grain statistics for the property to be refine. The adequate refinement model determines an ability to trust to the data without looking into each single spectrum/detector picture of each sample. The difference (quality) between calculated and measured diffraction patterns is characterised by the R_{wp} factor for the program MAUD (Formula 10, Figure 56). Difference between samples' R_{wp} is determined by internal properties of the sample. E.g. the worst R_{wp} for the sample with 2Cr is caused by bad grain statistics. The bad grain statistic gives too high or too low intensities of some peaks, which cannot be undoubtedly related to physical parameters of the calculated model and therefore yields to high R_{wp} values.

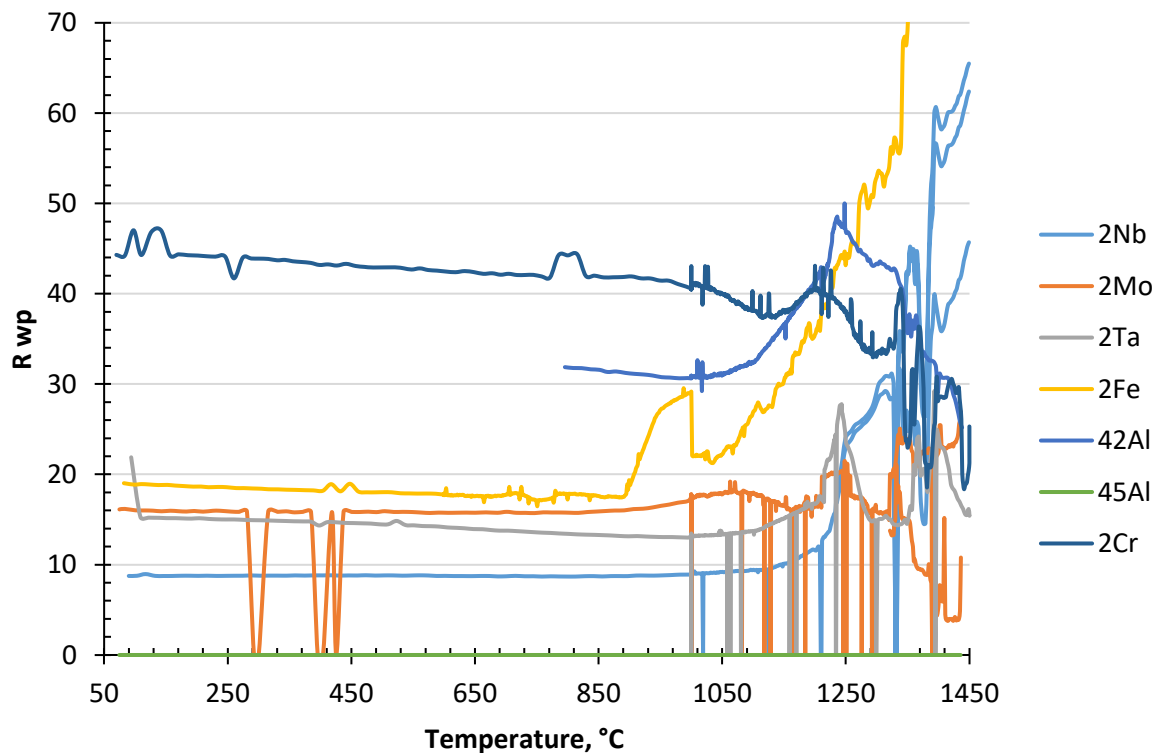


Figure 56 R_{wp} factors of synchrotron data interpretation.

The grain statistic situation of our samples is described in Appendix 2b. In the case of too detailed for refinement some parameters of the model could influence the refined spectrum simultaneously in an opposite way and their influence will be hardly distinguishable, or parameters will double their effect, but be interpreted as the influence of one of them. It is known from our experience: when many parameters were refined in parallel, the site occupancy + B-factor + microstructure (microstrain+crystalline size), it results in unphysical values. L. Lutterotti (the author of the program MAUD) explains that complex refinement situation could yield to the appearance of a local minimum in the difference between calculated and measured spectra, which is not the desirable result for the interpretation, while giving appropriate R_{wp} . Therefore some assumptions have been made which are shown in the part with theory of the refinement method and which resulted in the following uncertainties:

- Uncertainties of phase composition is ± 1 vol. % at room and ± 5 vol. % at high temperatures.
- Precision of lattice parameters refinement is determined as $\pm 0,01$ Å and difference in lattice parameters is the same $\pm 0,01$ Å (Appendix 7). During heating the lattice constants have been increased for 0.3-0.7 Å, which is a significantly higher value than the uncertainty.

Some additional assumption for microstructure

- The microstructure below 2-3 mm from the surface and in the middle part is the same after homogenization, therefore microstructure was assumed to be homogeneous in the whole sample. No SEM analysis has been performed between melting and heat treatment.
- The methodical/subjective uncertainties of the EDX measurements include the absence of an ideal reference for each ternary Ti-Al-X composition. The small amounts of third elements are detected with bigger mistakes than higher contents.

8.2 Complementarity of the different methods for study of β ordering phase transformation in γ -TiAl alloys

8.2.1 Comparison of experimental and evaluation methods

For study of β ordering phase transformation in γ -TiAl alloys standard methods widely applicable in material science analysis were used: quantitative metallography as SEM to determine the grain size and present phases, differential scanning calorimetry (DSC) and in situ high-energy X-ray diffraction (HEXRD), neutron diffraction. All of them are found to be helpful in a comprehensive view on the produced TiAl alloys.

HEXRD was conducted to study phase transformations and beside recrystallization processes in TiAl alloys were observed during in situ heating with high time resolution. *Neutron diffraction* gives high intensities for the superstructure peaks of ordered phases, but almost zero values for the main peaks, due to bcc and hcp structures of main phases and the special neutron contrast between Ti and Al atoms as it is also mentioned in the Chapter 2 Basics. Consequently, *in situ neutron diffraction experiments* could be the best method for determination of the ordered phase presence and ordering temperature of the α_2 - and β_0 - phases [CLEM2013]. But neutron diffraction could not be called an ideal tool to study order and disorder in the Ti-Al system due to the restrictions for phase content determination, when invisible disordered phases result in incorrect phase amounts after $\alpha_2 \rightarrow \alpha$ and $\beta_0 \rightarrow \beta$ phase transformations. The amount of ordered phases is only trustable below $\alpha_2 \rightarrow \alpha$ and $\beta_0 \rightarrow \beta$ transformations. Due to the absence of fundamental peaks neutron diffraction cannot be applied alone for the determination of the degree of ordering.

Step-wise heating. Currently available neutron sources provide weak intensities for diffraction investigations, so they need much more experimental time in comparison to synchrotron. The brightness of synchrotron sources allows much faster measurements (about a few seconds for synchrotron and up to one hour for good statistic with neutrons). Therefore, there are some restrictions for the investigation of fast changing processes in situ with neutrons. In order to be detected with neutrons at not very powerful neutron sources, a process or condition should remain constant in the material for at least one detector picture counting time. Synchrotron radiation is more convenient for in situ investigations of fast changing processes.

It is interesting to compare not only the neutron and synchrotron diffraction as well as the DSC results but also the two evaluation methods for both diffraction techniques. Appendix 5 contains two tables for both sample sets with phase transformation temperatures of the three experimental methods and both interpretation methods for the first sample set. The second sample set is currently analysed only by Gauss-fit. In order to avoid a misunderstanding, the data from APPENDIX 5 were compared further in the following order: (1) between neutron and synchrotron with the same evaluation method (Gauss fit) and DSC, and (2) between two evaluation methods.

8.2.1.1 Comparison of phase transformation temperatures between neutron and synchrotron with the same Gauss-fit evaluation method

Data of the second sample set are described here mainly according to the Gauss fit. This evaluation method for the first sample set was found to be more precise in comparison with Rietveld and matches very good under comparison of neutron and synchrotron data with DSC results. Describing in more details the data from Appendix 5 and based on the difference between neutron and synchrotron results, the values are divided into several groups. The data with a difference up to 10 °C between neutron and synchrotron results of the first sample set are marked green characters ($\beta_0 \rightarrow \beta$ phase transformation by neutron and synchrotron in Ti-42Al-2Fe; $\alpha_2 \rightarrow \alpha$ phase transformation in Ti-42Al-2Fe, Ti-42Al-2Nb, Ti-42Al, Ti-45Al, synchrotron data for Ti-42Al-2Cr and neutron data for Ti-42Al-2Mo and Ti-42Al-2Ta; and γ -solvus in synchrotron Ti-42Al, Ti-42Al-2Fe, Ti-42Al-2Mo); a difference between 10 and 20 °C is marked blue characters (β_0/β phase transformation in Ti-42Al-2Mo and Ti-42Al-2Cr, $\alpha_2 \rightarrow \alpha$ phase transformation in Ti-42Al-2Mo, Ti-42Al-2Cr, Ti-42Al-2Ta); higher differences e.g. γ -solvus in Ti-42Al-2Cr have a black colour. Summing up it is possible to mention that there is no tendency observed by any method (neutron or synchrotron nor even DSC) being higher than other methods, that would indicate a phase transformation heating rate dependency.

Comparing our results with literature data the reported temperatures are mainly different to our alloys. However, the literature TiAl alloy compositions differ to our chemical composition. Most of the investigated sample compositions in literature are quaternary or more complicated systems. E.g. in TNM alloys the amount of Nb reaches 4 at. % plus some amount of Mo.

8.2.1.2 Comparison between the Rietveld and Gauss (single peak) as evaluation methods

The differences in phase transformation temperatures between the Rietveld and Gauss (single peak) evaluation methods could be observed from the Appendix 5 by the blue colour of characters ground for the case of larger than 10 ° difference. For weak peaks a Gauss fit gives more precise values of the phase transformation temperatures than Rietveld method. As long as the analysis of only one peak is free from influence of the other peaks intensities (what is not the case in the Rietveld refinement). In most of the samples the phase transformation temperature difference between the evaluation methods does not exceed 10 °C. Especially at

high temperatures an uncertainty of ± 5 °C could be neglected as being half the heating step of neutron in situ measurements. The Rietveld and Gauss single peak evaluation methods theory are described in chapter 4. As short reminder, under MAUD temperature one should understand the temperature where the corresponding peak has been seen the last time as well as the SO values whereas for Gauss-fit the increase of FWHM is the decisive value. Some comments about Rietveld and Gauss methods differences were given in chapter results, as long as the difference was obvious from the described data. There is no tendency for one interpretation results would be higher than other method. Almost half the temperatures determined by Gauss-fit are few degrees higher and another half lower than the Rietveld refinement results. For γ -solvus the phase transformation temperature determined by Gauss is up to 20 °C different to that determined by Rietveld refinement.

Additionally to phase transformation comparison the lattice parameters determined by both methods could be compared. Rietveld refinement is known as more precise due to simultaneous refinement of a number of peaks. However it is not the case for our neutron data, as long as only 4 peaks were detected. E.g. as one can see lattice parameter a of γ phase in Figure 48, the Gauss-fit values are less fluctuating than the results of the Rietveld refinement of neutron data. In Appendix 7 the lattice parameters values are given according to Rietveld refinement of neutron and synchrotron data. One can see in the column headers the supposed initial model values and estimate the difference.

Not only phase transformation temperatures and lattice parameters could be compared, as well as the ability for phase content determination. So one should distinguish between qualitative and quantitative phase presence determination. Indeed a presence of the phase peak is an undoubtful sign of the phase presence. But for quantitative phase content determination several phase peaks should be taken into account, especially when ordered and disordered phases should be distinguished. The phase content difference by Rietveld refinement is shown in the results table of Appendix 6 for each diffraction method. The Rietveld and Gauss single peak fit interpretation method is described in the chapter 4. Only Rietveld method gives the quantitative phase content. While the Rietveld refinement is a powerful method, it is not sensitive to phase amounts smaller than 1-2 % (the value is taken from evaluation experience). Rietveld refinement of neutron data gives information about the ordered phase presence, that could be used to determine the degree of ordering of phases (more in details in subchapter 8.3).

8.3 Degree of ordering determination and other way quantitatively characterize the ordering

The degree of ordering, determined as the coefficient D by formula 4 was found not precise enough because with deviation from 50:50 element concentration the ordering could not be characterized as full ($D=1$). Its calculation from the SO values from Rietveld refinement gives not more information as comparison of the SO directly. Good values, analogical to degree of ordering, can be acquired from the correlation of the intensities of superstructure and fundamental peaks, that could be performed based on their Gauss-fit. The correlation values is better suited for determination of the disordering phase transformation temperature, especially because it is less fluctuating than SO refined by Rietveld method. The SO refinement was found to be less precise than the intensity relation, mainly because the model for refinement and the real alloy composition did not ideally match and the grain statistics was not ideal.

From our experience both fundamental and superstructure peaks are visible with synchrotron radiation. Therefore the synchrotron measurements play a major role in our investigation. Neutrons were found useful for determination of the amount of the β_0 phase assuming a perfect ordered phase. A comparison with the amount of β_0 phase from synchrotron (in samples Ti-

42Al-2Mo and Ti-42Al-2Fe, Appendix 6) shows undoubtedly that β is not in its perfect ordered state. The higher phase content by neutron data in sample Ti-42Al-2Cr occurs due to very coarse grains in the sample and during further heating the synchrotron phase content became higher again.

However, there is no possibility to determine the fundamental peaks via neutrons. With different chemical compositions, the fundamental peaks could be detected via neutrons as found in [CHAU1999]. That could be planned for the future work with different compositions if needed. In our current case for a direct comparison of the measured neutron intensities of the superstructure peak with synchrotron ones, a constant beam intensity should be provided for the time of both performed measurements. Unfortunately that was not the case, especially for the synchrotron spectrums.

Trying to combine the superstructure peak measured by neutrons and a fundamental one from synchrotron, it would be necessary to compare the neutron and synchrotron beam intensities as well as the beam intensity change measured during the full time of the experiment. One could combine neutron and synchrotron data when a special difference-factor would be calculated for each measured spectrum depending on time. Even if the neutron beam intensity is known to be stable during one measurement cycle, the synchrotron beam intensity can fluctuate during the long experiments because of technical reason (method of HEXRD beam production).

8.4 Future work

A more precise determination of the elemental composition of every phase could be better realized by Wavelength-Dispersive X-ray spectroscopy (WDX) because the EDX measurements errors are $\pm 5\%$ as long as no ideal reference sample of every nominal composition is available. The exact phase composition as well as the atom positions and present defects should be taken into account for spectrum refinement with possibly ideal references of 3rd element concentration. Good measuring point statistics should be provided.

A more complicated model for Rietveld refinement will include further details, however, it also requires fine grained microstructure and a “close to powder diffraction” grain statistics during measurements. A more detailed data interpretation can take into account the 3rd atom position, anti-site atoms and other possible defects. The vacancies present were also not taken into account up to now. The investigation of the vacancies present in our alloys could be performed by e.g. positron lifetime spectroscopy [BROS1994].

If additional samples for better grain statistic will be produced, there is also a need to determine the O₂ content, which, if present in medium or higher content, transfers the alloy from ternary to quaternary systems. That fact can make interpretation noticeably more complicated due to the possibility of the parallel presence of both ordered and disordered phases.

For sure confirmation of the solidification way, the microstructure analysis directly after arc melting could be useful. That was not performed for the currently investigated sample sets, but could be carried out for future sample sets.

Analogically to [BLE2013] atom location by channelling enhanced microanalysis (ALCHEMI) could be used to determine the site occupancy of alloying elements in the B2 phase.

Analysis of synchrotron spectrums measured during cooling. The influence of undercooling is the main thing to be found.

In the current study the B-factor is assumed to be isotropic and equal for all the atoms for all the phases. With availability of samples with more fine grained microstructure e.g. produced by HIP method, the anisotropy could be taken into account at a next step of data evaluation, when the base parameters are already well refined. Under base parameters we understand phase content, lattice parameters, and site occupancy. Some additional parameters may include third

atom presence, chemical composition, interatomic bonding types and other, which requires much more additional knowledge about TiAl alloys.

Probably amount of covalent and metal bonding types could be taken into account, as it corresponds to any intermetallics. Theoretically one can refine an electron density map of the unit cell. Depending on this map it is easy to decide whether a covalent, metallic or an ionic bonding exists in the phase. E. g. if electron density is smeared in the crystal, that could mean metallic bonding type, with more concentrated around atom positions – the ionic bonding, and concentrated between two atoms - the covalent one. However in order to refine it based on diffraction data a single crystal is needed. It is not easy to produce single crystals of our phases for performing a diffraction measurements. Also Density Functional Theory could calculate the electron density maps.

Summing up chapter 8, it is possible to say that, both Gauss fit and Rietveld refinement have found application in the data evaluation process and their comparison was needed for better understanding of samples itself and both methods possibilities. The errors during experiments and data evaluation are estimated not as bad to be critical. No pronounced dependency of phase transformation temperature from the heating rate was found in our samples. However, if possible, the same heating furnace and the same heating rate should be used at different beam sources for further β_0/β studies in TiAl alloys as well as for other in situ diffraction measurements. Meanwhile this is possible due to the presence of the dilatometer furnace at both sources, FRM II and DESY. Even if heating rate independent second order phase transformations should not be influenced by the heating rate, a similar heating ramp will reduce the doubt. However for an application of not a stepwise measurement, but with a constant heating rate, a higher beam intensity is necessary as well as a larger detector with higher counting abilities. Such possibilities hopefully would be achieved at the currently build European Spallation Source.

Conclusions

This unique project has realized an investigation of high potential materials for advanced aero engines with the most powerful methods of non-destructive analysis: the in situ neutron and synchrotron diffraction. The TiAl alloys represent a lightweight material, which application in the aero engines of most modern planes, e.g. Airbus A320neo, opens new possibilities for nowadays widening world aero connections. Particularly an application of TiAl increases the airlift capability with a simultaneous decrease in fuel consumption. The last point has a special meaning for the ecological situation of our planet and allows to reduce the negative influence of CO₂ emissions on the warming of the Earth's climate.

Indeed the performed measurements represent one of the first experiences in the world with the application of a dilatometer as a specimen environment for neutron diffraction. The experiments provide good starting information for further application of the dilatometer at more powerful neutron sources, e.g. ESS. On the one hand, the project demonstrated some restrictions on the application of the same heating ramp for the synchrotron and neutron in situ measurements. Therefore the detailed description of the experience of the performed Ph.D. project gives some recommendations for a more successful application in the future.

This thesis deals with the β phase ordering phenomena in binary and ternary γ -TiAl base alloys with such β stabilizing elements as Fe, Cr, Mo, Ta, Nb. The evolution of the β_0 /B2-phase with temperature was investigated in situ by means of high-energy XRD and neutron diffraction as well as conventional ex situ characterization methods. It allowed to look inside the material on the phase composition determining it quantitatively and qualitatively. The *in situ methods* HEXRD and neutron diffraction [KON2017] experiments were performed at Petra III DESY, Hamburg, and at MLZ neutron reactor FRM II in Garching near Munich respectively. The data of in situ and RT diffraction measurements were evaluated via Rietveld refinement for determination of phase content, site occupancies, w lattice parameters, and in some samples for the B-factor. Single peaks of α_2 101, β_0 100, and γ 110 were modeled by the Gauss function for both neutron and synchrotron results, and a change of the peaks intensity was used for disordering temperature determination. The ex situ methods included SEM, EDX and DSC, performed at Helmholtz-Zentrum-Geesthacht (now Helmholtz-Zentrum hereon). The results can be summarized as follows:

Influence of the β -stabilizing elements

Ternary alloys from the first sample set with Ti-42Al-2Fe, 2Cr, and 2Mo exhibited the β_0 phase between room temperature and 1000 °C. The amount of the β_0 phase in samples with Cr and Mo is unchanged up to 1000 °C. A $\beta_0 \rightarrow \tau_2 \rightarrow \beta_0$ phase transformation has been detected in samples with Fe between 800-900 °C.

Two at. % of the Ta and Nb are not enough to stabilize the β_0 phase. Between samples, with equal β stabilizing element content the sample with 2 at. % of Mo has the highest β_0 phase content, in comparison to samples with Cr and Fe.

All measured samples with higher than 2 at. % of β -stabilizing elements contain the β_0 phase above 1000 °C according to both synchrotron and neutron data. The samples Ti-42Al-3Fe, Ti-42Al-4Mo, Ti-42Al-6Mo, Ti-42Al-4Cr, and Ti-42Al-6Cr, contain β_0 phase at RT according to synchrotron data. An increase in the Cr, Mo, and Fe content results in an increase of the β_0 phase peaks. However, quantitative information about the β_0 decrease with temperature is currently not available. The content of the β_0 phase at RT in Ti-42Al-8.5Ta, Ti-42Al-8.5Nb, and Ti-42Al-10Nb is lower than that of the ω_0 phase. Ti-42Al-1Fe contains no β_0 at RT, but it appears at 1000 °C according to neutron data.

The temperature of the disordering phase transformation of β_0 in ternary alloys was determined for the Ti-42Al-2Mo, the Ti-42Al-2Cr, and the Ti-42Al-2Fe samples by two methods, via Rietveld refinement and Gauss-fit, and for samples with higher than 2 at. % of β -

stabilizing elements via Gauss-fit only. The difference between Gauss and Rietveld determined temperatures do not exceed 10 °C in most ternary samples.

The presence of the β phase is known to promise better forging properties of TiAl alloys. Thus for our alloys, the processing window could be recommended in the temperature region above the determined $\beta_0 \rightarrow \beta$ phase transformation. However, the $\beta \rightarrow \beta_0$ phase transformation temperature could be slightly lower than observed during heating due to overheating effect. No decrease of β_0 phase content below 1000 °C was observed. Thus the material is expected to be brittle between 700 – 800 °C and has deteriorated creep resistance due to the presence of the β_0 phase.

Additional phases have been detected in our samples below 1000 °C. In samples with 2 and 3 at. % of Fe there is a τ_2 phase. The τ_2 phase is present at RT together with the β_0 phase in 3 at. % Fe sample. In the samples with 8.5 and 10 at. % Ta and Nb the ω_0 phase was additionally found. At RT the ω_0 phase is present simultaneously with the β_0 phase in all 4 samples. The amount of ω_0 phase is higher in samples with Ta than with Nb.

The difference in lattice parameters between the samples does not correspond to the change in their atom radius or their electronegativity. It could be explained (1) by a complicated combination of kinds of chemical bondings where both atom parameters are important as well as (2) the small amount of the used 3rd element.

The γ phase was found in high content in all ternary and binary alloys except Ti-39Al and Ti-39Al-0.2B.

Influence of the amount of the β -stabilizing element

The increase of the content of β -stabilizing elements increases the β_0/β phase transformation temperature in some alloys (from 2Cr to 4Cr, from 2Mo to 4Mo), or decreases it (from 4Cr to 6Cr, from 4Mo to 6Mo, from 2Fe to 3Fe) and sometimes no difference is observed.

Most samples show a good correspondence between the phase transformation temperatures from neutron and synchrotron diffraction: Ti-42Al-3Fe, Ti-42Al-6Mo, Ti-42Al-10Nb, Ti-42Al-2Cr, Ti-42Al-2Fe, Ti-42Al-2Mo. Therefore the β_0/β transformation should be called heating rate independent. Problems with some other samples could be explained by insufficient grain statistics and heating interruptions during neutron measurements.

A correlation between the superstructure and fundamental peaks was used to determine the so-called “degree of ordering”. It reached 65 % for samples with 2 at. % of Cr and Fe, and 58 % for 2 at. % of Mo. This peak correlation was not yet refined for the second set of samples. The “degree of ordering” corresponds to not full ordering, which could explain the difference between β_0 and β phase content according to synchrotron and neutron data correspondingly.

The ordering of the β_0 or the α_2 phases could be also quantitatively determined via refinement of the site occupancy. An increase of the β stabilizing element content does not automatically cause a higher β_0/β phase site occupancy refined from synchrotron data by the Rietveld method at RT.

The more β -stabilizing elements are present, the more homogeneous and fine-grained microstructures could be observed. The β_0 - phase is mainly located along colony boundaries in the samples with 2 at. % of a β -stabilizing element. Ternary alloys with a β -stabilizing element content higher than 2 at. % have very small α_2 amounts, which most probably was replaced by the β_0 phase.

The maximum oxygen content in the samples of the first sample set was 863 $\mu\text{g/g}$.

No or very weak texture has been found in any samples neither by neutron nor by synchrotron diffraction, which means homogeneous distribution of the grains and thus no anisotropic strain/stress distribution in produced melts.

Can the β_0 phase appear at high temperatures in the binary alloys with 39-45 at. % Al?

No evidence for the presence of the β_0 phase in binary alloys was found neither by synchrotron nor by neutron diffraction.

Conclusions for improvement of technique of measurements

- The high-energy synchrotron technique has an advantage in the detection of phase presence occurring at limited temperature intervals and shows a higher amount of peaks (larger q space range). Neutrons unambiguously detected the ordered state presence of α and β phases.

- The modified dilatometer is a very powerful high-temperature equipment for TiAl investigations with more precise temperature control than the standard high-temperature furnace available at FRM II. The ideal case would be an application of the same equipment with the same heating ramp at both beam sources for the synchrotron and neutron in situ measurements.

- Some high heating rates are limited because of the longer exposure time needed using neutrons. Therefore an application of the described method will benefit from the availability of much brighter neutron sources, e.g. ESS in Lund, where the application of the same heating rate as with synchrotron radiation is expected to be possible.

- For our alloy composition both fundamental and superstructure peaks are visible with synchrotron radiation. Both peaks are needed to determine the degree of ordering, therefore the synchrotron measurements play a major role in our investigation. Neutrons gave only superstructure peaks with our sample compositions. However, with a less equal concentration of Ti and Al as well as under the presence of higher third element contents with higher scattering length, the fundamental peaks most probably could be detected also with neutrons.

- A fine-grained microstructure is desired for the neutron diffraction measurements more than for the synchrotron. Good grain statistic is also necessary for the application of a more detailed refinement model for better diffraction data interpretation. Rietveld refinement of not-high-statistical data could be controlled by Gauss-fit of single peaks intensities.

- In combination with a larger neutron detector than available at STRESS-SPEC, with higher beam intensity and the possibility to rotate the dilatometer in the beam by a few degrees it would be hard to imagine a more powerful scientific station for performing industry important investigation for the next decade.

In this work, the answers to all questions mentioned in the introduction are given, which provides experimental proof of the β_0 phase presence in binary and ternary alloys. The detailed description of the methods and results allowed to elaborate on the recommendation for higher-quality experimental data, that could streamline a possible industrial application of similar investigations.

Acknowledgements

I am deeply grateful to Dr. Andreas Stark, who was indeed supervised me during that long term of my PhD study, he supported me during most of experiments, allowed to follow him in his job at DESY learning how to perform the high qualitative experiments. For believe in me up to the end, fruitful discussions, answers of some thousands of questions I have had, as well as for support during foundation search for term prolongation. And especially I thank him for the moral support during Corona time, which I will appreciate all my life.

I am deeply grateful to the head of the WPM department Prof. Dr. Florian Pyczak for the idea of the PhD topic, hours of discussion of scientific questions, as well as introductions into CALPHAD and ab-initio method, invitations to conferences, provided working place and acceptance to command, being welcome in the group meeting and actually treatment as a real groupmate.

I would like to thank all WPM group and especially Dr. Jonathan Paul, Dr. Markus Rackel, Dr. Michel Oehring, Uwe Lorenz, Dirk Matthissen, Bernhard Eltzhig, Dr. Mark Langridge for tutition how to use equipment for sample preparation, measurements, as well as methodics of the sample preparation.

I would like to thank my previous roommate Dr. Soheil Sanamar and current roommate Dr. Katja Hauschild for constant support during daily life at work, useful advises.

I would like to thank Dr. Heike Gabrisch, Dr. Ulrich Fröbel, Dr. Peter Staron and other for provided books, friendliness, help with study of German language and just for support during life in foreign country. As well as Dr. Helmut Eckerlebe for my first working place at HZG and support during my first steps in Germany.

I would like to thank beam scientists Dr. Weimin Gan, Dr. Xiaohu Li for support during experiments, as well as some additional time for measurements. As well as those colleagues who visited experiments with me Dr. Michel Oehring, Dr. Alexey Sokolov, Dr. Gregor Nowak, Dr. Robert Koos.

I would like to thank my direct boss Dr. Jochen Fenske for allowance to participate in big number of conferences and schools over the word. As well as Prof. Dr. Brokmeier for support of my interest to the texture school, even if it is not the topic of the current thesis.

I would like to thank all administrative stuff of HZG, for answering my questions, support with document, visas, prolongations, especially Dr. Klaus Pranzas, Regina Rossmann, Nicola Kampner.

I would like to thank Prof. Dr. Sergei Grigoriev, without whom I would I would never have started the doctoral study in Germany.

I would like to thank Dr. Gleb Dovzhenko and Dr. Andreas Stark and Dr. Katja Hauschildt for my first steps in the Python programming and producing first codes for my data analysis.

I would like to thank Prof. Dr. Andreas Schreyer for the opportunity to work at HZG and a guidance. As well as for Prof. Dr. Martin Müller for the financial support of my PhD study.

Bibliography

- ALL2003 Allmann, R. (2003). Röntgen-Pulverdiffraktometrie, Springer.
- ANIE2011 Als-Nielsen, J. Elements of modern X-ray physics
- APPL1993 Appel, F., P. A. Beaven and R. Wagner (1993). "Deformation processes related to interfacial boundaries in two-phase γ -titanium aluminides." *Acta Metallurgica et Materialia* 41(6): 1721-1732.
- APPL1998 Appel F. and W. R. (1998). "Microstructure and deformation of two-phase γ -titanium aluminides." *Material Science And Engineering R22*: 187-268.
- APPL2000 Appel, F., M. Oehring and R. Wagner (2000). "Novel design concepts for gamma-base titanium aluminide alloys." *Intermetallics* 8: 1283-1312.
- APPL2003 Appel F., P. J. D. H., Oehring M., Buque C. (2003). "Recent Developments of TiAl Alloys Towards Improved High-Temperature Capability." *Gamma Titanium Aluminides 2003*, TMS,.
- APPL2003 Appel, F., J. D. H. Paul, M. Oehring, U. Fröbel and U. Lorenz (2003). "Creep behavior of TiAl alloys with enhanced high-temperature capability." *Metallurgical and Materials Transactions A* 34(10): 2149-2164.
- APPL2011 Appel, F., J. D. H. Paul and M. Oehring (2011). *Gamma Titanium Aluminide Alloys*, Wiley-VCH/ Science and Technology.
- ARAD <http://www.crystallmaker.com/support/tutorials/atomic-radii/>
- ARC-MELT Edmund Bühler GmbH Arc Melter furnace description, Schindächerstraße 8, D-772411, D-72411 Bodelshausen,
- AWH1975 A.W., H. (1975). "DESIGN FOR A CONVENTIONAL HIGH-RESOLUTION NEUTRON POWDER DIFFRACTOMETER." *Nuclear Instruments and Methods* 127: 361-370.
- BAKA2019 Bakan Emine, M. G., Sohn Yoo Jung, Schwebt Alexander, Rackel Markus Willi, Riedlberger Florian, Pyczak Florian, Peters Jan Oke, Mecklenburg Matthias, Gartner Thomas Maria, Vaßen Robert (2019). "Cold gas spraying of Ti-48Al-2Cr-2Nb intermetallic for jet engine applications." *Surface and Coating Technology* 371: 203 - 210.
- BAR1997 Bartolotta P., B. J., Kelly T., Smashey R. (1997). "<1997_Article_TheUseOfCastTi48Al2Cr2NbInJetE.pdf>." *JOM* May.
- BART2002 Bartels Arno, K. H., Clemens Helmut (2002). "Deformation behavior of differently processed γ -titanium aluminides." *Materials Science And Engineering A* 329-331: 153-162.
- BEN1991 BENDERSKY L. A. , B. W. J. a. R. A. (1991). "COHERENT PRECIPITATES IN THE B.C.C./ORTHORHOMBIC TWO-PHASE FIELD OF THE Ti-Al-Nb SYSTEM." *Acta metall, mater.* 39(8): 1959-1969.

- BEWL2013 Bewlay B.P, W. M., Kelly T., Suzuki A., and Subramanian P.R. (2013). "The Science, technology, and Implementation of TiAl Alloys in Commercial Aircraft Engines." Mater. Res. Soc. Symp. Proc. 1516.
- BLE2013 Blenkinsop Li, Y. G. P. A., Loretto M. H. and W. N. A. (2013). "Effect of aluminium ordering of highly stabilised β -Ti-V-Cr alloys." Materials Science and Technology 14(8): 732-737.
- BOC2009 Bochvar, N., T. Dobatkina, O. g. Fabrichnaya, V. Ivanchenko and D. M. Cupid (2009). "Aluminium – Chromium – Titanium." 11E1: 102-147.
- BOEH1958 Boehm, H., Loehberg, K., (1958). "A Superstructure CsCl Type Phase in the Titanium - Molybdenum - Aluminium System (in German), ." Z. Metallkd., (Crys. Structure, Experimental, #, 10) 49: 173-178
- BOLZ2015 Bolz S., O. M., Lindemann J., Pyczak F., Paul J., Stark A. , Lippmann T. , Schrüfer S. , Roth-Fagaraseanu D. , Schreyer A. , Weiß S. "Microstructure and mechanical properties of a forged β -solidifying γ TiAl alloy in different heat treatment conditions."
- BROK2004 BROKMEIER H.-G. , O. M., LORENZ U., CLEMENS H., and APPEL F., (2004). "Neutron Diffraction Study of Texture Development during Hot Working of Different Gamma–Titanium Aluminide Alloys " Metallurgical and materials transactions A 3.
- BROS1994 Brossmann, U., R. Wurschum, K. Badura and H. Schaefer (1994). "Thermal formation of vacancies in TiAl." Phys Rev B Condens Matter 49(10): 6457-6461.
- BRYD2018 Brydon R. E. , Burle J., Coenen J., Gan W. ,Hofmann M., Soinenen A. J., Wuttke J. , (2018) "Stress and texture calculator Steca", version 2
- BYST2010 Bystrzanowski, S., Bartels, A., Stark, A., Gerling, R., Schimansky, F. P., Clemens, H. (2010). "Evolution of microstructure and texture in Ti–46Al–9Nb sheet material during tensile flow at elevated temperatures." Intermetallics 18(5): 1046-1055.
- CHA2011 Cha, L., H. Clemens and G. Dehm (2011). "Microstructure evolution and mechanical properties of an intermetallic Ti-43.5Al-4Nb-1Mo-0.1B alloy after aging below the eutectoid temperature." International Journal of Materials Research 102: 703-708.
- CHAT2010 Chateigner, D. (2010). Combined Analysis, Wiley, ISTE.
- CHAU1999 Chaumat V. , R. E., Ouladdiaf B. , et al., (1999). "EXPERIMENTAL STUDY OF PHASE EQUILIBRIA IN THE Nb-Ti-Al SYSTEM." Scripta Materialia 40 905 (1999).
- CHE2011 Chen, Y., H. Niu, F. Kong and S. Xiao (2011). "Microstructure and fracture toughness of a β phase containing TiAl alloy." Intermetallics 19(10): 1405-1410.
- CHEM https://www.chemistryviews.org/details/ezine/2064331/100th_Anniversary_of_the_Discovery_of_X-ray_Diffraction.html
- CHEN1997 Chen, Z., Jones, I.P., Small, C.J., (1997). "The Structure of the Alloy Ti-50Al-15Mo between 800 and 1400 °C", ." Acta Mater., 45, 3801-3815 (1997) (Crys. Structure, Equi. Diagram, Experimental, 18).
- CHEN1998 Cheng T.T., L. M. H. (1998). "Decomposition Of beta phase in Ti-44Al8Nb and Ti-44Al-4Nb-4Zr-0.2Si Alloys." ActaMat 46.

- CHLAD2006 Chladil, H. F., Clemens, H., Leitner, H., Bartels, A., Gerling, R., Schimansky, F. P., Kremmer, S. (2006). "Phase transformations in high niobium and carbon containing γ -TiAl based alloys" *Intermetallics* 14: 1194-1198
- CHR2018 Christian, B. (2018). Auswirkungen unterschiedlicher Abkühlraten auf die Mikrostrukturentwicklung von neuartigen Gamma-TiAl Legierungen. Master Arbeit. T. U. Hamburg.
- CLEM2006 Clemens, H., Bartels, A., Bystrzanowski, S., Chaladil, H., Leitner, H., Dehm, G., Gerling, R., Schimansky, F. P. (2006). "Grain refinement in γ -TiAl-based alloys by solid state phase transformations." *Intermetallics* 14: 1380-1385.
- CLEM2008 Clemens, H., H. F. Chladil, W. Wallgram, G. A. Zickler, R. Gerling, K. D. Liss, S. Kremmer, V. Güther and W. Smarsly (2008). "In and ex situ investigations of the β -phase in a Nb and Mo containing γ -TiAl based alloy." *Intermetallics* 16(6): 827-833.
- CLEM2011 Clemens Helmut, M. S. (2011). "Intermetallisches Titanaluminid – Ein innovativer Leichtbauwerkstoff für Hochtemperaturanwendungen." *Berg- und Hüttenmännische Monatshefte* 156(7): : 255 – 260.
- CLEM2013 Clemens, H. and S. Mayer (2013). "Design, Processing, Microstructure, Properties, and Applications of Advanced Intermetallic TiAl Alloys." *Advanced Engineering Materials* 15(4): 191-215.
- CLEM2016 Clemens, H. and S. Mayer (2016). "Intermetallic titanium aluminides in aerospace applications – processing, microstructure and properties." *Materials at High Temperatures* 33(4-5): 560-570.
- DAS1993 Das, S., Jewett, T.J., Perepezko, J.H., (1993). "“High Temperature Phase Equilibria of Some Ternary Titanium Aluminides”, ." in "Structural Intermetallics", Darolia, R., Lewandowski, J.J., Liu, C.T., Martin, P.L., Miracle, D.B., Nathal, M.V., (Eds.), Min., Met., Mater. Soc., 420 Commonwealth Dr., Warrendale, Pens. 15086, 35-43 (1993) (Equi. Diagram, Experimental, Review, 48).
- DAS2003 Das K., D. S. (2003). "Order-disorder transformation of the body centered cubic phase in the Ti-Al-X (X=Ta, Nb, or Mo) system." *JOURNAL OF MATERIALS SCIENCE* 38: 3995 – 4002.
- DAS1993 Das, S., Mishurda, J.C., Allen, W.P., Perepezko, J.H., Chumbley, L.S., (1993). "“Development of a (γ + β_0) Lamellar Microstructure in a Ti45Al50Mo5 Alloy”,." *Scr. Metall. Mater.*, 28, 489-494 (1993) (Crys. Structure, Equi. Diagram, Experimental, 17).
- DEM2013 Деменюк А. О., Г. А. А., Деменюк О.Б., Кулаков Б. А. (2013). "Выбор легирующих элементов для сплавов на основе алюминидов титана." *Вестник ЮУрГУ. Серия "Металлургия"* 13(1): 95 - 102.
- DIAN2003 Dianoux Albert-Jose and L. Gerry (2003). *NeutronDataBooklet*.
- DIL805 "<DIL-805-Quenching-Dilatometer-Brochure.pdf>."
- DIV2008 Divinski, S. V., F. Hisler, T. Wilger, M. Friesel and C. Herzig (2008). "Tracer diffusion of boron in α -Ti and γ -TiAl." *Intermetallics* 16(2): 148-155.
- DJA1991 Djanarthany, S., Servant C., Penelle R. (1991). "Phase Transformations In Ti3Al and Ti3Al+Mo Aluminides." *J. Mater. Res.* 6 May(5).

- DJA1992-1 Djanarthany S , C. S. a. R. P. (1992). "Influence Of An Increasing Content Of Molybdenum On Phase Transformations Of TiAlMo Aluminides With Mechanical Properties." *Materials & Science and Engineering, A* 152: 48-53.
- DJA1992-2 Djanarthany, S., Servant, S., Lyon, O., (1992). "Phase Separation in a Ti-Al-Mo Alloy Studied by Anomalous Small-Angle X-Ray Scattering. A Synchrotron Radiation Experiment", *Philos. Mag.*, 66A, 575-590 (1992) (Crys. Structure, Equi. Diagram, Experimental, Theory, 14).
- DRUL <http://groups.mrl.uiuc.edu/chiang/czoschke/diffraction-selection-rules.html>
- DSC-Guide Differential Scanning Calorimetry Beginners Guide.
- ENEG <https://sciencenotes.org/electronegativity-definition-and-trend/>
- ERDL2015 Erdely, P., R. Werner, E. Schwaighofer, H. Clemens and S. Mayer (2015). "In situ study of the time-temperature-transformation behaviour of a multi-phase intermetallic β -stabilised TiAl alloy." *Intermetallics* 57: 17-24.
- ERDL2016 Erdely, P., T. Schmoelzer, E. Schwaighofer, H. Clemens, P. Staron, A. Stark, K.-D. Liss and S. Mayer (2016). "In situ Characterization Techniques Based on Synchrotron Radiation and Neutrons Applied for the Development of an Engineering Intermetallic Titanium Aluminide Alloy." *Metals* 6(1): 10.
- ERDL2017 Erdely, P., P. Staron, E. Maawad, N. Schell, J. Klose, S. Mayer and H. Clemens (2017). "Effect of hot rolling and primary annealing on the microstructure and texture of a β -stabilised γ -TiAl based alloy." *Acta Materialia* 126: 145-153.
- ERDL2019 Erdely, P., P. Staron, A. Stark, T. Klein, H. Clemens and S. Mayer (2019). "In situ and atomic-scale investigations of the early stages of γ precipitate growth in a supersaturated intermetallic Ti-44Al-7Mo (at. %) solid solution." *Acta Materialia* 164: 110-121.
- FAN2016 Fan, Y., W. Tian, Y. Guo, Z. Sun and J. Xu (2016). "Relationships among the Microstructure, Mechanical Properties, and Fatigue Behavior in Thin Ti6Al4V." *Advances in Materials Science and Engineering 2016*: 1-9.
- FISH2003 Fischer, F. D., F. Appel and H. Clemens (2003). "A thermodynamical model for the nucleation of mechanical twins in TiAl." *Acta Materialia* 51(5): 1249-1260.
- GAIZ2013 Gaitzenauer, Andrea, Schenk, Mathias, Kuchling, Wolfgang, Clemens, Helmut, Voigt, Patrick, Hempel, Robert, Mayer, Svea (2013) "Gefüge und Eigenschaften einer mehrphasigen intermetallischen Titanaluminidlegierung für innovative Leichtbauanwendungen", *BHM Berg- und Hüttenmännische Monatshefte* 513,158, 113-117
- GERT Gert, N. "PowderCell-InstructionManual."
- GhOSH2008 Ghosh, G. (2008). "Aluminium – Iron – Titanium." *11D1*: 280-318.
- GRYT2003 Grytsov A., R. P., Schmltdt H., Glester G. (2003). "Constitution of the Ternary System Al-Ru-Ti." *Journal of Phase Equilibria* Vol. 24 No. 6 2003.
- GÜN2014 Günter, G. (2014). *Materialwissenschaft und Werkstofftechnik Physikalische Grundlagen*, Springer.

- GÜTH2018 Güther, V., M. Allen, J. Klose and H. Clemens (2018). "Metallurgical processing of titanium aluminides on industrial scale." *Intermetallics* 103: 12-22.
- GUTT1956 Guttman Lester; (1956), "Order-Disorder phenomena in Metals" Guggenheim foundation Fellow
- HADD1994 HADDAD J. , ZEVIN L. , ELIEZER D. (1994) "Phase Relation In Titanium-Aluminide alloy-an X-ray study" *JOURNAL OF MATERIALS SCIENCE* 29 373-375
- HAL1991 HALL, S.-C. H. a. E. L. (1991). "The Effects of Cr Additions to Binary TiAl-Base Alloys." *METALLURGICAL TRANSACTIONS A VOLUME 22A, NOVEMBER* 2619 - 2627.
- HAMA1972 Hamajima, T., Luetjering, G., Weissman, S., (1972). "'Microstructure and Phase Relations for Ti-Mo-Al Alloys", ." *Metall. Trans.*, 3, 2805-2810 (1972) (*Crys. Structure, Equi. Diagram, Experimental, #, 15*).
- HAMM2016 Hammersley, A. P. (2016). "FIT2D: a multi-purpose data reduction, analysis and visualization program" *Journal of Applied Crystallography* 49, 2, 646-652
- HAO1999 HAO Y.L. , X. D. S., CUI Y.Y. , YANG R. and LI D. (1999). "THE SITE OCCUPANCIES OF ALLOYING ELEMENTS IN TiAl AND Ti3Al ALLOYS." *Acta materialia* 47 - 4: 1129 - 1139.
- HAOCrys. Structure, Experimenta l, 41 Hao, Y. L., Xu, D.S., Cui, Y.Y., Yang, R., Li, D., (1999). "'The Site Occupancies of Alloying Elements in TiAl and Ti3Al Alloys",." *Acta Mater.*, 47, 1129-1139 (1999) (*Crys. Structure, Experimental, 41*).
- HAUS2017 Unpublished Material by agreement of the author
- HAUS2018 Hauschildt Katja , S. A., Burmester Hilmar , Tietze Ursula, Schell Norbert , Müller Martin, and Pyczak Florian (2018). "Phase transformations in the brazing joint during transient liquid phase bonding of a γ -TiAl alloy studied with in situ high-energy X-ray diffraction " *Thermec-proceeding*.
- HAUS2020 Katja, H. (2020). "Mikrostrukturentwicklung während des TLP-Lötprozesses in γ -TiAl-Legierungen: In situ Experimente mit hochenergetischer Röntgenbeugung."
- HAUS-PERs Katja, H. (2017). "personal communication."
- HEL1998 Hellwig, A., M. Palm and G. Inden (1998). "Phase equilibria in the Al-Nb-Ti system at high temperatures." *Intermetallics* 6(2): 79-94.
- HEL2007 Helmut, M. (2007). *Diffusion in Solids Fundamentals, Methods, Materials, Diffusion-Controlled Processes* Berlin Heidelberg, Springer-Verlag
- HEWA1975 Hewat A.W., (1975) "DESIGN FOR A CONVENTIONAL HIGH-RESOLUTION NEUTRON POWDER DIFFRACTOMETER" *Nuclear Instruments and Methods* 127
- HOFM2015 Hofmann, M., W. Gan and J. Rebelo-Kornmeier (2015). "STRESS-SPEC: Materials science diffractometer." *Journal of large-scale research facilities JLSRF* 1.

- HOL2015-1 Holec Devid. (2015). "Preferential site occupancy of alloying elements in TiAl phases."
- HOL2015-2 Holec, D., D. Legut, L. Isaeva, P. Souvatzis, H. Clemens and S. Mayer (2015). "Interplay between effect of Mo and chemical disorder on the stability of β/β_0 -TiAl phase." *Intermetallics* 61: 85-90.
- HTF-MLZ . "Standart Hight Temperature furnace at FRM II." from <https://mlz-garching.de/englisch/instruments-und-labs/sample-environment/high-temperatures.html>.
- HUTC2005 Hutchings M.T. (2005) "Introduction to the characrerisation of residual stress by neutron diffraction" Taylor and Francis
- IBAC2009 Ibach Harald , Lüth Hans (2009) "Festkörperphysik_ Einführung in die Grundlagen", Springer-Lehrbuch
- IMA2007 Imayev, R. M., V. M. Imayev, M. Oehring and F. Appel (2007). "Alloy design concepts for refined gamma titanium aluminide based alloys." *Intermetallics* 15(4): 451-460.
- INDHEAT . "Inductive heating." from https://en.wikipedia.org/wiki/Induction_heating.
- ITC2005 (2005). International Tables of Crystallography.
- IZU2005 Izumi, T., T. Yoshioka, S. Hayashi and T. Narita (2005). "Oxidation behavior of sulfidation processed TiAl–2 at. %X (X=Si, Mn, Ni, Ge, Y, Zr, La, and Ta) alloys at 1173K in air." *Intermetallics* 13(7): 694-703.
- JIN2015 Jinan B. Al-Dabbagh, R. M. T., Mahadzir Ishak, Siti Aisyah Harun (2015). "Structural and phase formation of TiAl alloys synthesized by mechanical alloying and heat treatment." *Int. J. Nanoelectronics and Materials* 8: 23-32.
- KADUK2012 Kaduk, J. A. and J. Reid (2012). "Typical values of Rietveld instrument profile coefficients." *Powder Diffraction* 26(01): 88-93.
- KAIN1994 Kainuma R., Palm M. & Inden G. (1994) "Solid-phase equilibria in the Ti-rich part of the Ti-Al system" *Intermetallics* 2, 321-332
- KAIN2000 Kainuma, R., Y. Fujita, H. Mitsui, I. Ohnuma and K. Ishida (2000). "Phase equilibria among α (hcp), β (bcc) and γ (L10) phases in Ti–Al base ternary alloys." *Intermetallics* 8(8): 855-867.
- KAIN2000-B2 Kainuma R. Ohnuma I., I. K., Ishida K.(2000). "Stability of B2 ordered phase in the Ti-rich portion of Ti-Al-Cr and Ti-Al-Fe ternary systems." *Intermetallics* 8: 869-875
- KAS2015 Kassner, M. E. (2015). *Fundamentals of Creep in Metals and Alloys*. Departments of Aerospace and Mechanical Engineering, Chemical Engineering, and Materials Science University of Southern California Los Angeles, CA USA, Butterworth-Heinemann.

- KAZ2008 Kazantseva, N. V., N. V. Mushnikov, A. G. Popov, V. A. Sazonova and P. B. Terent'ev (2008). "Use of mechanoactivation for obtaining hydrides of titanium aluminides." *The Physics of Metals and Metallography* 105(5): 460-470.
- KIM1991 Kim, Y.-W. and D. M. Dimiduk (1991). "Progress in the understanding of gamma titanium aluminides." *JOM* 43(8): 40-47.
- KIM1992 Kimura, M., Hashimoto, K., Morikawa, H., (1992). "Study on Phase Stability in Ti-Al-X Systems at High Temperatures", .*Mater. Sci. Eng., A152*, 54-59 (1992) (Crys. Structure, Equi. Diagram, Experimental, #, 12).
- KIM2014 Kim, S.-W., J. K. Hong, Y.-S. Na, J.-T. Yeom and S. E. Kim (2014). "Development of TiAl alloys with excellent mechanical properties and oxidation resistance." *Materials & Design* (1980-2015) 54: 814-819.
- KITT2005 Charles, K. *Introduction To Solid State Physics*.
- KON2017 Kononikhina Victoria, S. A., Gan Weimin, Schreyer Andreas, and Pyczak Florian (2017). "Ordering and disordering of β/β_0 -phase in γ -TiAl based alloys investigated by neutron diffraction." 2016 MRS Fall Meeting.
- KOT2012 Kothari, K., R. Radhakrishnan and N. M. Wereley (2012). "Advances in gamma titanium aluminides and their manufacturing techniques." *Progress in Aerospace Sciences* 55: 1-16.
- KRAW Krawitz Aaron, () *Introduction to Diffraction in Materials Science and Engineering*
- KUN2010 Kunal, K. (2010). *MANUFACTURING TECHNIQUES FOR TITANIUM ALUMINIDE BASED ALLOYS AND METAL MATRIX COMPOSITES*. C. P. University of Maryland, College Park, MD, 20742, Approved for public release; distribution unlimited.
- LAI2017 Laipple, D., L. Wang, M. Rackel, A. Stark, B. Schwebke, A. Schreyer and F. Pyczak (2017). "Microstructure of gas atomised γ -TiAl based alloy powders." *MRS Advances* 2(25): 1347-1352.
- LAND-LIV Landau Lev, L. E. "Statistical Physiks. Course of Theoretical Physics." 5.
- LASA2006 Lasalmonie, Alain (2006) "Intermetallics: Why is it so difficult to introduce them in gas turbine engines" *Intermetallics* 14 1123-1129
- LASUR2021 Lazurenko, D.V.; Golkovsky, M.G.; Stark, A.; Pyczak, F.; Bataev, I.A.; Ruktuev, A.A.; Petrov, I.Y.; Laptsev, I.S. Structure and Properties of Ti-Al-Ta and Ti-Al-Cr Cladding Layers Fabricated on Titanium. *Metals* 2021, 11, 1139. <https://doi.org/10.3390/met11071139>
- LEYE2003 Christoph Leyens, Manfred Peters, *Titanium and Titanium Alloys: Fundamentals and Applications*, (2003) Wiley-VCH Verlag, doi:10.1002/3527602119
- LI1993 Li, Y. G., Loretto, M.H., (1993). "Antiphase Boundaries in Ti-48Al2Mo", .*Acta Metall. Mater.*, 41, 3413-3419 (1993) (Equi. Diagram, Experimental, 11).

- LI1994 Li, Y. G., Loretto, M.H., (1994). "Microstructure and Fracture Behaviour of Ti-44Al-xM Derivatives", *Acta Metall. Mater.*, 42, 2913-2919 (1994) (Crys. Structure, Equi. Diagram, Experimental, 12).
- LI2016 Li, H., Y. Qi, X. Liang, Z. Zhu, F. Lv, Y. Liu and Y. Yang (2016). "Microstructure and high temperature mechanical properties of powder metallurgical Ti-45Al-7Nb-0.3W alloy sheets." *Materials & Design* 106: 90-97.
- LI2018 Li, X.; Dippenaar, R.; Shiro, A.; Shobu, T.; Higo, Y.; Reid, M.; Suzuki, H.; Akita, K.; Funakoshi, K.I.; Liss, K.-D. Lattice parameter evolution during heating of Ti-45Al-7.5Nb-0.25/0.5C alloys under atmospheric and high pressures. *Intermetallics* 2018, 102, 120–131
- LIA2014 Liang, X., Y. Liu, H. Li, Z. Gan, B. Liu and Y. He (2014). "An investigation on microstructural and mechanical properties of powder metallurgical TiAl alloy during hot pack-rolling." *Materials Science and Engineering: A* 619: 265-273.
- LIN2011 Lin, J. P., L. L. Zhao, G. Y. Li, L. Q. Zhang, X. P. Song, F. Ye and G. L. Chen (2011). "Effect of Nb on oxidation behavior of high Nb containing TiAl alloys." *Intermetallics* 19(2): 131-136.
- LISS2006 Liss, K.-D., A. Bartels, H. Clemens, S. Bystrzanowski, A. Stark, T. Buslaps, F.-P. Schimansky, R. Gerling, C. Scheu and A. Schreyer (2006). "Recrystallization and phase transitions in a γ -TiAl-based alloy as observed by ex situ and in situ high-energy X-ray diffraction." *Acta materialia* 54(14): 3721-3735.
- LORI2000 Loria, E. A. (2000). "Gamma titanium aluminides as prospective structural materials." *Intermetallics* 8(9–11): 1339-1345.
- LÜTJ2007 Gerd Lütjering, James C. Williams, *Titanium*, (2007) Springer-Verlag Berlin Heidelberg, doi:10.1007/978-3-540-73036-1
- LUTT2015 Lutterotti, L. *Classical Rietveld Analysis*.
- LXRHT DHS 1100 Domed Hot Stage Heating Attachment for Four-Circle Goniometers
- MARK2003 Marketz W.T. , F. F. D., Clemens H. (2003). "Deformation mechanisms in TiAl intermetallics — experiments and modeling." *International Journal of Plasticity* 19.
- MAS1991 MASAHASHI Naoya. MIZUHARA Youji . MATSUO Munetsugu. HANAMURA Toshihiro, K. M. a. H. K. (1991). "High Temperature Deformation Behavior of Titanium-Aluminide Based Gamma Plus Beta Microduplex Alloy " *ISIJ International* Vol. 31,(No. 7,): 728 - 737.
- MAUD . "MAUD programm."
- MAYE2017 Mayer, S., P. Erdely, F. D. Fischer, D. Holec, M. Kasthuber, T. Klein and H. Clemens (2017). "Intermetallic β -Solidifying γ -TiAl Based Alloys – From Fundamental Research to Application " *Advanced Engineering Materials* 19(4): 1600735.
- MCCUS1999 McCusker L.B., V. D. R. B., Cox D.E., Louer D., Scardi P. (1999). "Rietveld refinement guidelines" *J. Appl. Cryst.* 32: 36–50.
- MEER1963 Meerson G.A., Segorcheanu T. (1963), "The Affinity Of Niobium For Oxygen" Translated from *Atomnaya Energy* 13 6

- MEHR2007 Mehrer Helmut (2007) "Diffusion in Solids Fundamentals, Methods, Materials, Diffusion-Controlled Processes" Springer-Verlag
- MLZE MLZ, Experimental Facilities Book
- MLZW <https://mlz-garching.de/stress-spec>
- MORR1994 Morris, M. A., Li, Y.G., Leboeuf, M., (1994). "Variation of the Phase Distribution in a Ti-44Al-2Mo Alloy by Annealing: Influence on its Strength and Ductility", . "Scr. Metall. Mater., 31, 449-454 (1994) (Crys. Structure, Equi. Diagram, Experimental, 11).
- MOSK2017 E, M. (2017). Приборное разрешение дифрактометров и спектрометров Lektion3.
- MUK2001 Mukherjee, A. K., & Mishra, R. S. (2001). Mukherjee. Encyclopedia of Materials, Science and Technology: 8977–8981.
- N.,1999 N., S. (1999). "PHASE EQUILIBRIA IN MULTI-COMPONENT γ -TiAl BASED ALLOYS." In "Gamma Titanium Aluminides 1999" eds.Y-W.Kim et al. (TMS Warrendale, PA) 183.
- NAKA1995 Nakai, K., Ono, T., Ohtsubo, H., Ohmori, Y., (1995). "'Phase Stability and Decomposition Processes in Ti-Al Based Intermetallics", ." Mater. Sci. Eng., A192, 922-929, (1995) (Equi. Diagram, Experimental, 21).
- NIU2012 Niu, H. Z., Y. Y. Chen, S. L. Xiao and L. J. Xu (2012). "Microstructure evolution and mechanical properties of a novel beta γ -TiAl alloy." Intermetallics 31: 225-231.
- NIU2015 Niu, H. Z., Y. Y. Chen, Y. S. Zhang, J. W. Lu, W. Zhang and P. X. Zhang (2015). "Producing fully-lamellar microstructure for wrought beta-gamma TiAl alloys without single α -phase field." Intermetallics 59: 87-94.
- NOLZ2017 Nolze Gert (2017). "PowderCell-InstructionManual" Federal Institute for Materials Research and Testing
- OHNM2000 Ohnuma, I., Y. Fujita, H. Mitsui, K. Ishikawa, R. Kainuma and K. Ishida (2000). "Phase equilibria in the Ti–Al binary system." Acta Materialia 48(12): 3113-3123.
- OKUL2015 Okulov, I. V., M. F. Sarmanova, A. S. Volegov, A. Okulov, U. Kühn, W. Skrotzki and J. Eckert (2015). "Effect of boron on microstructure and mechanical properties of multicomponent titanium alloys." Materials Letters 158: 111-114.
- OLIM <https://www.olympus-lifescience.com/en/microscope-resource/primer/lightandcolor/diffraction/>
- P07BEAM . "P07 beamline DESY." from http://photon-science.desy.de/facilities/petra_iii/beamlines/index_eng.html.
- PALM1995 Palm M., G. I., N. Thomas (1995). "The Fe-Al-Ti System " Basic and Applied Research: Section I.

- PALM1997 Palm M. , G. A., Letzig D. , Sauthoff G. , in: M.V. Nathal, R. Darolia, C.T. Liu, P.L. Martin, D.B. Miracle, R. Wagner, M. Yamaguchi (Eds.) (1997). Second International Symposium on Structural Intermetallics (ISSI-2), The Minerals, Metals and Materials Society, Champion, PA, September 21–25.: p. 885
- PALM2006 Palm, M. and J. Lacaze (2006). "Assessment of the Al–Fe–Ti system." *Intermetallics* 14(10-11): 1291-1303.
- PAUL1998 PAUL J. D. H. , A. F. a. W. R. (1998). "THE COMPRESSION BEHAVIOUR OF NIOBIUM ALLOYED γ -TITANIUM ALUMINIDES." *Acta materialia* 46(4): 1075-1085.
- PENG1996 PENG L.-M. , R. G., DUDAP S. L., ~V AND WHELAN M. J. (1996). "Debye-Waller Factors and Absorptive Scattering Factors of Elemental Crystals." *Acta Cryst A* 52(456-470)
- PER2019 Perrut (2019). "High Temperature Materials For Aerospace Applications: Ni-based Superalloys And Gamma-TiAl Alloys." *Comptes Rendus Physique*, Elsevier Masson, 2018, 19 (8),(hal-02073852): 657-671.
- PET2002 Peters, M., Leyens, C. (2002). *Titanium and Titanium Alloys*. Weinheim, Wiley-VCH.
- PFL2015 Pflumm, R., S. Friedle and M. Schütze (2015). "Oxidation protection of γ -TiAl-based alloys – A review." *Intermetallics* 56: 1-14.
- PFUL1993 Pfullmann Th., B. P. A. (1993). "On the relationship between lattice parameters and composition of the gamma-TiAl phase." *Scripta METALLURGICA* Pergamon Press Ltd. et MATERIALIA Printed in the U.S.A. All rights reserved 28: 275-280.
- POLM2005 Polmear, I. (2005). *Light Alloys_ From Traditional Alloys to Nanocrystals*-Butterworth-Heinemann. AMSTERDAM • BOSTON • HEIDELBERG • LONDON NEW YORK • OXFORD PARIS • SAN DIEGO SAN FRANCISCO • SINGAPORE • SYDNEY • TOKYO, Butterworth-Heinemann is an imprint of Elsevier.
- PORT1992 Porter D. A. , E. K. E. (1992). *Phase Transformations in Metals and Alloys*, Springer-Science+Business Media, B.Y.
- QIU2012-1 Qiu, C.-z., Y. Liu, L. Huang, b. Liu, W. Zhang, Y.-h. He and B.-y. Huang (2012). "Tuning mechanical properties for β (B2)-containing TiAl intermetallics." *Transactions of Nonferrous Metals Society of China* 22(11): 2593-2603.
- QIU2012-2 Qiu, C.-z. L., Yong; Huang, Lan; Zhang, Wei; Liu, Bin; Lu, Bin (2012). "Effect of Fe and Mo additions on microstructure and mechanical properties of TiAl intermetallics." *Transactions of Nonferrous Metals Society of China* 22(3): 521-527.
- R. 2018 R. E. Brydon, J. B., J. Coenen, W. Gan, M. Hofmann, A. J. Soininen, J. Wuttke, . (2018). "Stress and texture calculator Steca, version 2." from <https://github.com/scgmlz/Stecca2>
- RADV1987 Raghavan, V. (1987). *Phase diagrams of ternary iron alloys*.

- RAJI2020 Sadiq Abiola Raji, Abimbola Patricia Idowu Popoola, Sisa Leslie Pityana, Olawale Muhammed Popoola Characteristic effects of alloying elements on β solidifying titanium aluminides: A review. *Heliyon* 6 (2020) e04463
- RAMA1964 RAMAN A, S. K. (1964). "The occurrence of Zr₂Cu and Cr₂Al-type intermetallic compounds (in German)." *Z Metallkd.* 55: 798–804.
- RAND2011 Randau, C., U. Garbe and H. G. Brokmeier (2011). "StressTextureCalculator: a software tool to extract texture, strain and microstructure information from area-detector measurements." *Journal of Applied Crystallography* 44(3): 641-646.
- RAYN1988 Raynor G.V., R. V. G. (1988). "Phase Equilibria in Iron Ternary Alloys." The Institute of Metals London, UK: 20.
- SCHL2012 Schloffer, M., F. Iqbal, H. Gabrisch, E. Schwaighofer, F.-P. Schimansky, S. Mayer, A. Stark, T. Lippmann, M. Göken, F. Pyczak and H. Clemens (2012). "Microstructure development and hardness of a powder metallurgical multi phase γ -TiAl based alloy." *Intermetallics* 22: 231-240.
- SCHL2014 Schloffer, M., B. Rashkova, T. Schöberl, E. Schwaighofer, Z. Zhang, H. Clemens and S. Mayer (2014). "Evolution of the ω phase in a β -stabilized multi-phase TiAl alloy and its effect on hardness." *Acta Materialia* 64: 241-252.
- SCHM2010 Schmoelzer, T., K.-D. Liss, G. A. Zickler, I. J. Watson, L. M. Droessler, W. Wallgram, T. Buslaps, A. Studer and H. Clemens (2010). "Phase fractions, transition and ordering temperatures in TiAl–Nb–Mo alloys: An in- and ex-situ study." *Intermetallics* 18(8): 1544-1552.
- SCHM2011-1 Schmoelzer, T., K. D. Liss, P. Staron, S. Mayer and H. Clemens (2011). "The Contribution of High-Energy X-Rays and Neutrons to Characterization and Development of Intermetallic Titanium Aluminides." *Advanced Engineering Materials* 13(8): 685-699.
- SCHM2011-2 Schmoelzer, T., S. Mayer, C. Sailer, F. Haupt, V. Güther, P. Staron, K.-D. Liss and H. Clemens (2011). "In Situ Diffraction Experiments for the Investigation of Phase Fractions and Ordering Temperatures in Ti-44 at% Al-(3-7) at% Mo Alloys." *Advanced Engineering Materials* 13(4): 306-311.
- SCHM2012 Schmoelzer, T., A. Stark, E. Schwaighofer, T. Lippmann, S. Mayer and H. Clemens (2012). "In Situ Synchrotron Study of B19 Phase Formation in an Intermetallic γ -TiAl Alloy." *Advanced Engineering Materials* 14(7): 445-448.
- SCHM2013 Schmoelzer, T., K. D. Liss, C. Kirchlechner, S. Mayer, A. Stark, M. Peel and H. Clemens (2013). "An in situ high-energy X-ray diffraction study on the hot-deformation behavior of a β -phase containing TiAl alloy." *Intermetallics* 39: 25-33.
- SCHU2006 Schuster, J. C. and M. Palm (2006). "Reassessment of the binary aluminum-titanium phase diagram." *Journal of Phase Equilibria and Diffusion* 27(3): 255-277.
- SCHW2014 Schwaighofer, E., H. Clemens, J. Lindemann, A. Stark and S. Mayer (2014). "Hot-working behavior of an advanced intermetallic multi-phase γ -TiAl based alloy." *Materials Science and Engineering: A* 614: 297-310.

- SEFE2016 Sefer, B., J. J. Roa, A. Mateo, R. Pederson and M.-L. Antti (2016). "Evaluation of the Bulk and Alpha-Case Layer Properties in Ti-6Al-4V at Micro-And Nano-Metric Length Scale." 1619-1624.
- SING1997 Singh, A. K., Banerjee, D., (1997). "“Transformations in $\alpha_2+\gamma$ Titanium Aluminide Alloys Containing Molybdenum: Part II. Heat Treatment”, ." Metall. Mater. Trans., 28A, 1745-1753 (1997) (Equi. Diagram, Experimental, 7).
- SING2007 Singh, A. K., S. Kumar, S. Banumathy and R. K. Mandal (2007). "Structure of the B2 phase in Ti–25Al–25Mo alloy." Philosophical Magazine 87(34): 5435-5445.
- SING2008 Singh, A. K., S. Banumathy, D. Sowjanya and M. H. Rao (2008). "On the structure of the B2 phase in Ti–Al–Mo alloys." Journal of Applied Physics 103(10): 103519.
- STAR2008 Stark, A., A. Bartels, H. Clemens and F. P. Schimansky (2008). "On the Formation of Ordered omega-phase in High Nb Containing γ -TiAl Based Alloys." Advanced Engineering Materials 10(10): 929-934.
- STAR2010 Stark, A. (2010). Textur- und Gefügeentwicklung bei der thermomechanischen Umformung Nb-reicher Gamma-TiAl-Basislegierungen, Shaker Verlag.
- STAR2011 Stark, A., M. Oehring, F. Pyczak and A. Schreyer (2011). "In Situ Observation of Various Phase Transformation Paths in Nb-Rich TiAl Alloys during Quenching with Different Rates." Advanced Engineering Materials 13(8): 700-704.
- STAR2015 Stark, A., M. W. Rackel, T. A. T., M. Oehring, N. Schell, L. Lottermoser, A. Schreyer and F. Pyczak (2015). "In Situ High-Energy X-ray Diffraction during Hot-Forming of a Multiphase TiAl Alloy." Metals 5(4): 2252.
- ST-N2011 Staron, P., T. Fischer, T. Lippmann, A. Stark, S. Daneshpour, D. Schnubel, E. Uhlmann, R. Gerstenberger, B. Camin, W. Reimers, E. Eidenberger, H. Clemens, N. Huber and A. Schreyer (2011). "In Situ Experiments with Synchrotron High-Energy X-Rays and Neutrons." Advanced Engineering Materials 13(8): 658-663.
- ST-N2017 Staron P., Schreyer A., Clemens H., Mayer S. (2017) Neutrons and Synchrotron Radiation in Engeneering Materials Science. From Fundamentals to Applications. Wiley VCH.
- ST-N2021 Staron, P., Stark, A., Schell, N., Spoerk-Erdely, P., Clemens, H., (2021) Thermal Expansion of a Multiphase Intermetallic Ti-Al-Nb-Mo Alloy Studied by High-Energy X-ray Diffraction. Staron, Calphad 14 - 4
- STRC <https://www.atomic-scale-physics.de/lattice/struk/b2.html>
- STRESS-SPEC . "Stress-Spec description at FRM II web-site." from <https://mlz-garching.de/stress-spec>.
- STRY1988 Strychor, R., J. C. Williams and W. A. Soffa (1988). "Phase transformations and modulated microstructures in Ti-Al-Nb alloys." Metallurgical and Materials Transactions: A 19A: 225-234.
- SUN 2001 SUN FU-SHENG , C. C.-X., KIM SEUNG-EON , LEE YONG-TAI, and YAN MING-GAO (2001). "Alloying Mechanism Of Beta Stabili." METALLURGICAL AND MATERIALS TRANSACTIONS A 1574 — VOLUME 32A, JULY

- T.T.2000 T.T., C. (2000). "The mechanism of grain refinement in TiAl alloy by boron addition - an alternative hypothesis." *Intermetallics* 8.
- TAKEH2015 takehiro_okura (2015). "Materials for Aircraft Engines."
- TEXP ASM Ready Reference: Thermal Properties of Metals <https://www.owl.net.rice.edu/~msci301/ThermalExpansion.pdf>
- THCP "Thermocouples types."
- TRET2005-1 Tretyachenko Ludmila . "Aluminium – Molybdenum – Titanium." *Landolt-Börnstein New Series IV/11A3*.
- TRET2005-2 Tretyachenko Ludmila . "Aluminium – Niobium – Titanium." *Landolt-Börnstein New Series IV/11A3*.
- V., 2000 V., R. R. (2000). "Phase transformations in χ based titanium aluminides." *International Materials Reviews* 45(6).
- VELI2009 Velikanova, T., M. Turchanin, S. Ilyenko, G. Effenberg, V. Tomashik and D. Pavlyuchkov (2009). "Aluminium – Tantalum – Titanium." 11E1: 331-356.
- W.H.A. 1975 W., H. A. (1975). "DESIGN FOR A CONVENTIONAL HIGH-RESOLUTION NEUTRON POWDER DIFFRACTOMETER.pdf>." *Nuclear Instruments and Methods* 127: 361 - 370.
- WANG2000 Wang J.G., N. T. G. (2000). "Creep of a beta phase-containing TiAl alloy." *Intermetallics* 8: 737-748.
- WANG2012 Wang, G. (2012). *Thermodynamic Modelling of High Strength, High Toughness Ti Alloys*. S. o. M. a. Materials and U. o. Birmingham. University of Birmingham.
- WARL2018 Warlimont, H.; Martienssen, W. (Eds.) *Springer Handbook of Materials Data*; Springer: Berlin/Heidelberg, Germany, 2018.
- WATS2009 Watson, I. J., K.-D. Liss, H. Clemens, W. Wallgram, T. Schmoelzer, T. C. Hansen and M. Reid (2009). "In Situ Characterization of a Nb and Mo Containing γ -TiAl Based Alloy Using Neutron Diffraction and High-Temperature Microscopy." *Advanced Engineering Materials* 11(11): 932-937.
- WEBP http://en.cnki.com.cn/Article_en/CJFDTTotal-FMGC200504005.htm
- WEISS1998 Weiss, I.; Semiatin, S.L. *Thermomechanical Processing of Beta Titanium Alloys—An Overview*. *Mater. Sci. Eng. A* 1998, 243, 46–65.
- WILLY2017 Willy, R. M. (2017). *Aufklärung von komplexen intermetallischen γ -TiAl Legierungssystemen für Hochtemperaturanwendungen mittels hochenergetischer Synchrotronstrahlung*, <Dissertation - DO NOT COPY.pdf>.
- WITU2008-1 Witusiewicz, V. T., A. A. Bondar, U. Hecht, S. Rex and T. Y. Velikanova (2008). "The Al–B–Nb–Ti system I. Re-assessment of the constituent binary systems B–Nb and B–Ti on the basis of new experimental data." *Journal of Alloys and Compounds* 448(1-2): 185-194.

- WITU2008-2 Witusiewicz, V. T., A. A. Bondar, U. Hecht, S. Rex and T. Y. Velikanova (2008). "The Al–B–Nb–Ti system II. thermodynamic description of the constituent ternary system B–Nb–Ti." *Journal of Alloys and Compounds* 456(1-2): 143-150.
- WITU2008-3 Witusiewicz, V. T., A. A. Bondar, U. Hecht, S. Rex and T. Y. Velikanova (2008). "The Al–B–Nb–Ti system III. Thermodynamic re-evaluation of the constituent binary system Al–Ti." *Journal of Alloys and Compounds* 465(1-2): 64-77.
- WITU2009-1 Witusiewicz, V. T., A. A. Bondar, U. Hecht and T. Y. Velikanova (2009). "The Al–B–Nb–Ti system IV. Experimental study and thermodynamic re-evaluation of the binary Al–Nb and ternary Al–Nb–Ti systems." *Journal of Alloys and Compounds* 472(1-2): 133-161.
- WITU2009-2 Witusiewicz, V. T., A. A. Bondar, U. Hecht, J. Zollinger, L. V. Artyukh and T. Y. Velikanova (2009). "The Al–B–Nb–Ti system V. Thermodynamic description of the ternary system Al–B–Ti." *Journal of Alloys and Compounds* 474(1-2): 86-104.
- WITU2018 Witusiewicz, V. T., A. A. Bondar, U. Hecht, O. M. Stryzhyboroda, N. I. Tsyganenko, V. M. Voblikov, V. M. Petyukh and T. Y. Velikanova (2018). "Thermodynamic re-modelling of the ternary Al–Mo–Ti system based on novel experimental data." *Journal of Alloys and Compounds* 749: 1071-1091.
- WU2016 Wu, Z., R. Hu, T. Zhang, H. Zhou, H. Kou and J. Li (2016). "Microstructure determined fracture behavior of a high Nb containing TiAl alloy." *Materials Science and Engineering: A* 666: 297-304.
- XIA2001 Xia, Qiangfei, Wang, J. N., Yang, Jie, Wang, Yong (2001) "On the massive transformation in TiAl-based alloys" *Intermetallics* 9. 361-367
- XU,2017-1 Xu, S., Y. Xu, Y. Liang, X. Xu, S. Gao, Y. Wang, J. He and J. Lin (2017). "Phase equilibria of the Ti–Al–Nb system at 1300 °C." *Journal of Alloys and Compounds* 724: 339-347.
- XU2006 Xu, X. J., J. P. Lin, Y. L. Wang, J. F. Gao, Z. Lin and G. L. Chen (2006). "Microstructure and tensile properties of as-cast Ti–45Al–(8–9)Nb–(W, B, Y) alloy." *Journal of Alloys and Compounds* 414(1–2): 131-136.
- XU2017-2 Xu, W.-c., K. Huang, S.-f. Wu, Y.-y. Zong and D.-b. Shan (2017). "Influence of Mo content on microstructure and mechanical properties of β -containing TiAl alloy." *Transactions of Nonferrous Metals Society of China* 27(4): 820-828.
- YAVA1992 Yavari A. R. (1992). "Ordering and disordering in alloys" Elsevier applied science
- YEOH2007 Yeoh, L. A., K.-D. Liss, A. Bartels, H. Chladil, M. Avdeev, H. Clemens, R. Gerling and T. Buslaps (2007). "In situ high-energy X-ray diffraction study and quantitative phase analysis in the α + γ phase field of titanium aluminides." *Scripta Materialia* 57(12): 1145-1148.
- YONG1989 Yong-Won Kim (1989), *Intermetallic Alloys Based on Gamma Titanium Aluminide* JOM 41 7
- ZHANG2002 Zhang, W. J. and F. Appel (2002). "Effect of Al content and Nb addition on the strength and fault energy of TiAl alloys." *Materials Science and Engineering: A* 329–331: 649-652.

- ZHANG2018 Zhang, L., G. Ge, J. Lin, M. Aindow and L. Zhang (2018). "Effect of transition metal alloying elements on the deformation of Ti-44Al-8Nb-0.2B-0.2Y alloys." *Sci Rep* 8(1): 1 - 7.
- ZOLL2007 J. Zollinger, J. Lapin, D. Daloz, H. Combeau, (2007) "Influence of oxygen on solidification behaviour of cast TiAl-based alloys" *Intermetallics* 15 1343-1350

Appendix 1 Elementary theory of order for alloys with bcc lattice

Order of the phase transformations

This question was important for diffraction data interpretation as an allowance or an interdict of simultaneous presence of β_0 and β or α_2 and α . The chapter basics contains the thermodynamic basics in difference between the first and the second order phase transformation. This theory as a very fundamental one was expected to make things clear. Having said that it was found several literature sources exhibiting such properties of the β_0/β and $\beta_0 \rightarrow \beta$ phase transformation, which all together restrict the $\beta_0 \rightarrow \beta$ phase transformation to belong to one kind of phase transformation, or to change this kind when the alloy composition changes from ternary to containing more element alloys. Here literature extraction are collected for quicker achievement of them and main factors are discussed. This facts include:

- Composition AB or A_3B alloy
- Dependency from the heating rate, therefor visibility by DSC measurements
- Presence of both ordered and disordered phases simultaneously

Kinetics, or velocity of the phase transformations are different in the two kinds of phase transformation.

Crystallographic and thermodynamic description of ordering

The understanding whether the ordering phase transformation is the first or the second order could enable to the interpreter the easier refinement of the diffraction data. That allows or restricts presence of both the ordered and disordered phases simultaneously. Therefore some basics of thermodynamics according the kinds of phase transformation is given further.

Basics of thermodynamic description

In order to describe phase transitions in alloys one can use a thermodynamic approach. This approach implies an usage of thermodynamic functions such as entropy, Gibbs energy, enthalpy and others. For full understanding the usage of these functions describing the ordering phenomena the reader is referred to the book of Porter D.A, Easterling K.E. "Phase transformations in Metals and alloys" [PORT1992].

The most general approach to describe ordering and disordering in materials comes from terms of Long Range Order (LRO) met in crystalline materials and Short Range Order (SRO) met in any materials. The two kinds of the phase transformations known in thermodynamics: the first (Figure 1.1) and the second order (Figure 1.2) differs by way of change of the Long Range Order. As long as the LRO presents in any crystalline material, the "ordering" in our investigation means special position of different atom kinds in the unit cell. And "disordered" alloy means chaotically distributed of atoms between position, but still presence of the crystal structure and LRO. Ordering phase transformations are known [LAND-LIV] to be considered as the second order phase transformation because it is considered as change of symmetry without change of crystal lattice. However in some alloys ordering still is referred to the first order transformation [KITT2005].

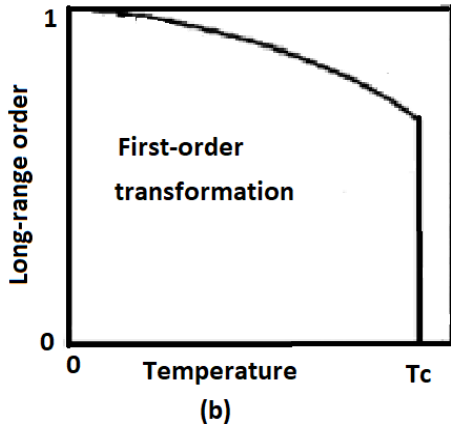


Figure 1.1 Long-range order for A_3B alloy. The transformation for this composition is of the first order. [KITT2005]

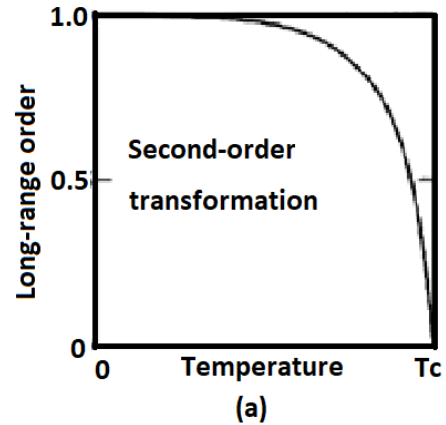


Figure 1.2 Long-range order versus temperature for AB alloy. The transformation is of the second order. [KITT2005]

During the first-order phase transformation the first derivatives of Gibbs free energy $\frac{\partial G}{\partial T}$ and $\frac{\partial G}{\partial P}$ at the transformation temperature are discontinuous (Figure 1.3, left) [PORT1992]. A prominent example of such a phase transformation is melting. Since $\frac{\partial G}{\partial T} = -S$ and $\frac{\partial G}{\partial P} = V$, first order transformations are characterized by discontinuous changes in S and V . There is also a discontinuous change in enthalpy H corresponding to the evolution of the latent heat of the transformation. Due to the change in enthalpy H , the first order phase transformations are very good visible with DSC.

For the second-order transformation the second derivatives of Gibbs free energy $\frac{\partial^2 G}{\partial T^2}$ and $\frac{\partial^2 G}{\partial P^2}$ are discontinuous (Figure 1.3 right) [PORT1992]. The first derivatives, however, are continuous which means that H is also continuous. Consequently since

$$\frac{\partial^2 G}{\partial T^2} = -\left(\frac{\partial S}{\partial T}\right)_P = \frac{1}{T}\left(\frac{\partial H}{\partial T}\right)_P = \frac{C_p}{T} \quad (3)$$

there is no latent heat, only a high specific heat, associated with the transformation.

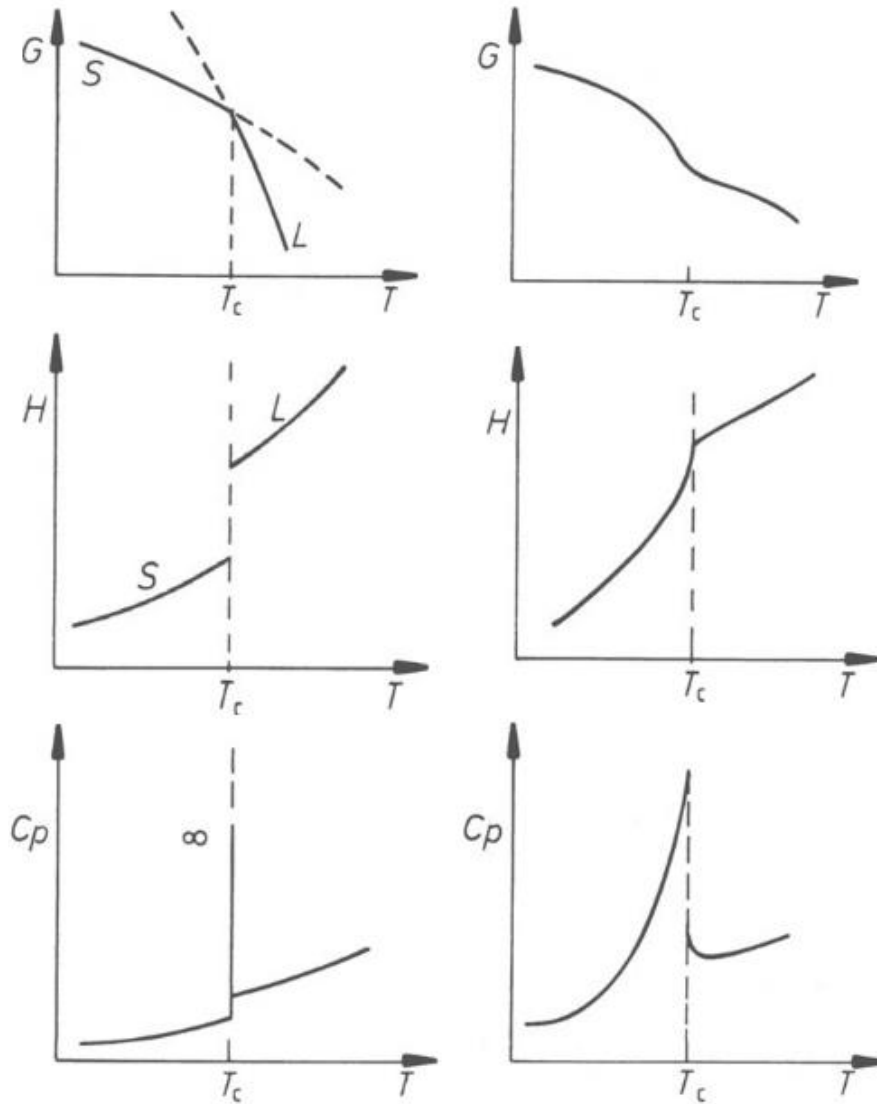


Figure 1.3 First - left and Second - right order phase transformation thermodynamic parameters change [PORT1992]

In the case of A_3B with fcc or hcp structure there is a first order transition marked by a latent heat. [KIT2005]. According to the explanation given above the $\alpha_2 \rightarrow \alpha$ phase transformation should be the first order phase transformation. With a first order phase transformation there is always a two phase region below the ordering temperature for non-stoichiometric compositions. Indeed looking on the binary phase diagram shown one can find a $\alpha_2 + \alpha$ region between pure the α_2 and the α phases at room temperature in the Al concentration range 10 – 20 at. % and an additional small one at temperatures above 1100 °C in the Al concentration range 30 – 40 at. %. That means that the $\alpha_2 \rightarrow \alpha$ phase transformation could be a first order phase transformation but we do not expect the two phase region within our Al concentration range in the binary TiAl diagram. Therefore if only this property is the decisive factor, then a strange variation is existing: the $\alpha_2 \rightarrow \alpha$ phase transformation changes from a first order to a second order transformation depending on the Al content. [PORT1992, DAS2003]

It is important to mention, that first order phase transformations depend on the velocity of heating and cooling [LAND-LIV]. That knowledge should be taken into account when the $\alpha_2 \rightarrow \alpha$ phase transformation will be taken as a reference.

In case of any AB type of alloy with bcc structure there was observed a second order transition between ordered and disordered phases marked by discontinuity in the heat capacity (Figure 1.3). “The second order phase transformations are not rate limited by nucleation” [DAS2003]. That means under changing heating and cooling rates, the second order phase transformation should always take place more or less at the same temperature range [DAS2003] and we should expect to have similar temperatures determined from the data with different heating rates applied. However, the second order phase transformation never takes place at a constant temperature, instead it occurs over a range of temperatures [PORT1992].

In literature [DAS2003] and [CHA1999] the disordering β_o/β phase transition in TiAl alloys is often explained as a second order phase transformation. For the second order transformation this two-phase region never exists [PORT1992, DAS2003]. Thus as a consequence of the phase transformation of the second order [PORT1992, DAS2003] we should not expect to see the presence of both β_o and β phases simultaneously during the in situ diffraction data interpretation. However in more complicated systems than ternary, a simultaneous presence of the β_o and β phases is possible e.g. Kainuma et al. [KAIN2000-B2]. In quaternary system the β -Ti become the ordered B2 structure by progressive substitution of Ti by Fe and Al. At 1000 °C they found a continuous range of solid solutions between β -Ti (A2) and FeTi (B2) with a second order disorder-order transition [PALM2006]. Additionally they show a diagram (Figure 1.4 [KAIN2000-B2]) that contains both A2 and B2 phases simultaneously. The Fe region where both phases are present is between 20 and 50 at. % and with Al contents between 0 – 20 %. This composition differs from the alloys investigated in the present work, but the fact of a possible presence of both ordered and disordered beta phases is detected. The presence of a region with both phases means a first order phase transformation, which “may change to the second order at somewhat higher temperatures” [PALM2006].

No binary TiAl phase diagram contains a region of both β_o/β phases.

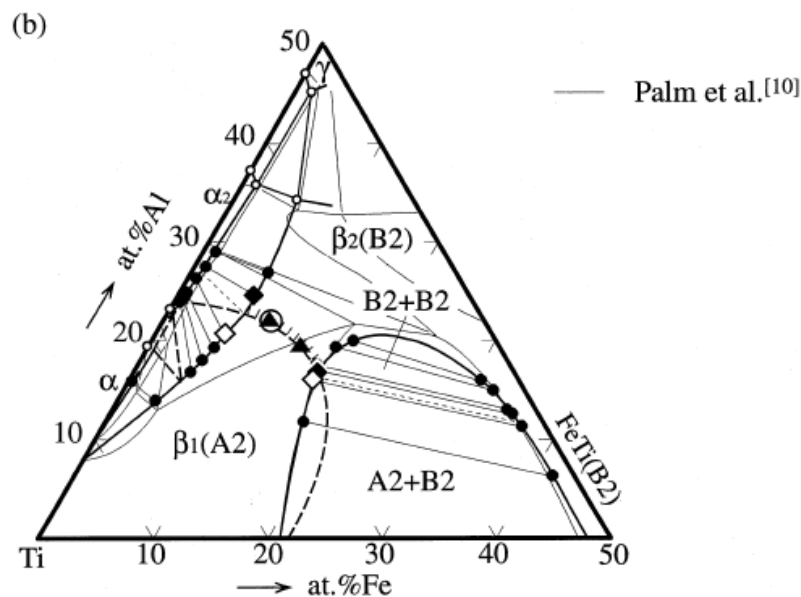


Figure 1.4 Isothermal ternary phase diagram at 1000 °C of the Ti-rich portion of the Ti-Al-Fe systems, which contains both A2 and B2 phases. The thick broken lines indicate

the critical boundary of the A2/B2 ordering experimentally estimated. Taken from [KAIN2000-B2].

The DSC detects phase transformations via a change in heat flow or enthalpy with temperature increase. As it is known only first order phase transformations are conjugated with heat exchange [KITT2005]. Therefore these phase transformations are visible by DSC and are assumed by the thesis author to be depend from the heating rate. E.g. our DSC results include only the $\alpha_2 \rightarrow \alpha$, γ -solvus and the $\alpha \rightarrow \beta$ temperatures and no $\beta_o \rightarrow \beta$ phase transformation. Additionally the first order phase transformations could have regions with two phases [LAND-LIV]. According to the temperature the first peak of the DSC curve corresponds to the $\alpha_2 \rightarrow \alpha$ phase transformation. The $\beta_o \rightarrow \beta$ phase transformation is invisibility by DSC which could be explained not only by another type of phase transformation but also by its very close temperature to the $\alpha_2 \rightarrow \alpha$ phase transformation, that restricts a separation of the two phase transformations in some alloys.

According to Gibbs phase rule in ternary alloys no $\alpha_2+\alpha$ or $\beta_o+\beta$ could appear. Therefore by the author's opinion the α_2/α and the β_o/β should not be referred to the first order phase transformations and therefore are not-influenced by heating rate. Once should consider the α_2/α and β_o/β transformations as proposed by Guttman Lester [GUTT1956] as just atom rearrangements and therefore should be referred to the second order. The dependence from the heating ramp could be determined by the need of changing the chemical composition via diffusion during the phase transformation. By analysing of the binary phase diagram the order of the α_2/α transformation could depend on the position in the phase diagram (the Al content), that means that during heating the chemical composition can change. However, at an Al concentration above 39-40 at. % the α_2/α phase field shows no two phase region in the binary phase diagram. For a sample composition close to our, the α_2/α phase transformation is experimentally [CHLAD2006] found to be slightly dependent from the heating ramp (± 5 °C). The β_o/β phase transformation is expected to be heating rate independent because no change of chemical composition is needed, only the change of positions between the closest neighbours.

Appendix 2a Debay-Waller Factor

In chapter “Basics” description of the Rietveld contain following formula for calculated intensity:

$$I_i^{calc} = S_F \sum_{j=1}^{N \text{ phases}} \frac{f_i}{V_j^2} \sum_{k=1}^{N \text{ peaks}} L_k |F_{k,j}|^2 S_j (2\theta_i - 2\theta_{j,k}) P_{k,j} A_j + bkg_i$$

There is the so called structure factor $|F_{k,j}|^2$, which depends from the temperature Debay-Waller factor B_n

$$|F_{k,j}|^2 = m_k \left| \sum_{n=1}^N f_n e^{-B_n \frac{\sin^2 \theta}{\lambda^2}} (e^{2\pi i (G = h\bar{b}_1 + k\bar{b}_2 + l\bar{b}_3)}) \right|^2$$

$e^{-B_n \frac{\sin^2 \theta}{\lambda^2}}$ – is the temperature factor or the Debye-Waller factor, or displacement parameter of the site j. B_n is the temperature factor or Debye parameter, this parameter is refined in MAUD program. B_n is proportional to $\langle u_j^2 \rangle$ – the mean-square isotropic thermal displacement of the atom on its site, in a direction normal to the diffracting plane, expressed in \AA^2 . In the anisotropic case instead of one B-factor a tensor value should be calculated:

$$B_o = \begin{pmatrix} B_{11} & B_{12} & B_{13} \\ B_{21} & B_{22} & B_{23} \\ B_{31} & B_{32} & B_{33} \end{pmatrix} = 8\pi^2 \begin{pmatrix} u_{11}^2 & u_{12}^2 & u_{13}^2 \\ u_{21}^2 & u_{22}^2 & u_{23}^2 \\ u_{31}^2 & u_{32}^2 & u_{33}^2 \end{pmatrix}$$

In this study the B-factor is assumed to be isotropic. And anisotropy could be taken into account at a next step of data interpretation, when the base parameters are already sure refined.

The B-factor refined in our project very often highly exceeds the expected values (Figure 2a.1). The maximum reached values are 42 and 18 \AA^2 which correspond to u^2 values of 0.532 and 0.22 \AA^2 . According to literature data these values have no physical meaning for metals, but are rather corresponding to bio-materials. Too high calculated values could be explained by peculiarities of the MAUD program where the mathematical algorithm minimizes the least square function regardless of the physical meaning. The typical values in inorganic crystals lie in the region between 0.005 and 0.02 \AA^2 for the heavy atoms.

Figure 2a.1 exhibits the really calculated B-factors for different samples. Thus in the investigated temperature range 1000-1250 °C a fixed B-factor was chosen 1.5 contains for all temperature values applied in the refinements.

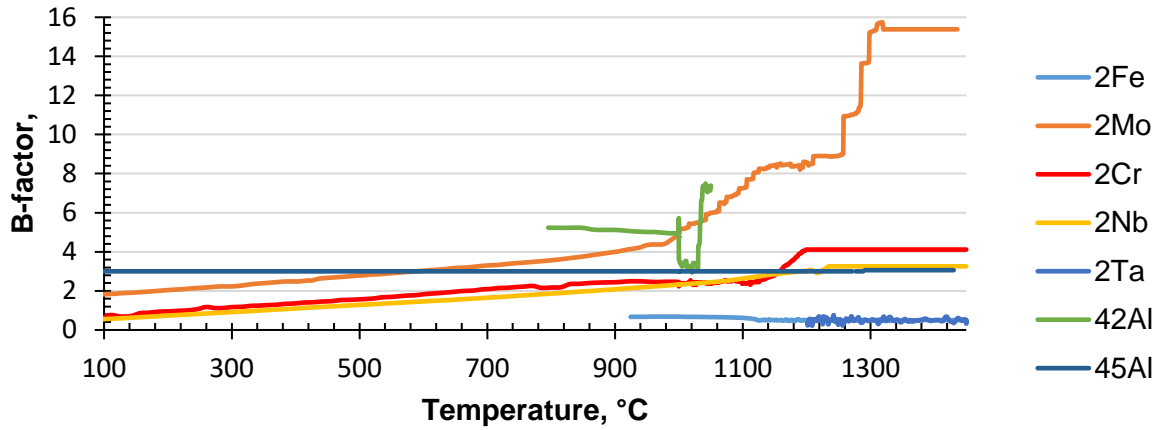


Figure 2a.1 The most wrong refinement results according the B-factor. Values of refined and fixed B-factor for first sample set (based at HEXRD, heating).

Table 2a.1 B-factors values applied in the refinement.

Sample composition	Synchrotron	Neutrons	Extrapolated from [PENG1994] Maximum at 1400 °C
Ti-39Al	Not refined	1.5	3.53
Ti-42Al	Fixed from 1291 °C(483file) B=3	1.5	3.57
Ti-45Al	Fixed from RT B=3	1.5	3.62
Ti-42Al-2Fe	Not fixed B 0.5	1.5	3.55
Ti-42Al-2Mo	Not fixed B 15.38 Out2MoAllparam(2)	1.5	3.54
Ti-42Al-2Cr	Fixed from 1999.4 °C(393file) B=4.11329	1.5	3.54
Ti-42Al-2Nb	Fixed from 1235.585 °C(281file) B=3.254	1.5	3.56
Ti-42Al-2Ta	Fixed from 1215 °C (281file) B=3	1.5	3.55

One can see that values of fixed B-factor are lower then the extrapolated values. However it provided good refined spectrums. The values of fixation were chosen also according to fluctuation of other parameters.

Appendix 2b Grain statistics

Quantitative versus qualitative data interpretations

Qualitative analysis is the determination of the presence of different phases without an estimation of the amount of the phases. Quantitative research is used to quantify the properties by generating numerical data such as the just mentioned phase amount or lattice parameters as well as e.g. site occupancy or B-factor. In our alloys, as in many others the quantitative analysis is more desirable than a qualitative one because it offers more possibilities to compare the influence of the β stabilizing elements on the β_0/β and other phase transformations. However, the negative influence of grain coarsening at high temperatures hampers the quantitative analysis and plays a decisive role to choose often the qualitative data analysis instead of the quantitative one. The problem with bad grain statistic has been met at HT for all samples and at RT for Ti-39Al and Ti-39Al-0.2B.

Influence of grain coarsening at high temperatures

A quantitative analysis is hampered by the problem of bad grain statistics that appeared for most of the samples at high temperatures above 1300 °C. Below 1250 °C no problem with data interpretation was found (except for Ti-39Al and Ti-39Al-0.2B). However the data at HT could be still used for the qualitative analysis of β_0/β phase presence.

The mechanism of grain statistic change during heating is simple. Above 1300 °C, when the single phase regions appears, (α or β for the alloys containing initially the β_0 phase) the grains are growing which makes the grain statistic worse. The spectrums are no longer quantitatively interpretable because the intensities of the peaks do no longer correspond to the intensities of an ideal “powder sample”. Big grains start to absorb the small ones and thus the big grains are “moving” and changing orientation. Due to change of the orientation grains temporary fulfil the reflection conditions and bright wide peaks are appearing and disappearing with temperature thus a highly fluctuating intensity could be observed in the diffraction spectrums. Figure 2b.1 shows the detrimental influence of the bad grain statistic in the area framed in red at high temperature. The jump of the β and α phase could be explained by bad grain statistic at temperature above 1300 °C. Fine grained microstructures provide the higher amount of scattering points and as a result the more homogenous ring.

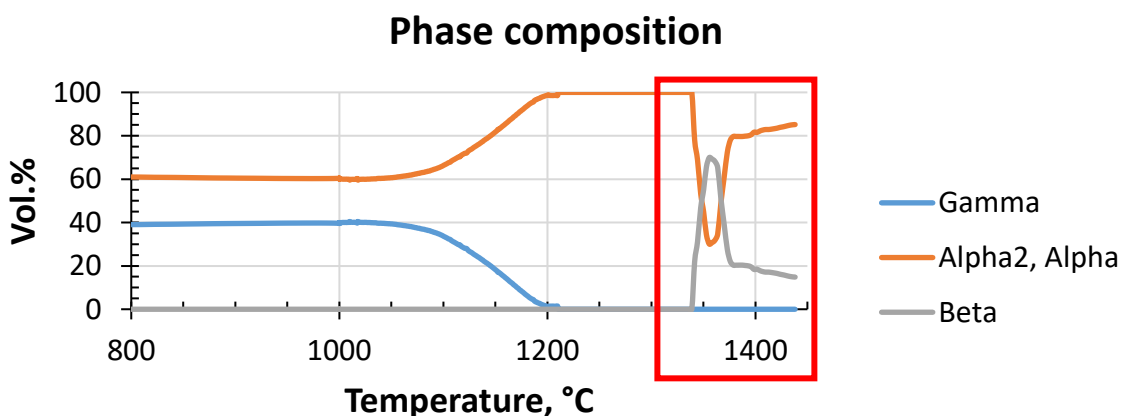
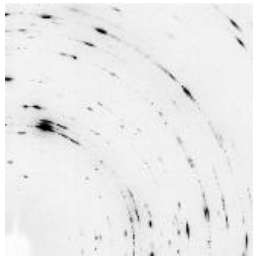
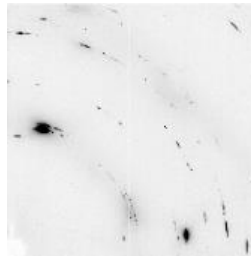


Figure 2b.1 Phase composition of Ti-42Al based on HEXRD during heating. Red marked area exhibits the temperature region with jumping phase composition due to bad grain statistics.

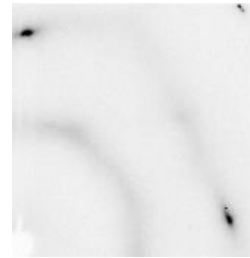
The same behaviour as shown in Figure 2b.1 could be observed with lattice parameters and other parameters e.g. the site occupancy refinement. Usually not only one but several parameters show jumps of their values, aiming to better fit to the high intensity of big grains. Then the summation of the high intensive spots result in a wrong estimation of the phase composition. Additionally the large spots broaden the peaks thus problems with peak position determination occurs. Figure 2b.2 shows synchrotron detector images of samples with bad (Ti-42Al-2Cr) and good (Ti-42Al-2Nb) grain statistics. The summation of rare but high intensive spots gives a wrong estimation of both the phase composition and (in less extend) lattice parameters. Additionally the large spot makes the peak broader and peak position determination problems occur.



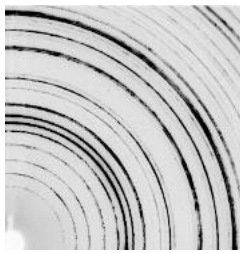
a Ti-42Al-2Cr, 1000 °C



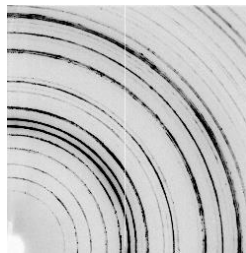
b Ti-42Al-2Cr, 1300 °C



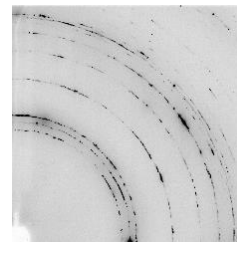
c Ti-42Al-2Cr, 1450 °C



d Ti-42Al-2Nb, 287 °C



e Ti-42Al-2Nb, 1000 °C



f Ti-42Al-2Nb, 1250 °C

Figure 2b.2 Quarters of detector images of two measured samples in order to demonstrate the grain statistic. a, b, c and f are examples for bad grain statistics; d and e allow a quantitative phase analysis.

Influence of grain statistic on neutron measurements

Same as in the case of synchrotron investigation the bad grain statistics plays a negative role in the data interpretations every diffraction techniques. Even the larger size of neutron beam did not play a decisive role, due to the lower beam intensity compared to synchrotron and the smaller section of the diffraction rings.

Figure 2b.3 shows some examples of neutron detector images where one can see the presence of several big grains of β_0 phase in Ti-42Al-2Mo (figures a-c) and the bad statistic of Ti-39Al alloy (figures d-f). Qualitative analysis allows to determine the temperatures where peaks have been seen the last time for the first sample set.

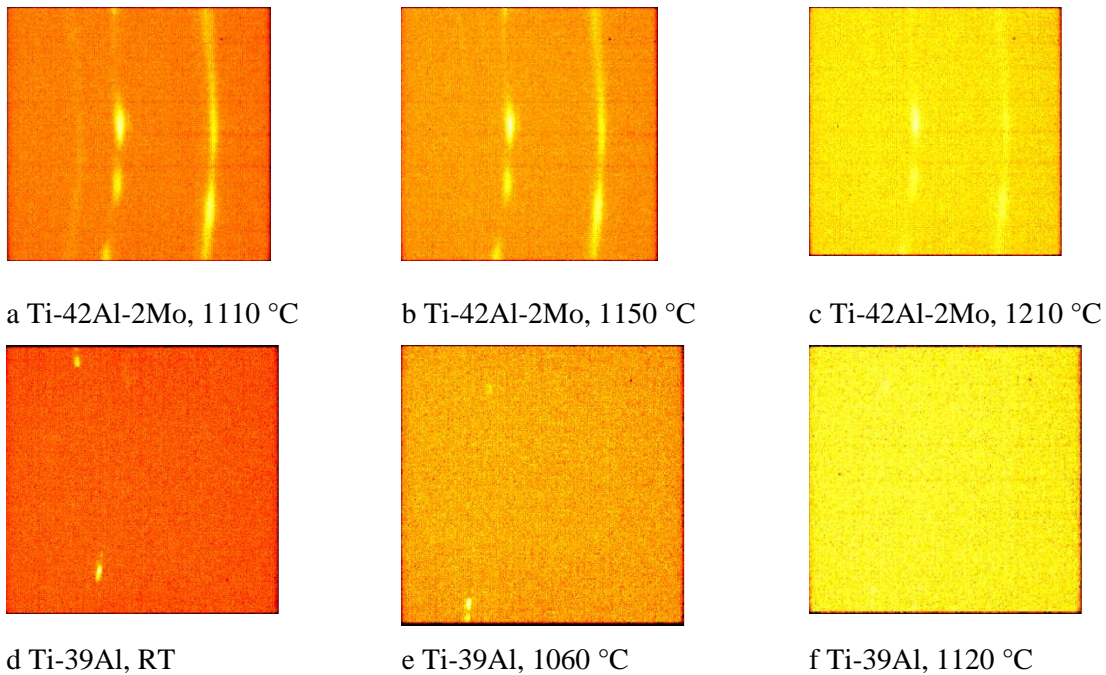
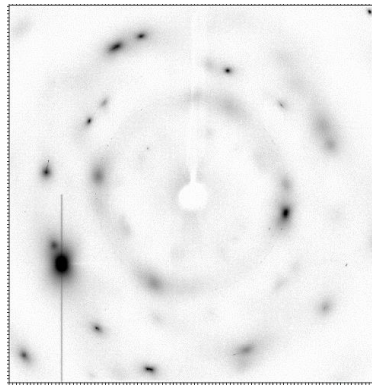


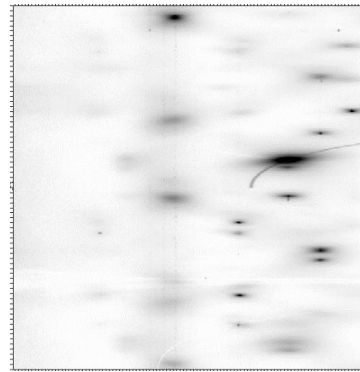
Figure 2b.3 Examples of the bad grain statistics.

Bad grain statistic from the RT: Ti-39Al and Ti-39Al-0.2B alloys in more details

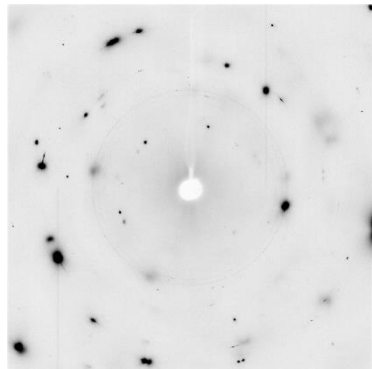
The binary alloys Ti-39Al and Ti-39Al-0.2B have already after production and heat treatment very coarse grained microstructures (see SEM results: grain size above 200 μm), thus a negative influence of the bad grain statistics can be observed already at RT: constantly too high or too low peak intensities are measured (Figure 2b.4, Figure 2b.5), that depends whether the big grains are in the reflection condition.



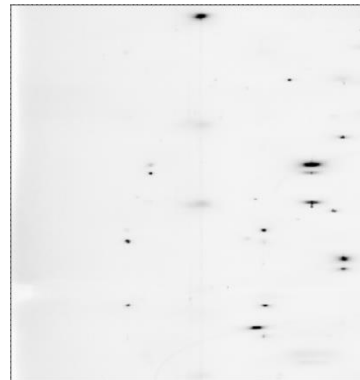
a



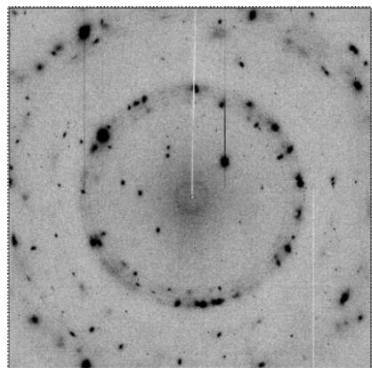
b



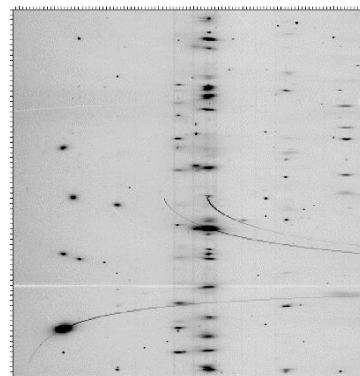
c



d



e

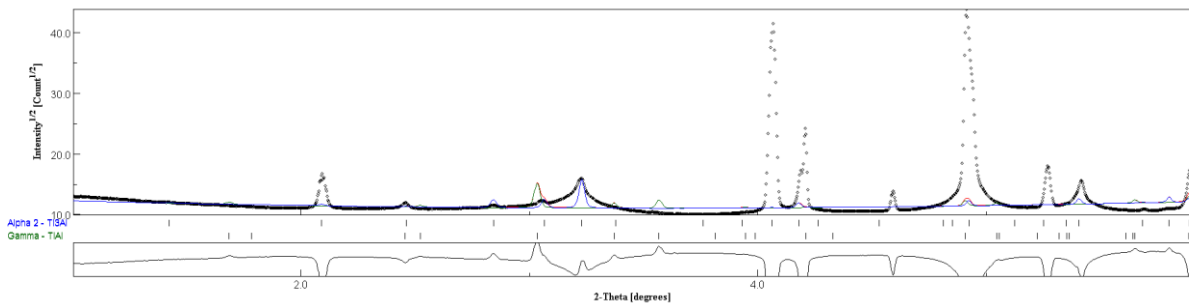


f

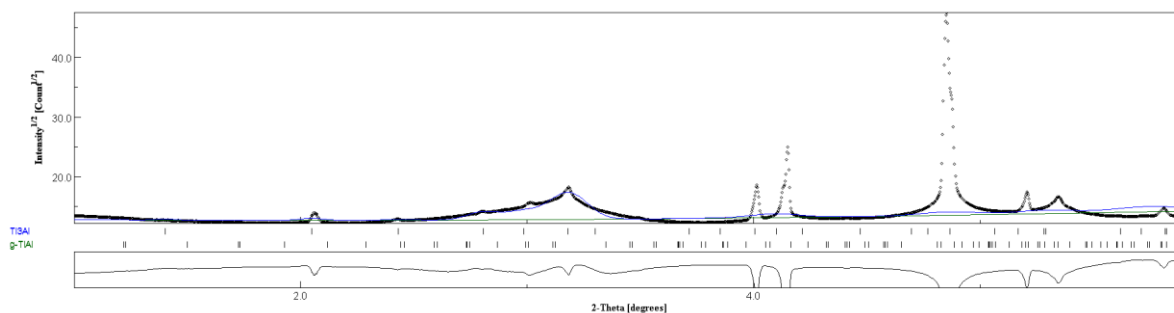
Detector pictures

Unrolled rings

Figure 2b.4 Detector picture and its unrolled modification for Ti-39Al a,b - at 1000 °C; c,d - RT, e,f - Results synchrotron measurements of second set sample Ti-39Al-0.2B at RT



a. RT



b. 1000 °C

Figure 2b.5 Synchrotron spectrums of Ti-39Al: a. RT, b. 1000 °C

The Figure 2b.5 shows explicitly how inconsistent can look like spectrum in the case of low grain statistics.

It is evidently a need to control the microstructure of samples before experiment to avoid uninterpretable data of diffraction measurements. Unfortunately only a tendency to form coarse grained microstructure is known, but neither the real chemical composition nor the heat treatment by itself could be identified as the main reason for grains coarsening. So it is hard to estimate before melting which of the samples could give bad grain statistics.

Possible improvements for the case of the bad grain statistic

The problem of grain statistic is known to be solved with small boron additions. Therefore the new alloys Ti-39Al-0.2B and Ti-42Al-0.2B were produced for the second sample set. However only samples with Ti-42Al-0.2B has shown significant improvements and the grain size of Ti-39Al-0.2B stayed still too coarse. Figure 2b.4 shows a small improvement of the grain statistic (grain refinement) for Ti-39Al-0.2B compared to Ti-39Al. The small improvement was not sufficient for a good quantitative refinement and especially at HT the grain statistic will be only worse.

Additional demands for better measurements and data analysis are fine grained microstructures without texture. This is even more desired for the neutron diffraction than for synchrotron measurements, because part of the ring is detected only by the STRESS-SPEC instrument.

The case of low phase content yield to the weak intensity of the ring, that obliges to apply the summation as of detector pictures, as well as the segmentation (unrolling) of the ring during interpretation. Thus both homogeneous ring and its high intensity, are really necessary for the best diffraction data interpretation. For neutron diffraction due to the lower beam intensity, intensity of signal becomes less, that needs longer exposure time. In the case of high intensity neutron beam as e.g. ESS the grain statistic situation could be improved, especially together with oscillation of the sample or dilatometer position and the highest possible the detector counting statistics.

Unfortunately it should be mentioned that in the case of neutron as well as for synchrotron measurements it is hard to rotate either the sample inside the dilatometer or the whole dilatometer in the beam, which would result in the best statistics achievement. The impossibility for rotation of the sample inside the dilatometer occurs due to the welded thermocouples, which would lose the contact to the sample. The rotation of the whole dilatometer positioned on a goniometer, as applied at FRM II, is limited to a few degrees because internal parts of dilatometer might move between beam sample and detector during rotation.

Appendix 2c Correspondence of the SO and Phase composition graphs.

Further going graphs of site occupancies of the β phase are compared first sample set based on synchrotron data. One can see correlation: the temperature of the SO reached 0.5 to the temperature below the local maximum and minimum phase contents occur.

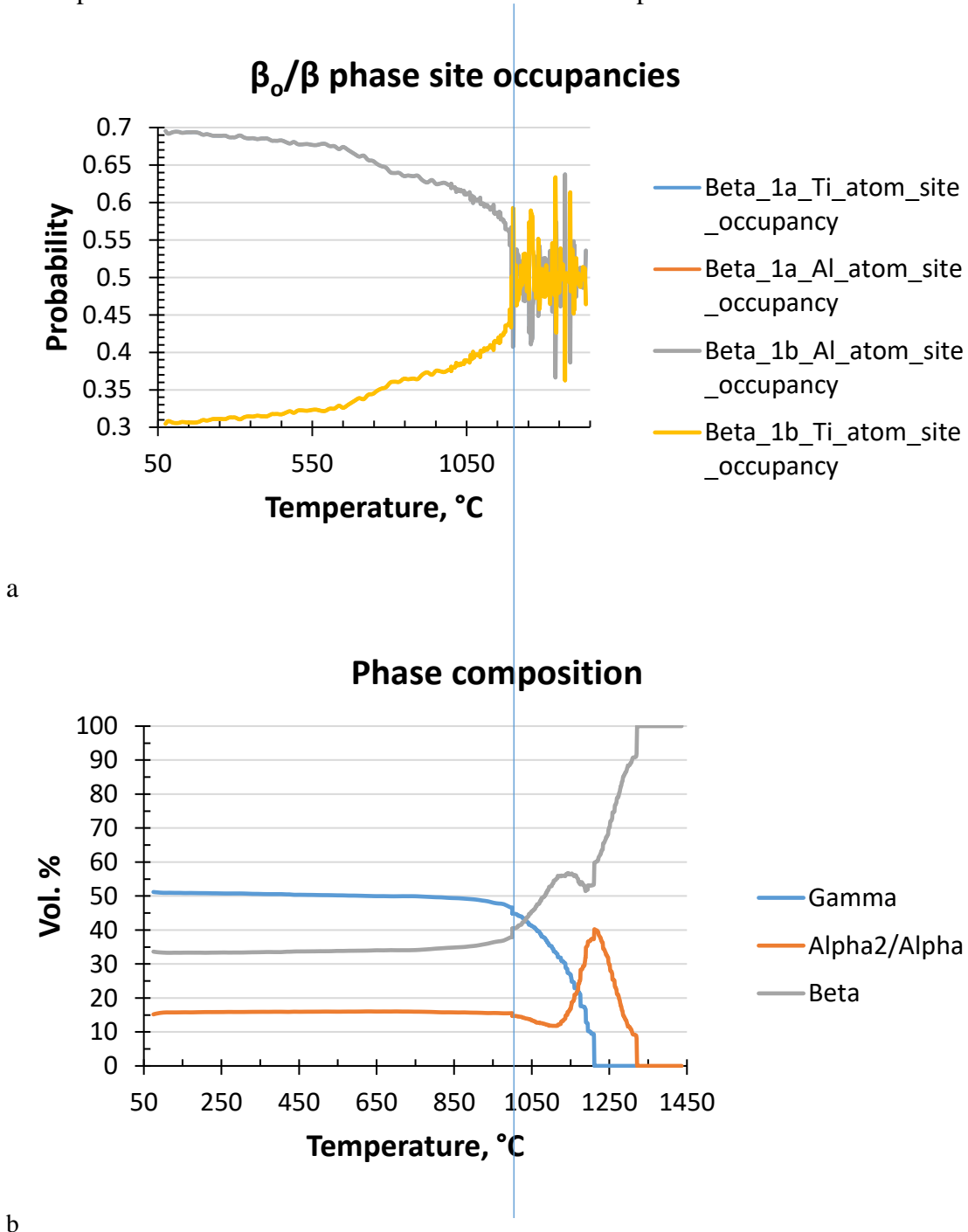
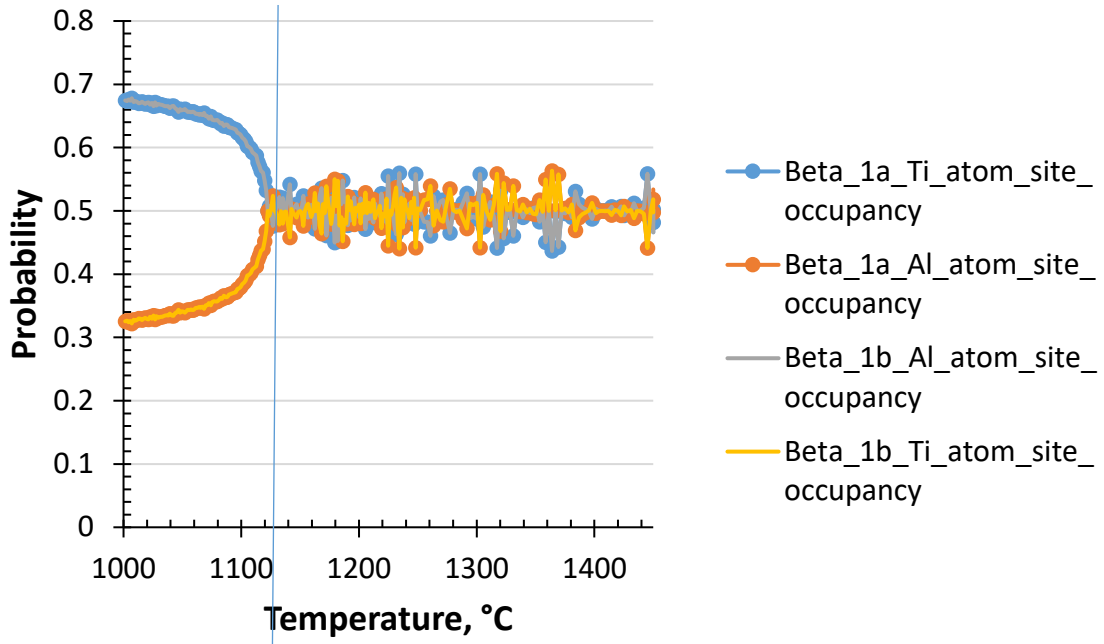


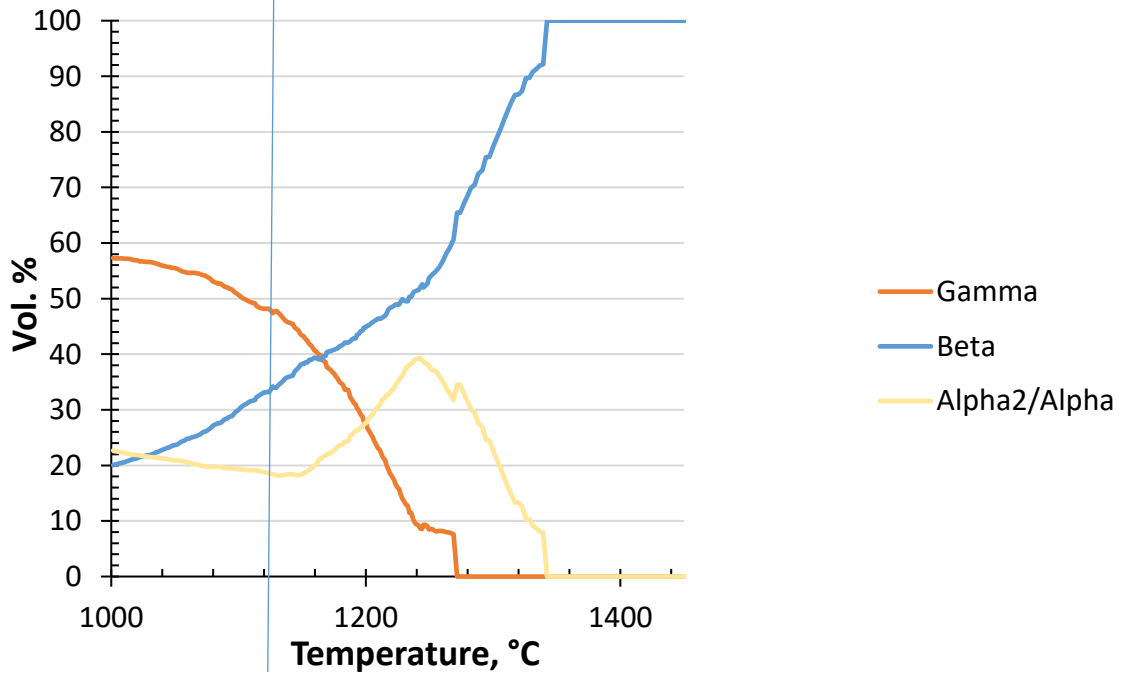
Figure 2c.1 2Ti-42Al-2Mo

β_0/β phase site occupancies



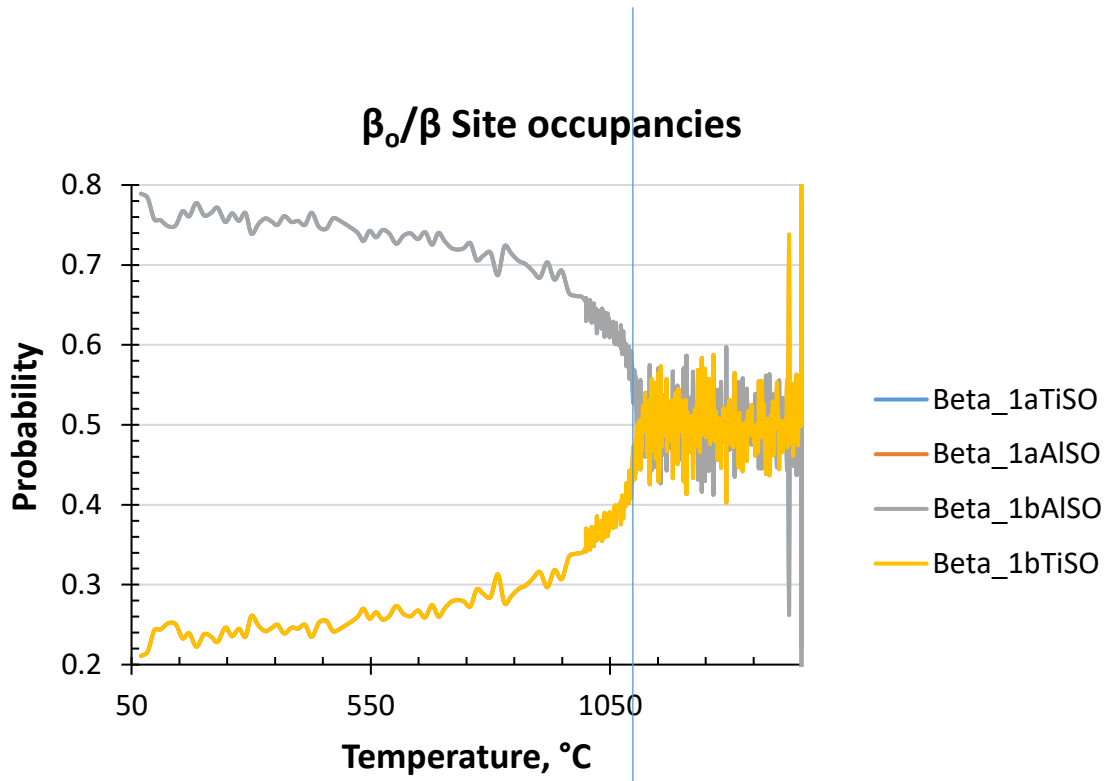
a

Phase composition

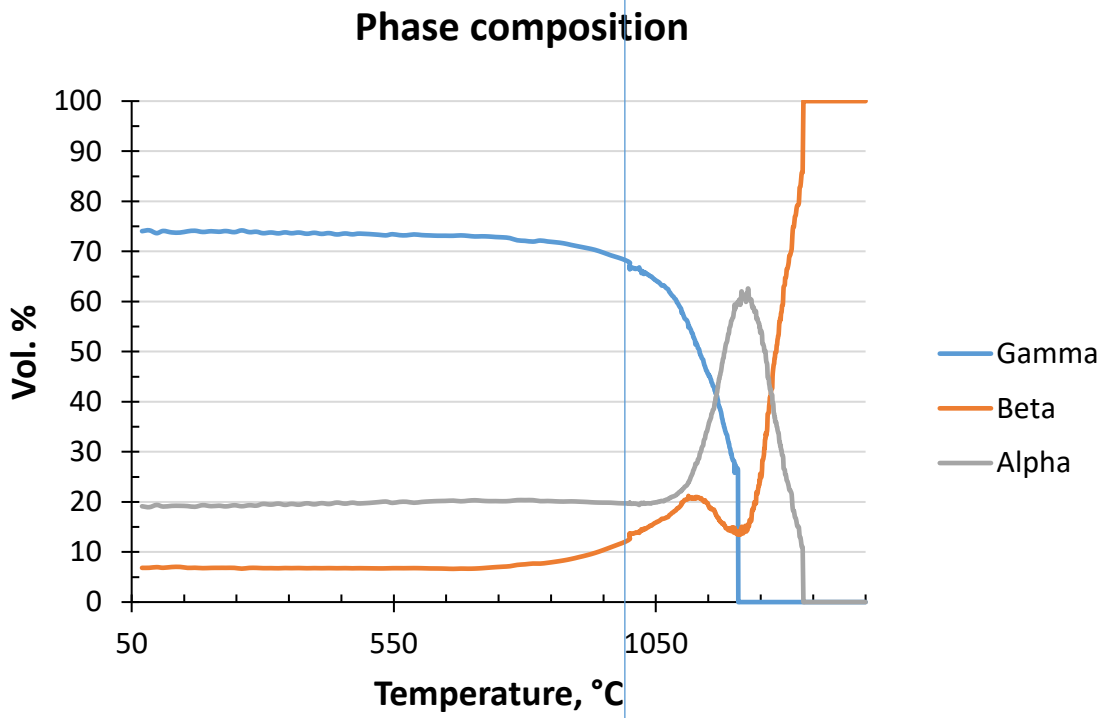


b

Figure 2c.2 Ti-42Al-2Fe



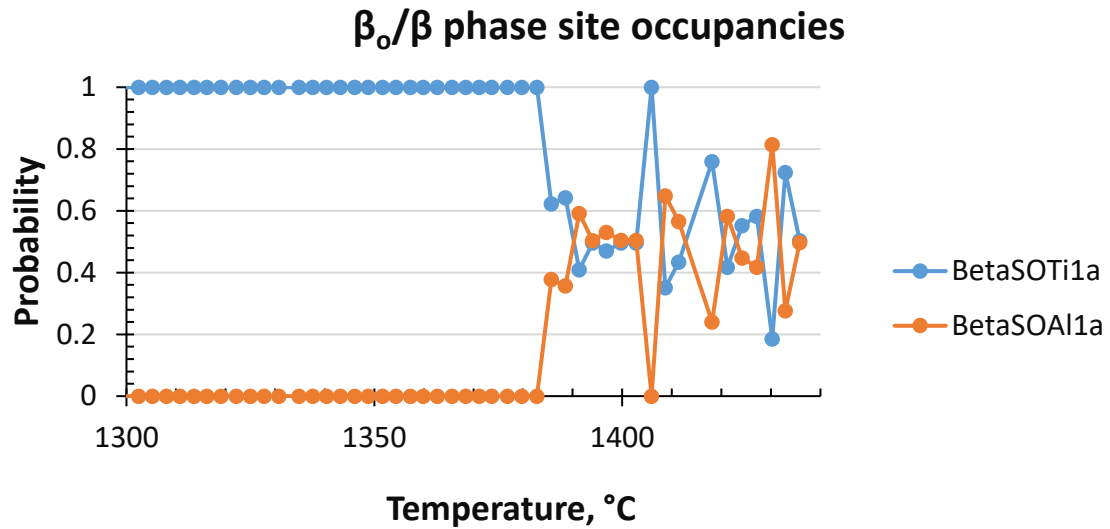
a



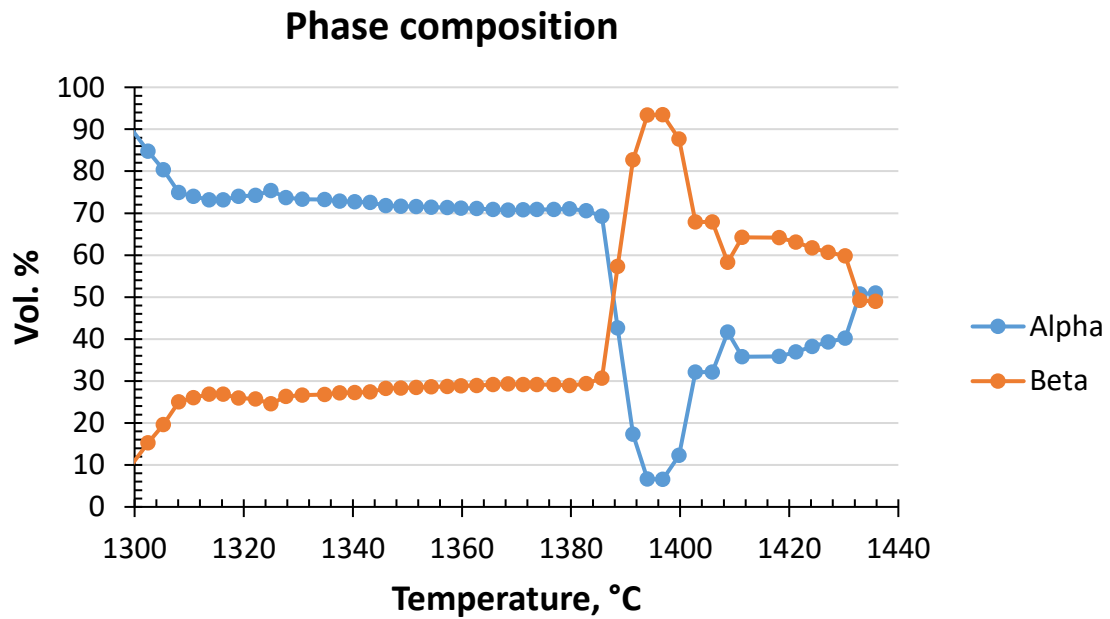
b

Figure 2c.3 Ti-42Al-2Cr

An attempt to find for β_0 phase in binary alloys. The much fluctuating SO at HT, that no undoubtful presence of β_0 phase could be confirmed. The MAUD Refinement finds the superstructure peak within the background, and it is not confirmed by the manual spectrum check. This is the same for further going Ti-45Al, Ti-42Al, Ti-42Al-2Ta, Ti-42Al-2Nb.

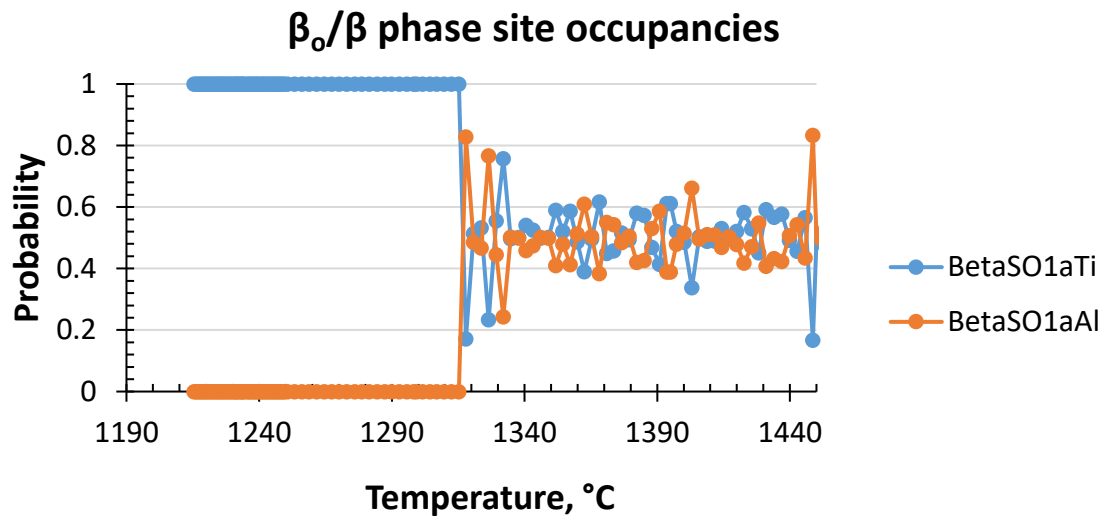


a

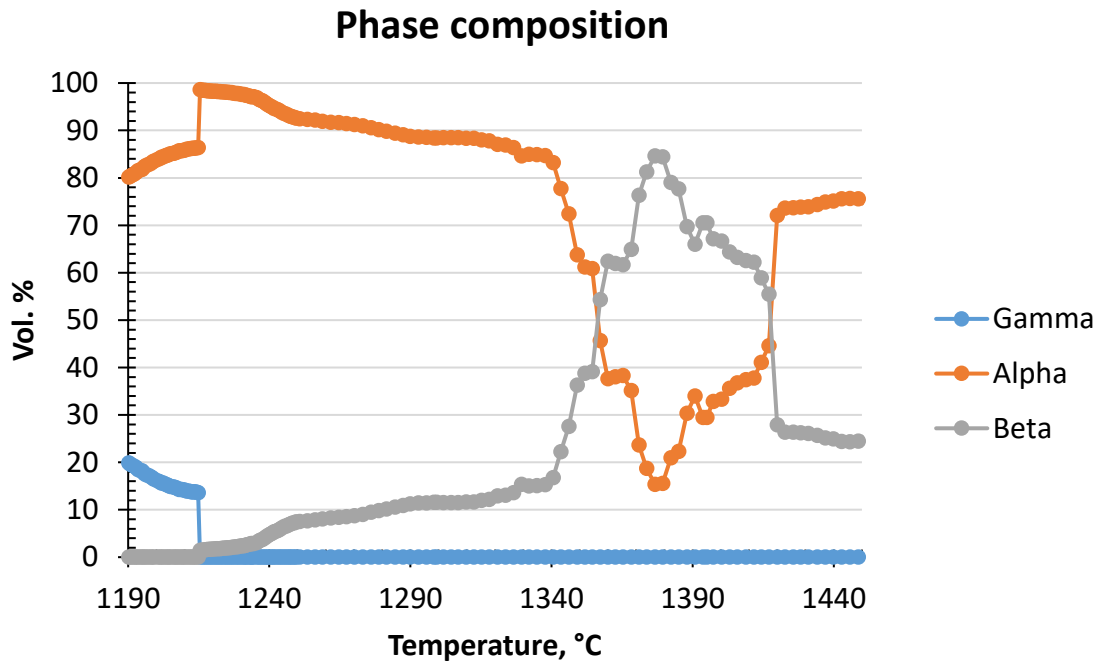


b

Figure 2c.4 Ti-45Al

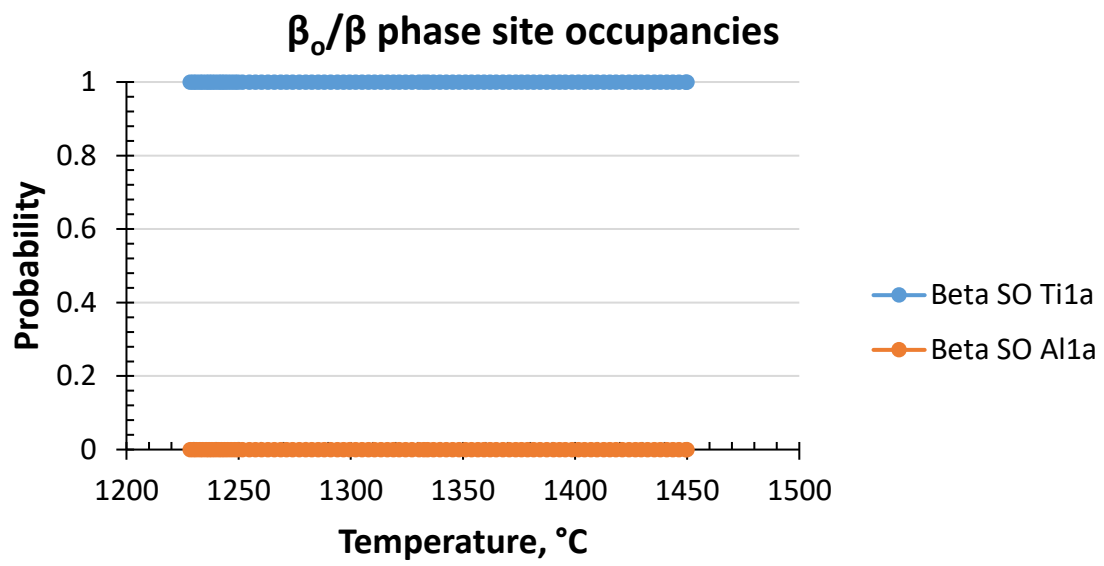


a

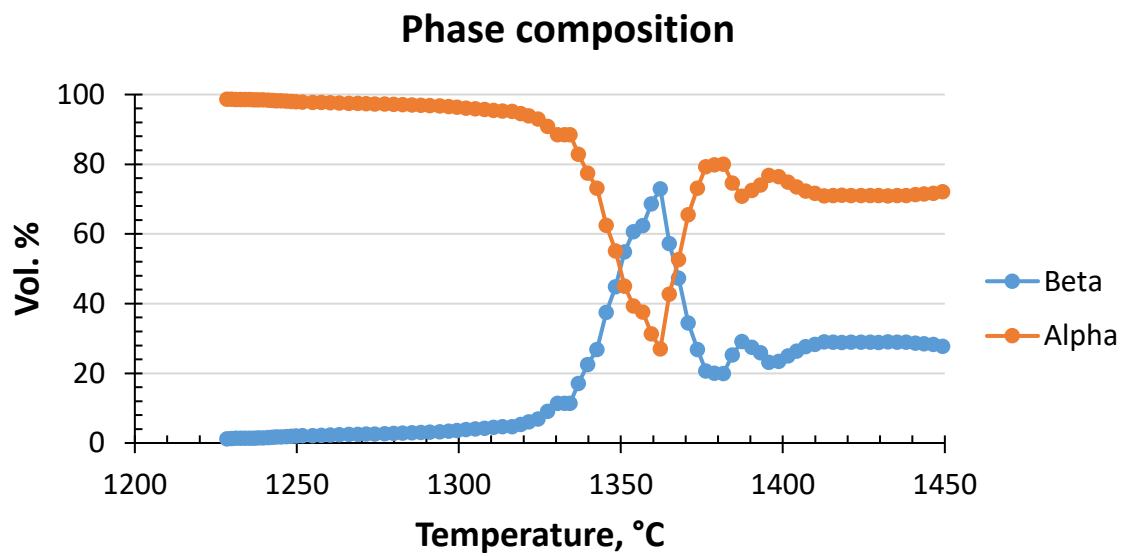


b

Figure 2c.5 Ti-42Al-2Ta

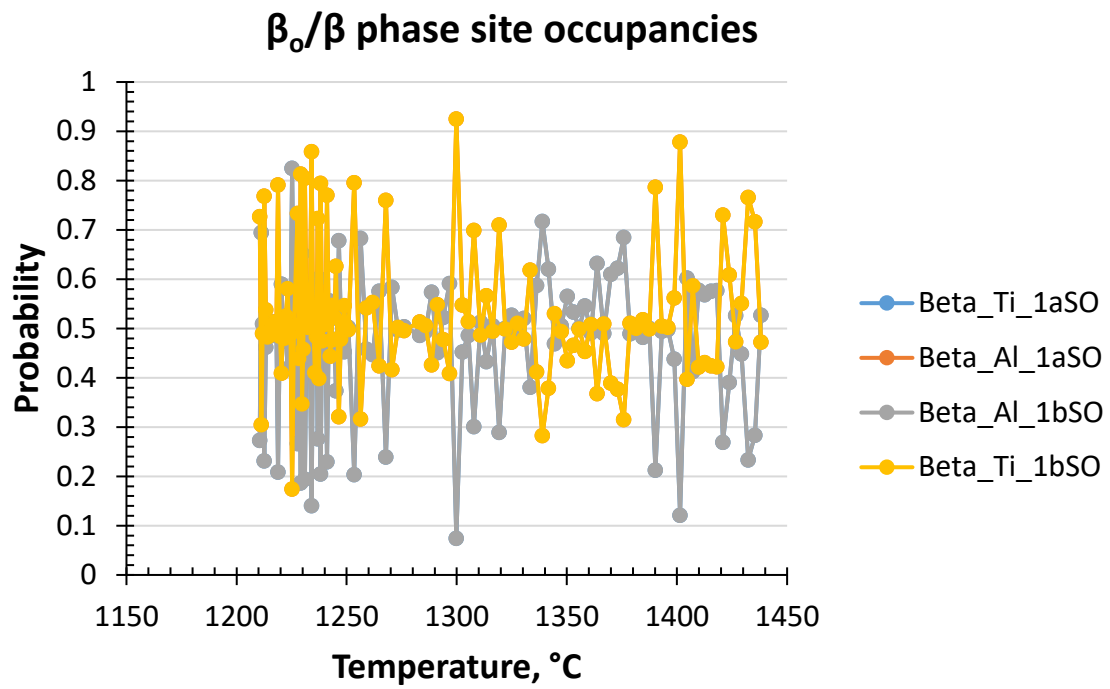


a

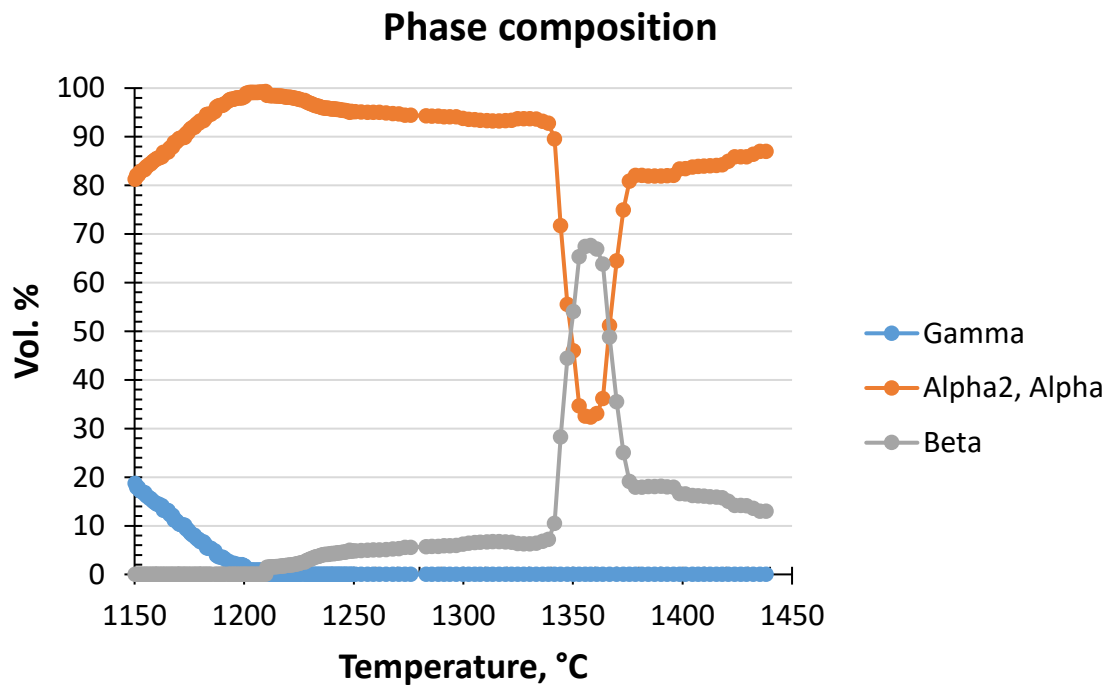


b

Figure 2c.6 Ti-42Al-2Nb



a



b

Figure 2c.7 Ti-42Al

Appendix 3a Difference between nominated and weighted element composition in grams

Sample composition	Calculated	Weighted	Calculated	Weighted	Calculated	Weighted	Sum.Mass of Elements	Real mass	mass diff.
	Grams of Al		Grams of Ti		Grams of El				
The First sample set									
Ti-42Al-2Fe	9.508	9.237	22.492	21.852	0.911	0.906	31.994	31.898	0.096
Ti-42Al-2Cr	9.256	9.253	21.895	21.894	0.849	0.847	31.995	31.918	0.077
Ti-42Al-2Mo	9.053	9.052	21.414	21.413	1.533	1.534	31.998	31.941	0.057
Ti-42Al-2Nb	9.067	9.072	21.447	21.448	1.487	1.487	32.007	31.899	0.107
Ti-42Al-2Ta	8.684	8.689	20.542	20.542	2.773	2.774	32.005	31.763	0.243
Ti-39Al	8.477	8.479	23.523	22.725	0.000	0.000	31.204	31.963	0.759
Ti-42Al	9.276	9.277	22.724	22.725	0.000	0.000	32.002	31.951	0.051
Ti-45Al	10.100	10.105	21.900	21.898	0.000	0.000	32.003	31.979	0.024
The second sample set									
Ti-42Al-1Fe	9.391	9.398	22.609	22.613	0.456	0.457	32.468	32.396	0.072
Ti-42Al-3Fe	9.629	9.663	22.371	22.374	1.363	1.364	33.401	33.258	0.143
Ti-42Al-4Cr	9.237	9.251	21.068	21.081	1.695	1.698	32.030	31.986	0.043
Ti-42Al-6Cr	9.217	9.211	20.245	20.304	2.538	2.544	32.059	31.947	0.112
Ti-42Al-4Mo	8.841	8.845	20.165	20.175	2.994	2.994	32.014	31.817	0.197
Ti-42Al-6Mo	8.638	8.638	18.974	18.977	4.388	4.393	32.008	31.935	0.074
Ti-42Al-10Nb	8.317	8.319	16.864	16.870	6.819	6.819	32.008	31.899	0.109
Ti-42Al-8.5Ta	7.194	7.197	15.042	15.047	9.764	9.772	32.016	31.742	0.274
Ti-42Al-10Ta	6.920	6.921	14.030	14.052	11.050	11.062	32.035	31.817	0.218
Ti-39Al-0.2B	8.493	8.492	23.489	23.4909	0.017	0.018	31.203	31.946	0.744
Ti-42Al-0.2B	9.293	9.293	22.689	22.693	0.018	0.018	32.004	31.979	0.025

**Appendix 3b Estimation of the sample chemical composition
under an assumption of only Al loss during arc-melting based on
the mass of the melted button.**

Samples name, at. %	Phase composition, estimated with Al loss only, at. %	Difference in element concentration, assuming only Al loss, at. %		
		Ti	Al	El
First sample set				
Ti-42Al-2Fe	Ti-41.7Al-2Fe	-0.26	0.26	0.00
Ti-42Al-2Cr	Ti-41.8Al-2Cr	-0.21	0.20	0.00
Ti-42Al-2Mo	Ti-41.8Al-2Mo	-0.16	0.15	0.01
Ti-42Al-2Nb	Ti-41.7Al-2Nb	-0.28	0.27	0.01
Ti-42Al-2Ta	Ti-41.3Al-2Ta	-0.67	0.65	0.02
Ti-39Al	Ti-38.9Al	-0.10	0.10	
Ti-42Al	Ti-41.9Al	-0.13	0.13	
Ti-45Al	Ti-45Al	-0.04	0.04	
Second sample set				
Ti-42Al-1Fe	Ti-41.8Al-1Fe	-0.17	0.18	-0.01
Ti-42Al-3Fe	Ti-41.8Al-2.9Fe	-0.23	0.34	-0.11
Ti-42Al-4Mo	Ti-41.5Al-4Mo	-0.55	0.51	0.04
Ti-42Al-6Mo	Ti-41.8Al-6Mo	-0.21	0.19	0.03
Ti-42Al-4Cr	Ti-41.9Al-4Cr	-0.09	0.08	0.01
Ti-42Al-6Cr	Ti-41.6Al-6Cr	-0.38	0.35	0.04
Ti-42Al-10Nb	Ti-41.7Al-10.1Nb	-0.32	0.27	0.05
Ti-42Al-8.5Ta	Ti-41.1Al-8.5Ta	-0.94	0.80	0.14
Ti-42Al-10Ta	Ti-41.2Al-10.1Ta	-0.81	0.67	0.14
Ti-42Al-0.2B	Ti-41.9Al-0.2B	-0.08	0.28	0.01
Ti-39Al-0.2B	Ti-38.9Al-0.2B	-0.07	0.07	0.00

Appendix 3c Difference of the middle, estimated by many points according to RT with Rotation DESY measurements, and nominal sample composition

Samples name, at. %	Phase composition, at. %
First sample set	
Ti-39Al	Ti – 39.1 Al
Ti-42Al	Ti - 44.3 Al DO WE HAVE SIMILAR phase compositionn to Ti-45Al
Ti-45Al	Ti - 44.9 Al
Ti-42Al-2Fe	Ti - 42.1 Al - 1.2 Fe
Ti-42Al-2Mo	Ti – 42.21 Al – 4.50 Mo
Ti-42Al-2Cr	Ti - 41.2 Al - 2.6 Cr
Ti-42Al-2Nb	Ti - 55.6 Al - 1.61 Nb
Ti-42Al-2Ta	Ti - 40.9 Al - 1.66 Ta
Second sample set	
Ti-42Al-1Fe	Ti - 39.75 Al – 1 Fe
Ti-42Al-3Fe	Ti – 42.43 Al - 1.92 Fe
Ti-42Al-4Mo	Ti - 40.0 Al - 2.0 Mo
Ti-42Al-6Mo	Ti - 41.9 Al - 3.5 Mo
Ti-42Al-4Cr	Ti - 45.08 Al – 2.97 Cr
Ti-42Al-6Cr	Ti - 42.2 Al - 3.2 Cr
Ti-42Al-8.5Nb	Ti – 42.02 Al – 8.66 Nb
Ti-42Al-10Nb	Ti - 40.6 Al - 7.88 Nb
Ti-42Al-8.5Ta	Ti – 41.6 Al – 8.80 Ta
Ti-42Al-10Ta	Ti – 38.79 Al – 10.94 Ta
Ti-42Al-0.2B	Ti - 41.3 Al
Ti-39Al-0.2B	Ti - 37.8 Al

**Appendix 3d Difference of the element content in different
phases for the second sample set acc. EDX**

a α_2/α -phase

Sample composition	Al		Ti		El	
		Stand. Dev.		Stand. Dev.		Stand. Dev.
Ti-39Al-0.2B	38.71	5.45	61.29	1.43		
Ti-42Al-0.2B	38.11	1.00	61.83	1.00		
Ti-42Al-1Fe	40.11	0.00	58.71	0.00	0.92	0.00
Ti-42Al-2Fe	37.36	5.56	63.46	1.50	0.00	
Ti-42Al-3Fe	36.78	5.58	62.03	1.43	1.20	7.22
Ti-42Al-2Mo	35.24	5.55	61.27	1.63	3.49	2.30
Ti-42Al-4Mo	0.00		0.00		0.00	
Ti-42Al-6Mo	0.00	0.00	0.00	0.00	0.00	0.00
Ti-42Al-2Cr	36.56	5.65	59.38	1.52	4.07	4.14
Ti-42Al-4Cr	36.30	5.61	59.48	1.45	4.21	3.45
Ti-42Al-6Cr	37.02	5.56	60.47	1.44	2.51	3.80
Ti-42Al-2Nb	59.57	1.53	38.79	5.46	1.64	3.13
Ti-42Al-10Nb	0.00	0.00	0.00	0.00	0.00	0.00
Ti-42Al-2Ta	45.53	5.19	53.23	1.64	1.24	6.40
Ti-42Al-10Ta	39.77	5.22	52.06	2.28	8.17	2.94

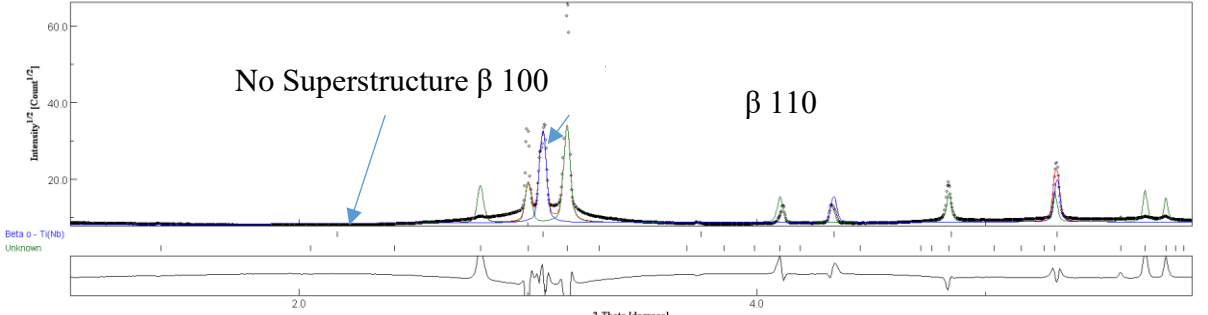
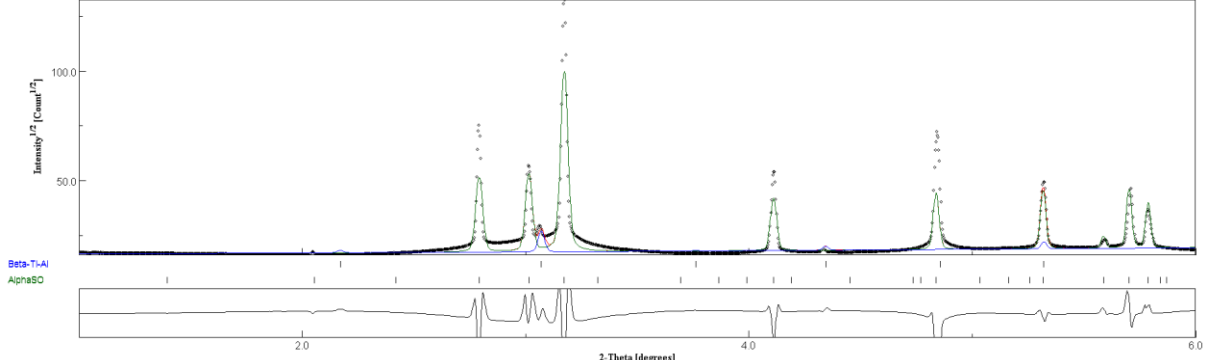
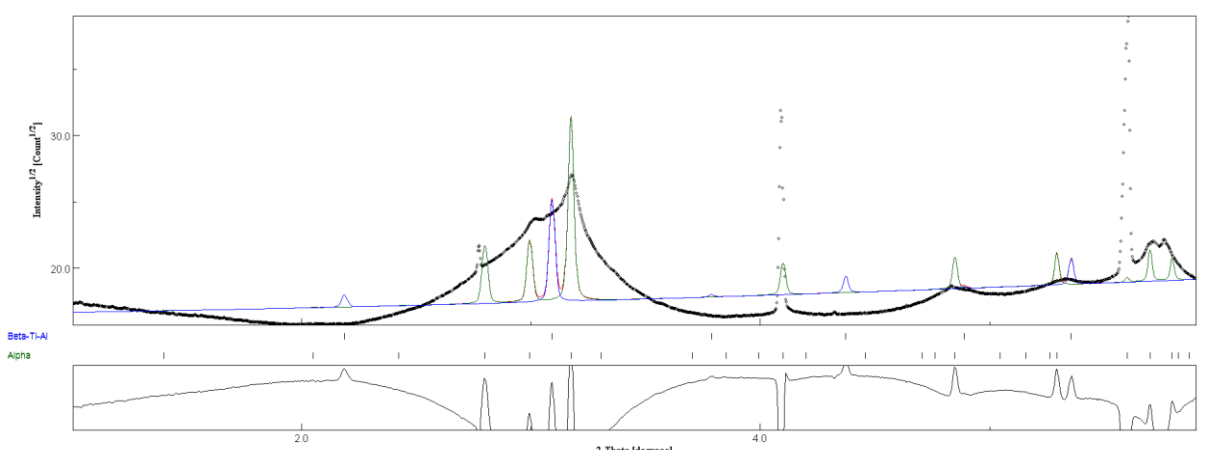
b β_0/β -phase

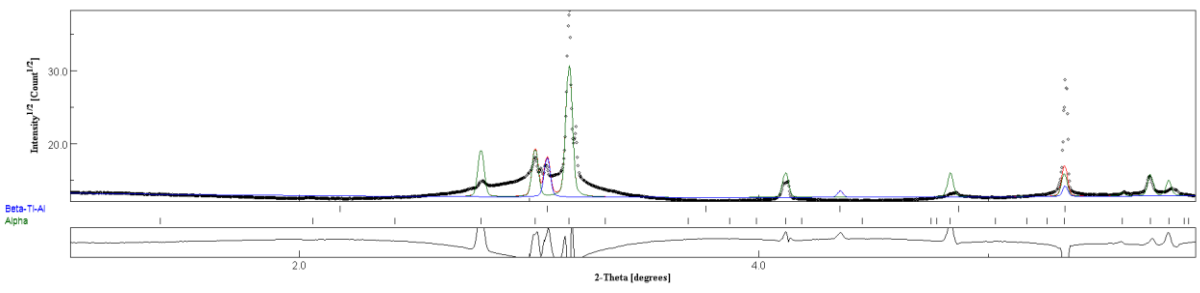
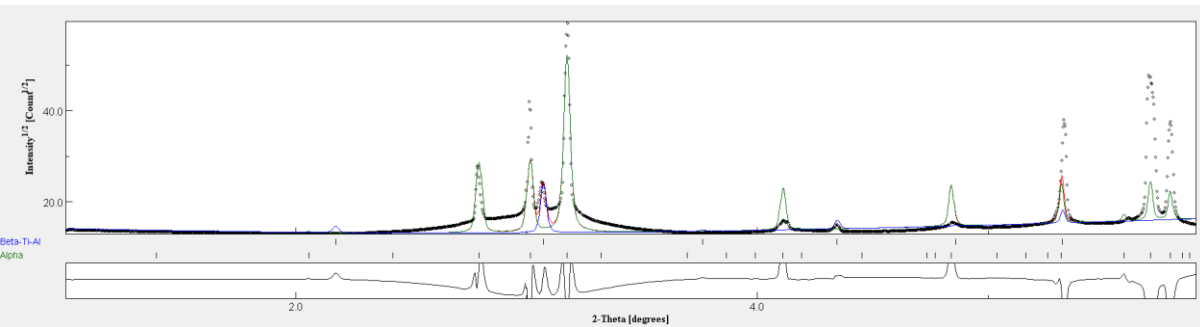
Sample composition	Al		Ti		El	
		Stand. Dev.		Stand. Dev.		Stand. Dev.
Ti-39Al-0.2B						
Ti-42Al-0.2B						
Ti-42Al-1Fe	32.36		60.45		7.18	
Ti-42Al-2Fe	32.37	5.96	60.83	1.53	6.80	3.21
Ti-42Al-3Fe	33.46	5.83	61.29	1.46	5.25	3.04
Ti-42Al-2Mo	37.67	5.48	61.70	1.47	0.63	3.75
Ti-42Al-4Mo	34.96	5.56	59.80	1.74	5.24	2.15
Ti-42Al-6Mo	35.55	5.53	56.37	1.90	8.09	2.05
Ti-42Al-2Cr	36.69	5.66	58.22	1.53	5.10	3.88
Ti-42Al-4Cr	43.13	5.37	52.50	1.50	4.37	3.53
Ti-42Al-6Cr	33.91	5.73	59.27	1.46	6.82	3.25
Ti-42Al-2Nb	0.00	0.00	0.00	0.00	0.00	0.00
Ti-42Al-10Nb	36.45	5.43	48.72	1.88	7.39	2.66
Ti-42Al-2Ta	0.00	0.00	0.00	0.00	0.00	0.00
Ti-42Al-10Ta	36.99	5.23	50.74	2.55	12.27	2.57

c γ -phase

Sample composition	Al		Ti		El	
		Stand. Dev.		Stand. Dev.		Stand. Dev.
Ti-39Al-0.2B						
Ti-42Al-0.2B	44.93	1.00	55.03	1.00		
Ti-42Al-1Fe	37.62	0.00	61.45	0.00	1.06	0.00
Ti-42Al-2Fe	45.07	5.23	54.93	1.64	1.48	6.37
Ti-42Al-3Fe	45.87	5.25	53.47	1.50	0.66	5.09
Ti-42Al-2Mo	46.16	5.20	53.49	1.50	0.36	4.84
Ti-42Al-4Mo	43.30	5.29	55.33	1.00	1.02	3.96
Ti-42Al-6Mo	46.58	5.18	43.30	5.29	1.02	3.96
Ti-42Al-2Cr	44.46	5.33	54.16	1.55	1.38	5.09
Ti-42Al-4Cr	46.00	47.00	51.60	52.60	2.40	3.40
Ti-42Al-6Cr	46.01	5.24	52.43	1.49	1.57	4.04
Ti-42Al-2Nb	52.13	1.58	46.30	5.20		
Ti-42Al-10Nb	43.89	5.21	48.72	1.88	7.39	2.66
Ti-42Al-2Ta	39.27	5.39	59.03	1.65	1.70	5.30
Ti-42Al-10Ta	46.54	5.04	46.97	2.21	6.49	3.13

Appendix 4 Spectrums at HT and temperatures of β phase appearance in binary and ternary alloys without ordered β_0 phase at RT

Sample Composition	°C	Graphs
Ti-42Al	1338	
Ti-42Al -0.2B	1330	
Ti-45Al	1377	 <p data-bbox="311 1870 606 1915">Too bad grain Statistic</p>

Ti-42Al-2Ta	1329	
Ti-42Al-2Nb	1327	

Appendix 5 Phase transformation temperatures determined by DSC as well as synchrotron and neutron diffraction methods, interpreted by 2 methods: Rietveld refinement and Gauss fit of one reflex

a. 1st Sample Set

Sample	$\beta_0 \rightarrow \beta$, °C			$\alpha_2 \rightarrow \alpha$, °C			γ -solvus, °C			ω ₀ /T ₂ →β ₀ , °C	Synchrotron
	Synchrotron	Neutrons		Synchrotron	Neutrons		Synchrotron	Neutrons			
	Single peak Gauss fit 100	MAUD	Single peak Gauss fit 100	Single peak Gauss fit 101	MAUD	Single peak Gauss fit 101	Single peak Gauss fit 001	MAUD	Single peak Gauss fit 110	MAUD corrected	DSC
Ti-42Al				1123	1115	1120	1211	1210	1190	1210	1207
Ti-45Al				1114	1110	1120	1286	1288	1283	1310	1288
Ti-42Al-2Fe	1123	1122	1120	1167	1160	1160	1252	1269	> 1210	> 1210	1242
Ti-42Al-2Mo	1204	1197	1230	1136	1125	1140	1206	1212, 4	1210	1220	1234
Ti-42Al-2Cr	1111	1110	1090	1128	1131	1110	1209	1211	1170	1170	1193
Ti-42Al-2Nb				1135	1130	1120	1238	1235	1190	1190	1217
Ti-42Al-2Ta				1128	1136	1100	1215	1201	1180	1190	1212

*The data with a difference up to 10°C between neutron and synchrotron results of the first sample set are marked green characters (β₀/β phase transformation by neutron and synchrotron in Ti-42Al-2Fe; α₂→α phase transformation in Ti-42Al-2Fe, Ti-42Al-2Nb, Ti-42Al, Ti-45Al, synchrotron data for Ti-42Al-2Cr and neutron data for Ti-42Al-2Mo and Ti-42Al-2Ta); and γ-solvus in synchrotron Ti-42Al, Ti-42Al-2Fe, Ti-42Al-2Mo); a difference between 10 and 20°C is marked blue characters (β₀/β phase transformation in Ti-42Al-2Mo and Ti-42Al-2Cr, α₂→α phase transformation in Ti-42Al-2Mo, Ti-42Al-2Cr, Ti-42Al-2Ta); higher differences e.g. γ-solvus in Ti-42Al-2Cr have a black colour.

**The differences in phase transformation temperatures between the Rietveld and Gauss (single peak) evaluation methods could be observed by the blue color of characters ground for the case of larger than 10° difference.

b. The 2nd Sample Set. DSC measurements are not performed

Sample with neutron	$\beta_0 \rightarrow \beta$, °C		$\alpha_2 \rightarrow \alpha$, °C		γ -solvus, °C		$\omega_0/\tau_2 \rightarrow \beta_0$, °C
	Synchrotron Gauss	Neutrons Gauss	Synchrotron Gauss	Neutrons Gauss	Synchrotron Gauss	Neutrons Gauss	
Ti-42Al-1Fe	1180	1100	1100		1332	1190/1200	Synchrotron MAUD Very weak τ_2
Ti-42Al-3Fe	1128	1130	1170		1285	1230	948
Ti-42Al-4Mo	1213, but not clear	1250 (1260)	1200	α_2 101 reflex overlapped by Al_2O_3	Not measured yet	1230(1240)	
Ti-42Al-6Mo	1261	1250	1310		1240	1260	
Ti-42Al-4Cr	1004	1120 (1130)	1110		1190	1190 (1200)	
Ti-42Al-6Cr	1194	1110 (1120)			1190	1180	
Ti-42Al-8.5Ta	1080	1066	1150		1200	1200	960
Ti-42Al-10Ta			1190		1240	1240	850
Ti-42Al-8.5Nb	1170	Double Reflex	Overlapped with something		1200	1200	920
Ti-42Al-10Nb	1174/1320*	1180	1066				920
Ti-42Al-0.2B			1117	1120	1360	1170	

* Small reflex at 1174° but it stays so above 1320°C

** Not Measured

Appendix 6 Neutron and synchrotron phase content comparison at RT by Rietveld refinement

Sample	β_0/β , vol. %			a_2 , vol. %			γ , vol. %		
	RT_Syn ch. With rotation	Synch.	Neutr.	RT_Synch. With rotation	Synch	Neutr.	RT_Synch. With rotation.	Synch.	Neutr.
Ti-42Al				52.98	60.99	55.48	47.02	39.01	44.52
Ti-45Al				20.09	18.76	19.88	79.91	81.24	80.12
Ti-42Al-2Fe (with τ_2 phase)	4.6	3.10	0.10 But 0.22 τ_2	31.73	34.35	28.99	63.36	61.14	70.69
Ti-42Al-2Mo	22.16	33.64	18.74	17.96	15.17	15.34	59.86	59.89	65.92
Ti-42Al-2Cr	21.83	11.62	18.65	27.44	18.04	15.23	50.73	70.34	66.12
Ti-42Al-2Nb				No data	47.34	47.36	No data	52.66	52.64
Ti-42Al-2Ta				49.07	47.94	45.44	50.93	52.06	54.56

Appendix 7 Comparison of the lattice parameter values between Rietveld refinement of 2 diffraction

methods at RT

a. α/α phase

Sample	a=5.775			c=4.638			c/a = 0.803		
	Synchrotron	Neutrons	Difference	Synchrotron	Neutrons	Difference	Synchrotron	Neutrons	Difference
Ti-42Al	5.818	5.744	0.074	4.675	4.599	0.076	0.804		
Ti-42Al-2Cr, Z=24	5.762	5.733	0.029	4.62	4.629	-0.009	0.802	0.807	-0.005
Ti-42Al-2Mo, Z=42	5.765	5.733	0.032	4.631	4.628	0.003	0.803	0.807	-0.004
Ti-42Al-2Fe, Z=26	5.766	No RT		4.619	4.617	0.002		No RT	
Ti-42Al-2Nb, Z=41	5.764	5.755	0.009	4.632	4.604	0.028	0.804	0.8	0.004
Ti-42Al-2Ta, Z=73	5.761	5.759	0.002	4.629	4.603	0.026	0.803	0.799	0.004
Ti-45Al	5.766	5.749	0.017	4.628	4.601	0.027	0.803	0.8	0.003
MAX	5.818	5.759	0.074	4.675	4.629	0.076	0.804	0.807	0.004
MIN	5.761	5.733	0.002	4.619	4.599	-0.009	0.802	0.799	-0.005
MAX-MIN	0.057	0.026	0.072	0.056	0.03	0.085	0.002	0.008	0.009

b. β_0/β phase

Sample	a = 3,21			Difference
	Synchrotron	Neutrons		
Ti-42Al-2Cr, Z=24	3.19	No RT		
Ti-42Al-2Mo, Z=42	3.208	3.199		0.008
Ti-42Al-2Fe, Z=26	3.218	No RT		
MAX	3.218	3.2		0.008
MIN	3.19	3.2		0.008
MAX-MIN	0.028	0		0.008

c. γ - phase

Sample	a=4.012			c=4.065			c/a 1.013
	Synchrotron	Neutrons	Difference	Synchrotron	Neutrons	Difference	
Ti-42Al	4.058	4.011	0.047	4.09			1.008
Ti-42Al-2Cr, Z=24	4.015	4.019	-0.004	4.049	4.065	-0.016	1.008
Ti-42Al-2Mo, Z=42	4.022	4.019	0.003	4.057	4.065	-0.008	1.009
Ti-42Al-2Fe, Z=26	4.012	4.005	0.007	4.049	4.065	-0.016	
Ti-42Al-2Nb, Z=41	4.019	4.015	0.004	4.061	4.06	0.001	1.01
Ti-42Al-2Ta, Z=73	4.018	4.017	0.001	4.059	4.06	-0.001	1.01
Ti-45Al	4.015	4.009	0.006	4.057	4.065	-0.008	1.01
MAX	4.058	4.019	0.047	4.09	4.065	0.001	1.010
MIN	4.012	4.005	-0.004	4.049	4.06	-0.016	1.0080
MAX-MIN	0.046	0.014	0.051	0.041	0.005	0.017	0.0020

d. τ_2 phase

Sample	Synchrotron	Neutrons
Ti-42Al-2Fe, Z=26	12.135	12.137